Targeting Muscle Stem Cells for the Treatment of Spinal Muscular Atrophy

TARGETING MUSCLE STEM CELLS FOR THE TREATMENT OF SPINAL MUSCULAR ATROPHY

A DISSERTATION PRESENTED

BY

REBECCA MIEKO GIBBS

TO

THE DIVISION OF MEDICAL SCIENCES

IN PARTIAL FULFILLMENT OF THE REQUIREMENTS

FOR THE DEGREE OF

DOCTOR OF PHILOSOPHY

IN THE SUBJECT OF

BIOLOGICAL AND BIOMEDICAL SCIENCES

HARVARD UNIVERSITY

CAMBRIDGE, MASSACHUSETTS

DECEMBER 2019

TARGETING MUSCLE STEM CELLS FOR THE TREATMENT OF SPINAL MUSCULAR ATROPHY

ABSTRACT

Spinal muscular atrophy (SMA) is a genetic neuromuscular disease caused by insufficient expression of the Survival of Motor Neuron (SMN) protein. SMA is the most common genetic cause of infant mortality and there is currently no cure. Although SMA is primarily characterized by motor neuron death in the spinal cord and subsequent nerve degeneration and muscle atrophy, accumulating evidence suggests that SMN deficiency may directly impair skeletal muscle development and maturation.

Skeletal muscle stem cells, known as satellite cells, play a critical role in postnatal muscle growth and regeneration after damage. In this dissertation, we used novel SMA mouse models and induced pluripotent stem cell (iPSC) models to demonstrate that SMN deficiency decreases satellite cell proliferation in a cell-autonomous manner, causing insufficient production of myogenic precursors to support muscle growth.

In addition, we recently demonstrated that systemic administration of therapeutic agents can enhance skeletal muscle growth by proliferating endogenous satellite cells *in situ*. Therefore, we hypothesized that small molecule-based, satellite cell-targeted therapies could potentially ameliorate muscle-intrinsic defects in SMA. Here, we performed a phenotypic screen and discovered small molecules across distinct drug classes that stimulate wild type satellite cell proliferation *in vitro*. We further identified a subset of compounds capable of proliferating SMN-deficient satellite cells *in vitro* and in SMA mice *in vivo*. These enhancements in satellite cell proliferation were associated with increased muscle size and motor strength in SMA mouse models.

We propose that satellite cells are an important therapeutic target for treating SMA, through correction of the satellite cell-intrinsic defect or by pharmacological stimulation of their activity to regenerate atrophic muscle. If this approach proves efficacious, small molecule-based, satellite cell-targeted therapy could provide significant benefit for many neuromuscular and muscle disorders, such as Duchenne muscular dystrophy (DMD), amyotrophic lateral sclerosis (ALS), acute muscle trauma, or age-related sarcopenia.

TABLE OF CONTENTS

LIST OF FIGURES AND TABLES

CHAPTER 1

CHAPTER 2

CHAPTER 3

CHAPTER 4

To my father-

It was all because of you.

ACKNOWLEDGMENTS

First and foremost, I would like to thank my dissertation advisor, Dr. Lee Rubin, for providing me with a wonderful lab and the scientific freedom to pursue my interests. I feel so fortunate to have worked with such a genuinely kind, patient, wise, and supportive person. Lee opened my eyes to the possibility of developing innovative therapeutics for patients with devastating neurodegenerative disorders, and I cannot wait to see the clinical impact of his work in the future.

I would also like to sincerely thank Dr. Feodor Price, my primary collaborator and direct mentor in the Rubin lab. His incredible passion for stem cell biology inspired me every day, and this dissertation would not have been possible without him. Also, a heartfelt thank you to my undergraduate mentee Soumyaa Mazumder, for learning and trudging alongside me throughout the years.

I would also like to thank all of the Rubin Lab members for making Sherman Fairchild a home away from home. In particular, a huge thank you to Jane LaLonde and Kathy Pfaff for keeping the lab afloat, to my fellow graduate students Brittany Mayweather and Michelle Watts for their constant encouragement, and to Sean Buchanan and Natalia Muela-Rodriguez for their intellectual guidance.

I would also like to thank my former mentor Dr. Chien-Ping Ko. He was the first professor I ever worked with many years ago, back when I was an English major with a sudden dream of developing therapies for neuromuscular diseases. He took a chance on me despite the fact that I had no scientific background, and forever changed the course of my life.

I would also like to thank the advisors who guided my thesis research, including Dr. Amy Wagers, my Dissertation Advisory Committee members Drs. Tracy Young-Pearse, Jay Rajagopal and Andrew Lassar, and my Dissertation Defense Committee members Drs. Charlotte Sumner, Brian Wainger, and Vandana Gupta. I am incredibly fortunate to have had such brilliant professors shape my intellectual journey.

Finally, an exceedingly heartfelt thank you to my family and friends for their immeasurable love and support throughout the years. In particular, I am eternally grateful to Joe Luquette for providing a constant source of joy and love throughout graduate school. For the rest of my life, when I remember Harvard, I will picture this brilliant and wonderful man. Also, a huge thank you to Chris Pettit and my four siblings, Nate, Rachel, Anela and Ben, who stood beside me through everything. Most importantly, I would like to thank my parents, Del and Maude Gibbs, for their unwavering love and support. Their resilience in the face of hardship inspired me to face each day with optimism, even during the most challenging parts of this journey. There are no words to convey my love for them all.

CHAPTER 1

INTRODUCTION

Spinal muscular atrophy pathogenesis and clinical presentation

Spinal muscular atrophy (SMA) is an autosomal recessive, neuromuscular disorder characterized by lower motor neuron death and widespread muscle atrophy. Most commonly occurring in children, SMA was originally described more than a century ago by physicians Guido Werdnig and Johann Hoffman, who observed infants with flaccid muscles, degeneration of spinal cord motor neurons, and extreme muscle weakness[1,2]. Today, SMA is viewed as a heterogeneous disorder with a continuum of phenotypes, and clinical characterizations have been refined to categorize patients according to the severity of their symptoms (Table 1.1).

Table 1.1. Severity of SMA clinical subtypes is inversely correlated with SMN2 copy number.

Clinical SMA Type	Approximate SMN2 Copy Number	Age of Onset	Key Clinical Features	Life Expectancy
Type 0	1	In utero	Widespread motor and sensory neuronal loss, congenital cardiac defects	Perinatal
Type I	2	<6 months	Poor feeding and head control, hypotonia, respiratory distress	<24 months
Type II	3	6-18 months	Cannot walk, respiratory muscle weakness	30-50 years depending on respiratory function
Type III	4	>18 months	Unable to climb stairs	Normal
Type IV	4	Adulthood	Mild muscle weakness and tremors	Normal

Adapted from Bowerman et al., 2017[3]

Type I SMA (also called Werdnig-Hoffman disease) is the most fatal and common form, typically presenting before 6 months of age and resulting in death within two years. With an incidence of ~1:10,000 live births, Type I accounts for 60% of new SMA cases[4]. Type I patients present with extensive generalized muscle weakness (hypotonia) and are unable to control head movement or sit unaided. Muscle weakness is usually symmetrical, but it tends to be more severe in proximal muscles

and leg muscles. Although there is relative sparing of the diaphragm, patients usually succumb to respiratory failure and death in the absence of respiratory support[5].

Type II patients have similar but more mild symptoms beginning within the first 18 months of life. Type II patients can sit independently, but they are never able to walk and often require surgical intervention for scoliosis. Type II patients live beyond two years of age, and the majority reach 20 years of age. Type III patients have an even milder form of SMA, with an age of onset beyond 18 months. Type III is highly variable in presentation, with some patients requiring wheelchair assistance while others are able to walk unaided. Type III patients live into adulthood but suffer from muscle weakness throughout their lives. Less common forms of SMA have also been described, including Type 0 SMA, which begins prenatally and causes death within the first 6 months of life, and adult-onset Type IV SMA, which presents with very mild symptoms and a normal life expectancy.

The genetics and molecular basis of spinal muscular atrophy

Spinal muscular atrophy is caused by deficient Survival of Motor Neuron (SMN) expression

SMA is an autosomal recessive, monogenic disorder. All patients have a deletion or loss of function (LOF) mutation in the *Survival of Motor Neuron 1* gene, which was mapped to chromosome 5q13 by linkage analysis in 1995 and named for its purported role in SMA[6]. In the same region of the causative SMA gene, there is an inverted duplication that shares a high degree of homology with *SMN1*[7]. This duplicated telomeric gene (*SMN2* or SMN^{T}) only differs from the disease-causing centromeric *SMN* (*SMN1* or SMN^{C}) by a single synonymous C→T mutation in exon 7 and four other single base substitutions in non-coding regions. Although the nucleotide transition in the coding region of *SMN2* is translationally silent, it causes exon 7 to be skipped in a majority of transcripts (Figure 1.1). Thus, *SMN2* primarily produces a truncated and highly unstable SMN protein lacking the region corresponding to exon 7 (SMNΔ7). However, approximately 10% of the time, *SMN2* is

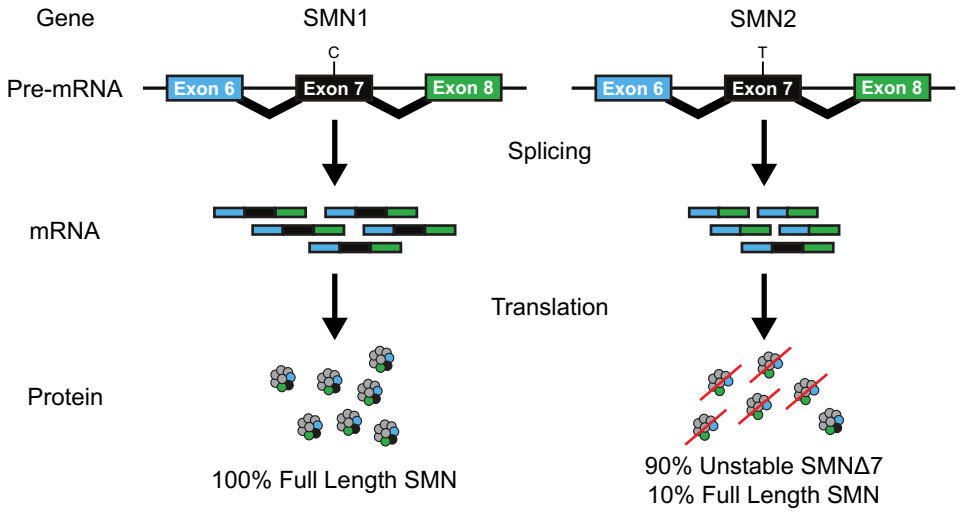

Figure 1.1. Genetics of spinal muscular atrophy. Schematic showing *SMN1* and *SMN2* gene architecture in humans. *SMN1* produces full length SMN protein, but a C→T transition in exon 7 of *SMN2* causes exon 7 skipping during splicing. *SMN2* primarily produces a truncated and unstable SMN protein. SMA patients have a deletion or LOF mutations in *SMN1* and retention of 0-4 copies of *SMN2*.

correctly spliced and produces low levels of functional, full-length SMN. Since *SMN2* exists in variable copy number in the population, there is a range of SMN protein levels that correlates with disease subtype (Table 1.1). Thus, although SMA is caused by the loss of *SMN1*, higher copy numbers of *SMN2* can compensate and modify disease severity.

Heterozygous carriers of *SMN1* deletions/LOF mutations occur at a frequency of ~1:50-1:100 across various ethnic groups, and are generally considered to be healthy and unaffected by SMA-related pathologies[4,7].

Survival of Motor Neuron (SMN) functions to assemble snRNPs

SMN is a ubiquitously expressed 38 kDa protein found in a diffused pattern throughout the cytoplasm and in focal structures called gems in the nucleus. Gems exist in close proximity to Cajal bodies, nuclear substructures thought to play a role in small nuclear ribonucleoprotein (snRNP)

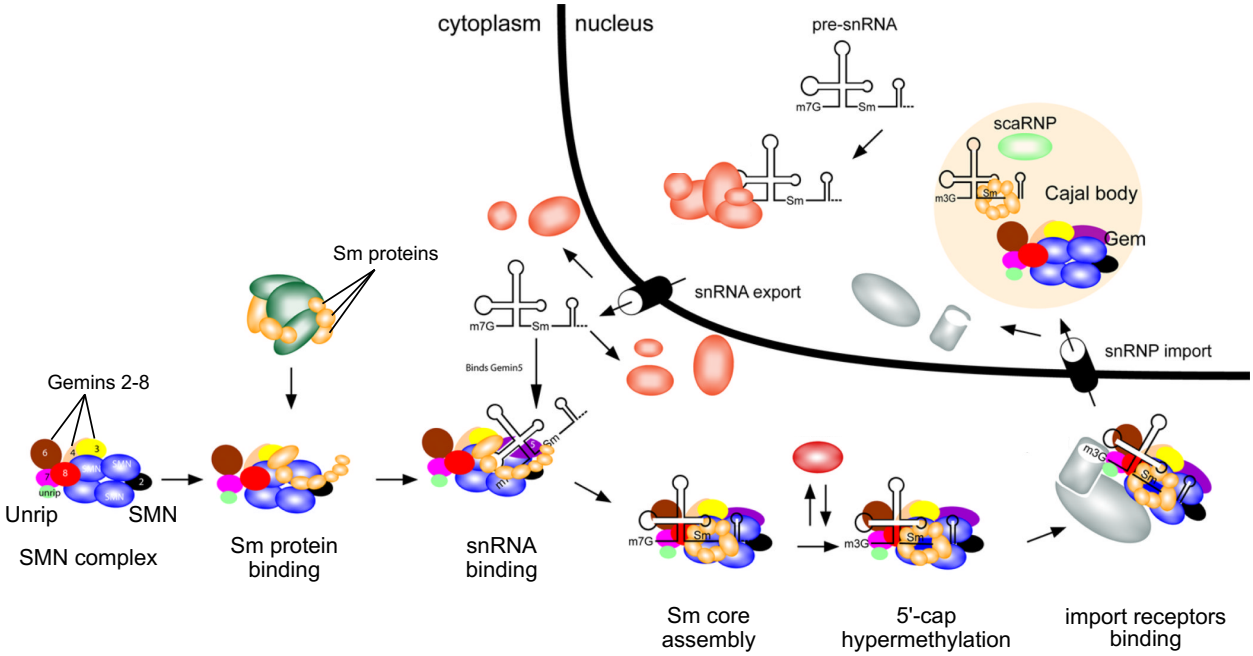

Figure 1.2. The SMN complex functions to assemble snRNPs. SMN complexes with Gemins 2-8 and Unrip and loads Sm proteins onto snRNA. The entire complex is imported into the nucleus, where it associates with Cajal bodies for snRNP maturation. Figure modified from Burghes & Beattie, 2009[8].

biogenesis and pre-mRNA splicing[9]. SMN plays a critical role in the assembly of snRNPs, RNA-protein complexes that form the spliceosome with pre-mRNA (Figure 1.2). SMN oligomerizes and forms a complex with a number of proteins, including Gemins 2-8 and unr interacting protein (Unrip). The SMN complex then facilitates the transfer of a heptameric ring of Sm proteins onto snRNA, which is originally transcribed in the nucleus and transported to the cytoplasm[10]. The entire SMN complex and associated snRNA are then imported into the nucleus, where they localize to Cajal bodies for further snRNP maturation[11].

The role of Survival of Motor Neuron (SMN) in SMA pathology

Exactly how SMN deficiency causes SMA is not well understood, although there are two primary hypotheses. The first is that SMN deficiency disrupts the formation of snRNPs and in turn

causes mis-splicing of genes important for motor neuron function. In support of this hypothesis, neural and non-neural extracts from severe SMA mice have lowered snRNP assembly activity, and administration of assembled snRNPs rescues SMN-dependent motor axon defects in zebrafish[12,13].

To examine the consequence of disrupted snRNP formation, many studies have evaluated splicing abnormalities secondary to SMN deficiency. Interestingly, the loss of SMN does not uniformly reduce snRNPs, but causes tissue-specific and snRNA-specific deficits. For example, there is a greater reduction of minor snRNPs, such as those containing U11, U12, and U4atac snRNA in the brain, spinal cord and heart of SMA mice, but these same snRNAs are relatively unaffected in skeletal muscle and kidney tissue[13,14]. RNA-sequencing studies also identified elevated U12-intron retention across multiple tissues in SMA mice[15]. Overall, these differential defects in snRNP profiles lead to widespread splicing abnormalities across a diverse set of genes, with a preferential disruption in genes containing a large number of introns[14]. However, in spite of these broad splicing defects, it has been difficult to elucidate abnormalities driving disease pathology versus those occurring as a secondary consequence to SMA phenotypes. Several studies have suggested that SMA may result from mis-spliced transcripts involved in motor neuron-related pathologies such as neurite outgrowth and calcium homeostasis, but no clear splicing-dependent mechanism has emerged that entirely accounts for the SMA phenotype[15,16].

The second core hypothesis for how SMN deficiency causes SMA involves the role of SMN in axons. SMN localizes to granules that are actively transported and distributed throughout neuronal axons and growth cones. Since these SMN granules co-localize with Gemin proteins but not Sm proteins, SMN's function in the axon might be independent of its role in snRNP assembly[11,17]. Furthermore, several studies have identified motor axon phenotypes in SMA models. For example, SMN knockdown in zebrafish disrupts motor axon pathfinding in a motor neuron-autonomous manner, and disruption of SMN's ability to interact with its binding partners or preventing SMN granule secretion from the Golgi apparatus impairs neurite outgrowth and morphology[18-20]. Studies of

SMN-deficient motor neuron cultures have also revealed shorter axons and reduced β-actin mRNA transport to the distal axon, leading to disrupted Cav2.2 channels in axonal growth cones and impaired electrophysiological activity[21,22]. These deficits may disrupt neurotransmission to skeletal muscle, partially explaining the weakness phenotype. However, in spite of the evidence supporting a role of SMN in motor axons, there is no clear consensus regarding the exact mechanism by which axonal SMN deficiency underlies SMA.

Animal Models of SMA

C. elegans, drosophila and zebrafish models of SMA

SMA is a disease unique to humans. Only chimpanzees possess the *SMN2* gene duplication, which occurred at least 5 million years ago, but only *Homo sapiens* possess the exon 7 nucleotide conversion that confers low levels of SMN in the absence of *SMN1*[23]. In all other species, *SMN* is present as a single gene, loss of which causes embryonic lethality[24]. Regardless, animal models have been crucial for elucidating SMA disease mechanisms. In *Caenorhabditis elegans*, the SMN ortholog *CeSMN* is expressed throughout development and adulthood, and disruption causes severe locomotive defects and embryonic lethality in progeny[25]. In *Drosophila melanogaster*, the SMN ortholog *dSMN* is expressed more highly during development than in adulthood. Homozygous deletion disrupts locomotion, decreases muscle size, impairs sensory-motor circuit function, and ultimately causes death during the larval stage[26,27]. In addition, some hypomorphic *dSmn* mutations cause acute muscle atrophy and weakness, as well as impaired axon arborization[28]. Aside from invertebrate models, zebrafish *Danio rerio* have been used to model SMA via antisense morpholino knockdown of SMN throughout the embryo, which results in motor axon pathfinding defects[20].

Mouse models of SMA

Murine models are perhaps most widely used to study SMA biology and for therapeutics development. Since mice only have one *Smn* gene, which leads to embryonic lethality upon deletion, modeling SMA in mice generally involves disrupting the endogenous *mSmn* gene either ubiquitously or in a tissue-specific manner and supplementing the lack of Smn with transgenic human *SMN* (*hSMN*). In the original SMA mouse model, a lacZ-neo cassette was inserted into *mSmn* exon[29]. When heterozygous mice were crossed, there were no *mSmn*$^{-/-}$ progeny and embryos homozygous for this null mutation displayed massive early cell death at the blastocyst stage. These results are not altogether surprising, given SMN's important role in snRNP assembly and pre-mRNA processing.

To circumvent the embryonic lethality issue, and to more faithfully recapitulate disease-relevant SMN levels, a subsequent study modified the *Smn*-knockout mouse by introducing a transgene containing the *hSMN2* gene and promoter[30]. *mSmn*$^{-/-}$;*hSMN2* mice are indistinguishable from littermates for the first two days after birth. However, they rapidly deteriorate due to extensive motor neuron death and motor behavioral deficits, and ultimately die by postnatal day 4-6 (P4-P6). Although these mice have been useful for studying SMA, their short life span limits the types of experiments that can be performed.

To create a mouse with a less severe SMA phenotype, a cDNA sequence encoding *hSMN* lacking exon 7 (*SMNΔ7*) was introduced into the severe *mSmn*$^{-/-}$;*hSMN2* background[31]. These "SMNΔ7" mice are initially indistinguishable at birth, but they begin to diverge in body weight at P5. SMNΔ7 experience postnatal motor neuron death, widespread muscle atrophy, neuromuscular junction denervation, and early death around two weeks of age. The SMNΔ7 model is most commonly used in the SMA field and will be referenced throughout this dissertation.

SMA pathologies outside of the central nervous system

SMA is a multisystem, non-motor neuron autonomous disorder

SMA has traditionally been viewed as a motor neuron disorder. Indeed, the core SMA pathologies likely arise from the loss of SMN in motor neurons, which not only causes motor neuron death and subsequent muscle atrophy, but also impairs synaptic transmission in fully innervated muscles[32,33]. In addition to electrophysiological deficits, NMJ structural abnormalities are apparent. Accumulation of neurofilament protein in the presynaptic nerve terminal is a hallmark of SMA, and postsynaptic acetylcholine receptors retain fetal expression of AchR isoforms and remain in an immature plaque-like structure instead of progressing to the more mature, pretzel-like configuration[34].

However, many studies have demonstrated that in addition to motor neuron defects, SMA is actually a multisystem disorder with direct effects in non-motor neuron cell types. In fact, in a mouse model expressing Cre driven by Olig2, a marker of motor neurons and oligodendrocytes in the spinal cord, SMN knockdown did not fully recapitulate SMA[35]. The mutant mice displayed only mild neuromuscular symptoms and lived for one year, compared to SMA mice with ubiquitous SMN knockdown, which only live for two weeks[31]. Furthermore, a series of fascinating studies demonstrated that peripheral SMN restoration conferred long-term survival benefits in SMA mice, whereas SMN restoration in the central nervous system alone only improved survival by several days[36]. The phenotypic rescue achieved with systemic restoration persisted even when the effects of SMN-elevation were blocked in the CNS[37]. Altogether, these studies suggest that SMN deficiency in peripheral tissues directly contributes to SMA pathology.

Indeed, many studies have described peripheral organ defects, including cardiac defects, compromised bone structure and bone mineral density, vascular structure and perfusion issues, necrosis of digits, and dysfunction of the pancreas and intestine[38-45]. Interestingly, using a bioinformatics analysis of SMA patients' electronic medical records, our lab recently identified a range

of non-neuromuscular phenotypes in SMA patients that actually preceded clinical presentation of any neuromuscular symptoms[46]. Overall, the plethora of systemic issues observed in SMA patients highlights the need for therapeutics that address a wide range of symptoms, and suggests that the loss of SMN may cause direct consequences in a tissue-specific manner.

Skeletal muscle and neuromuscular junction structure and function

Of the peripheral organs thought to play a role in SMA pathology, skeletal muscle in particular has emerged as a key therapeutic target. Accounting for 40% of adult human body weight, skeletal muscle provides an important source of trophic support for motor neurons. In fact, skeletal muscle-derived factors are critical for the survival of motor neurons during embryonic development[47,48]. More broadly, skeletal muscle acts as an autocrine, paracrine, and endocrine organ, secreting "myokines" that regulate systemic processes via cross-talk with other organs, including the liver, pancreas, and brain[49].

Skeletal muscle is composed of bundles of multinucleated myofibers that attach by tendons to bones (Figure 1.3). As the structural and functional unit of the muscle, myofibers are arranged in parallel and are composed of actin and myosin filaments, which occur in repeated segments called sarcomeres[50]. Each muscle fiber is innervated at a specialized synapse called the neuromuscular junction, where motor axons extending from the ventral root of the spinal cord contact myofibers. In response to a nerve impulse from the motor axon, acetylcholine (ACh) is released from the presynaptic nerve terminal and binds acetylcholine receptors (AChRs) at post-synaptic motor endplates, which are regions on the muscle fiber with high AChR densities. Neurotransmission depolarizes the myofiber, stimulating calcium release from the sarcoplasmic reticulum and causing movement of the actin and myosin filaments. This contraction shortens the sarcomere to generate muscle force[51].

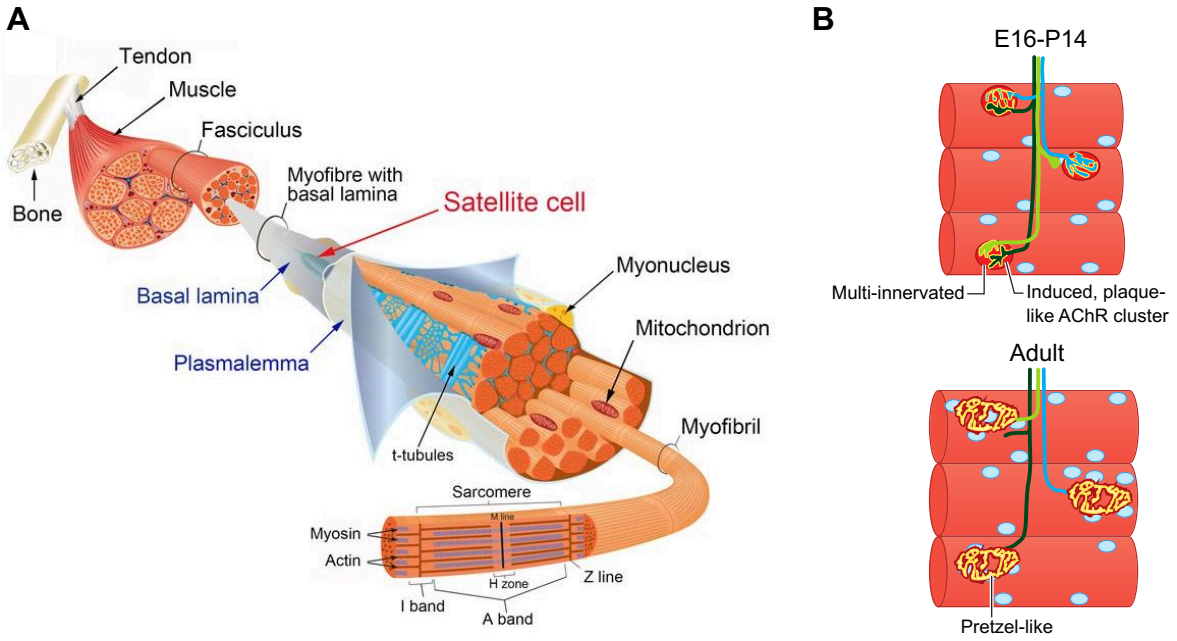

Figure 1.3. Skeletal muscle and neuromuscular junction structure and function. A) Schematic of skeletal muscle structure. Figure modified from Relaix & Zammit, 2012[52]. B) Schematic of neuromuscular junctions in developing and adult muscle. During late embryonic and early postnatal stages, NMJs are innervated by multiple axons and form immature, plaque-like AchR clusters. In adults, NMJs mature into a complex, pretzel-like morphology. Figure modified from Li et al., 2019[51].

SMN deficiency in skeletal muscle may contribute to SMA pathology

There is abundant evidence that skeletal muscle may be directly affected by SMN deficiency in SMA, and that atrophy may not merely be a secondary consequence of motor neuron death. SMA patient muscle fibers are much smaller than normal and exhibit molecular features of delayed maturation, including altered expression of myogenic regulatory factors, as well as reduced mitochondrial content and activity[53,54]. Muscle structural degeneration does not typically occur, suggesting that impaired muscle maturation along with atrophy are the primary pathological events.

The same phenomenon occurs in SMA mouse models, which express abnormal levels of myogenic regulatory factors and display a drastic reduction in muscle size, accompanied by significant loss of force production[34,54]. This occurs even prior to motor neuron death and motor axon loss. Interestingly, as with SMA patients, not all muscle groups are equally affected. We and others have

shown a selective vulnerability of different muscle groups to neuromuscular junction denervation, with proximal muscles near the head and trunk being generally more severely affected than distal muscles of the limb[55,56]. Remarkably, however, even muscles that remain fully innervated at the disease end stage display drastic reductions in muscle size, suggesting a uniform growth deficit occurring independently from motor neuron death-induced atrophy.

Even though synaptic transmission deficits likely contribute to muscle weakness, skeletal muscle-autonomous defects may also contribute to SMA pathology due to SMN deficiency in muscle fibers and myogenic precursors. In fact, myoblasts derived from SMA mice display cell-autonomous proliferation, motility and fusion deficits that are rescued by restoring SMN levels[57,58]. In addition, *mSmn* deletion in skeletal muscles of mice results in a severe dystrophic phenotype, which improves when background (non-skeletal muscle) SMN levels are elevated[59,60]. Interestingly, one study directly addressed if motor neuron, synaptic transmission, and muscle size deficits are attributed to the loss of SMN in motor neurons versus skeletal muscle[61]. The authors conditionally restored SMN in either motor neurons or all skeletal muscle precursors in SMA mice. Both resulted in a ~50% increase in survival and significant improvements in motor behavior. However, while motor neuron death and synaptic impairments were only rescued when SMN was restored in motor neurons, SMN restoration in muscle precursors completed rescued myofiber size. These results underscore the importance of SMN in skeletal muscle for normal growth, independent of NMJ and motor neuron deficits. Furthermore, since motor neuron-specific SMN restoration only moderately increased muscle size in SMA mice, muscle-targeted therapy may be critical for SMA patients, in addition to SMN elevation to sustain motor neuron survival.

Therapeutic approaches for SMA

SMN-elevating therapeutics

Until very recently, treating SMA patients primarily involved palliative care and the use of assistive technologies, such as respirators, nutritional support, and orthopedic devices. However, following the discovery that inactivation of *SMN1* and retention of *SMN2* underlies SMA, a great number of therapeutic developments have been underway that focus on elevating SMN levels to prevent motor neuron death (reviewed in Howell, Gibbs and Rubin, 2019)[62]. Fortunately, there are now two promising FDA-approved SMA drugs on the market with several more in preclinical and clinical development. These SMN-elevating therapeutics mostly fall into three categories: 1) small molecule splicing modifiers; 2) antisense oligonucleotides (ASOs) that increase the amount of full length SMN produced by *SMN2*; and 3) AAV9-mediated gene therapy to introduce a functional *SMN* gene into patients' motor neurons[62].

The first drug approved for SMA in 2016 was nusinersen (Spinraza), developed by Ionis Pharmaceuticals and Biogen. Nusinersen is an ASO that masks an *SMN2* intronic splicing silencer element in intron 7 to efficiently enhance exon 7 inclusion, leading to increased levels of SMN protein[36,63]. A phase III clinical trial of patients with severe SMA found that nusinersen treatment significantly improved motor milestones achieved, and a significantly higher percentage of patients survived without ventilatory support compared to control groups[64]. In addition, in clinical trials of Type II SMA, an increased percentage of patients achieved higher motor function compared to the control group[65]. Although the approval of nusinersen was a major milestone for the SMA community, there are several limitations to this approach. Firstly, since nusinersen does not cross the blood-brain barrier, the drug must be administered by intermittent intrathecal injections. Recurring injections may require sedation and can cause complications and respiratory risk for SMA patients, particularly for those who have spinal rods due to scoliosis. Furthermore, since ASO distribution is higher in lumbar and thoracic spinal cord regions, the more limited distribution to the rostral spinal cord may limit efficacy[66].

The second FDA-approved therapy is AVXS-101 (Zolgensma; AveXis, Novartis), a gene therapy that leverages a nonpathogenic, self-complementary recombinant AAV9 vector to express exogenous *SMN1* cDNA in patients' motor neurons. Since recombinant AAVs can persist for long periods in post-mitotic cells such as motor neurons, AVXS-101 is administered as a one-time intravenous treatment. AVXS-101 demonstrated dramatic benefits in preclinical studies and significantly improved motor milestones achieved in SMA patients, which led to its FDA approval in 2019[67,68]. While SMN gene therapy has great promise, limitations include the possibility of immune response in patients who develop antibodies to the virus, and the potential dilution of the recombinant AAVs over time in proliferating tissue[69].

Two other therapies in clinical development are branaplam (Novartis) and risdiplam (Roche, PTC Therapeutics, SMA Foundation), small molecule splicing modifiers that increase the production of full length SMN produced by *SMN2*[70,71]. These orally bioavailable drugs are easier to administer than nusinersen and AVXS-101 and enable SMN upregulation in peripheral tissue. Both compounds showed dramatic benefits in SMA animal models and clinical results have been promising thus far[62,72].

Limitations of SMN-elevating therapeutics

In spite of early successes, neither nusinersen nor AVXS-101 are curative, particularly in older patients in chronic phases of the disease when motor neurons have been largely lost. In all cases of SMN-elevating therapies, timing and tissue distribution are critical factors to consider. In both animal models and patients, early intervention has proven crucial for achieving better outcomes, as there appears to be a critical developmental window when SMN elevation has the greatest impact on improving motor neuron survival. In fact, natural history studies have demonstrated that SMA follows an up-front disease course, with the majority of motor neuron death occurring very early, followed by a much slower degenerative phase (Figure 1.4)[73]. Furthermore, in humans, SMN levels in the spinal

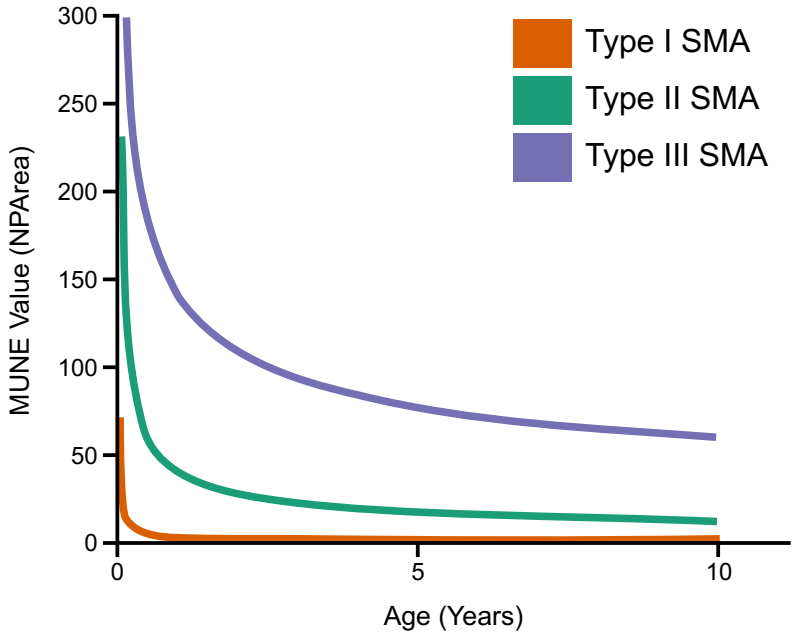

Figure 1.4. SMA presents clinically with early motor neuron death. Motor neuron numbers (reflected by the motor unit number estimation value on the Y-axis) decrease sharply shortly after birth, followed by a long plateau phase characterized by slower neurodegeneration. The severity of the initial drop in motor neuron numbers correlates with SMA clinical subtype. Figure adapted from Swoboda et al., 2005.[73]

cord are highest during fetal development, then decrease to low levels postnatally[66]. In SMA mice, SMN restoration in the early neonatal period rescues the disease phenotype, but later restoration has no therapeutic benefit[74]. Conversely, SMN depletion in mice after P17, when postnatal skeletal muscle development and neuromuscular junction maturation is complete, has almost no effect. The only exception is in the case of skin, muscle or motor axon damage, during which global SMN deficiency impairs regeneration[75]. Thus, SMN-elevation at an early age, prior to the onset of motor neuron death, may have the greatest benefit. This implies that early diagnosis is imperative for nusinersen and AVXS-101 to be maximally effective.

Aside from the timing issue, it is important that SMN-elevating therapies are administered systemically for maximal benefit. Interim results from an ongoing clinical trial demonstrated that even when nusinersen was administered to genetically diagnosed, pre-symptomatic SMA patients, not all

patients achieved expected motor milestones[76]. Given that nusinersen is administered intrathecally, these results could partially be due to insufficient elevation of SMN outside the central nervous system. Thus, it will be important for future therapeutics to accomplish SMN elevation both in the CNS and peripheral tissues, or to complement SMN elevation in the CNS with drugs targeting key peripheral tissues.

SMN-independent therapeutics for SMA

There are several SMN-independent therapies being developed, which mostly focus on correcting skeletal muscle defects. The pharmaceutical company Scholar Rock is developing SRK-015, an antibody against myostatin, which is a negative regulator of muscle growth[77]. By blocking the activation of myostatin, SRK-015 increases muscle size and strength in SMA mice, and is currently being evaluated in clinical trials[78,79]. Another muscle-targeted approach by Cytokinetics and Astellas Pharma is reldesemtiv, a small molecule that increases muscle force by sensitizing the muscle to calcium, resulting in amplified contractions even with submaximal nerve stimulation. Ongoing clinical trials have demonstrated beneficial improvements in ambulation and reduced muscle fatigue in Type II and III SMA patients[80]. Going forward, it will be important to assess the combined benefit of SMN elevation and muscle-targeted therapies. Furthermore, as patients treated with nusinersen and AVXS-101 begin to live longer, it will be important to identify additional peripheral symptoms that may require targeted correction.

Enhancing muscle growth in SMA

Satellite cells in muscle growth and regeneration

The muscle-targeted therapies described above focus on improving the strength of muscle fibers that have already developed. An alternative strategy to enhance muscle growth is to target the actual cell that gives rise to muscle in the first place—the satellite cell.

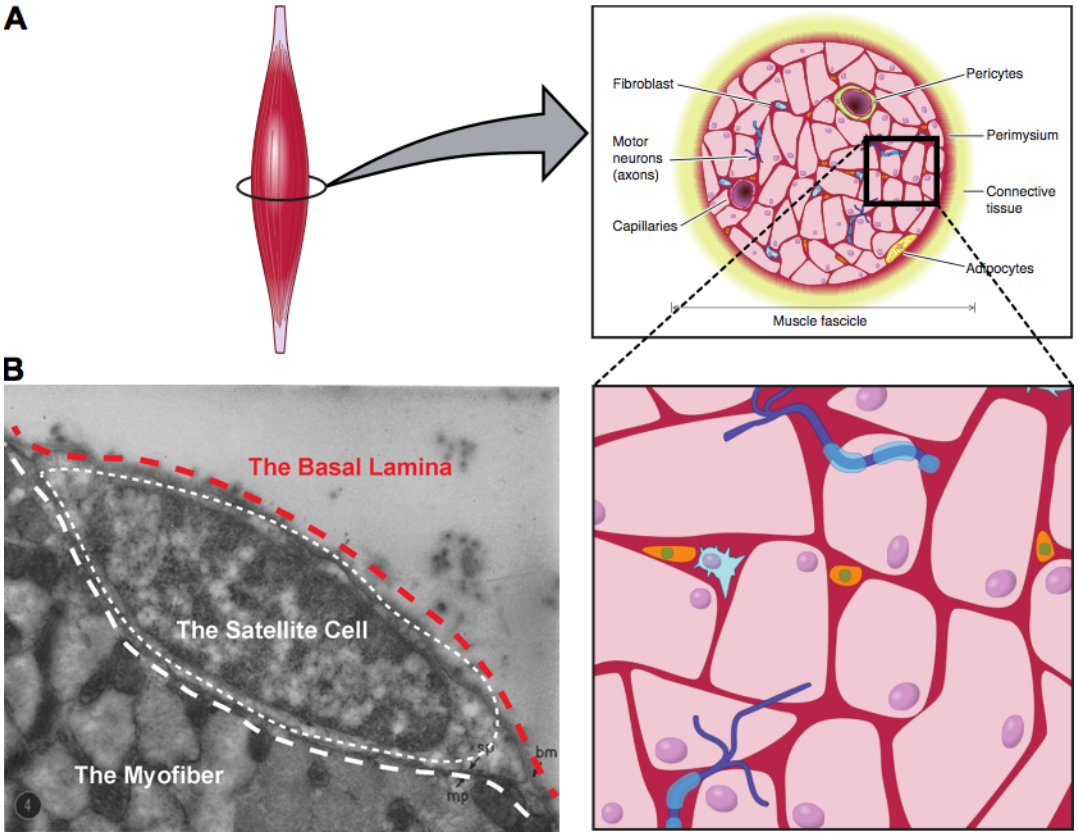

Figure 1.5. Satellite cells occupy a niche between the sarcolemma and basal lamina of muscle fibers. A) Schematic showing the location of satellite cells (orange) wedged between myofibers (pink). Myofibers are arranged in parallel within the muscle, which contains other cell types such as fibroblasts and adipocytes. Figure generated by co-author Dr. Feodor Price. B) Electron micrograph from the first study to identify the satellite cell as a mononucleated cell within the basal lamina surrounding myofibers. EM image modified from Mauro, 1961[81].

Skeletal muscle is composed of contractile multinucleated fibers that form in several phases. During embryonic development, skeletal muscle arises from the paraxial mesoderm, which segments into somites on each side of the body axis[82]. In the dorsal portion of somites, called the dermomyotome, $Pax3^{+}$ cells specified to the myogenic lineage upregulate the myogenic transcription

factor Myf5, proliferate and fuse to form the primary myotome[52]. Following myotome formation, $Pax3^+$ cells migrate from the dermomyotome to the developing limb buds, where they upregulate Pax7 and initiate myogenesis through the sequential expression of muscle regulatory factors Myf5, Myf6, MyoD and myogenin. Pax3 is downregulated in myogenic precursors toward the end of embryonic development, but Pax7 is maintained in satellite cells, which occupy a niche between the sarcolemma and basal lamina of muscle fibers (Figure 1.5)[52,81].

After birth, the number of fibers in a muscle remains constant, but there is a rapid period of postnatal muscle growth characterized by robust myonuclear accretion (Figure 1.6)[83]. Since muscle fibers are post-mitotic, the increase in nuclei is entirely attributed to $Pax7^+$ satellite cells, which activate and divide to produce: 1) an identical daughter cell that repopulates the niche (self- renewal), and 2) a myoblast, a muscle precursor cell committed to the myogenic lineage[84]. Myoblasts, which express both Pax7 and MyoD, robustly proliferate to form a transit amplifying muscle precursor pool[85]. Myoblasts then terminally differentiate into elongated $myogenin^+$ myocytes, which upregulate muscle structural myosin proteins (MyHC) before fusing with existing muscle fibers. This process of myonuclear accretion contributes new nuclei to meet the demands of the growing muscle fiber.

The postnatal period of muscle growth demands massive production of satellite cells and myoblasts, resulting in a five-fold increase in the number of myofiber nuclei within the first three postnatal weeks in wild type mice[86]. In humans, this active satellite cell period corresponds to approximately the first few months after birth[87]. After this growth period, >99% of satellite cells return to mitotic quiescence within their niche. However, satellite cells remain absolutely critical for muscle regeneration throughout life[88]. In response to muscle damage, satellite cells robustly reactivate, transitioning from a G0 to a G1 phase of the cell cycle, then proliferate, differentiate, and fuse to repair damaged fibers or to form new fibers *de novo*.

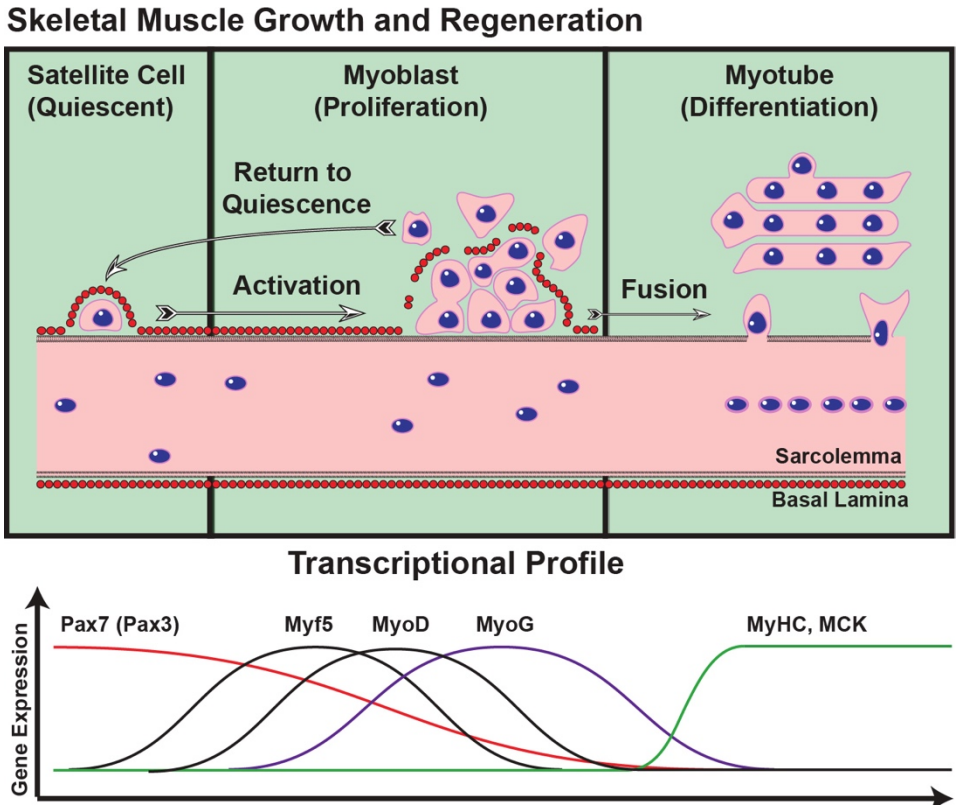

Figure 1.6. Satellite cell function during muscle growth and regeneration. During muscle growth and regeneration after damage, quiescent satellite cells activate and divide to produce myoblasts. Myoblasts robustly proliferate, terminally differentiate, and fuse to existing myofibers or to form new fibers *de novo*. Fluctuating levels of myogenic transcription factors (Pax7, Pax3, Myf5, MyoD, MyoG) and muscle fiber proteins (MyHC, MCK) characterize each cell state. Figure generated by co-author Dr. Feodor Price.

Satellite cells in SMA

Multiple SMA studies have proposed that weakness begins at the muscle, since it occurs in some cases prior to motor neuron death. Although nervous system deficits certainly play a role, we believe that the loss of SMN may directly impair skeletal muscle growth and maintenance. Intriguingly, although severe SMNΔ7 mice are the same size as littermate controls at birth, their muscle growth begins slowing down at P5 and plateaus at P10[54]. This exactly coincides with the most dynamic period of satellite cell-mediated skeletal muscle growth[86].

In fact, accumulating evidence suggests that satellite cell defects underlie growth failures in SMA. Conditional SMN restoration in post-mitotic muscle using the human skeletal actin (HSA) promoter has no effect on muscle size or survival of SMA mice, but SMN restoration in all muscle cell types (including satellite cells and myoblasts) completely rescues muscle size, improves motor behavior, and moderately increases lifespan[61,89]. Furthermore, we recently demonstrated that satellite cells in a severe SMA mouse model prematurely differentiate *in vivo* and display reduced myofiber formation *in vitro*[90]. These results suggest that myogenic precursors, including satellite cells and myoblasts, are critical targets of SMN deficiency.

In addition, we and others have established that SMN has an important function in cell proliferation, and that the loss of SMN reduces the proliferative capacity of multiple cell types[58,91,92]. Therefore, we hypothesized that SMN deficiency decreases satellite cell and myoblast proliferation, causing insufficient production of myogenic precursors to support postnatal muscle growth in SMA.

In this dissertation, we demonstrate that satellite cells play a role in SMA pathology. Specifically, we identified a loss of proliferating satellite cells in a mouse model with ubiquitous SMN deficiency, and further demonstrated that conditional SMN reduction in satellite cells impairs satellite cell-mediated muscle growth. These findings argue for the importance of peripheral SMN elevation during the postnatal period, possibly in combination with therapies that stabilize the motor neuron pool. Furthermore, given the remarkable regenerative capacity of satellite cells, we believe that stimulating satellite cell proliferation can increase muscle growth and ameliorate disease manifestations independent of SMN deficiency. To explore this possibility, we performed a phenotypic screen and identified multiple compounds across discrete drug classes that are capable of stimulating satellite cell proliferation, and additionally demonstrated that one compound was capable of ameliorating muscle atrophy in both severe and intermediate mouse models of SMA. This work suggests that satellite cells

may represent a novel therapeutic target for restoring strength to patients suffering from SMA and other devastating muscle diseases.

CHAPTER 2

SMN DEFICIENCY IN SATELLITE CELLS IMPAIRS SKELETAL MUSCLE GROWTH IN SPINAL MUSCULAR ATROPHY

Introduction

Spinal muscular atrophy (SMA) is a genetic neuromuscular disorder caused by a deletion or loss of function (LOF) mutation in *SMN1* and retention of one or more copies of the highly homologous *SMN2* gene[6,24]. SMA pathologies are primarily driven by the loss of Survival of Motor Neuron (SMN) protein in motor neurons, which causes motor neuron death, nerve degeneration, and subsequent skeletal muscle atrophy[8]. However, accumulating evidence suggests that SMN deficiency may cause intrinsic skeletal muscle growth failures, independent of muscle atrophy occurring as a secondary consequence to motor neuron death[54,93].

Skeletal muscle growth is primarily driven by muscle stem cells called satellite cells, which occupy a niche within the basal lamina surrounding muscle fibers. Satellite cells are normally quiescent. However, during postnatal growth and in response to muscle damage, they activate, proliferate, differentiate, and fuse with existing fibers to increase the size of multinucleated fibers (Figure 1.6)[50]. We and others have demonstrated that satellite cell defects may impair muscle growth in SMA. For example, we recently demonstrated that satellite cells in a severe SMA mouse model prematurely differentiate *in vivo* and display reduced myofiber formation *in vitro*[90]. Furthermore, studies have shown that conditional SMN restoration in post-mitotic muscle has no effect on muscle size or survival of SMA mice, but SMN restoration in all muscle cell types, including satellite cells and myoblasts, completely rescues muscle size, improves motor behavior, and moderately increases lifespan[61,89].

In addition, SMN-deficiency has been shown to decrease the proliferative capacity of multiple cell types, including fibroblasts, myoblasts, and cells in the hippocampus[58,91,92]. Therefore, we hypothesized that SMN deficiency decreases satellite cell and myoblast proliferation, causing insufficient production of myogenic precursors to support postnatal muscle growth in SMA. If satellite cell function is impaired, muscle growth may be limited even if motor neuron survival is corrected in patients.

To test this hypothesis, we characterized satellite cell defects in the well-established SMNΔ7 mouse model of severe SMA, which features inactivation of the single endogenous mouse *Smn* gene and the presence of low levels of SMN provided by human *SMN2* and *SMNΔ7* transgenes[31]. SMNΔ7 mice faithfully recapitulate similar patterns of motor circuit vulnerability observed in patients, including motor neuron death, neuromuscular junction denervation, and muscle atrophy. These mice only live for two weeks, which exactly corresponds to the most dynamic period of postnatal muscle growth and satellite cell activity in mice[86]. To investigate if SMN deficiency impairs satellite cell function in a cell-autonomous manner, we also generated satellite cell-conditional SMN knockout and knockdown mouse models.

Here, we demonstrate that myogenic precursors undergo defective proliferation in the severe SMNΔ7 mouse model, which occurs as a direct consequence of SMN deficiency in satellite cells. These findings suggest that satellite cells may be an important therapeutic target for treating SMA and highlight the need for peripheral SMN restoration during the postnatal muscle growth period, when satellite cells are most active. In addition, since satellite cells are typically quiescent after postnatal development, elevating SMN levels in post-symptomatic patients may have limited effects on enhancing muscle growth. This suggests that SMN elevation therapies may need to be supplemented with muscle-targeted therapies that stimulate satellite cell activity.

Results

Satellite cell proliferation defects impair muscle growth in SMNΔ7 mice *in vivo*

To determine if SMN deficiency impairs satellite cell proliferation, we first examined if there is a decrease in the number of proliferating satellite cells in the skeletal muscle of end-stage SMNΔ7 mice. To label proliferating satellite cells, we injected end-stage (postnatal day 14) SMA and age-matched littermate control mice with 5-Ethynyl-2'-deoxyuridine (EdU), a thymidine analog that

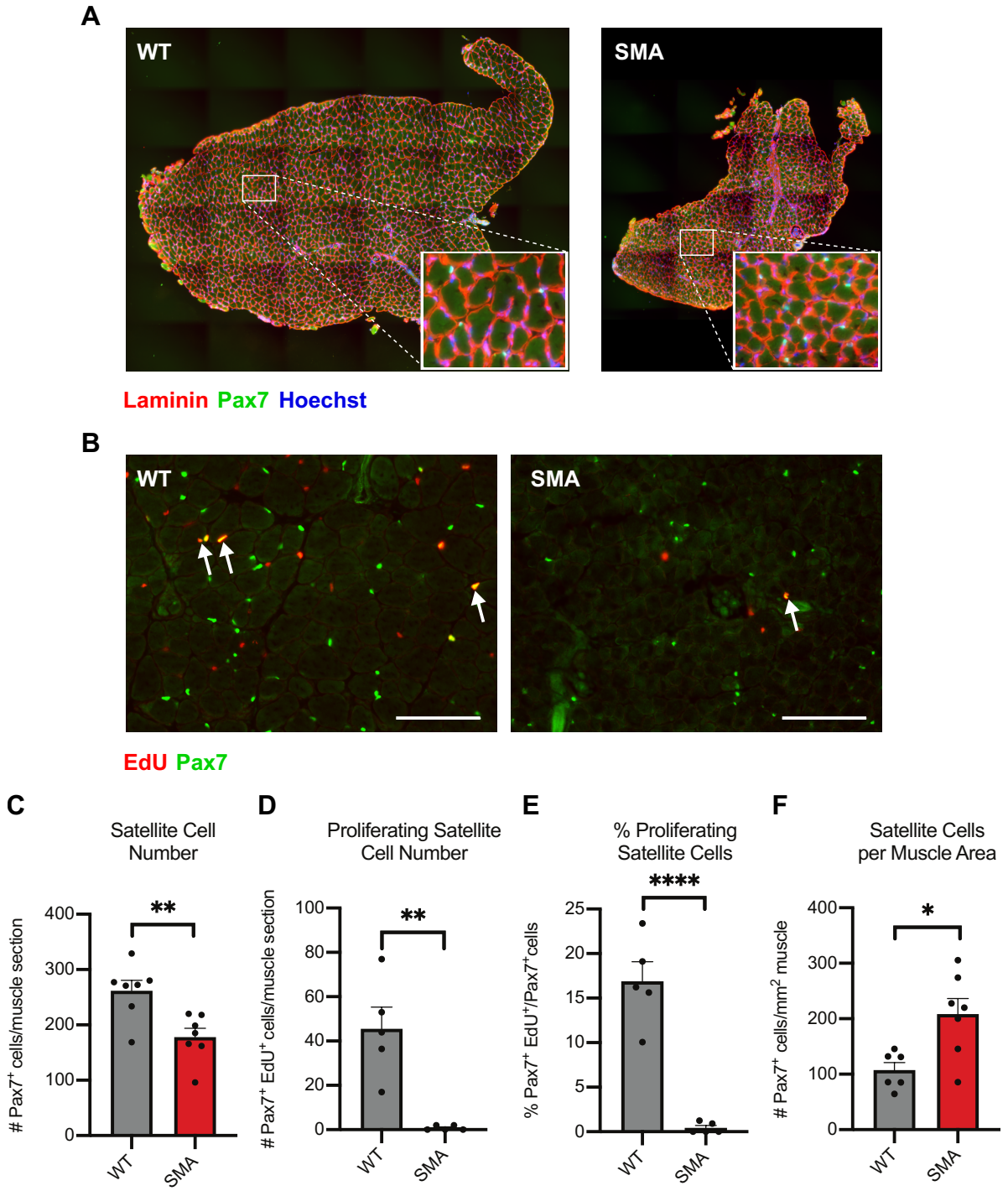

Figure 2.1. Satellite cell proliferation is reduced in end-stage SMNΔ7 mice. A) Whole TA muscle cross sections and larger magnification inserts from wild type (WT) and SMNΔ7 mutant (SMA) mice at P14. Satellite cells are immunolabeled with anti-Pax7 (green) and the basal lamina surrounding muscle fibers with anti-laminin (red). B) Muscle cross sections showing proliferating satellite cells labeled with anti-Pax7 (green) and EdU (red). Scale bars=100μM. Arrows show examples of Pax7/EdU co-localization. C) Number of $Pax7^+$ satellite cells per TA muscle cross section. N=7 per group, p=0.0054, unpaired t test. D) Number of proliferating $Pax7^+$ EdU^+ satellite cells per TA muscle

Figure 2.1 (continued) cross section. N=5 per group, p= 0.0019, unpaired t test. E) Percent of $Pax7^+$ satellite cells that are proliferating. N=5 per group, p= <0.0001, unpaired t test. F) Total number of $Pax7^+$ satellite cells per mm^2 TA muscle. N=6-7 per group, p=0.0108, unpaired t test. Data presented as mean ± SEM.

rapidly incorporates into the DNA of dividing cells. After a 4-hour chase period, we isolated the hindlimb tibialis anterior (TA) muscle and immunolabeled satellite cells in muscle cryosections with antibodies against Pax7 and a Click-iT Plus EdU Imaging Kit (Figure 2.1A-B). We specifically selected the TA muscle because unlike more severely atrophic muscles, it never loses neuromuscular innervation. This partially mitigates the contribution of motor neuron death to any observed satellite cell defects[55].

Interestingly, we observed a 32% reduction in the total number of $Pax7^+$ satellite cells in SMA muscle, as well as a 97% reduction in the percentage and 98% reduction in the total number of actively proliferating EdU^+Pax7^+ satellite cells (Figure 2.1C-E). When normalized to the overall muscle cross sectional area, which is substantially smaller in end-stage SMA mice, there was a 94% increase in the density of satellite cells in SMA muscle (Figure 2.1F). These findings suggest that SMN-deficient satellite cells not only fail to proliferate, but also fail to fuse with growing muscle fibers. This is consistent with previous reports showing reduced fusion of SMN-deficient myoblasts *in vitro*[57].

Similar but less dramatic impairments in satellite cell proliferation were also evident in early symptomatic (postnatal day 7) SMA mice (Figure 2.2A). Specifically, we observed a 20% reduction in total satellite cell number and a 35% reduction in proliferating satellite cell number (Figure 2.2B-C). In addition, consistent with the end-stage data, we observed trends towards reduced percentage of proliferating satellite cells and increased number of satellite cells normalized to muscle area (Figure 2.2D-E). Based on previous reports that SMA muscle size begins to diverge from wild type littermates during the early symptomatic stage, our findings suggest that the onset of satellite cell proliferation defects coincide with the onset of impaired muscle growth in SMA mice[54].

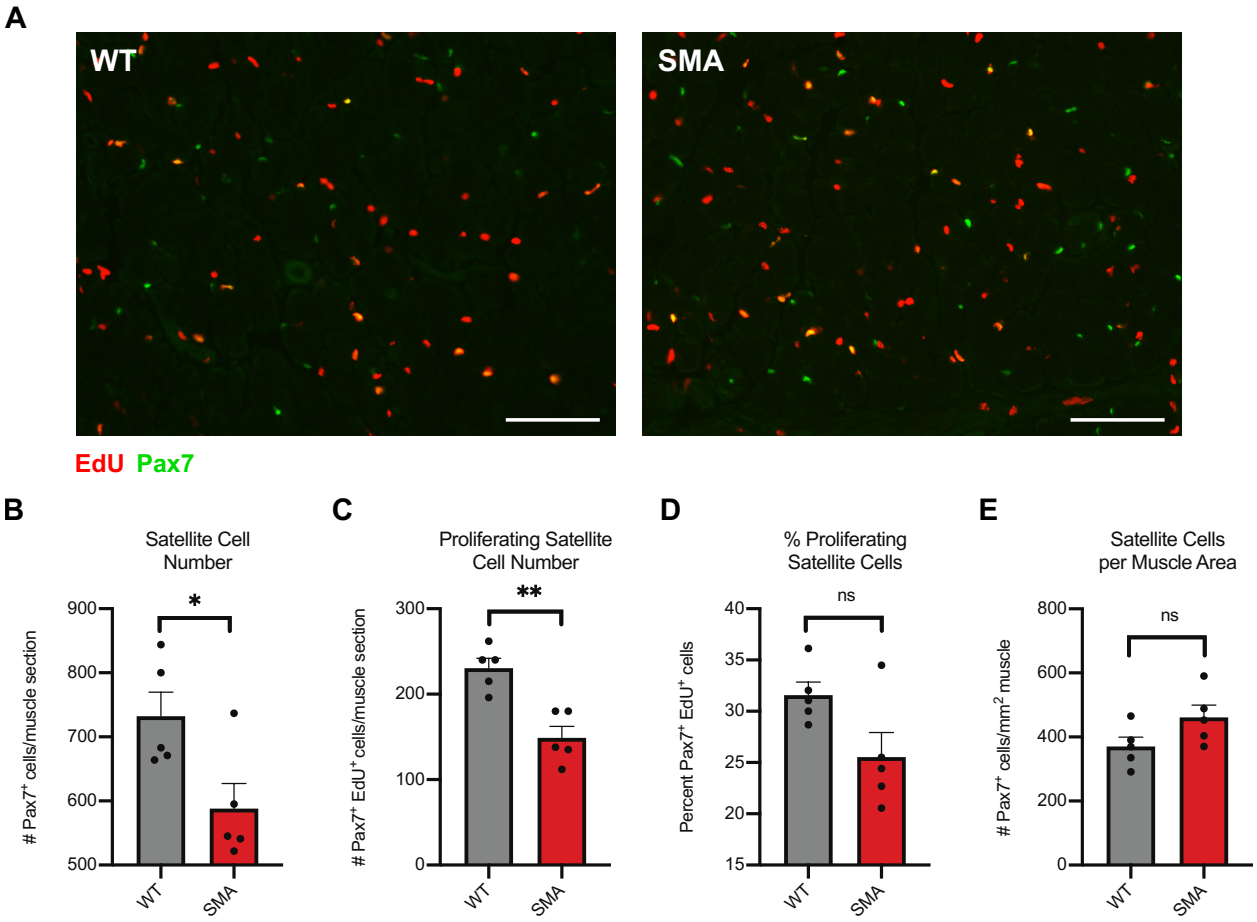

Figure 2.2. Satellite cell proliferation is reduced in early symptomatic SMNΔ7 mice. A) TA muscle cross sections from WT and SMA mice at P7 showing proliferating satellite cells labeled with anti-Pax7 (green) and EdU (red). Scale bars=100μM. B) Number of Pax7+ satellite cells per TA muscle cross section. N=5 per group, p=0.0284, unpaired t test. C) Number of proliferating $Pax7^+$ EdU^+ satellite cells per TA muscle cross section. N=5 per group, p=0.0017, unpaired t test. D) Percent of $Pax7^+$ satellite cells that are proliferating. N=5 per group, p>0.05, unpaired t test. E) Total number of $Pax7^+$ satellite cells per mm^2 TA muscle. N=5 per group, p>0.05, unpaired t test. Data presented as mean ± SEM.

Next, we investigated whether the observed satellite cell proliferation deficits were associated with a failure of muscle fibers to grow by myonuclear accretion, which is the fundamental terminal muscle differentiation step leading to muscle growth during the postnatal period (Figure 1.6). In support of our hypothesis, we observed a decrease in the number of nuclei incorporated within single myofibers isolated from SMA versus WT muscles at the disease end stage (Figure 2.3A-B). Overall,

these results suggest that SMN deficiency impairs satellite cell proliferation, thus impeding skeletal muscle growth during postnatal myogenesis.

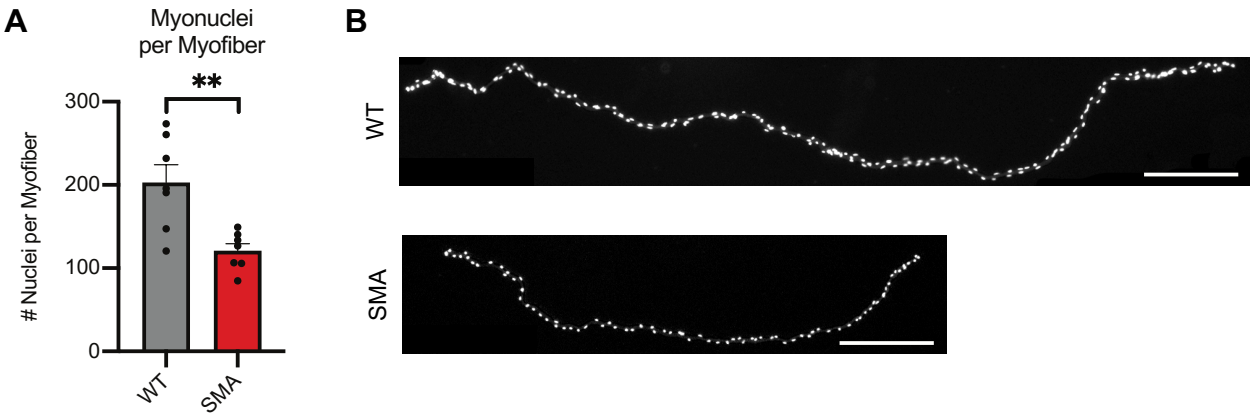

Figure 2.3. Reduced myonuclear accretion in end-stage SMNΔ7 mice. A) Number of nuclei incorporated within single extensor digitorum longus (EDL) myofibers isolated from WT and SMA mice. N=7 per group, p=0.0039, unpaired t test. Data presented as mean ± SEM. B) Representative images of single EDL myofibers from WT and SMA mice. Myonuclei are labeled with Hoechst. Scale bars=200μM.

Satellite cell-autonomous SMN deficiency impairs muscle growth during regeneration

Our observation of impaired satellite cell proliferation in SMA mice highlights the importance of skeletal muscle as a therapeutic target in SMA. However, it remained unclear if skeletal muscle-intrinsic defects were driving the satellite cell impairments. In the SMNΔ7 model, where SMN is ubiquitously reduced, satellite cell defects could arguably be neurogenic in origin, resulting from muscle atrophy induced by motor neuron deficits. To directly determine if SMN deficiency contributes to muscle growth failures in a satellite cell-autonomous fashion, we used a tamoxifen-inducible Cre/loxP approach to generate two separate satellite cell-conditional SMN *knockout* and *knockdown* mouse models. We reasoned that the complete SMN knockout model would allow us to assess the necessity of SMN for satellite cell function, while the SMN knockdown model would more

appropriately recapitulate the role of SMN-deficient satellite cells in SMA pathology (since patients always retain low levels of SMN).

To knockout SMN in satellite cells, we generated the *Pax7:SMN*-KO mouse model by breeding the commercially available strains Pax7-CreER^{T2} and Smn^{F7} (Figure 2.4A and Supplementary Figure 2.1). The Pax7-CreER^{T2} transgene consists of an IRES-CreER^{T2} inserted after the endogenous Pax7 stop codon, driving Cre-ER^{T2} expression in satellite cells while preserving Pax7 function[94]. Pax7-CreER^{T2} mice have been validated extensively in the literature for their use in achieving highly specific satellite cell-conditional genetic modifications[95,96]. When crossed with Smn^{F7} mice, which possess endogenous mouse *Smn* exon 7 flanked by loxP sites, Cre-mediated recombination can be induced with tamoxifen to excise *Smnex7* and produce truncated *SMN* transcripts, similar to *SMN2* in humans

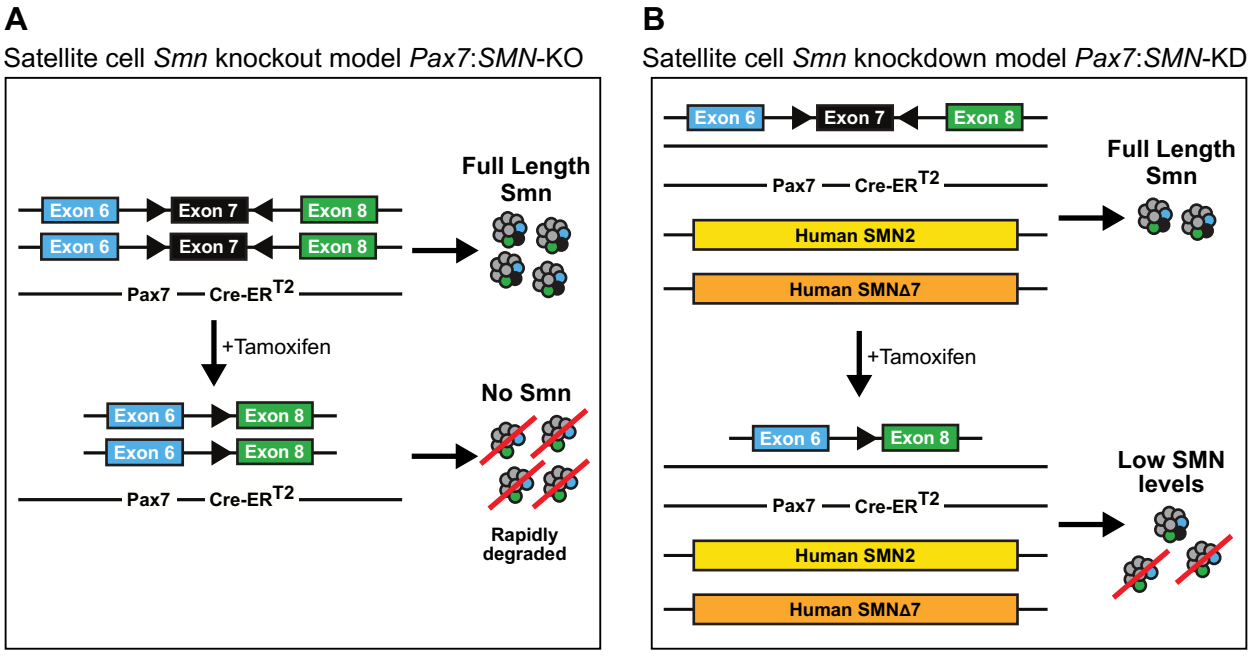

Figure 2.4. Genetics of satellite cell-conditional, tamoxifen-inducible SMN knockout and SMN knockdown mouse models. A) *Pax7:SMN*-KO mice possess Pax7-CreER^{T2} and homozygous SMN$^{F7/F7}$ alleles, which cause complete loss of full length SMN in satellite cells due to Cre-mediated excision of *mSmn* exon 7. B) *Pax7:SMN*-KD mice carry SMN$^{F7/-}$, where a single allele of *mSmn* is knocked out and the other is floxed. They additionally possess Pax7-CreER^{T2}, hSMN2 and hSMNΔ7 transgenes, which provide low levels of SMN to compensate for the complete knockout.

(Figure 2.4A)[97]. This approach allowed us to knockout *Smn* in adult satellite cells, when Pax7 expression is restricted to satellite cells in skeletal muscle, instead of inducing non-cell autonomous phenotypes due to widespread Pax7 expression during development. In addition, we crossed these mice with a Rosa26-floxed stop tdTomato line to allow lineage tracing of satellite cells after tamoxifen administration[98].

To knockdown SMN in satellite cells, we generated the *Pax7:SMN*-KD mouse model by breeding *Pax7:SMN*-KO mice with SMNΔ7 mice, which carry a null mouse Smn mutation and *hSMN2* and *hSMNΔ7* transgenes. In offspring that inherit the floxed-*Smn* on one allele and the null *mSmn* mutation on the other allele ($SMN^{F7/-}$), we can achieve tamoxifen-induced depletion of *mSmn* in satellite cells with retention of low levels of *hSMN* in the background (Figure 2.4B). Overall, this results in low levels of SMN expression in satellite cells, as opposed to complete depletion. This strategy has been used extensively in the SMA literature to reduce SMN levels in other cell types, including motor neurons, neuronal progenitors, and post-mitotic skeletal muscle[35,59,60,99].

To validate these mouse models, we first ensured that Cre-mediated SMN depletion was confined to satellite cells and downstream myogenic progenitors and muscle fibers. Briefly, we treated *Pax7:SMN*-KD mice with tamoxifen *in vivo* for one week, then allowed a one-month chase period, which is the standard time frame used in forthcoming experiments. Using primers designed to amplify the 460 bp recombined exon 7 product, we confirmed via PCR that Cre-mediated deletion of exon 7 only occurred at very low levels in skeletal muscle and not at all in other organs. We only observed a very faint band in skeletal muscle that was completely absent in cardiac muscle, spinal cord, brain or liver tissues (Figure 2.5A). As a control for the DNA extraction, we demonstrated that the 635 bp band corresponding to the floxed SMN allele was present in all organs tested (Figure 2.5A).

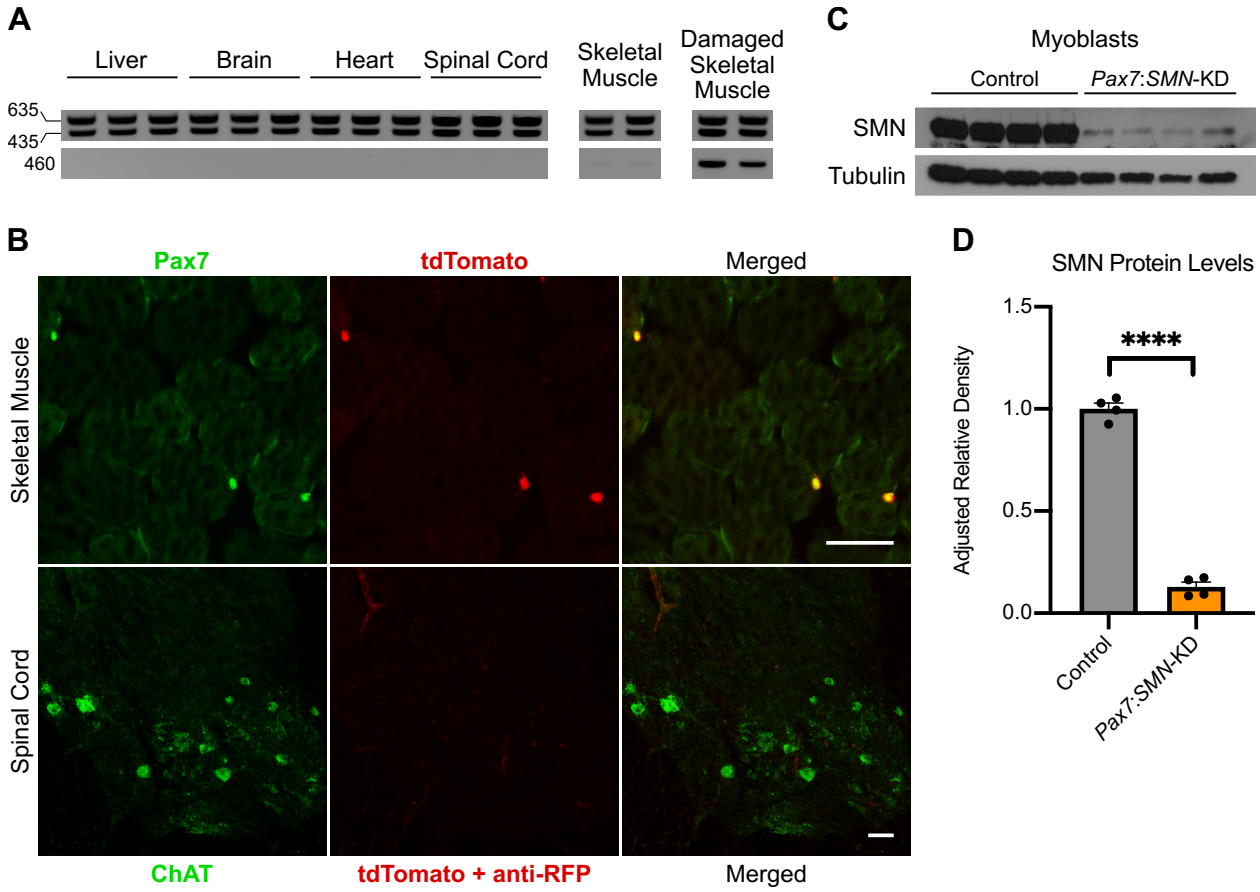

Figure 2.5. Validating Cre-mediated recombination and SMN protein knockdown in *Pax7:SMN*-KD mice. A) PCR analysis confirming Cre-specificity in *Pax7:SMN*-KD mice homozygous for the floxed SMN allele ($SMN^{F7/F7}$). *GS8/Ex7sou1* primers were used to detect the presence of the SMN^{F7} band (635 bp) and *GS8/PHR5* primers were used to amplify the recombined exon 7 product (460 bp). Detection of Cre-mediated exon 7 deletion is only slightly detectable in skeletal muscle and significantly detectable in damaged skeletal muscle that has been reconstituted with satellite cells. B) Representative skeletal muscle and spinal cord images from *Pax7:SMN*-KD mice. Cre activity only induces recombination and subsequent tdTomato (red) expression in $Pax7^{+}$ (green) satellite cells, and not in muscle fibers or $ChAT^{+}$ (green) motor neurons. Anti-RFP (red) immunostaining was also used to confirm the absence of tdTomato in motor neurons. Scale bars=50μM. C-D) Western blot and quantification of SMN protein levels in *Pax7:SMN*-KD control and mutant myoblasts treated with 4-OHT to induce recombination. N=4 per group, p<.0001, unpaired t test. Data presented as mean ± SEM..

Since it is technically infeasible to separate skeletal muscle fibers from satellite cells, which are closely associated with the fibers and scattered throughout the muscle tissue, we expected to observe low levels of exon 7 excision in bulk skeletal muscle. To ensure that Cre expression is restricted to the

satellite cell within skeletal muscle, we analyzed tdTomato expression in muscle cross-sections obtained from tamoxifen-treated *Pax7:SMN*-KD mice. As expected, we observed robust tdTomato labeling co-localized with Pax7 expression (Figure 2.5B). We did observe occasional tdTomato-positive fibers in skeletal muscle, suggesting low levels of Cre-mediated *SMNex7* deletion. However, this is expected given the normal turnover of satellite cells occurring over a 5-week period[100]. Importantly, to be certain that recombination did not occur in motor neurons, we confirmed the complete absence of tdTomato expression in *Pax7:SMN*-KD spinal cords (Figure 2.5B). We assessed both endogenous tdTomato and anti-RFP labeling (which recognizes tdTomato), and we did not see co-localization in either case with ChAT+ motor neurons (Figure 2.5B).

Having confirmed that Cre-mediated deletion is largely restricted to satellite cells within skeletal muscle, and is completely absent from non-muscle tissue, we next validated that SMN was substantially depleted in $Pax7^+$ cells. We derived primary myoblast lines from FACS-purified satellite cells isolated from *Pax7:SMN*-KD mice and Cre-only littermate controls. We used a FACS method outlined in the Methods section that was developed by our collaborator, Dr. Amy Wagers. Using western blotting, we confirmed that SMN was knocked down by approximately 90% in *Pax7:SMN*-KD myoblasts treated with 4-hydroxytamoxifen (4-OHT), a potent tamoxifen metabolite commonly used to replace standard tamoxifen in cell culture experiments (Figure 2.5C-D). These very low SMN levels are similar to those observed in severe SMA patients.

After validating our new model, we addressed the hypothesis that the loss of SMN impairs satellite cell function in a cell-autonomous manner. We first focused on *Pax7:SMN*-KO mice, since any satellite cell defects would be more readily apparent in this model. To assess satellite cell function, we used an *in vivo* cardiotoxin muscle regeneration assay. Cardiotoxin is a snake venom that causes muscle necrosis and immune infiltration, resulting in satellite cell activation, proliferation and myofiber repair over several weeks[101]. Although such severe muscle damage does not occur in SMA patients, it

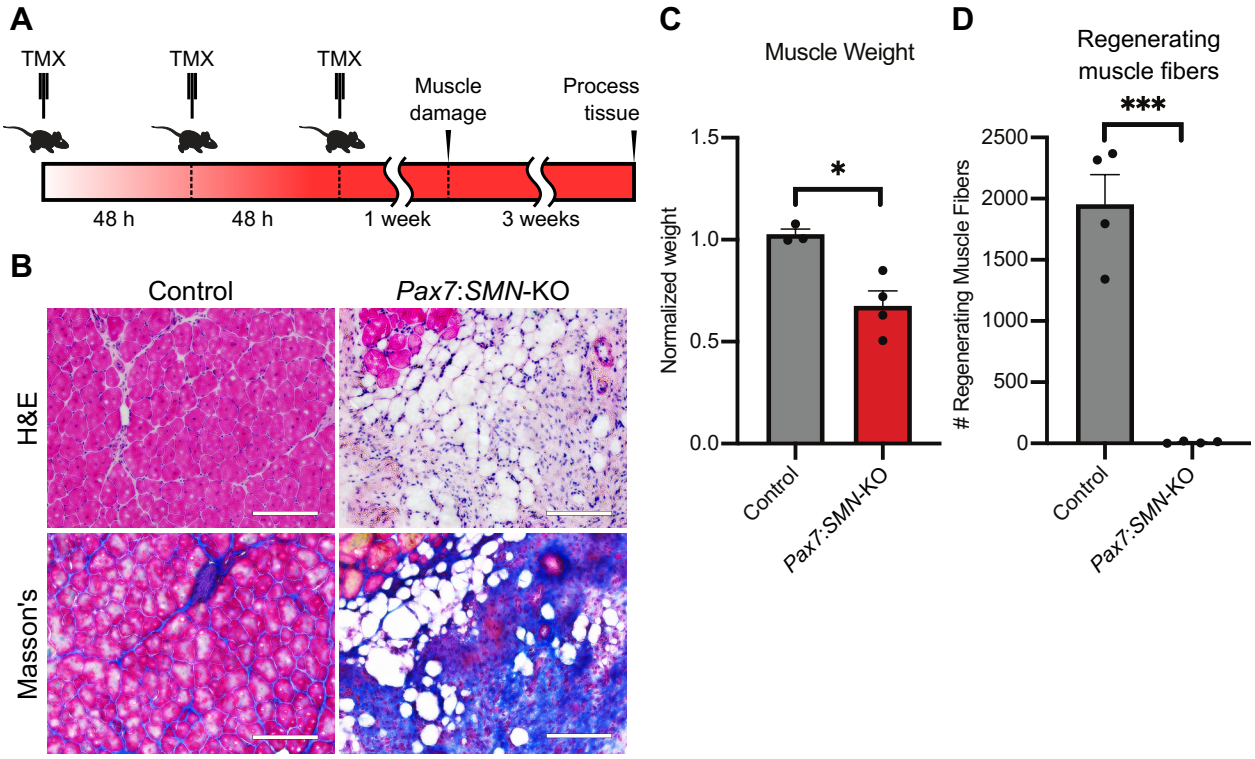

Figure 2.6. SMN knockout in satellite cells prevents muscle regeneration *in vivo*. A) Experiment schematic for assessing muscle regeneration in *Pax7:SMN*-KO mice three weeks post-damage. B) Representative muscle histology images of *PAX7:SMN*-KO control and mutant mice. H&E shows the overall tissue architecture (muscle fibers are pink, nuclei are blue). Masson's stain shows collagenase infiltration (muscle fibers are pink, collagen is blue). Scale bars=100μM. C) Damaged TA muscle weight normalized to contralateral undamaged muscle. N=3-4 per group, p=0.0107, unpaired t test. D) Number of regenerating muscle fibers in the TA muscle. N=4 per group, p=0.0002, unpaired t test. Data presented as mean ± SEM.

provides an excellent surrogate assay for satellite cell function and muscle growth, since satellite cell activity is crucial for muscle regeneration. In accordance with previously published protocols, we treated adult *Pax7:SMN*-KO mutant and Cre-only control mice systemically with tamoxifen, allowed a one-week chase period for SMN to become depleted, and induced muscle damage by intramuscular cardiotoxin injection in the hindlimb TA muscle (Figure 2.6A). We then waited three weeks for muscles to regenerate, which is typically sufficient for nearly full recovery of muscle size and strength in wild type mice[101]. To evaluate muscle regeneration, we analyzed histology sections and quantified the number of centrally-nucleated muscle fibers, which is a standard indicator of skeletal muscle that

has undergone regeneration via satellite cell fusion[102]. For both control and mutant mice, small, discrete regions of the tissue were sometimes undamaged due to incomplete cardiotoxin perfusion throughout the muscle. This is a typical issue with this technique, and such areas, which are apparent from a lack of centrally-nucleated muscle fibers, were excluded from all analyses throughout this study.

Strikingly, we found that damaged skeletal muscle completely failed to regenerate in *Pax7:SMN*-KO mutant mice compared to Cre-only control mice. Mutant mice experienced a 35% reduction in muscle weight and a near complete absence of centrally-nucleated, regenerating muscle fibers, with the damaged area instead occupied by extensive fibrosis (Figure 2.6B-D). These results demonstrate that SMN is critical for satellite cell-mediated muscle regeneration, and the near complete absence of regenerated fibers suggests that satellite cells may have not only failed to proliferate, but also died under conditions of SMN depletion.

To further elucidate how the loss of SMN in satellite cells causes a muscle growth deficit, we analyzed myoblast activity *in vitro*. Briefly, we dissociated and FACS-purified satellite cells from *Pax7:SMN*-KO mutant and Cre-only control mice in the absence of tamoxifen, passaged the cells to generate primary myoblast lines, treated the cultures with 4-OHT *in vitro* to knockout SMN, then analyzed cell growth starting from equal seeding densities (Figure 2.7A). As predicted, we observed a cell death phenotype, where the total number of myoblasts decreased over time, resulting in an 83% decrease in myoblast number after one week (Figure 2.7B-C).

Furthermore, we also observed a proliferation deficit, where surviving myoblasts failed to incorporate EdU (Figure 2.7D-E). Since these *in vitro* experiments were only performed in biological duplicate (with 8 technical replicates per condition), we will need to confirm that these results are reproducible. However, thus far we have observed a dramatic effect size and small variability and the *in vitro* results are consistent with our *in vivo* observations. Overall, our findings suggest that SMN depletion in satellite cells prevents sufficient production of myogenic precursors to support skeletal

muscle growth during regeneration, and are consistent with previous reports that SMN depletion causes death across numerous cell types[29,59].

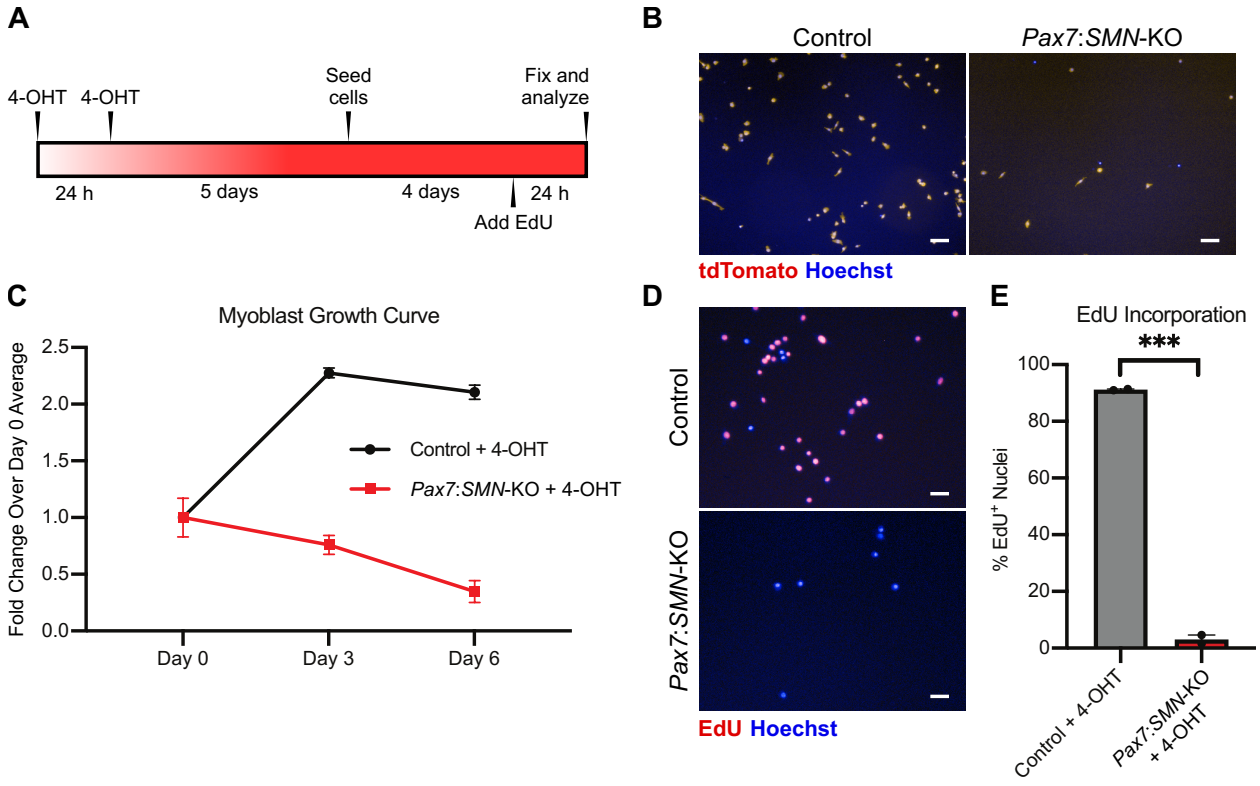

Figure 2.7. SMN knockout in myoblasts causes cell death and loss of proliferation. A) Experiment schematic for assessing proliferation of *Pax7:SMN*-KO myoblasts. B) Representative images of tdTomato^{+} (red) *Pax7:SMN*-KO control and mutant myoblasts after 4-OHT treatment *in vitro*. C) Myoblast growth curve. N=2 biological replicates. Error bar represents SD. D) Representative images showing EdU incorporation (pink) in *Pax7:SMN*-KO control and mutant myoblasts *in vitro*. E) Percent of nuclei with EdU incorporated. N=2 per group, p=0.0003, unpaired t test. Data presented as mean ± SEM. All scale bars=100μM.

The SMN knockout results were striking and demonstrate that SMN is required for normal satellite cell function. However, it may be difficult to translate these results to patients, who suffer from low SMN levels as opposed to complete SMN depletion. Therefore, to examine the effect of SMN *reduction* on satellite cell function, we performed a muscle regeneration assay as described above using *Pax7:SMN*-KD mice (Figure 2.8A). We found that SMN reduction in *Pax7:SMN*-KD satellite

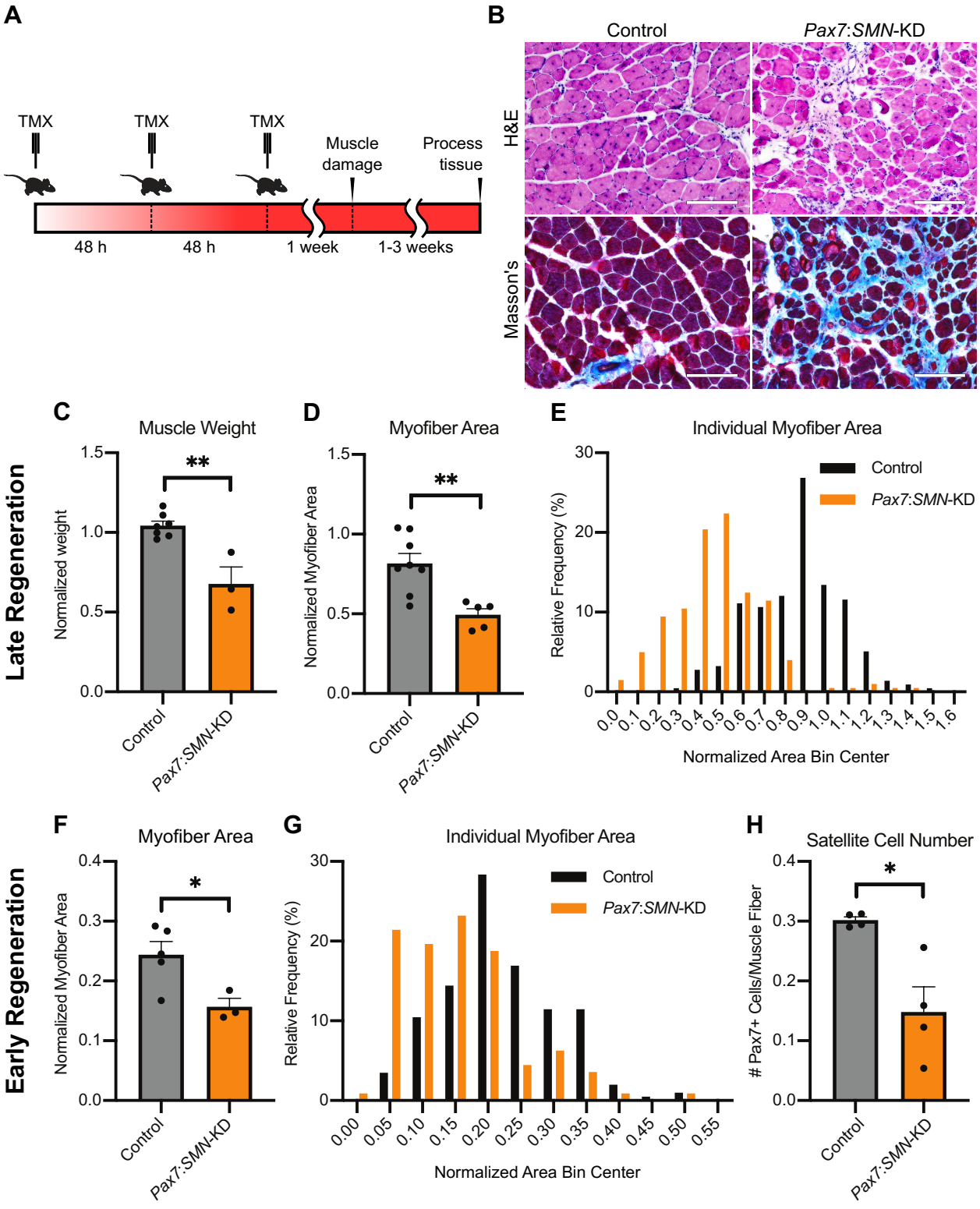

Figure 2.8. SMN knockdown in satellite cells impairs muscle regeneration and reduces satellite cell production *in vivo*. A) Experiment schematic for assessing muscle regeneration in adult *Pax7:SMN*-KD mice three weeks post-damage. B) Representative muscle histology images showing H&E and Masson's trichrome stain in *PAX7:SMN*-KD control and mutant mice. Scale bars=100μM.

Figure 2.8 (continued) C) Damaged TA muscle weight normalized to contralateral undamaged muscle in *PAX7:SMN*-KD control and mutant mice 3 weeks post-damage (late regeneration). N=3-7 per group, p=0.0015, unpaired t test. D) Average normalized individual myofiber areas corresponding to Graph C. N=5-8 per group, p=0.0034, unpaired t test. E) Histogram of normalized individual myofiber area corresponding to Graph C. F) Average individual myofiber areas of damaged muscle normalized to contralateral undamaged muscle in *PAX7:SMN*-KD control and mutant mice 1-week post damage (early regeneration). N=3-5 per group, p=0.0322, unpaired t test. G) Histogram of normalized individual myofiber area corresponding to Graph F. H) Number of $Pax7^+$ satellite cells per muscle fiber in *PAX7:SMN*-KD control and mutant muscle 1-week post damage. N=4 per group, p=0.0110, unpaired t test. Data presented as mean ± SEM.

cells resulted in a 35% reduction in muscle weight and 39% reduction in the size of regenerating muscle fibers compared to Cre-only controls (Figure 2.8B-E). In addition, we identified robust levels of Cre-mediated exon 7 deletion, since the skeletal muscle had been partially reconstituted by satellite cells (Figure 2.5A).

These results suggest that normal SMN levels are required for satellite cell-mediated muscle regeneration. However, it was unclear if the phenotype resulted from the loss of SMN in satellite cells versus the loss of SMN in the regenerating muscle fiber itself (i.e. the muscle failing to regenerate due to reduced satellite cell activity versus regenerating and then degenerating over time due to the loss of SMN in the muscle fiber). To differentiate between these two possibilities, we examined muscle histology one week after cardiotoxin damage. At this early regeneration phase, satellite cells are most proliferative and fibers have completed necrosis[101]. We found that even at this early time point, muscle fibers in *Pax7:SMN*-KD mutant mice were 36% smaller compared to control muscle fibers and had a 51% decrease in the number of satellite cells per muscle fiber (Figure 2.8F-G). These results suggest that in the case of SMN deficiency, at SMN levels similar to those in SMA patients, satellite cells are dysfunctional in proliferation and unable to efficiently contribute to skeletal muscle growth.

To further explore how SMN deficiency impairs muscle growth, we analyzed primary myoblast lines derived from *Pax7:SMN*-KD and Cre-only control mice (Figure 2.9A). Similar to SMN

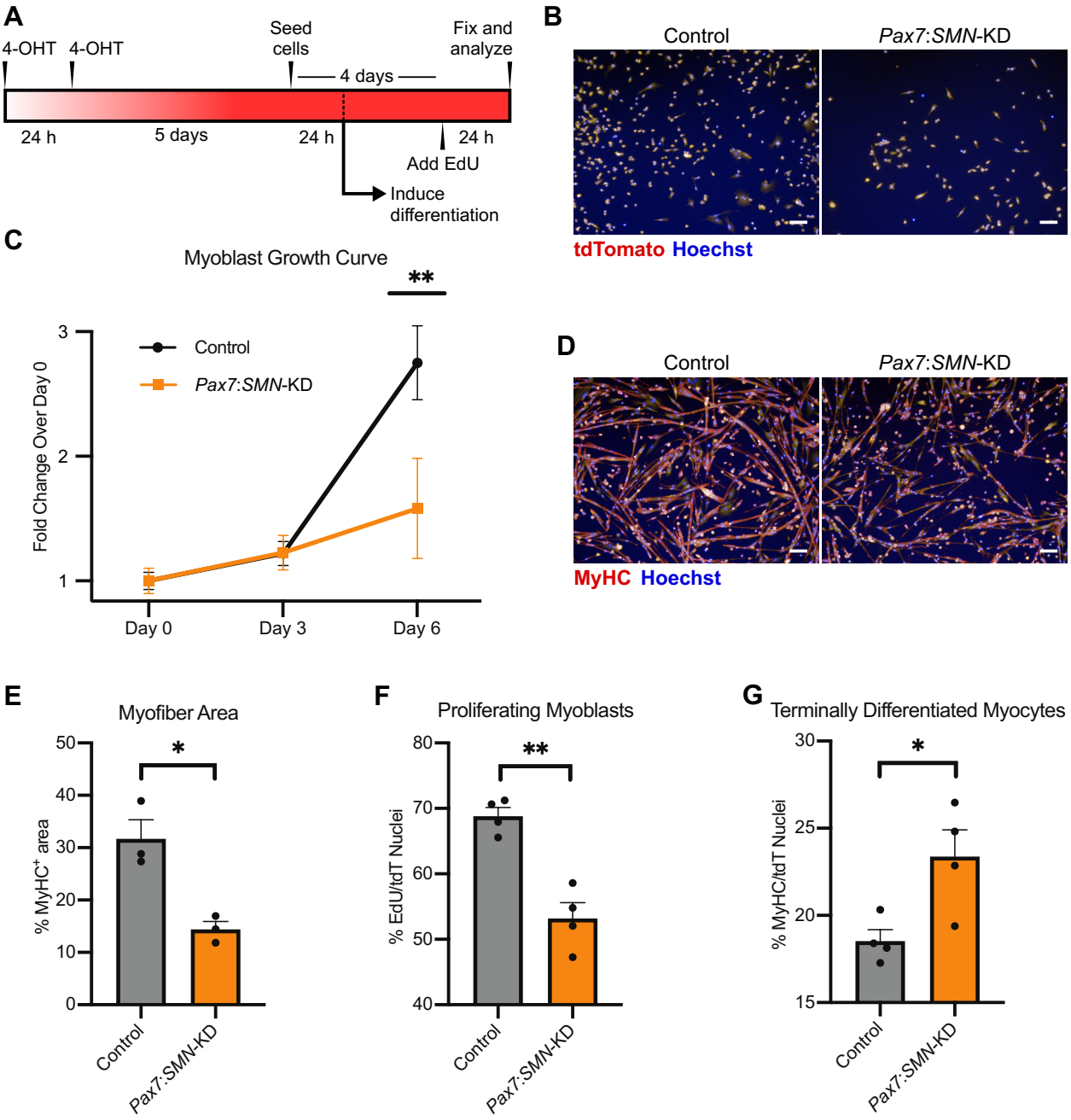

Figure 2.9. SMN knockdown impairs proliferation and myofiber formation *in vitro*. A) Experiment schematic for assessing proliferation and differentiation of *Pax7:SMN*-KD myoblasts. B) Representative images of tdTomato$^+$ (red) proliferating *Pax7:SMN*-KD control and mutant myoblasts after 4-OHT treatment *in vitro*. C) Myoblast growth curve. N=3 per group, p=0.0034, post-hoc unpaired t test at final time point. Error bar represents SD. D) Representative images showing *Pax7:SMN*-KD control and mutant MyHC$^+$ (red) myofibers 5 days after inducing terminal differentiation. E) Percent of culture positive for MyHC myofibers after terminal differentiation. N=3 per group, p=.0116, unpaired t test. F) Percent of tdTomato$^+$ myogenic nuclei with EdU incorporated. N=4 per group, p=0.0012, unpaired t test. G) Percent of tdTomato$^+$ myogenic nuclei expressing MyHC. N=4 per group, p=0.0262, unpaired t test. Data presented as mean ± SEM. All scale bars=100μM.

knockout conditions, we observed deficits in myoblast growth *in vitro*. Under serum-rich growth promoting conditions, *Pax7:SMN*-KD myoblasts displayed a 43% reduction in growth compared to control myoblasts (Figure 2.9B-C). Furthermore, when cultured in high-density, serum-starved conditions, which induce terminal muscle differentiation and fusion, *Pax7:SMN*-KD myoblasts displayed deficits in myofiber formation. This was apparent by a 55% reduction in the area of the culture covered by myofibers expressing the muscle structural protein MyHC (Figure 2.9D-E). These results suggest that SMN-deficient myoblasts not only fail to grow, but also fail to efficiently form muscle fibers.

Next, we wanted to better understand why SMN-deficient myoblasts fail to grow. We previously demonstrated that SMN deficiency causes satellite cells to prematurely differentiate in severe SMA mice[90]. Since terminally differentiated myocytes are not proliferative, we hypothesized that a shift towards a more differentiated myogenic state could explain reductions in proliferation. To address this, we cultured *Pax7:SMN*-KD myoblasts in EdU for 24 hours and immunolabeled terminally differentiated myocytes with anti-myogenin. Consistent with our hypothesis, we observed a 23% reduction in EdU incorporation concurrent with a 26% increase in myogenin^{+} myocytes, even under serum-rich growth promoting conditions that normally maintain healthy myoblasts in a non-differentiated state (Figure 2.9F-G). Altogether, these *in vivo* and *in vitro* results demonstrate that reducing SMN to levels physiologically relevant to patients results in decreased muscle growth due to impaired satellite cell and myoblast function. However, it is important to note that the satellite cell phenotypes in *Pax7:SMN*-KD (knockdown) mice were far less severe than what we observed in *Pax7:SMN*-KO (knockout) mice. This means that SMN-deficient satellite cells are indeed capable of undergoing proliferation, albeit at a rate insufficient to sustain healthy muscle growth.

We additionally examined whether or not the impaired size of regenerating muscle due to SMN-deficiency in satellite cells causes a functional deficit in muscle force production. Briefly, we

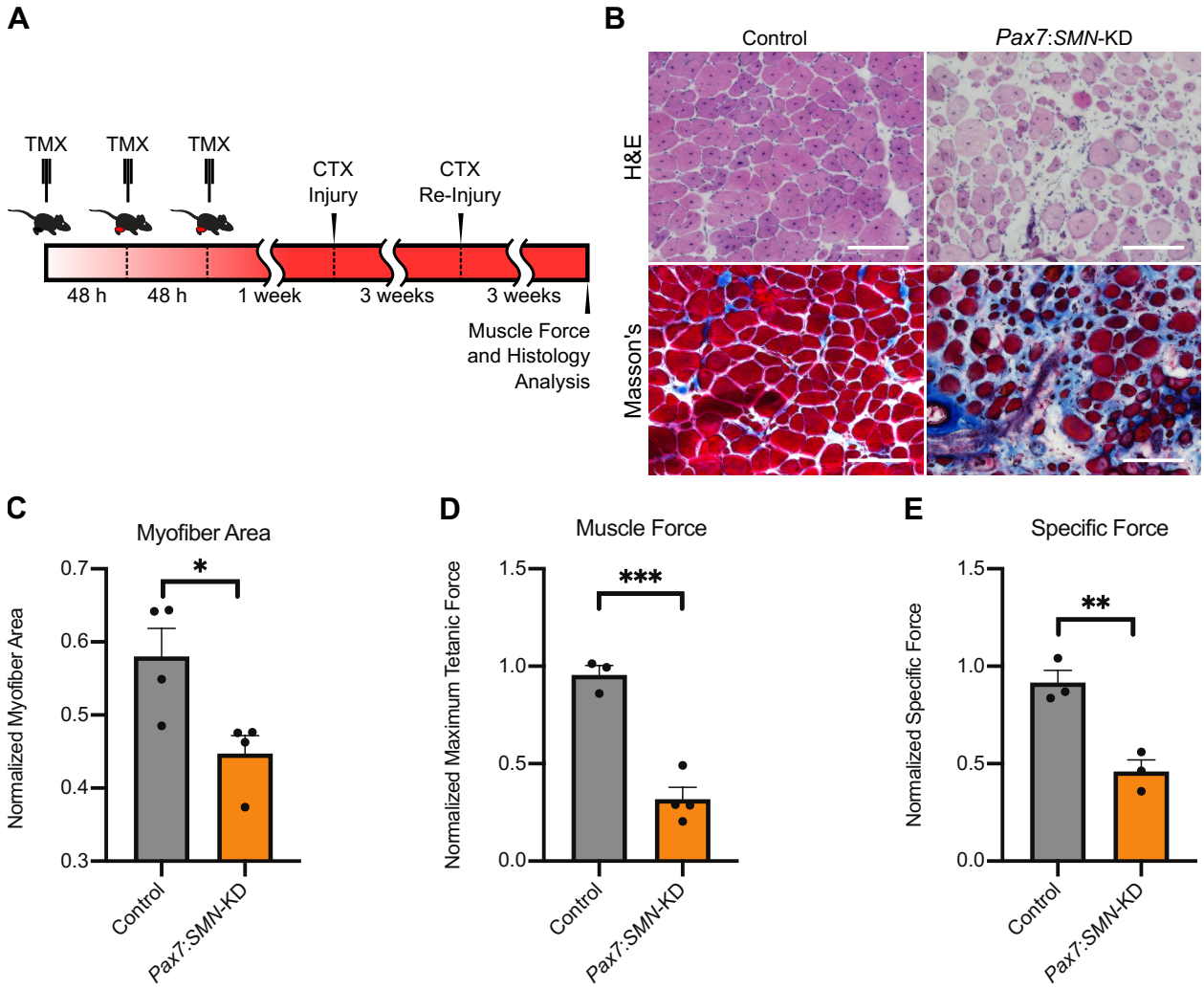

Figure 2.10. SMN knockdown impairs muscle force production after regeneration. A) Experimental schematic of muscle force experiment. Tamoxifen-treated *Pax7:SMN*-KD mice were damaged twice with cardiotoxin followed by a three week regeneration period. In situ muscle force measurements were performed as described in the Materials and Methods section. B) Representative images of TA muscles 3-weeks post second damage. Scale bars=100μM. C) Individual myofiber cross-sectional area normalized as in Graph C. N=4 per group, p=0.0286, Mann-Whitney test. D) Maximum tetanic force generated with 150Hz direct stimulation by regenerating *Pax7:SMN*-KD control and mutant TA muscles. Force produced by the damaged leg was normalized to the force produced from the contralateral undamaged leg to account for natural variability in size between mice. N=3-4 per group, p=0.0006, unpaired t test. E) Specific force generated by *Pax7:SMN*-KD control and mutant muscle normalized as in Graph C. N=3 per group, p=0.0062, unpaired t test. Data presented as mean ± SEM.

repeated the muscle regeneration protocol, but we performed two rounds of cardiotoxin injections to ensure that the whole TA muscle was thoroughly damaged (Figure 2.10A). This accounted for any variability in the extent of cardiotoxin damage, which would have impacted the overall muscle force

generated by the entire muscle. We then performed *in situ* muscle force measurements of the TA muscle with direct stimulation (150 Hz) at the neuromuscular junction band.

We observed a 67% deficit in maximum muscle force accompanied by a 23% reduction in muscle fiber area in *Pax7:SMN*-KD versus control muscle (Figure 2.10B-D). To determine if the muscle force impairment was attributed to the smaller muscle size, we calculated the specific force by normalizing maximum muscle force to muscle cross-sectional area. Here, we observed that mutant mice displayed a 50% reduction in specific force, meaning that SMN-deficient muscles are intrinsically weaker (Figure 2.10E). Overall, the loss of SMN in satellite cells not only impairs proliferation and muscle growth, but also leads to a profound functional deficit in muscle strength that is consistent with the motor weakness observed in both SMA patients and animal models.

Cell cycle pathways are downregulated in SMN-deficient myoblasts

Finally, to better understand transcriptional profile changes associated with SMN deficiency in myogenic cells, we performed RNA-sequencing of *Pax7:SMN*-KD myoblasts. RNA was extracted from *Pax7:SMN*-KD mutant and Cre-only control myoblasts following 4-OHT treatment *in vitro*. RNA sequencing libraries were constructed by a 3'-digital gene expression (DGE) single cell protocol adapted for bulk samples (Figure 2.11A; quality assessment in Supplementary Figures 2.2-2.3). Notably, the 3'-DGE protocol incorporates unique molecular identifiers (UMIs) to improve gene expression quantitation, but it is optimized to analyze several multiplexed libraries simultaneously at the cost of reduced sequencing depth. Differential expression analysis identified 71 genes with significantly altered expression levels (with a false discovery rate of 0.1), of which 22 were upregulated and 49 were downregulated in SMN-knockdown conditions (Figure 2.11B and full list in Supplementary Table 2.1). Interestingly, we identified downregulation of multiple genes related to cell proliferation, including

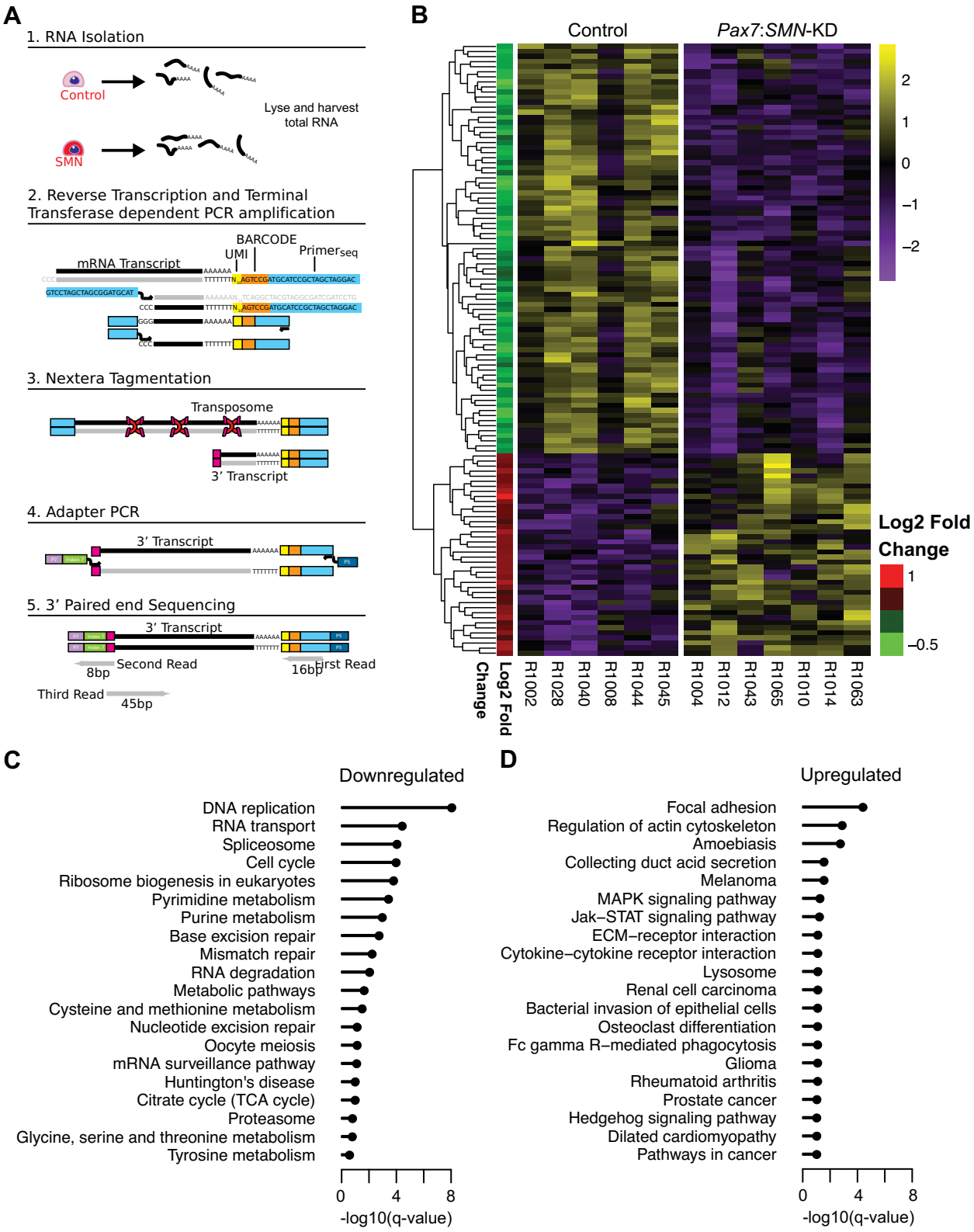

Figure 2.11. RNA sequencing reveals downregulation of cell cycle pathways after SMN knockdown in myoblasts *in vitro*. A) 3'-DGE RNA sequencing method, including RNA isolation, library construction and multiplex barcoding strategy. B) Heat map of top 50 differentially expressed

Figure 2.11 (continued) genes in *Pax7:SMN*-KD control and mutant myoblasts by q-value. Yellow to purple gradient represents normalized expression values. Red to green gradient represents log2 fold change per group. X-axis represents individual replicates. N=6-7 per group. See Table 6.2 for sample IDs. C-D) Top 20 significantly (FDR=10%) downregulated and upregulated KEGG pathways.

Cdk1, *Fen1*, *Cdca3*, *Prc1* and *Pcna*. In addition, 4 out of the 5 top-scoring hits in a gene set enrichment analysis of KEGG pathways included downregulation of pathways related to cell cycle (DNA replication and cell cycle) or SMN deficiency (RNA transport and spliceosome) (Figure 2.11C-D). GO term analysis revealed a similar trend, highlighting pathways such as cell division and chromosome segregation (Figure 2.12). These transcriptional changes are consistent with the cell growth deficits observed both *in vitro* and *in vivo* in SMN-deficient myoblasts.

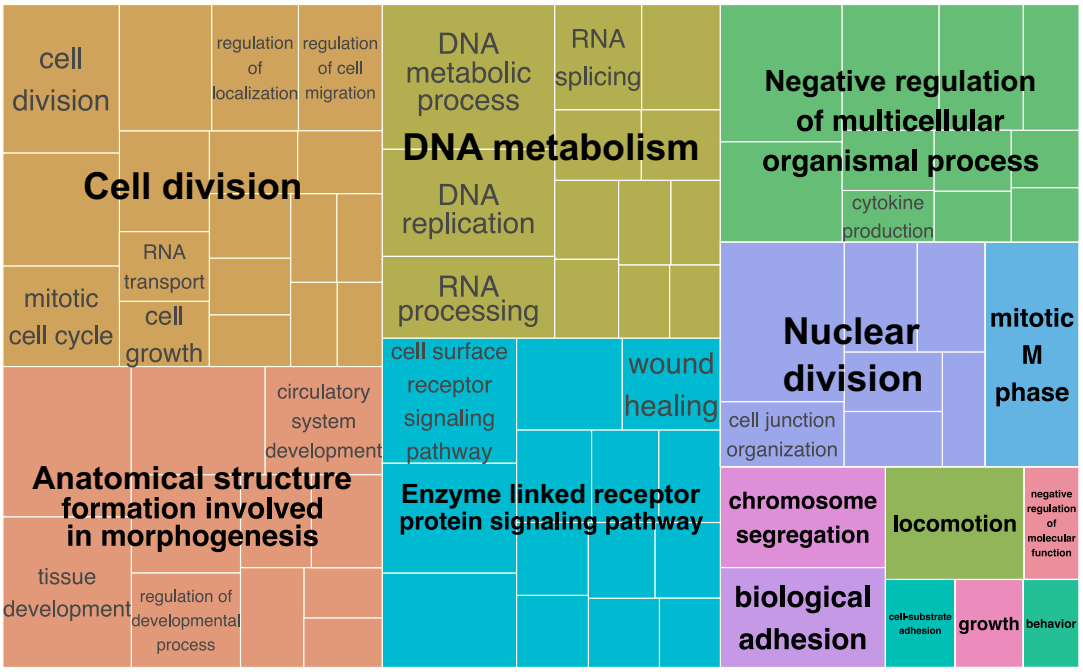

Figure 2.12. Gene ontology analysis of SMN-deficient myoblasts reveals cell cycle disruption. GO analysis of *Pax7:SMN*-KD control versus mutant myoblasts as visualized by REVIGO[103]. Larger size of blocks represents greater significance of GO terms.

Discussion

The contribution of satellite cell deficits to muscle growth pathologies in SMA

In this study, we demonstrated that severe failures in satellite cell proliferation are present at the end stage of SMA, when skeletal muscles have stopped growing[54]. Furthermore, we showed that defects in satellite cell function occur as a consequence of SMN deficiency in a cell autonomous manner. RNA sequencing data reinforced the presence of a proliferation deficit in SMA, as we observed that many cell cycle pathways are disrupted in SMN-deficient myoblasts. Therefore, we propose a model where SMN-dependent proliferation deficits impair satellite cell function during muscle growth in SMA, which is a period normally characterized by robust myoblast expansion. If correct, muscle hypotrophy occurring early in SMA patients may be distinct from atrophy that occurs later in the disease as a consequence of motor neuron death[54,72]. In fact, in SMNΔ7 mice, we observed satellite cell proliferation defects in the hind limb TA muscle, which remains fully innervated at the disease end stage[55]. This supports the idea that in relatively spared muscles, hypotrophy may be a direct consequence of impaired satellite cell-mediated muscle growth, as opposed to atrophy due to motor neuron death and neuromuscular junction denervation. It would be interesting to determine the relative contribution of muscle growth versus muscle atrophy by conditionally restoring SMN in all myogenic precursors on an SMA background and assessing myofiber size in muscles that undergo severe denervation, such as the semispinalis capitis of the neck or the paraspinal back muscles[55].

How SMN deficiency impairs cell growth is still unknown, but it may result from precocious terminal differentiation. Indeed, we observed an abnormal increase in terminally differentiated and non-dividing myocytes in SMA cultures, even under growth promoting conditions. Furthermore, it has been shown that SMNΔ7 muscle expresses abnormally high levels of the terminal differentiation factor myogenin[104]. If there is a tendency for proliferative cells to precociously differentiate, this could explain the reduction in satellite cells over time. This phenomenon is likely not specific to myogenic

cells. We have observed that multiple SMA patient-derived iPSC lines tend to spontaneously differentiate *in vitro* (Lynes and Gibbs et al., manuscript in preparation). Thus, SMN deficiency may impair the balance between proliferation and differentiation in multiple cell types.

Ultimately, we would also like to study the effects of satellite cell-conditional SMN deficiency during the postnatal muscle growth period, which more closely mimics SMA patient biology. Here, we chose an adult muscle regeneration model because it is a very well-characterized method of testing satellite cell function *in vivo*, and because we unfortunately observed severe tamoxifen toxicity in neonatal mice. In future studies, it would be interesting to administer low doses of tamoxifen to neonatal *Pax7:SMN*-KD mice to achieve mosaic recombination in satellite cells, then lineage trace SMN-deficient satellite cells based on tdTomato expression. This would allow us to truly address the question of how SMN-deficiency specifically in satellite cells affects postnatal myogenesis.

The role of satellite cells in neuromuscular defects

SMA is characterized not only by motor neuron loss, but also by neuromuscular phenotypes including denervation, impaired synaptic transmission, and immaturity of neuromuscular junctions[34,55,56,105]. Conditional SMN restoration in motor neurons has been shown to rescue many of these neuromuscular phenotypes[61]. However, it is possible that defective satellite cell function could exacerbate motor neuron and neuromuscular junction defects. Interestingly, satellite cell depletion in wild type mice has been shown to exacerbate muscle atrophy and impair reinnervation and maturation of neuromuscular junctions after nerve damage[106]. Therefore, if satellite cells are completely dysfunctional in SMA, as they appear to be at the end stage in SMNΔ7 mice, this may partially contribute to neuromuscular deficits.

The relationship between SMN levels and phenotypic severity

By generating separate mouse models of conditional SMN *knockout* and *knockdown* in satellite cells, we observed a differential phenotype associated with the extent of SMN deficiency. When SMN was completely depleted by Cre-mediated deletion of *Smnex7*, we observed myoblast cell death both in primary *in vitro* cultures and after muscle damage *in vivo*. This led to a complete failure in muscle regeneration consistent with previously published models of diphtheria toxin-A induced satellite cell ablation[88]. However, when we knocked SMN down by approximately 90%, satellite cells were capable of regenerating muscle, albeit to a lesser degree (Figure 2.8). Consistent with the range of SMA clinical subtypes, which correlates with SMN expression levels in patients, our results suggest that the severity of the SMA satellite cell phenotype is correlated with the extent of SMN deficiency.

Therapeutic implications of satellite cell defects in SMA

Our study suggests that early SMN elevation in peripheral tissues is important for conferring maximal benefit to patients. In addition, patients on SMN-elevating drugs may benefit from additional muscle-targeted therapies. One method of increasing skeletal muscle growth in SMA is to enhance the number of activated satellite cells in the tissue. In theory, this could be accomplished by satellite cell transplantation, SMN-elevation in endogenous satellite cells to protect them from death or premature differentiation, or enhancing the proliferation of endogenous satellite cells with therapeutic agents.

However, for satellite cells to be a therapeutic target for treating SMA, it will be important to better understand their defects in patients. Motor axon denervation has been shown to stimulate satellite cell activation, but chronic denervation substantially reduces satellite cell populations over time[106-108]. Therefore, it will be important to understand the impact of chronic denervation on satellite cell populations of older patients with milder forms of SMA. If satellite cells in chronically denervated muscles can no longer proliferate, they may not be capable of enhancing muscle growth in response

to SMA therapies. Older patient populations with chronic muscle denervation may instead need to pursue muscle-targeted therapies that do not rely on the satellite cell to enhance growth, such as myostatin inhibition or molecules that enhance muscle contractility.

Author Contributions:

Rebecca Gibbs[1,2] and Dr. Lee Rubin[1,2] designed experiments. Lovelace J. Luquette[3] and Kristina Holton[1,2] performed bioinformatics analyses of RNA sequencing data. Dr. Feodor Price[1,2] and Mark Matyas[1,2] performed muscle force measurements. Dr. Ceren Ozek[1,2] performed a subset of western blotting experiments. Dr. Sarah Boswell[4] constructed libraries for RNA sequencing. All other experiments were performed and analyzed by Rebecca Gibbs.

[1] *Department of Stem Cell and Regenerative Biology, Harvard University, Cambridge, MA*

[2] *Harvard Stem Cell Institute, Cambridge, MA*

[3] *Department of Biomedical Informatics, Harvard Medical School, Boston, MA*

[4] *Laboratory of Systems Pharmacology, Harvard Medical School, Boston, MA*

CHAPTER 3

DEFECTIVE MYOGENESIS IN A HUMAN INDUCED PLURIPOTENT STEM CELL MODEL OF SPINAL MUSCULAR ATROPHY

Introduction

In chapter 2, we provided evidence from various SMA mouse models that SMN deficiency impairs satellite cell proliferation in a cell-autonomous manner. These results raised the question of whether or not SMN loss also impairs skeletal muscle growth in SMA patients. To address this question, we utilized an *in vitro* human induced pluripotent stem cell (iPSC) model of SMA, which allowed us to study the effects of SMN deficiency on myogenesis without the influence of motor neurons.

Since the discovery by Takahashi and Yamanaka that a combination of transcription factors can reprogram adult somatic cells into iPSCs, many studies have used iPSCs to model neurodegenerative diseases. For example, in our lab, we have studied the role of ER stress and autophagy in SMA patient iPSC-derived motor neurons, and performed screens to identify compounds that promote ALS patient-derived motor neuron survival[109-111].

In this study, we used a skeletal muscle directed differentiation protocol, which utilizes growth factors and small molecules to recapitulate endogenous signaling pathways that normally occur during mesoderm development[112]. The process coaxes pluripotent stem cells towards a muscle fate without requiring transgenic overexpression of master transcription factors such as *Pax7* or *MyoD*[113,114]. Thus, this transgene-free approach reduces the potential for random transgene integration in the genome and subsequent disruption of cell function. Several directed differentiation protocols exist for making muscle. For example, pluripotent stem cells can be driven towards a presomitic mesoderm fate through a combination of Wnt activation and BMP inhibition, then further differentiated into satellite-like cells and mature muscle fibers by the addition of myogenic growth factors HGF, IGF-1 and FGF-2[115]. For our study, we used a directed differentiation system developed by Genea Biocells, which efficiently generates activated satellite cells, myoblasts, and skeletal muscle fibers from iPSCs/hESCs using a small-molecule-based, FACS-free approach[116]. This method allows for scalable and consistent

differentiations and, in contrast to many other monolayer skeletal muscle protocols, has a duration of less than four weeks.

Here, we demonstrate that SMA patient iPSCs display SMN-dependent defects in myogenesis, including reduced production of myogenic precursors and impaired muscle fiber formation. These results are consistent with our previous findings of myogenic defects in SMA models. We further demonstrate that $Pax7^+$ satellite cells are present in SMA patient muscle tissue, suggesting that in spite of myogenic deficits, satellite cells are not depleted and remain a potential therapeutic target for ameliorating muscle atrophy.

Results

SMA iPSCs exhibit defects in skeletal muscle formation

Our lab previously derived and characterized a large collection of iPSC lines from SMA patient fibroblasts, providing an *in vitro* system to study SMA pathogenesis across a range of SMN levels and disease severities (Lynes and Gibbs et al., manuscript in preparation). For the purposes of this study, we selected 3 SMA iPSC lines from Type 0 and Type I patients, and 4 control iPSC and ESC lines (Table 3.1).

Table 3.1. iPS/ES cell lines used for myogenic differentiation experiments.

Cell Line	Diagnosis	Line Type	Reprogramming Method
WA01	Healthy control	ESC	--
BJ siPS-D	Healthy control	iPSC	Sendai
Hues66	Healthy control	ESC	--
E3A	Healthy control	iPSC	Sendai
15A	SMA Type 0	iPSC	Sendai
38D	SMA Type 1	iPSC	Sendai
2-18C	SMA Type 1	iPSC	Sendai

As expected, all SMA lines had significantly lower SMN protein levels compared to control iPS or ES cells as assessed by western blot (Figure 3.1B). Line 15A, a Type 0 patient line, had the lowest SMN expression, with <5% SMN protein compared to control lines. Lines 38D and 2-18C, Type I patient lines, expressed approximately 5% SMN protein compared to control lines.

Using this panel of SMA iPSCs expressing disease-relevant levels of SMN protein, we addressed the question of whether or not SMN loss impairs skeletal muscle growth in a human system. To model this phenotype *in vitro*, we generated skeletal muscle cells from each line using the Genea Biocells skeletal muscle directed differentiation system, a proprietary three-part medium kit (Figure 3.1A). Briefly, iPSCs/ESCs were cultured in Skeletal Muscle Induction Medium, which facilitates the production of proliferating $Pax3^+/Pax7^+$ satellite cells. The cultures were then dissociated and reseeded in Myoblast Cell Culture Medium, which promotes the conversion of satellite cells to committed myogenic precursors called myoblasts, which express the myogenic commitment transcription factor MyoD. Finally, myoblasts were cultured in Myotube Fusion Medium to generate $MyoG^+$ (myogenin) terminally differentiated myocytes, which fuse into multinucleated muscle fibers expressing the contractile skeletal muscle structural protein MyHC.

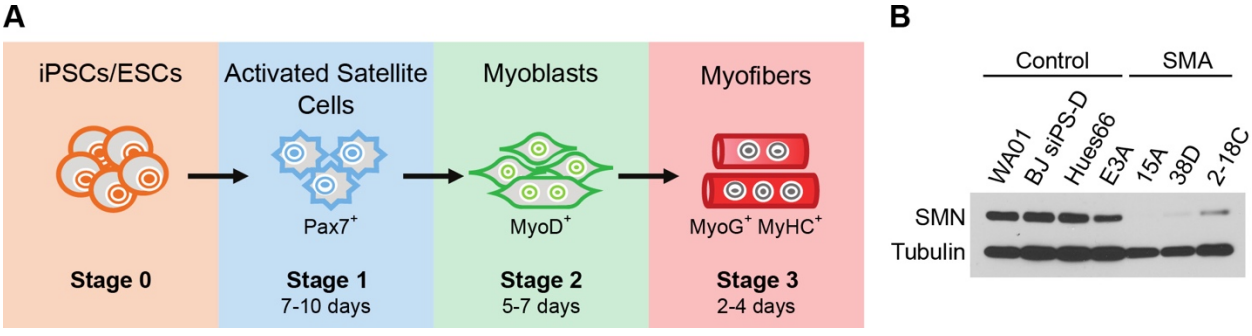

Figure 3.1. Experimental details for generating SMA iPSC-derived skeletal muscle. A) Schematic of Genea Biocells skeletal muscle differentiation protocol, which is divided into three stages. Stage 1: differentiation of iPSCs/hESCs into activated satellite cells, Stage 2: conversion of activated satellite cells into myoblasts, and Stage 3: fusion of myoblasts into myotubes. B) Western blot showing reduced SMN levels in SMA patient iPSCs compared to healthy control lines.

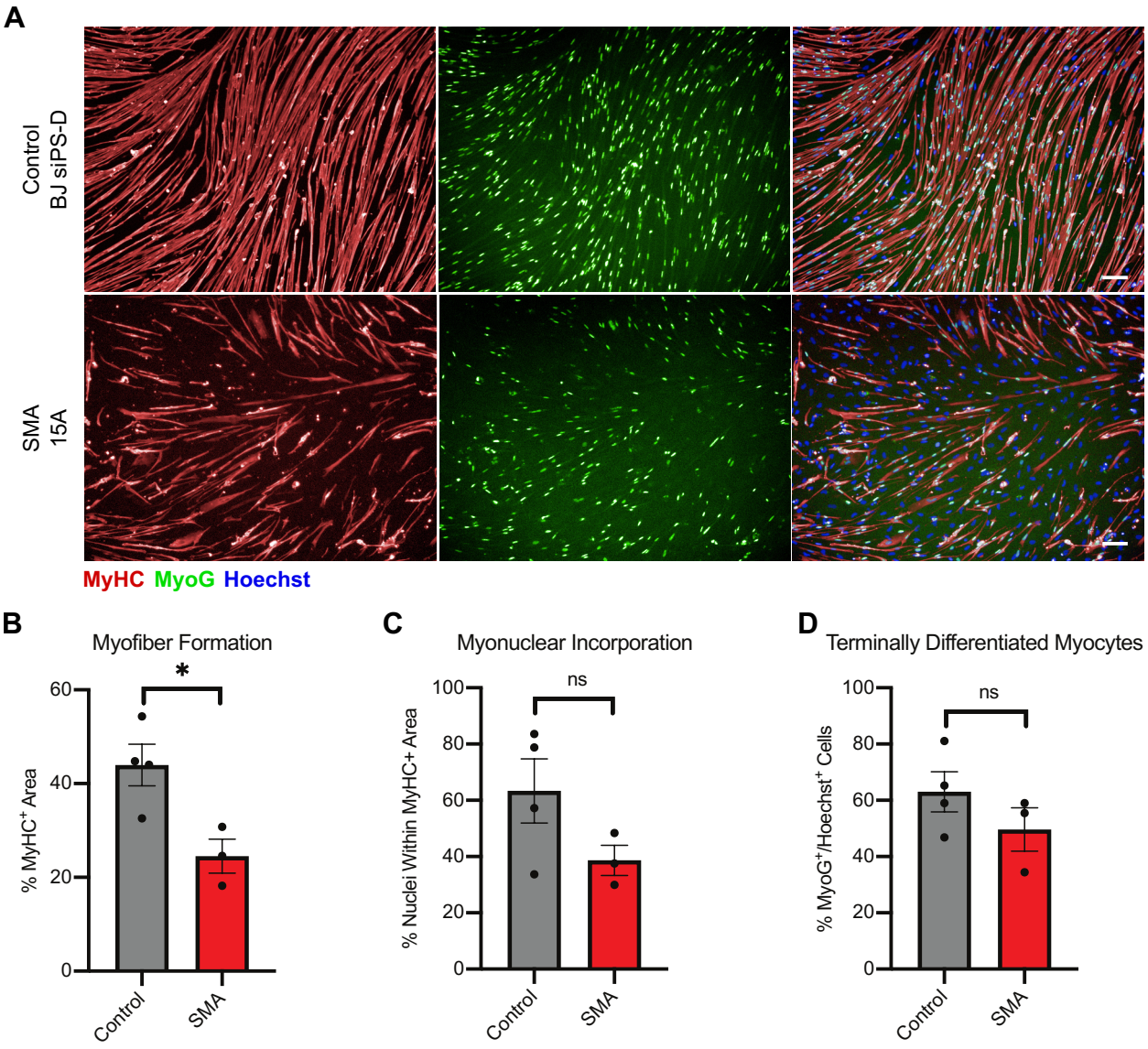

Figure 3.2 SMA iPSCs exhibit defects in skeletal muscle formation. A) Representative images of myofibers produced from a control line (BJ-SiPS-D) and a Type 0 SMA line (15A) 4 days after inducing terminal differentiation. Myofibers were stained at the end stage of the differentiation for muscle structural protein MyHC (red), terminal muscle differentiation transcription factor MyoG (green), and nuclear marker Hoechst (blue). Scale bars=100μM. B) Percentage of $MyHC^+$ culture area. N=3-4 individual patient iPSC lines per group, p=0.0240, unpaired t test. C) Percentage of total nuclei incorporated within $MyHC^+$ area. N=3-4 per group, p>0.05, unpaired t test. D) Percentage of $MyoG^+$ nuclei. N=3-4 per group, p>0.05, unpaired t test. Data presented as mean ± SEM.

To assess myogenesis in SMA versus control iPSC lines, we compared the formation of muscle cells at the end stage of the differentiation using the aforementioned markers of myogenic progression. We found that SMA lines produced significantly fewer myofibers compared to control lines, as

demonstrated by a 44% reduction in the total area of $MyHC^+$ muscle fibers in the culture (Figure 3.2A-B). In addition, SMA lines showed a notable but non-significant trend towards reduced myonuclear incorporation, demonstrated by a reduced percentage of nuclei incorporated within $MyHC^+$ muscle fibers, as well as a trend towards reduced formation of terminally differentiated $MyoG^+$ myocytes (Figure 3.2C-D). These results suggest that SMA patient-derived iPSCs undergo defective myogenesis, which leads to reduced skeletal muscle growth *in vitro*.

SMN deficiency directly impairs myogenesis

Although SMA is widely considered a monogenic disorder resulting from a deletion or LOF mutation in *SMN1*, our observation of impaired myogenesis in SMA lines cannot necessarily be attributed to the loss of SMN protein. SMN-independent differences in patients' genetic backgrounds could contribute to the observed myogenic defects. Furthermore, our experiment assessing myogenic defects across multiple SMA lines yielded highly variable results, likely due to the intrinsic variability in differentiation capacity widely known to exist between iPSC/ESC lines. In fact, a power calculation using the results in Figure 3.2C predicted that given the variance and effect size observed, we would need to assess 13 SMA and control iPSC lines for our study to be sufficiently powered to detect a true difference between the means. Though feasible, performing such a large-scale experiment is not practical. Therefore, to determine if SMN reduction directly impairs myogenesis using a more controlled experimental system, we knocked down SMN using a pool of SMN-targeted siRNAs in a control iPSC line and assessed muscle formation.

Briefly, iPSCs were transfected at two time points prior to initiating skeletal muscle differentiation and three additional time points throughout the differentiation. This protocol ensured that SMN levels were knocked down to at least less than 50% compared to the scrambled control throughout the experiment (Figure 3.3C). The scrambled siRNA sequence did not negatively impact

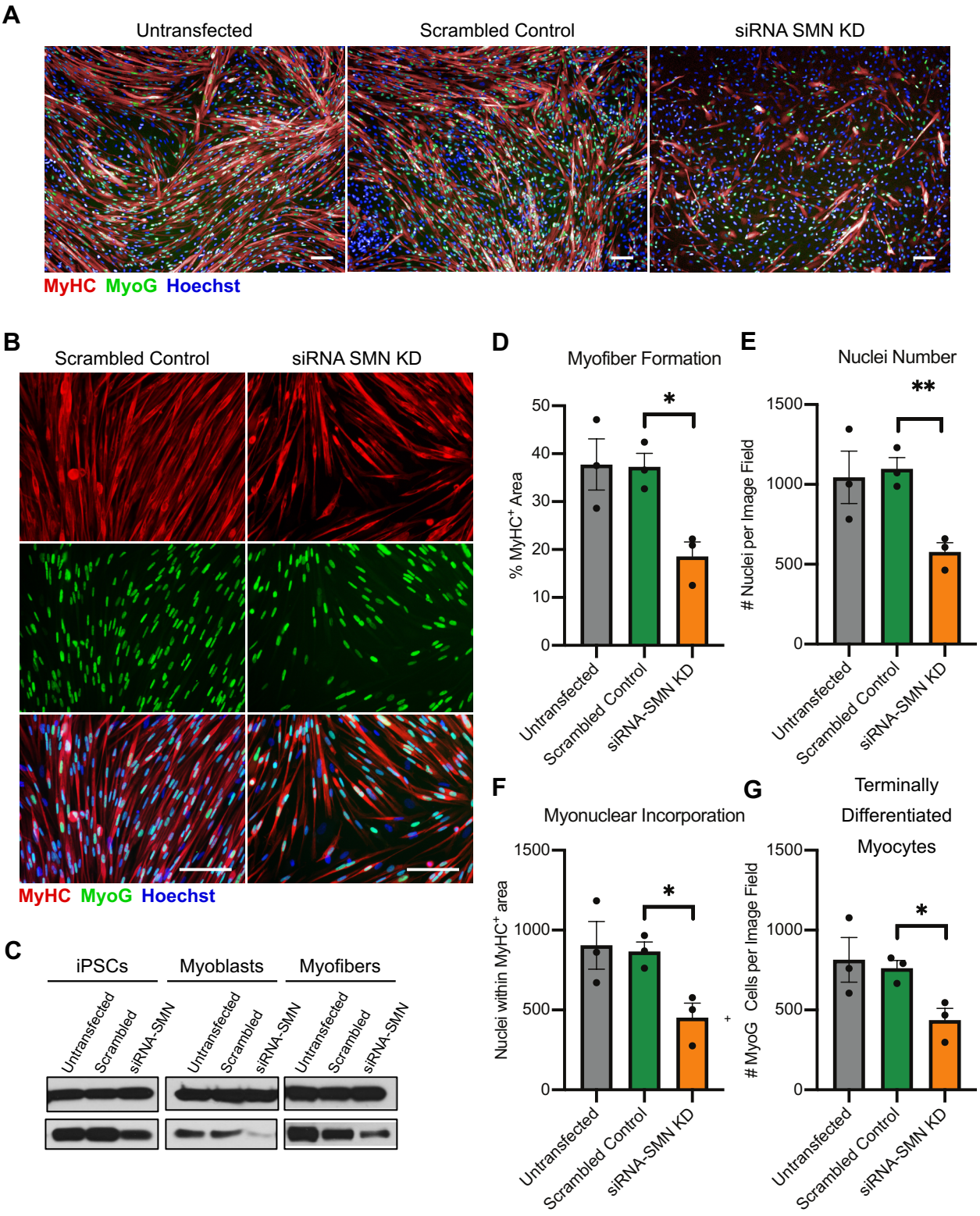

Figure 3.3 SMN deficiency directly impairs myogenesis. A-B) Representative 10X and 20X images of myofibers from untransfected, scrambled siRNA and SMN siRNA knockdown (KD) cultures 4 days after inducing terminal differentiation. Myofibers were stained at the end stage of the

Figure 3.3 (continued) differentiation for MyHC (red), MyoG (green) and Hoechst (blue). All scale bars=100μM. C) Western blot showing SMN protein levels in iPSCs, iPSC-derived myoblasts, and iPSC-derived myofibers in untransfected cultures or after treatment with an siRNA against SMN or a scrambled control. D) Percentage of $MyHC^+$ culture area. N=3, p=0.0108, unpaired t test. E) Total number of nuclei per image field. N=3, p=0.0048, unpaired t test. F) Percentage of total nuclei incorporated within $MyHC^+$ area. N=3, p=.0185, unpaired t test. G) Total number of $MyoG^+$ nuclei per image field. N=3, p=.0209, unpaired t test. Data presented as mean ± SEM.

any parameters of myogenesis compared to untransfected controls, meaning that the siRNA reagents did not cause any observable toxicity (Figures 3.3A, D-G). We found that SMN knockdown impaired myogenesis, resulting in decreased production of myogenic cells and defective muscle fiber formation. At the end stage of the differentiation, myofiber formation was reduced by 50%, total nuclei number was reduced by 47%, myonuclear incorporation was reduced by 43%, and myocyte production was reduced by 43% in SMN knockdown versus scrambled control conditions (Figures 3.3A-B, D-G). These myogenic impairments approximately phenocopy the deficits observed in muscle cultures derived from SMA iPSC lines and would possibly be even more pronounced if SMN was knocked down to levels typically observed in severe SMA patients.

SMN deficiency causes early defects in myogenesis

Our previous studies in SMA mice suggested that muscle growth deficits are caused by insufficient production of early myogenic precursors, including satellite cells and myoblasts. To determine if the same phenomenon occurs in a human SMA iPSC system, we assessed myogenesis at an earlier time point in the differentiation. At this stage, cells have committed to the myogenic lineage and express the muscle commitment transcription factor MyoD. We found that SMN knockdown reduced myoblast production, causing a 30% decrease in the percentage of $MyoD^+$ cells and a 42% reduction in overall cell number (Figure 3.4A, C-D). When cells were cultured in the presence of EdU, we observed a 17% reduction in the percentage of EdU+ myoblasts, underscoring once again the

Figure 3.4 SMN deficiency causes early defects in myogenesis. Representative images of myoblasts (A) and myocytes (B) from scrambled siRNA and SMN siRNA cultures 5-7 days after inducing myoblast formation (Stage 2). Myoblasts and myocytes were stained for MyoD or MyoG (green), MyHC (red), and Hoechst (blue). All scale bars=100μM. C) Percentage of $MyoD^+$ cells. N=3, p=0.0124, unpaired t test. D) Number of nuclei per image field. N=3, p=0.0001, unpaired t test. E) Percent of proliferating EdU^+ $MyoD^+$ myoblasts. N=3, p=0.0079, unpaired t test. F) Percentage of $MyHC^+$ culture area. N=3, p=0.0017, unpaired t test. G) Percentage of total nuclei incorporated within $MyHC^+$ area. N=3, p=.0044, unpaired t test. H) Percent of $MyoG^+$ nuclei. N=3, p=.0004, unpaired t test. Data presented as mean ± SEM.

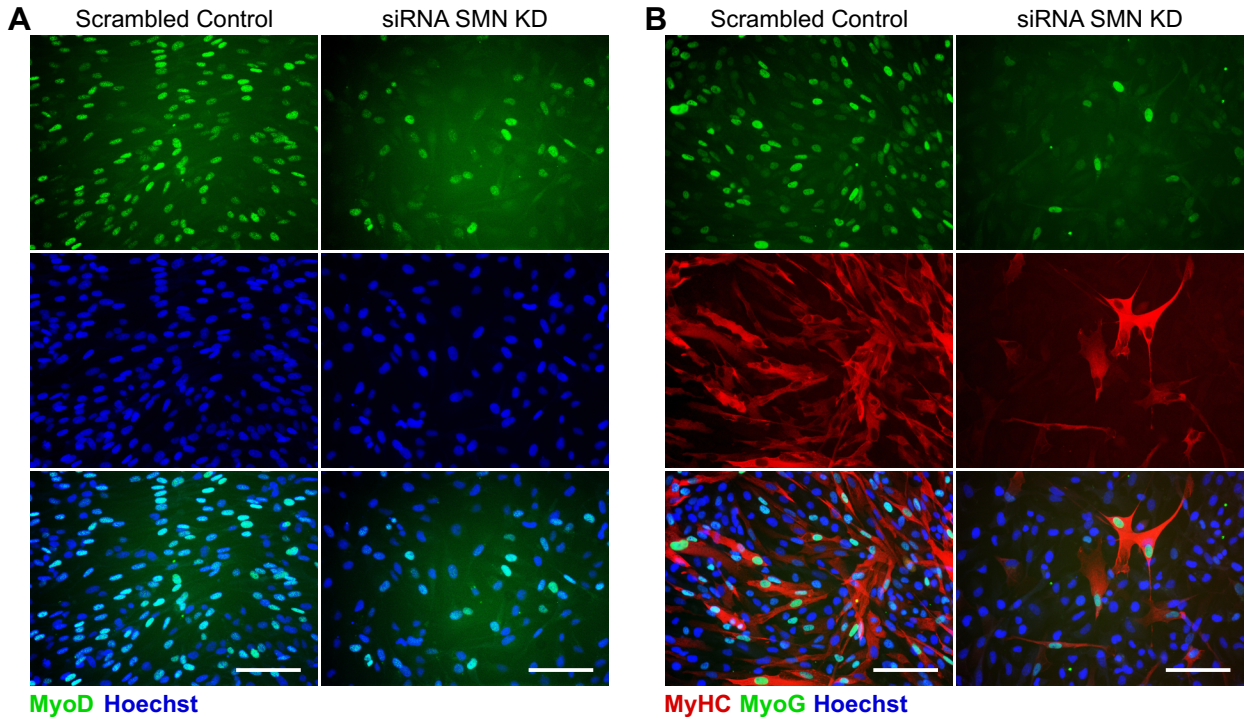
A
Scrambled Control
siRNA SMN KD
MyoD Hoechst
B
Scrambled Control
siRNA SMN KD
MyHC MyoG Hoechst

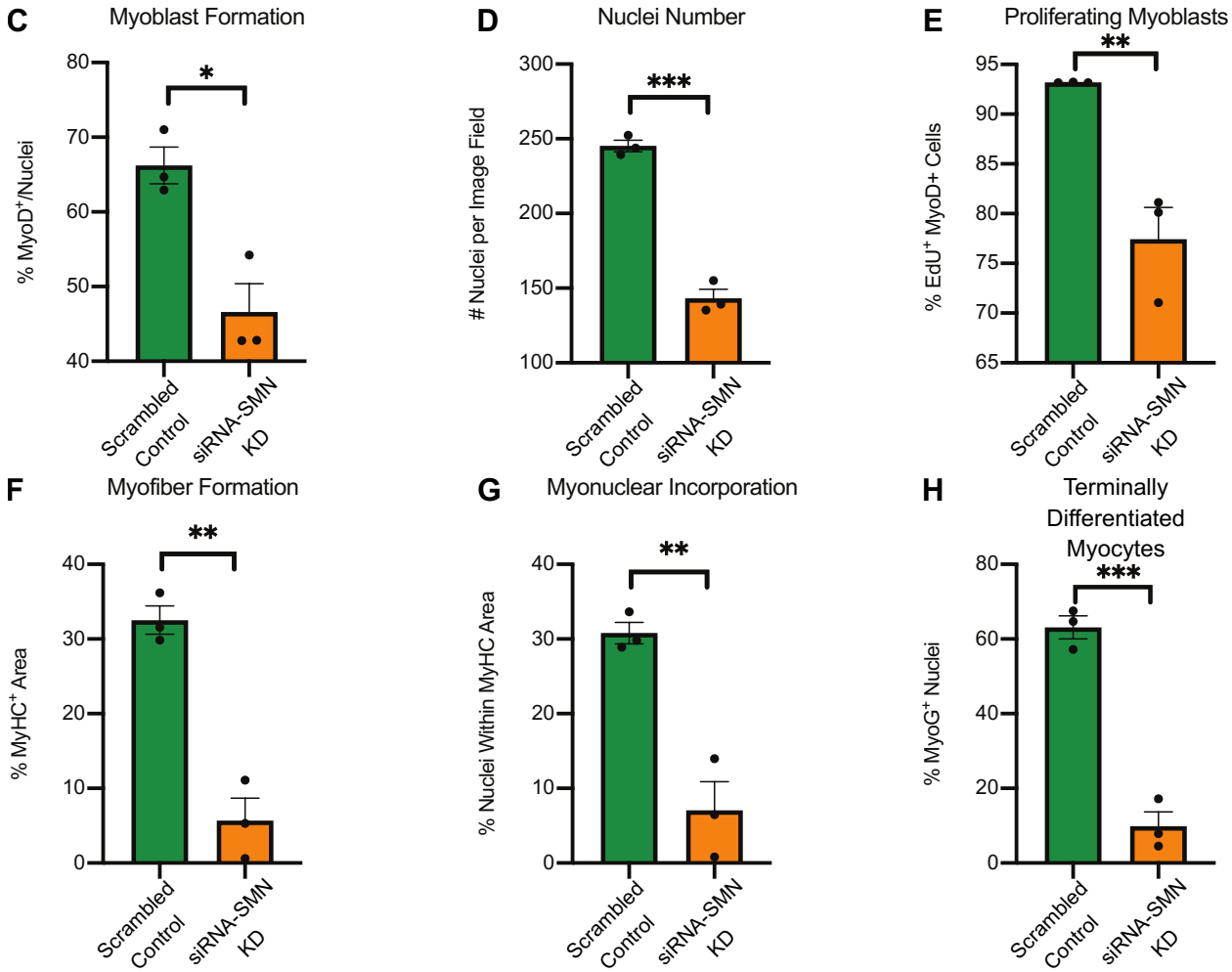
C
Myoblast Formation
% MyoD+/Nuclei
80
70
60
50
40
*
Scrambled Control
siRNA-SMN KD
D
Nuclei Number
Nuclei per Image Field
300
250
200
150
100
***
Scrambled Control
siRNA-SMN KD
E
Proliferating Myoblasts
% EdU+ MyoD+ Cells
95
90
85
80
75
70
65
**
Scrambled Control
siRNA-SMN KD
F
Myofiber Formation
% MyHC+ Area
40
30
20
10
0
**
Scrambled Control
siRNA-SMN KD
G
Myonuclear Incorporation
% Nuclei Within MyHC Area
40
30
20
10
0
**
Scrambled Control
siRNA-SMN KD
H
Terminally Differentiated Myocytes
% MyoG+ Nuclei
80
60
40
20
0
***
Scrambled Control
siRNA-SMN KD

reduction in proliferating myogenic cells caused by SMN deficiency (Figure 3.4E). Furthermore, we observed an 84% reduction in the percentage of terminally differentiated myocytes, an 83% reduction in myofiber formation, and a 77% reduction in myonuclear incorporation in SMN knockdown versus scrambled control conditions (Figure 3.4B, F-H). These results suggest that not only does the loss of SMN decrease the efficiency of differentiating down the muscle lineage from a pluripotent stem cell state, but also causes a loss of myoblast proliferation once the myogenic cells have formed. Ultimately, SMN deficiency directly impairs multiple stages of myogenesis, and the reduced production of myogenic precursors underlies defects in skeletal muscle formation.

The satellite cell pool is not depleted in SMA patient skeletal muscle

Given that SMN deficiency impairs skeletal muscle growth by reducing the proliferation of satellite cells and myoblasts, it is important to understand if this pathogenic process leads to a depletion of the satellite cell pool over time, especially in muscles that are severely impacted in the disease. This is a particularly important question because satellite cells are a critical mechanism by which muscle fibers increase in size. From an SMA cellular mechanism perspective, it is important to understand if the depletion of satellite cells creates a bottleneck that prevents muscle growth and regeneration. From a therapeutics perspective, we are interested in determining if healthy satellite cells remaining in the tissue can be driven to regenerate atrophic muscle.

To determine if the satellite cell pool is depleted in SMA, we obtained SMA patient skeletal muscle biopsies from a repository maintained at Johns Hopkins University (see Methods for additional details). The de-identified tissue samples were collected during spinal fusion surgeries or standard autopsies of SMA patients varying from severe Type I infants to moderately affected Type II older children (Table 3.2). Type I SMA diaphragm and iliopsoas muscles and Type II SMA paraspinal muscles were cross-sectioned and labeled with anti-Pax7 and Hoechst to identify satellite cells. We

Table 3.2 SMA patient and control muscle samples used for satellite cell analysis

Diagnosis	Muscle type	Age
Type I SMA	Diaphragm	7 weeks
Type I SMA	Iliopsoas	7 weeks
Type II SMA	Paraspinal	9 years
Control (I)	Diaphragm	3 years
Control (I)	Iliopsoas	41 days
Control (II)	Paraspinal	13 years

analyzed 2-3 patient samples per group and age-matched controls. Remarkably, we identified the presence of large numbers of $Pax7^+$ satellite cells in the majority of SMA muscle samples analyzed, suggesting that the satellite cell pool is *not* necessarily depleted in SMA (Figure 3.5). Interestingly, satellite cells were present in both the iliopsoas muscle, which is clinically severely affected in SMA, as well as the diaphragm, which is relatively spared[104]. We occasionally observed SMA samples without $Pax7^+$ staining, but this appeared to be caused by excessively high background signals in particularly atrophic muscles (data not shown). Further optimization will be required to determine if there are any SMA cases with a complete loss of $Pax7^+$ cells.

Discussion

Myogenic deficits of human SMA iPSCs resemble SMA mouse muscle pathologies

In this study, we identified SMN-dependent myogenic deficits in SMA patient-derived iPSCs that were consistent with the myogenic deficits observed in SMA mouse models. First, we found that SMN-deficient iPSCs make fewer and small muscle fibers *in vitro*, similar to the reduced myofiber formation observed in SMNΔ7 mice *in vivo* (Chapter 2). We further discovered that this phenotype arises as a consequence of reduced myoblast proliferation during earlier stages of the differentiation, similar to the proliferation deficits observed in SMNΔ7, *Pax7:SMN*-KO and *Pax7:SMN*-KD mouse

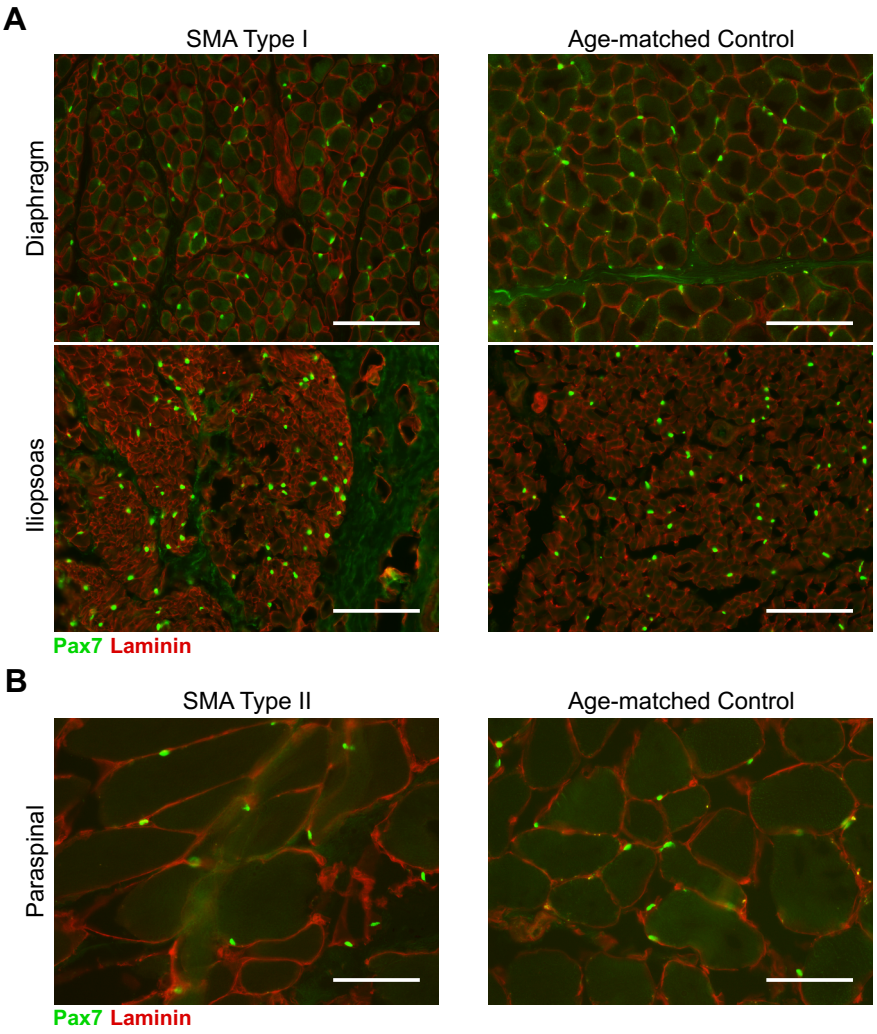

Figure 3.5. Type I and Type II SMA patient skeletal muscle contains abundant quantities of Pax7$^+$ cells. A) SMA Type I and age-matched control diaphragm and iliopsoas muscles labeled with Pax7 (green). B) SMA Type II and age-matched control paraspinal muscles labeled with Pax7 (green) and laminin (red). All scale bars=100μM.

models. Lastly, since there were no motor neurons in the cultures, our results point to a muscle-intrinsic impact of SMN deficiency, similar to our observation of impaired muscle regeneration in *Pax7:SMN*-KO and *Pax7:SMN*-KD mice.

One explanation for the observed myogenic deficits is that SMN deficiency causes precocious terminal differentiation of stem cells. Our lab previously found that satellite cells in a very severe SMA mouse model spontaneously differentiate *in vitro* and *in vivo*, leading to reduced muscle fiber

formation[90]. In addition, we found that SMA iPSCs are themselves defective in maintaining pluripotency, instead demonstrating spontaneous differentiation and a bias towards forming ectodermal lineages (Lynes and Gibbs et al., manuscript in preparation). These data suggest that SMN loss may dysregulate stem cell fate, which could have broad developmental implications impacting skeletal muscle satellite cells and other adult stem cell populations in patients.

Approximating postnatal muscle development with an SMA iPSC model

While iPSC models afford the opportunity to study patient biology *in vitro*, iPSC-derived cells often resemble early embryonic tissues instead of maturing to adult stages[117]. Indeed, our preliminary qPCR experiments identified embryonic skeletal muscle isoforms of MyHC (*MyH3, MyH8*) rather than adult isoforms (*MyH1*, *MyH4*) in SMA iPSC-derived muscle cultures (data not shown). However, muscle is generated through two waves of development *in vivo*. During embryogenesis, myoblasts proliferate, differentiate and fuse to form muscle fibers *de novo*. After birth, satellite cells proliferate, differentiate and fuse with existing fibers to increase muscle size through myonuclear accretion. Both myogenic processes are similar, and thus the results from our iPSC model are still applicable to understanding postnatal muscle growth. Furthermore, given the embryonic nature of iPSC-derived muscle, our results suggest that SMA could potentially involve an embryonic development component. Understanding these earliest consequences of SMN deficiency will be critical for designing optimal treatment methods.

Satellite cells remain a potential therapeutic target in SMA patient muscle tissue

Having data from both human and animal models substantiates our claim that SMN-dependent defects play a role in muscle development pathologies in SMA, and also raises the question of whether or not defective myogenesis depletes the satellite cell pool in SMA patients over time.

Fortunately, we identified abundant numbers of satellite cells remaining in both Type I and Type II SMA patient muscle tissue, and in both clinically affected and relatively spared muscles. However, the myogenic capacity of these cells is not known. These $Pax7^+$ cells could potentially be incapable of regenerating muscle if they are terminally differentiated, senescent, or undergoing apoptosis. In fact, in Chapter 2, we found that substantial numbers of $Pax7^+$ cells are present in end-stage SMA mice, but they are completely non-proliferative. Therefore, in future studies, we will need to more fully characterize the satellite cell state in SMA patient tissue.

Author Contributions:

Rebecca Gibbs[1,2] and Dr. Lee Rubin[1,2] designed experiments. Experiments and data analyses were performed by Rebecca Gibbs and Soumyaa Mazumder[1,2].

[1] *Department of Stem Cell and Regenerative Biology, Harvard University, Cambridge, MA*

[2] *Harvard Stem Cell Institute, Cambridge, MA*

CHAPTER 4

SMALL MOLECULE-BASED, SATELLITE CELL-TARGETED THERAPY FOR SPINAL MUSCULAR ATROPHY

Introduction

Spinal muscular atrophy (SMA) is a devastating neuromuscular disease characterized by motor neuron death and widespread muscle atrophy. Although the principal pathologies underlying SMA likely result from the loss of Survival of Motor Neuron (SMN) protein in spinal cord motor neurons, we and others have demonstrated that some SMA pathologies may be directly caused by SMN deficiency outside the central nervous system[93]. Fortunately, following the discovery of the disease-causing *SMN1* and *SMN2* genes nearly 25 years ago, two very promising SMA therapeutics are now available, with several others in clinical development[6,72]. The two FDA-approved therapies include nusinersen, an antisense oligonucleotide that enhances the amount of functional SMN protein produced by *SMN2*, and AVXS-101, a gene therapy that provides exogenous *SMN1* expression.

Despite the great therapeutic advances achieved thus far, SMN elevation strategies have not yet proved curative. Although patients treated with both drugs experience significant improvements in motor function, they still lag behind healthy infants in motor development[76]. This has raised concerns that SMN elevation alone may not be sufficient to restore maximal benefit to patients. This could be due to insufficient uptake of the compounds into motor neurons, or the fact that treatment sometimes commences after motor neuron death has occurred[72]. Another possibility is that these strategies may not effectively restore SMN in non-motor neuron cell types that are critical to SMA pathology. For example, nusinersen is administered intrathecally, and may therefore have limited effects outside of the central nervous system[118]. AVXS-101, a systemically-injected one-time treatment, is capable of crossing the blood brain barrier when administered at high doses. However, although AAVs can achieve long-term expression in post-mitotic motor neurons, they do not remain stably expressed in proliferative tissues[69]. Therefore, it is unclear if AVXS-101 provides sufficient SMN rescue in postnatally developing muscle.

Furthermore, even if SMN-elevating therapies were capable of targeting all systemic tissues, it is unclear if SMN elevation would lead to meaningful improvements once motor neuron pathologies have already manifested, as opposed to merely protecting against further degeneration. In fact, it has been demonstrated in SMA mice that SMN restoration in post-mitotic skeletal muscle does not increase muscle fiber size, suggesting that patients already suffering from muscle atrophy may not experience muscle gains from SMN-enhancing therapy[89]. These challenges suggest that alternative, SMN-independent therapeutic strategies targeting specific tissue types should be explored. In particular, skeletal muscle is an attractive therapeutic target, given its important role in regulating systemic functions and the extensive muscle hypotrophy that manifests early in SMA patients[49,72].

In Chapter 2 of this dissertation, we demonstrated that SMN deficiency directly impairs satellite cell proliferation, leading to insufficient production of myogenic precursors to support skeletal muscle growth. As the resident skeletal muscle stem cells, satellite cells are normally quiescent. However, during postnatal development and in response to muscle damage or chronic denervation, they activate and proliferate to form a transit amplifying progenitor population of myoblasts, which terminally differentiate and fuse to growing muscle fibers[50].

Although satellite cell-independent paths to muscle growth are possible, such as myostatin-inhibition, we believe that increasing the number of viable satellite cells in muscle tissue can enhance fiber growth and strength[119]. Most muscle stem cell therapies have focused on transplanting satellite cells or myoblasts directly into skeletal muscle[120]. For example, several studies have successfully replenished the satellite cell pool in irradiated, injured or dystrophic muscles of mice, and myoblast transplantation has been tested in clinical trials for the treatment of muscle disorders[121-123]. In addition, in pilot experiments, we performed satellite cell transplants in damaged muscles after SMN knockout in satellite cells and observed a substantial rescue of regenerating fibers (Supplementary Figure 4.1). However, muscle cell therapy has many limitations to overcome, including immune rejection, failed

engraftment, and the inability of myoblasts to repopulate the satellite cell niche. Furthermore, in the case of SMA, which causes widespread muscle atrophy, a cell therapy approach would be hindered by the sheer number of muscles that would require intramuscular delivery.

An alternative approach is to systemically-administer therapeutic agents that enhance skeletal muscle growth by selectively proliferating endogenous satellite cells *in situ*. A small molecule-based approach could potentially circumvent many of the issues associated with cell therapy, while still leveraging the robust regenerative potential of endogenous satellite cells. We previously found that the small molecule receptor tyrosine kinase inhibitor CEP701 stimulated wild type satellite cell proliferation and increased the size of regenerating muscle fibers after damage (Buchanan and Price et al., manuscript in preparation). These results provided a proof-of-concept that compounds that increase satellite cell proliferation *in vitro* can stimulate muscle regeneration and increase muscle size *in vivo*. Therefore, since SMN deficiency results in insufficient production of satellite cells, we hypothesized that small molecule-based modulation of endogenous satellite cells can promote functional muscle growth in SMA.

In this study, we performed a phenotypic screen and discovered multiple small molecules across distinct drug classes that stimulate satellite cell proliferation *in vitro*. We further determined that treating SMA mice with one of these compounds resulted in increased satellite cell proliferation *in vivo*. These enhancements in satellite cell proliferation were associated with increases in muscle fiber size in both severe and intermediate SMA mouse models. We propose that satellite cell-targeted, small molecule therapy may represent a novel approach to increasing muscle growth and strength in SMA patients, as a complement to SMN-elevating therapies that stabilize the motor neuron pool. If this approach proves efficacious, small molecule-based, satellite cell-targeted therapy could provide significant benefit for many neuromuscular and muscle disorders, including amyotrophic lateral sclerosis (ALS) and age-related sarcopenia.

Results

A phenotypic screen identifies small molecules that induce wild type satellite cell proliferation *in vitro*

We performed a chemical screen to identify compounds that increase proliferation of wild type murine satellite cells. Satellite cells were isolated by enzymatic dissociation and FACS purification from transgenic reporter Tg:Pax7-nGFP mice expressing nuclear localized nGFP in Pax7+ satellite cells[124]. Notably, once satellite cells are removed from their niche within the basal lamina of myofibers, they rapidly exit quiescence and become mitotically active[50]. Therefore, this was a screen for compounds that act on activated satellite cells. We seeded FACS-purified GFP^+ satellite cells on 96-well plates in serum free growth medium (Figure 4.1A). Following 24 hours in culture, we treated cells with compounds from the NIH Library of Integrated Network of Cellular Signatures (LINCS). The LINCS library is composed primarily of kinase inhibitors and chromatin-targeting small molecules totaling to 386 compounds. We screened each compound at 3 concentrations (0.1μM, 0.3μM and 1μM) and in biological triplicate. After 3 days of culture, cells were fixed and labeled with Hoechst using an automated liquid handling system, which ensures minimal disruption of cells, then imaged and quantified using high content automated analysis software, as is routinely performed in our lab for drug screening[111,125]. DMSO was used as a negative control and JAK3 inhibitor VI was used as a positive control, based on previous results in our lab showing robust enhancement of satellite cell proliferation in response to JAK inhibition. Hit compounds were defined based on a fold increase in proliferation of 2 standard deviations above the average DMSO control per plate. From this screen, we identified 61 compounds that enhance satellite cell proliferation, including 28 compounds that increased proliferation by >2X and 33 compounds that increased proliferation by >3X the standard deviation of DMSO controls (Figure 4.1B-D and full table of hits in Supplementary Table 4.1). This

Figure 4.1. Small molecule screen identifies satellite cell proliferating compounds. A) Schematic of satellite cell screen timeline. B) Representative images of Hoechst^{+} myogenic nuclei on Day 4 of the screen. DMSO is the negative control and Jak3 VI is the positive control. C) Relative fold change of 40 hit compounds compared to DMSO average. D) Representative image of hits from LINCS1-4.3 libraries when screened at a 1μM concentration. The X-axis represents individual compounds (averaged from triplicate wells) and the Y-axis shows fold change in cell number compared to DMSO. Dark red circles show hits at least >2X greater than the standard deviation of DMSO. Light red circles show negative compounds. Green and blue circles show DMSO negative and Jak3-VI positive controls, respectively.

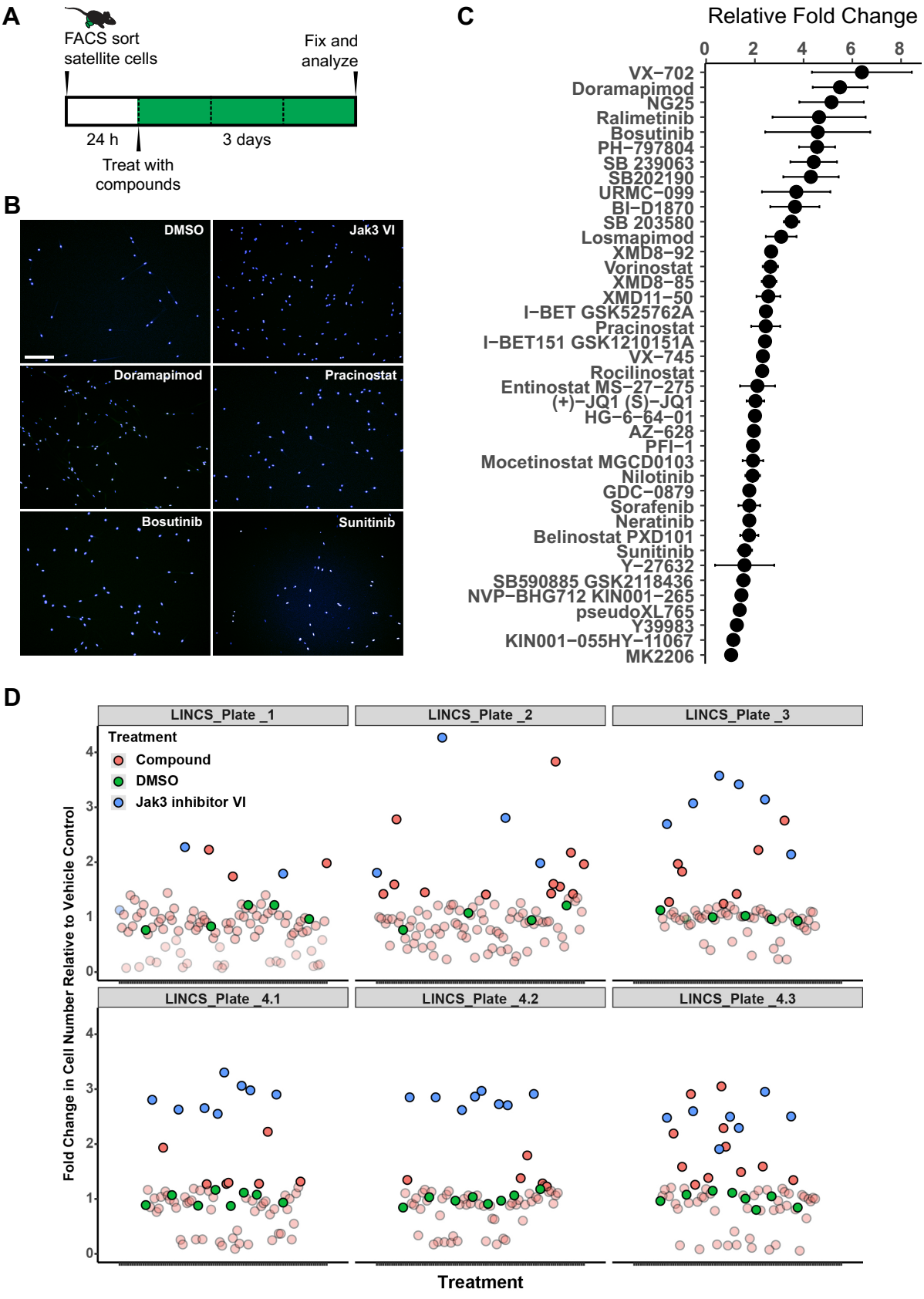
A
FACS sort satellite cells
Fix and analyze
24 h
3 days
Treat with compounds
B
DMSO
Jak3 VI
Doramapimod
Pracinostat
Bosutinib
Sunitinib
C
Relative Fold Change
0
2
4
6
8
VX−702
Doramapimod
NG25
Ralimetinib
Bosutinib
PH−797804
SB 239063
SB202190
URMC−099
BI−D1870
SB 203580
Losmapimod
XMD8−92
Vorinostat
XMD8−85
XMD11−50
I−BET GSK525762A
Pracinostat
I−BET151 GSK1210151A
VX−745
Rocilinostat
Entinostat MS−27−275
(+)−JQ1 (S)−JQ1
HG−6−64−01
AZ−628
PFI−1
Mocetinostat MGCD0103
Nilotinib
GDC−0879
Sorafenib
Neratinib
Belinostat PXD101
Sunitinib
Y−27632
SB590885 GSK2118436
NVP−BHG712 KIN001−265
pseudoXL765
Y39983
KIN001−055HY−11067
MK2206
D
LINCS_Plate _1
LINCS_Plate _2
LINCS_Plate _3
LINCS_Plate _4.1
LINCS_Plate _4.2
LINCS_Plate _4.3
Treatment
Compound
DMSO
Jak3 inhibitor VI
Fold Change in Cell Number Relative to Vehicle Control
0
1
2
3
4
Treatment

amounted to a total hit rate of ~16%, which is within the range of other phenotypic screens that our lab has performed with annotated compound libraries (unpublished results).

To validate hit compounds and identify optimal concentrations that induce satellite cell proliferation, we performed an 8-point dose response curve ranging from 50nM-5μM. We observed a large range of potency and efficacy, with fold increases between 1.2-6.4X and maximum effective doses between 50nM-5μM (Figure 4.2). Sunitinib, a multi-targeted receptor tyrosine kinase inhibitor, enhanced proliferation in a range of 800nM-1μM, resulting in a maximal 1.6X increase in proliferation. Doramapimod, a pan-p38 MAPK inhibitor, enhanced proliferation in a range of 200nM-5μM,

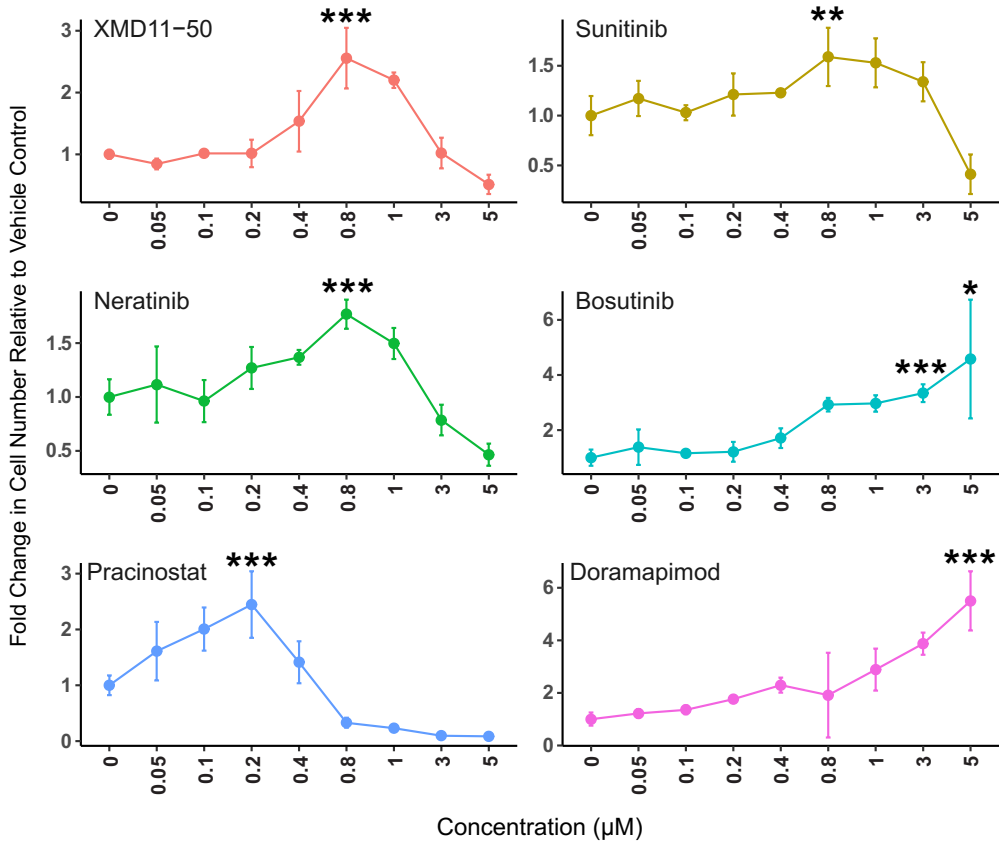

Figure 4.2. Dose response curves for selected hit compounds from the satellite cell screen. Dose response graphs for 4-day satellite cell treatment with six selected compounds. The X-axis shows eight compound concentrations between 0-5μM and the Y-axis shows fold change relative to a DMSO control. Statistical analysis was conducted using a one-way ANOVA followed by post-hoc Welch's t-test. * Indicates a $p< 0.05$, ** indicates $p < 0.01$ and *** indicates $p<0.001$.

resulting in a maximal 5.5X increase in proliferation. Pracinostat, an HDAC inhibitor, enhanced proliferation in a range of 50nM-200nM, resulting in a maximal 2.5X increase in proliferation. Finally, the positive control JAK3 inhibitor VI increased proliferation by 3X at a concentration of 600nM (Figure 4.1D).

We additionally tested for synergy between the compounds, assessing 3 doses each of 2 different compounds in various combinations (Supplementary Figure 4.2). However, we did not observe any additional increases in satellite cell proliferation with any of the combinations. It is possible that a longer assay would reveal additional proliferative benefits of combination treatments.

Selected compounds induce SMA satellite cell proliferation *in vitro*

Since our ultimate goal is to identify compounds that increase satellite cell-mediated muscle growth for the treatment of SMA, we next wanted to determine if hit compounds from the screen are also capable of stimulating the proliferation of SMN-deficient satellite cells. Our previous work identified satellite cell proliferation deficits due to SMN deficiency, so it was possible that satellite cell-activating compounds would have limited effects on SMA satellite cells. Since it was not feasible to test all ~60 hits in SMA mice *in vivo*, we first performed preliminary *in vitro* drug testing of a selected subset of compounds on satellite cells derived from our *Pax7:SMN*-KD mouse model, which features tamoxifen-inducible SMN knockdown and tdTomato expression specifically in $Pax7^+$ satellite cells (Figure 2.4). Briefly, we treated adult *Pax7:SMN*-KD mice with tamoxifen over the course of one week, allowed a one-week chase period for SMN depletion and tamoxifen clearance, then FACS purified satellite cells based on tdTomato fluorescence expression (Figure 4.3A). tdTomato proved a strong reporter and allowed efficient separation of a discrete $tdTomato^+$ satellite cell population (Figure 4.3B). Satellite cells were seeded at low density and treated after 24 hours with a subset of 10

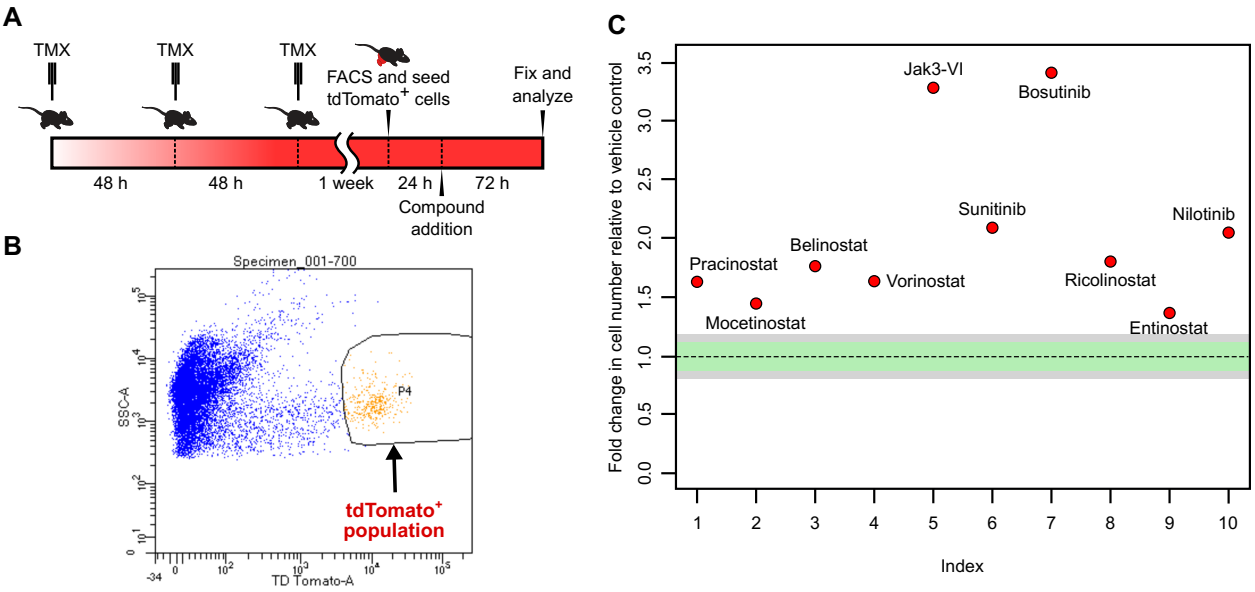

Figure 4.3. Selected compounds enhance the proliferation of SMN-deficient satellite cells. A) Schematic of satellite cell isolation from *Pax7:SMN*-KD mice and *in vitro* drug treatment. B) Representative FACS plot showing separation of distinct tdTomato$^+$ cell population (P4, yellow). The plot shows tdTomato expression on the X-axis and side scatter on the Y-axis. C) Dot plot showing the effect of 10 compounds on stimulating SMA satellite cell proliferation. The Y-axis represents fold change in satellite cell number relative to a DMSO control. The rectangles show 2X (green) and 3X (grey) the DMSO standard deviation. N=2 biological and 4 technical replicates per compound.

hit compounds identified in the screen, using optimal doses based on the dose response curves performed in wild type cells. Interestingly, all 10 compounds stimulated the proliferation of SMN-deficient satellite cells to a similar degree as observed in the wild type screen. For example, for both wild type and SMA satellite cells, bosutinib increased proliferation by ~4X, sunitinib by ~2X, and pracinostat by ~2X compared to a DMSO vehicle control (Figures 4.1C and 4.3C).

These results suggest that SMA satellite cells are indeed capable of proliferating in response to satellite cell-targeted compounds and can in some cases achieve robustly enhanced growth rates. In addition, it appears that multiple discrete compound classes are capable of stimulating SMA satellite cell growth, including HDAC inhibitors and tyrosine kinase inhibitors. Although we have not determined the mechanism by which these compounds increase SMA satellite cell growth, we believe

that increased growth is not simply due to increases in SMN levels, since these compounds show similar efficacy in both SMA and wild type cells with normal SMN levels.

Pracinostat increases satellite cell proliferation and ameliorates skeletal muscle atrophy in a severe SMA mouse model *in vivo*

We next wanted to determine if any of the hit compounds from the screen are capable of ameliorating muscle atrophy by increasing satellite cell-mediated skeletal muscle growth in SMA mice. We reasoned that we should first test an HDAC inhibitor, since HDAC-inhibition has previously been shown to improve several aspects of SMA pathology, including enhancing motor neuron function, muscle size and life span[126]. However, to our knowledge, no one has identified a role of satellite cells in mediating HDAC inhibitors' benefits in SMA. Since multiple HDAC inhibitors stimulated the proliferation of satellite cells in a cell-autonomous manner *in vitro*, and since the compounds worked on wild type satellite cells that express normal SMN levels, our approach could potentially represent an SMN-independent, satellite cell-targeted mechanism of action.

For this experiment, we selected pracinostat, a potent HDAC inhibitor that has never been tested in SMA. Pracinostat selectively inhibits all HDACs in Class I, II, and IV, with the exception of HDAC6, and is FDA-approved for acute myeloid leukemia[127]. We administered daily subcutaneous injections of 10 mg/kg pracinostat or a DMSO vehicle control to SMNΔ7 mutant and wildtype mice from birth until P14, which is the typical disease end-stage in untreated mice. Pracinostat treatment increased body weight of SMA mice at P14 by 35% (Figures 4.4A-B). However, pracinostat appeared to cause some toxicity, as evident by the reduced body weight of pracinostat-treated wild type mice. Therefore, it is possible that a lower pracinostat dose with fewer toxic side effects could result in an even more substantial rescue in body weight. Regardless, pracinostat treatment substantially improved motor strength of SMA mice as assessed by multiple behavioral assays, including a 56% improvement

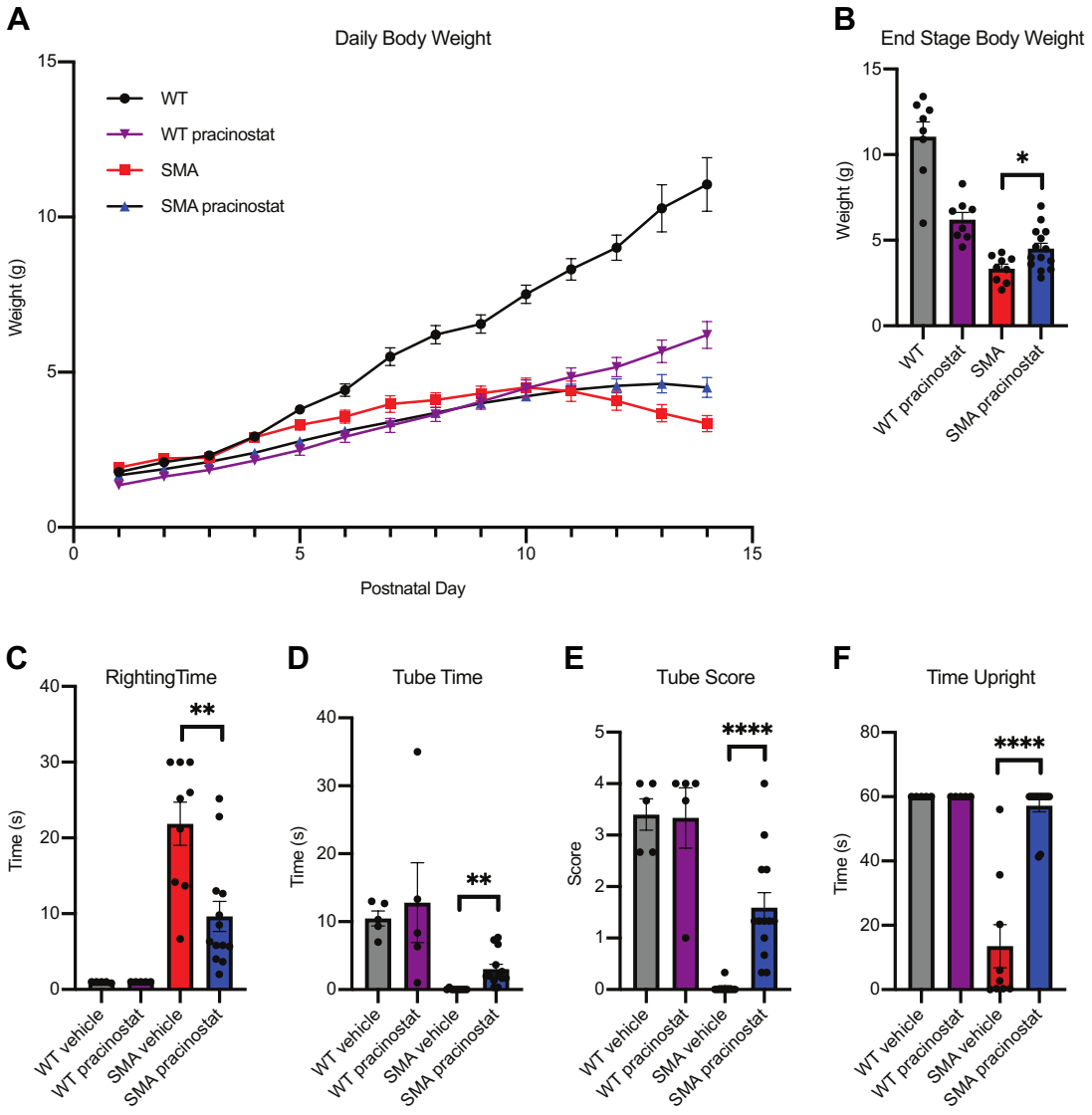

Figure 4.4. Pracinostat improves body weight and motor strength of severe SMNΔ7 mice *in vivo*. A) Daily body weight of SMNΔ7 mutant and wildtype mice treated with pracinostat or DMSO. B) End-stage (postnatal day 14) body weight. N=8-14 per group, p=0.0188, unpaired t test. C) Righting latency time. N=5-13 per group, p=.0011, Mann-Whitney test. D) Hind limb tube test. N=5-13 per group. p=0.0023, unpaired t test. E) Hind limb tube score test. N=5-13 per group, p=<0.0001, Mann-Whitney test. F) Time standing upright. N=5-13 per group, p=<0.0001, Mann-Whitney test. Data presented as mean ± SEM.

in righting latency, an 81-fold increase in hind limb suspension time, a 42-fold increase in hind limb scores, and a striking complete rescue of time standing upright (Figures 4.4C-F)[128].

We also observed a 27% increase in hind limb muscle fiber cross sectional area and a substantial 155-fold increase in the number and 113-fold increase in the percentage of proliferating

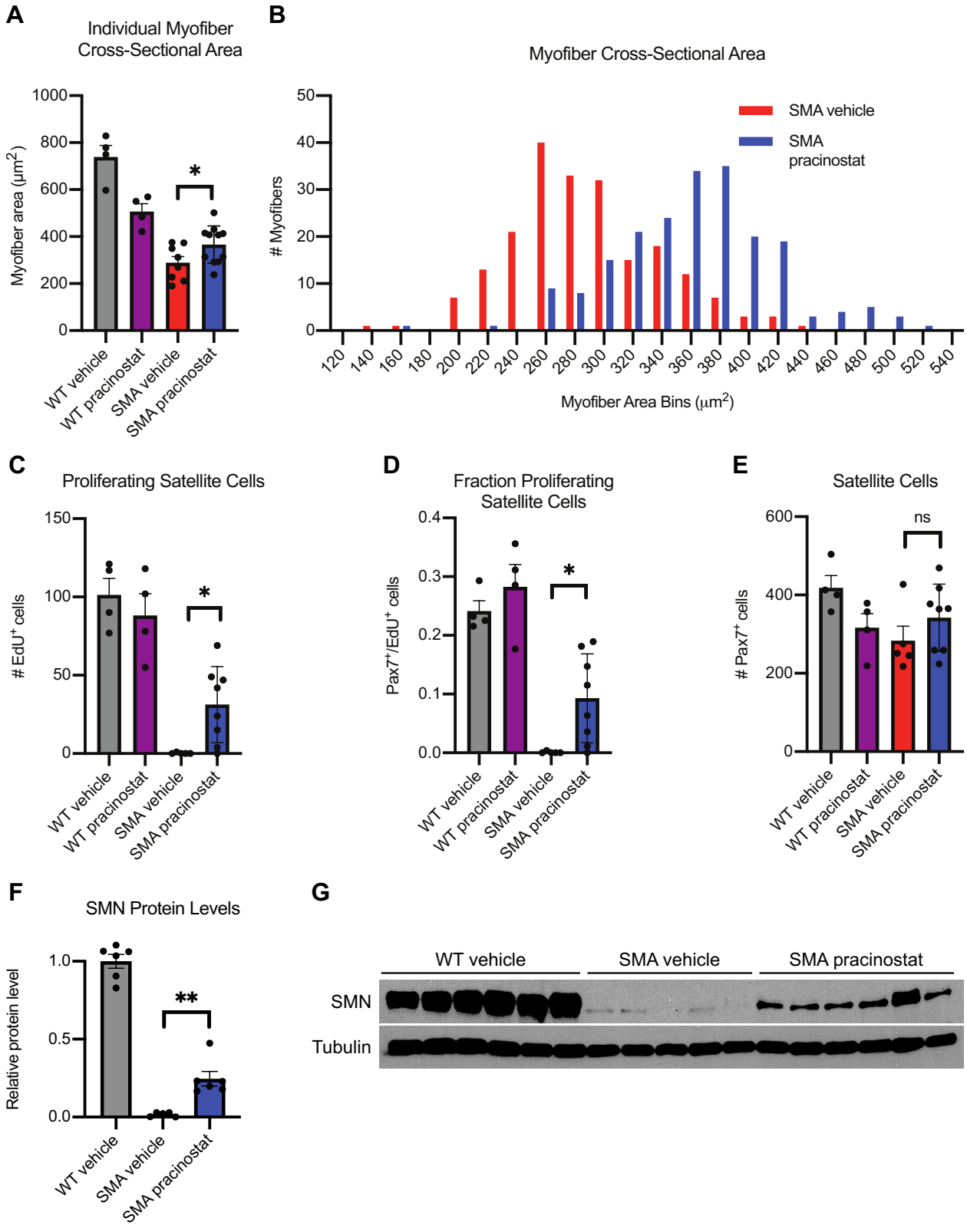

Figure 4.5. Pracinostat increases satellite cell proliferation and muscle fiber size in severe SMA mice *in vivo*. A) Quantification of individual tibialis anterior myofiber cross-sectional area.

Figure 4.5 (continued) N=4-11 per group, p=.0462, unpaired t test. B) Histogram showing distribution of individual myofiber cross-sectional area. C) Total number of proliferating EdU^+Pax7^+ satellite cells in hind limb muscle cross sections. N=4-8 per group, p= 0.0170, unpaired t test. D) Proportion of proliferating $EdU^+/Pax7^+$ satellite cells in hind limb muscle. N=4-8 per group, p= 0.0214, unpaired t test. E) Total number of $Pax7^+$ satellite cells in hind limb muscle cross sections. N=4-8 per group, p>0.05, unpaired t test. F-G) Western blot and quantification of relative SMN protein levels in wild type and SMNΔ7 mutant mice treated with a DMSO vehicle or pracinostat. Tubulin was used as a loading control. Data presented as mean ± SEM.

satellite cells, which represents an approximate 30-40% rescue to wild type levels (Figures 4.5A-E and Supplementary Figure 4.3). These results suggest that pracinostat is capable of improving satellite cell-mediated skeletal muscle growth, which is correlated with improvements in motor strength and body weight.

To determine if pracinostat treatment affected SMN levels, we performed western blotting of hind limb skeletal muscle tissue. We found that pracinostat resulted in a minor but significant increase in SMN expression. However, even with treatment, the total SMN protein levels were <25% compared to wild type mice (Figures 4.5F-G). Based on these results, we cannot completely exclude the possibility that pracinostat exerted its positive effect by ubiquitously increasing SMN levels. Regardless, we conclude that pracinostat is capable of stimulating satellite cell proliferation in a cell-autonomous manner, even in wild type cells that already express normal SMN levels, and that *in vivo* treatment substantially protects against the loss of proliferating satellite cells, ultimately leading to greater muscle size and strength.

We also tested six additional hit compounds from the screen in SMNΔ7 mice, including bosutinib, doramapimod, CEP-701, ralimetinib, AD80, and JQ1. Doses were selected based on the literature, although most previous studies tested these compounds in adult mouse models. Unfortunately, we found that the treatments either caused significant toxicity, thus preventing downstream analysis, or did not increase muscle fiber size (Table 4.1). This was not altogether surprising, given that all of these compounds are cancer therapeutics that cause cytotoxicity in various

cancer cells, and would likely be toxic in rapidly developing neonatal mice. Therefore, we will need to perform basic pharmacokinetic/pharmacodynamic studies in neonatal mice to optimize dosing for each compound before repeating these experiments.

Table 4.1. Small molecules tested in SMNΔ7 mice.

Drug	Dose	Treatment Days	Outcome
Bosutinib	25 mg/kg; daily	P5-P8	Fatally toxic in all mice
Doramapimod	10 mg/kg; daily	P3-P9	Fatally toxic in SMA mutants
CEP-701	10 mg/kg; daily	P9-P14	No effect on myofiber size
Ralimetinib	20 mg/kg; twice daily	P5-P8	Fatally toxic in all mice
AD80	10 mg/kg; daily	P5-P7	Toxic; terminated experiment
JQ1	5 mg/kg; daily	P5-P12	Toxic, terminated experiment

Pracinostat ameliorates skeletal muscle atrophy in the intermediate pharmacological SMA mouse model *in vivo*

Next, we wanted to determine if pracinostat is capable of stimulating skeletal muscle growth in an adult SMA mouse model. Because severe SMNΔ7 mice only live for two weeks, we could only assess the effects of pracinostat during the postnatal skeletal muscle growth phase, when satellite cells are already actively dividing[86]. Similarly, our screen was performed in satellite cells that were removed from their niche and were therefore entering a mitotically active state. Thus far, we have not determined if compounds that stimulate activated satellite cell proliferation are also capable of driving satellite cells out of quiescence. This is an important distinction, because adult satellite cells are typically quiescent under healthy conditions, suggesting that compounds that only stimulate proliferation of actively cycling satellite cells may have no effect on healthy, adult muscle. However, since it has been shown that long-term, chronic denervation leads to satellite cell activation, we believe it may be possible to stimulate satellite cell proliferation in SMA skeletal muscle tissue, even in the absence of acute muscle damage[107]. This would be important in considering treatment for older SMA

patients with milder forms of the disease, who are likely past the robust satellite cell proliferation phase of postnatal muscle development, which ends before the first year of life in humans[87].

To address this question, we used the intermediate "pharmacological" SMA mouse model. Pharmacological SMA mice are standard SMNΔ7 mice treated daily with a low dose of C1, an SMN-elevating small molecule originally developed and currently undergoing clinical trials by Roche[70]. Low C1 doses slightly boost SMN levels in severe SMA mice, enabling them to live up to 5-6 weeks and resulting in a milder SMA phenotype. This mouse model has been used in SMA preclinical studies to demonstrate drug efficacy of both SMN-elevating and SMN-independent, tissue-targeted compounds[79,129]. SMNΔ7 mutant and wild type littermate control mice were treated daily with 0.1 mg/kg C1 by subcutaneous injection from P1-P42. Mice were additionally treated once daily with 10 mg/kg pracinostat or DMSO from P24-P42. We selected P24 as a starting point, since postnatal skeletal muscle growth is completed and satellite cells become quiescent by P21[86].

We found that pracinostat treatment did not improve body weight and may have actually caused moderate toxicity in SMA mice, as demonstrated by a moderate loss in body weight throughout the experiment (Figure 4.6A). In addition, pracinostat treatment did not increase the size of myofibers in the hind limb TA muscle (Figure 4.6B). However, we did observe a significant 18% increase in myofiber size of the semispinalis muscle, a proximal muscle located in the neck that we previously found to be severely denervated and atrophic in SMA mice (Figures 4.6C-D and Supplementary Figure 4.4)[55]. In addition, we observed a small percentage of centrally nucleated myofibers in both DMSO and pracinostat-treated semispinalis muscles, suggesting that there is a low rate of satellite cell-mediated muscle regeneration in this chronic, adult SMA model (data not shown). Overall, pracinostat treatment ameliorated muscle atrophy in a more severely affected muscle, but it did not uniformly improve skeletal muscle size. Given the moderate toxicity observed, it will be important to repeat this experiment with a lower dose and a longer treatment window.

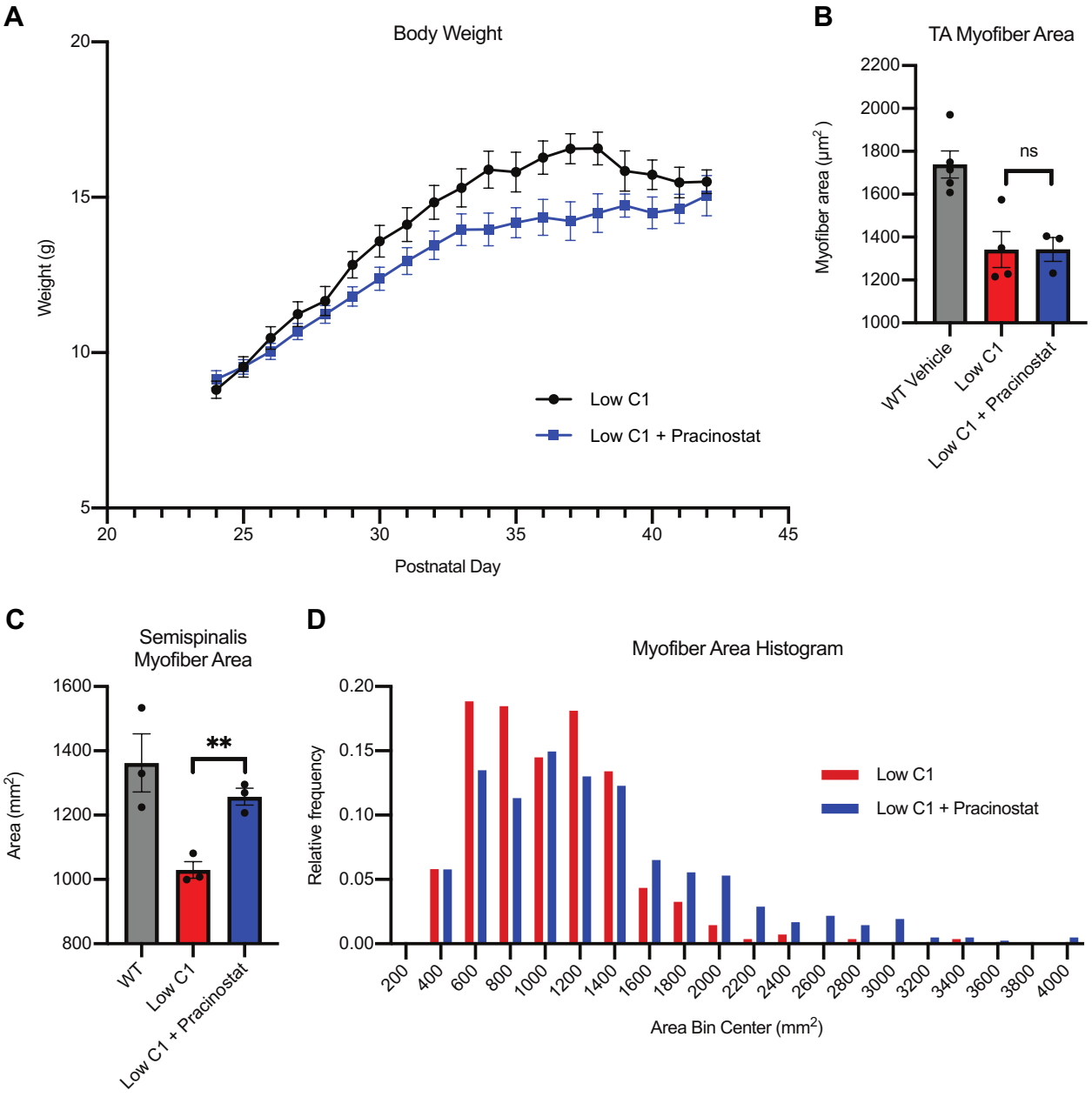

Figure 4.6. Pracinostat ameliorates muscle atrophy in intermediate pharmacological SMA mice *in vivo*. A) Daily body weight of SMNΔ7 mutant mice treated with a low dose of C1 only or a low dose of C1 and 10 mg/kg pracinostat. B) Hind limb TA individual myofiber area at P42. N=3-5 per group, p=>0.05, unpaired t test. C) Semispinalis individual myofiber area at P42. N=3 per group, p=.0035, unpaired t test. D) Histogram showing distribution of semispinalis individual myofiber cross-sectional area. Data presented as mean ± SEM.

In addition to pracinostat, we tested CEP701 in the pharmacological SMA model. We previously demonstrated that this tyrosine kinase inhibitor stimulated wild type satellite cell proliferation *in vitro* and increased muscle size and satellite cell number *in vivo* in a model of muscle trauma (Buchanan and Price et al., manuscript in preparation). Twice daily, subcutaneous 10 mg/kg CEP701 injections were administered as described above. Unfortunately, we did not observe any benefits of CEP701 treatment in terms of body weight or myofiber size improvements (Supplementary Figure 4.5). It is possible that the dose selected was not optimally effective, or that CEP701 is not capable of acting on a satellite cell population that is mostly quiescent.

Hit compounds target known satellite cell-activating pathways

Lastly, we wanted to characterize the molecular pathways targeted by the hit compounds in our screen. We previously found that annotations for compounds in chemical libraries are often not all-inclusive and can be misleading, particularly because most mechanistic work on compounds is performed in cancer cells. For example, we previously found that the known FLT3 inhibitor CEP701 robustly stimulates satellite cell proliferation. However, after extensive mechanistic work to elucidate the role of FLT3 inhibition in satellite cell growth, we discovered that FLT3 is not expressed in satellite cells, and CEP701 was in fact exerting its effect through the entirely distinct GDNF/RET signaling pathway (Buchanan and Price et al., manuscript in preparation).

Therefore, we used an unbiased bioinformatics approach to reveal the pathways most likely involved in mediating the satellite cell proliferative effect of our compounds. First, we ran a clustering algorithm to group drugs based on shared protein interactions, using data from the STITCH protein-chemical interaction database[130]. Protein-chemical associations are based on a number of factors, such as co-expression or text-mining data, but we only selected interactions that met a high confidence threshold set by the database. We found that most compounds separated into distinct branches

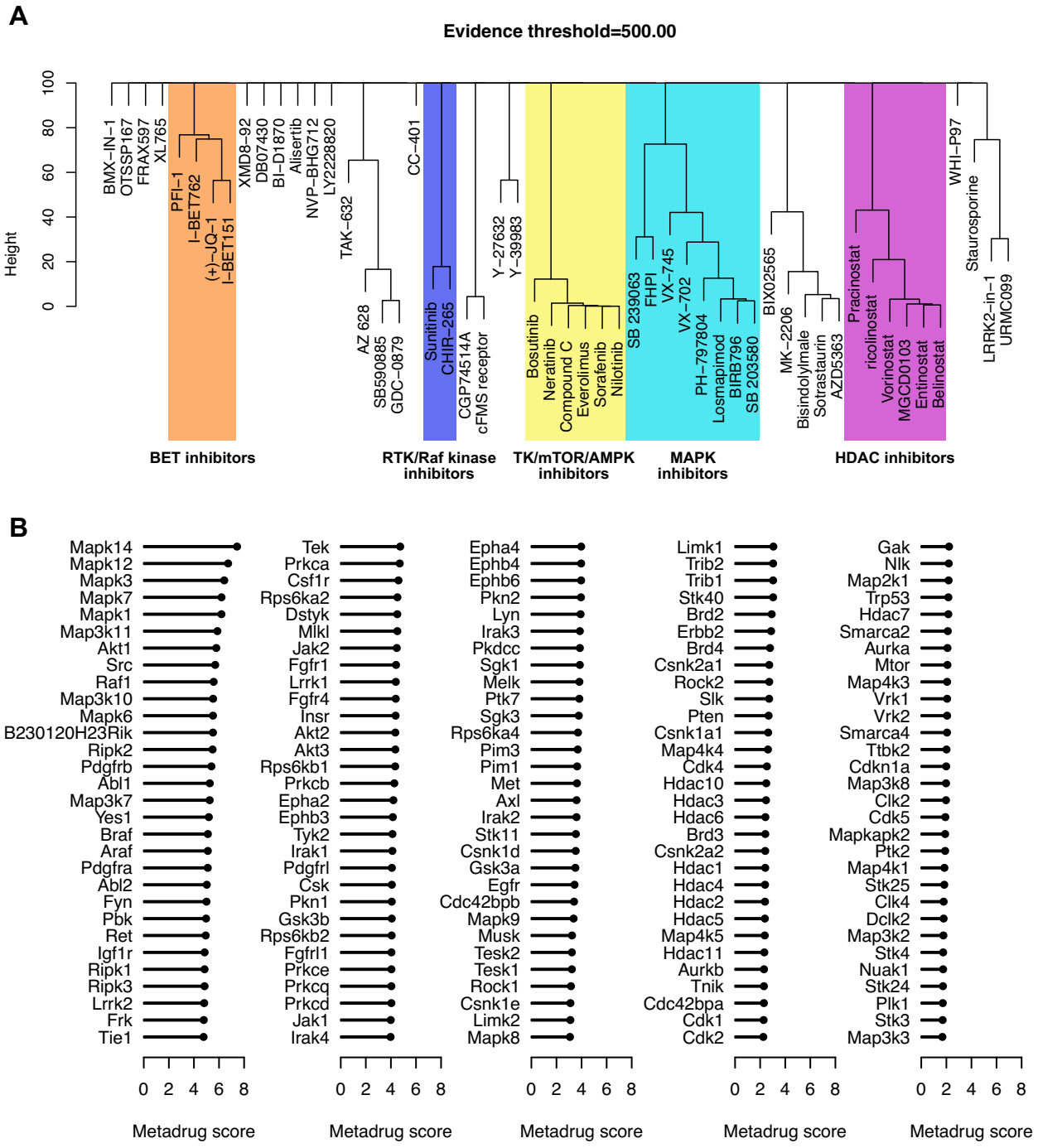

Figure 4.7. Bioinformatics analysis of satellite cell proliferating hit compounds. A) Unbiased clustering of hit compounds based on shared protein associations annotated in STITCH. B) Frequency of proteins associated with hit compounds. The Y-axis represents the number of distinct "metadrug" classes that are associated with each protein. Metadrug profiles were generated by clustering hit compounds into 10 profiles based on shared protein associations. This normalization corrects for a bias towards pathways targeted by highly similar compounds.

representing known compound classes (Figure 4.7A). For example, all of the HDAC inhibitors separated into a distinct branch and 4 known BET inhibitors split out into their own branch. These results helped us rapidly characterize distinct molecular pathways represented by our hits.

Next, to reveal molecular targets potentially involved in satellite cell proliferation, we overlapped the drug-protein interactions with satellite cell RNA-sequencing data previously generated in our lab. We then created a list of the proteins most frequently associated with the hits that are also expressed in satellite cells (Figure 4.7B). As a positive control, we confirmed that this analysis successfully filtered out FLT3, the annotated target of CEP701 that we previously found to be dispensable for mediating the satellite cell proliferation effect.

Interestingly, even compounds with distinctly different protein-association profiles converged onto common satellite cell growth pathways. For example, the top proteins on the list were mitogen-activated protein kinase (MAPK) family members, such as Mapk12, Mapk14, and Mapk3. This is of particular interest, since p38-MAPK signaling has been shown to regulate multiple myogenic stages, from satellite cell quiescence to terminal myogenic differentiation[131]. In fact, the hits that produced the greatest fold changes in the screen were p38 inhibitors VX-702 and doramapimod. Other proteins high on the protein-chemical list included Ret and Jak2, both previously shown to regulate myogenesis[132,133]. These results suggest that the combination of phenotypic drug screening, RNA-sequencing, and unbiased bioinformatics analysis of protein-chemical interactions may be useful for uncovering interesting biological mechanisms governing cell behavior. Overall, this analytical approach will serve as a basis for follow-up mechanistic experiments and future screens on broader compound class libraries.

Discussion

Satellite cell-targeted therapy for SMA

In this study, we identified novel compounds across distinct drug classes that stimulate wild type and SMA satellite cell proliferation *in vitro*, and demonstrated that systemic treatment with the HDAC-inhibitor pracinostat increased satellite cell proliferation and skeletal muscle size in SMA mice. We also identified nilotinib, bosutinib, sunitinib, and JAK3 inhibitor VI as compounds capable of stimulating SMA satellite cell proliferation *in vitro*. Given that all of the compounds tested in SMA satellite cells increased proliferation to a similar degree as in wild type cells, it is likely that many more hits from the screen will also be able to proliferate SMN-deficient muscle cells. These results provide a promising proof-of-concept that small molecule-based, satellite cell-targeted therapy could potentially stimulate skeletal muscle growth for the treatment of SMA. Furthermore, this study represents one of the few instances reported to date of utilizing small molecules that specifically target skeletal muscle stem cells to increase muscle growth. This approach may have broad applications for the treatment of other muscle disorders, such as ALS, DMD, acute trauma, or age-related sarcopenia.

Going forward, it will be important to determine if satellite cells in SMA patients are capable of responding to pro-proliferative agents. Our compound screen was performed on satellite cells that were freshly removed from the niche and were thus entering a mitotically active state. At this point, we do not know if our hit compounds have any effect on quiescent satellite cells, since different pathways regulate quiescence versus proliferation. Therefore, we need to determine if satellite cells in SMA patients ever exist in an activated state. We believe that this is possible, since chronic denervation is known to activate satellite cells, and because we observed small numbers of centrally nucleated fibers in denervated muscles of adult SMA mice. Furthermore, the fact that pracinostat improved muscle size in denervated but not innervated muscles suggests that its effect may have been mediated

through activated, but not quiescent, satellite cells. In future studies, we aim to characterize satellite cell activity in SMA patient muscle tissue.

In addition, it will be important to consider satellite cell-targeted therapy as a combination with SMN elevation, which is clearly critical for promoting motor neuron survival. Furthermore, given that SMN deficiency causes premature differentiation and myoblast fusion deficits in addition to proliferation deficits, merely boosting satellite cell production may not be sufficient to enhance muscle growth in SMA patients. In future studies, we plan to test the combination of satellite cell-targeted compounds plus a peripheral SMN-elevating therapeutic like AVXS-101.

Understanding satellite cell-targeting pathways

Using a bioinformatics approach to characterize our hit compounds, we identified several known pathways that regulate satellite cell proliferation, such as p38-MAPK, JAK-STAT, and FGF signaling[131,132,134-136]. The fact that discrete drug classes emerged in our screen suggests that various molecular mechanisms can be leveraged to pharmacologically enhance satellite cell-mediated skeletal muscle growth. However, before translating these compounds into therapies, we need to first elucidate the mechanisms by which each compound exerts its pro-proliferative effect. For example, p38-MAPK signaling is critical for driving myogenic differentiation, since it inhibits the proliferation-inducing JNK pathway[137]. Therefore, while p38-MAPK inhibitors enhance satellite cell proliferation, they also prevent myoblast fusion into myotubes. In such cases, cyclic instead of sustained delivery may be optimal. Understanding these types of nuances will be critical for determining their potential benefit in SMA patients.

Author Contributions:

Rebecca Gibbs[1,2], Dr. Lee Rubin[1,2], Dr. Feodor Price[1,2] and Dr. Chien-Ping Ko[3] designed experiments. Dr. Feodor Price and Erica Wolin[1,2] performed initial satellite cell drug screen and dose response experiments. LINCS compound libraries were provided by Dr. Peter Sorger[4] and were prepared by Stuart Rudnicki[5] and Jen Smith[5]. Lovelace J. Luquette[6] and Rebecca Gibbs performed bioinformatics analysis of drug hits. Dr. Zhihua Feng[3] performed pharmacological SMA mouse model drug injections. All other experiments were performed and analyzed by Rebecca Gibbs.

[1] *Department of Stem Cell and Regenerative Biology, Harvard University, Cambridge, MA*

[2] *Harvard Stem Cell Institute, Cambridge, MA*

[3] *Department of Biological Sciences, University of Southern California, Los Angeles, CA*

[4] *Department of Systems Biology, Harvard Medical School, Boston, MA*

[5] *ICCB-Longwood Screening Facility, Harvard Medical School, Boston, MA*

[6] *Department of Biomedical Informatics, Harvard Medical School, Boston, MA*

CHAPTER 5

DISCUSSION

Summary of dissertation

In this dissertation, we sought to understand the role of satellite cell and skeletal muscle defects in SMA, and to envision novel stem cell-mediated therapeutic methods for ameliorating muscle atrophy. In Chapter 2, we demonstrated that satellite cells undergo defective proliferation during postnatal development in a mouse model of SMA featuring ubiquitous SMN deficiency. This proliferative defect begins during early symptomatic stages, coinciding with the onset of skeletal muscle growth deficits and worsening over time, until the number of activated satellite cells becomes completely depleted. Satellite cells seem unable to complete myogenic differentiation and fusion, instead accumulating in the interstitial spaces between muscle fibers. This phenotype thus results in muscle fibers that are not only smaller, but that contain drastically reduced numbers of nuclei. Using two novel satellite cell-conditional models of SMN depletion, we further demonstrated that SMN is required for normal satellite cell function. While complete loss of SMN causes satellite cell death and renders the muscle unable to repair from damage, disease-relevant levels of SMN deficiency also impair satellite cell proliferation, muscle regeneration and force production after damage.

In Chapter 3, we extended our explorations of skeletal muscle deficits to SMN-deficient human tissue. Specifically, we identified SMN-dependent myogenic deficits in SMA patient-derived iPSCs, including reduced production of myoblasts and impaired myotube formation. The results from Chapters 2 and 3 raised the question of whether or not the reduced production of myogenic precursors would deplete the satellite cell pool over time in SMA patients. Fortunately, we found that abundant numbers of satellite cells still exist in SMA patient muscle tissue, even at the disease end stage, although the myogenic potential of these cells remains to be determined.

Finally, in Chapter 4, we searched for new therapeutic agents capable of ameliorating skeletal muscle atrophy in SMA. We performed a phenotypic screen for pro-myogenic agents and identified 61 compounds, 10 of which successfully stimulated SMA satellite cell proliferation *in vitro*. We

additionally determined that treatment with pracinostat, an HDAC inhibitor, substantially increased satellite cell proliferation and muscle size in SMA mice *in vivo*. These promising results suggest that satellite cell-targeted therapeutics may be capable of enhancing skeletal muscle growth for the treatment of SMA.

Proposed model of satellite cell defects in SMA

As a whole, our data supports the following model: the loss of SMN in satellite cells and myoblasts decreases their proliferation, possibly due to premature terminal differentiation, which leads to insufficient production of functional myogenic precursors during the postnatal period. These deficits lead to reduced myonuclear accretion, thus impeding skeletal muscle growth. Simultaneously,

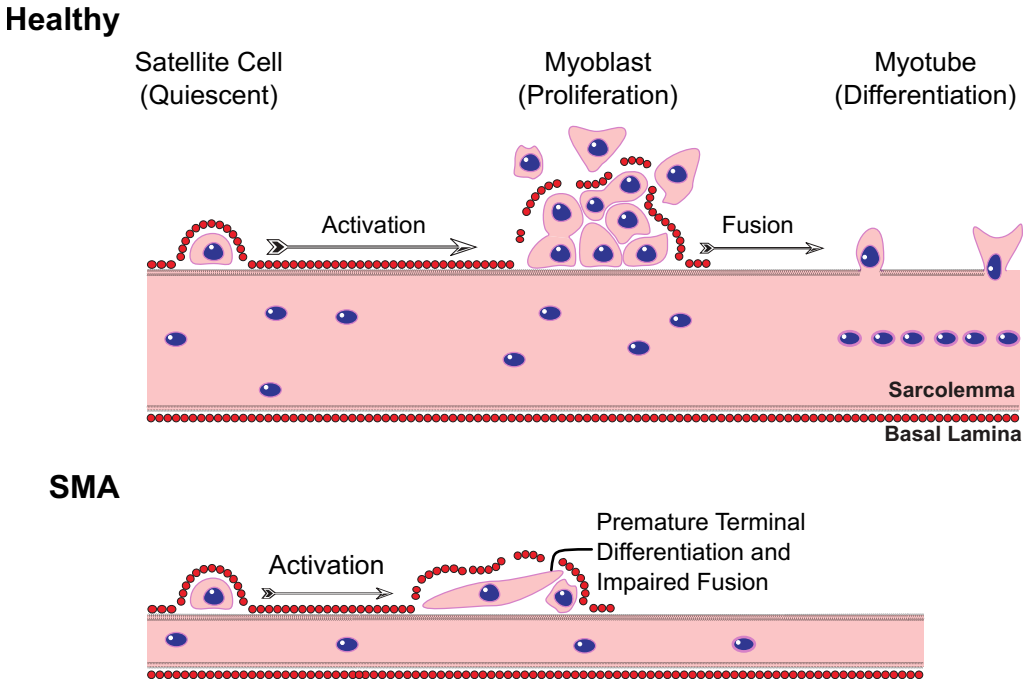

Figure 5.1. Proposed model of satellite cell-dependent muscle growth defects in SMA. In healthy muscle, proliferating satellite cells and myoblasts differentiate and fuse with myofibers to increase muscle size. In SMA, premature differentiation, reduced proliferation, and impaired myocyte fusion decreases myonuclear accretion and muscle growth. Figure generated by co-author Dr. Feodor Price.

in certain severely affected muscles, motor axon degeneration and neuromuscular junction denervation leads to muscle atrophy. The reduced muscle growth combined with atrophy secondary to motor neuron death causes the profound loss of strength characteristic of SMA.

In addition to a muscle development issue, our findings that inducible SMN knockdown impairs regeneration in adult mice suggest that SMA may also present with a muscle maintenance issue. In healthy adults, satellite cells activate and turnover at a low rate to maintain muscle mass. In the TA hind limb muscle of mice, approximately 20% of fibers are maintained by satellite cell turnover over a period of two weeks[100]. Muscle maintenance is not typically discussed in the context of SMA, as the profound atrophy due to motor neuron death is the leading pathogenic driver. However, as patients treated with SMN-elevating therapeutics begin living longer, it will be important to ensure that they are capable of maintaining normal muscle mass. In future studies, it would be interesting to administer tamoxifen to adult *Pax7:SMN*-KD mice and assess muscle health over long periods of time in the absence of muscle damage. This would allow us to determine if SMN deficiency directly impairs muscle maintenance independent of neurodegeneration.

Do satellite cell defects exacerbate neuromuscular defects?

It is well appreciated that motor neurons are important for supporting muscle health, as their loss leads to muscle atrophy and eventual satellite cell depletion[107,108]. Aside from motor neuron death, hallmark characteristics of SMA mice include neuromuscular junction denervation, impaired synaptic transmission, and accumulation of neurofilament protein at motor end terminals[55,56,105]. In addition, SMN deficiency arrests the maturation of NMJs, which remain largely in an immature plaque-like formation instead of progressing to a mature pretzel-like morphology (Figure 1.3)[34]. While motor neurons significantly contribute to neuromuscular phenotypes, it is interesting to consider whether defective satellite cell function exacerbates motor neuron and neuromuscular junction defects in SMA,

in addition to directly impairing muscle maturation. In a series of fascinating studies performed in wild type mice, it was shown that satellite cells play an important role in neuromuscular junction innervation and maturation after nerve damage. The authors expressed tamoxifen-inducible, Cre-mediated diphtheria toxin-A in satellite cells to deplete them in adult mice, then performed sciatic nerve transection and tracked neuromuscular regeneration[95,106]. Interestingly, satellite cell depletion significantly exacerbated muscle atrophy and loss of force production after nerve damage. Furthermore, satellite cell depletion nearly doubled the percentage of motor endplates that were denervated and displayed an immature, plaque-like morphology. These phenotypes are reminiscent of those observed in multiple SMA models. Therefore, if satellite cells are completely dysfunctional, as they appear to be at the end stage in SMNΔ7 mice, this may exacerbate neuromuscular deficits in SMA.

Intriguingly, several SMA studies support this possibility. First, we previously demonstrated that initial NMJ formation is not impaired in muscles that eventually become denervated in SMNΔ7 mice[55]. Instead, the nerve-muscle contacts are initially formed during late embryonic stages, but then lost several days after birth. Another study ubiquitously knocked down SMN in adult mice and performed a sciatic nerve crush[75]. In the absence of normal SMN, motor axon regeneration and contact with muscle proceeded normally. Fascinatingly, however, the reformed NMJs in SMN deficient mice failed to mature, remaining in an arrested and fragmented state. Although the loss of SMN in motor neurons impairs synaptic integrity, the similarities between these studies and the satellite cell depletion studies warrant further investigation into the role of satellite cells in stabilizing NMJs in SMA.

Conflicting evidence from the literature

Some studies have concluded that skeletal muscle does not play an important role in SMA pathology. For example, one study demonstrated that SMN restoration under the human skeletal actin (HSA) promoter provided no improvements in motor behavior or survival of SMA mice, and did not increase muscle fiber size[89]. However, since HSA is only expressed in mature, fully formed muscle fibers, this study did not account for the effect of SMN loss in myogenic precursors during muscle growth. In fact, when SMN was restored in all myogenic precursors, including satellite cells and myoblasts, muscle fiber size in SMA mice was completely corrected to wild type levels[61]. Therefore, satellite cells and myoblasts may be more critical as targets of SMN-enhancing therapeutics than muscle fibers themselves.

Another study did not demonstrate any skeletal muscle defects after Myf5-driven, Cre-mediated *mSmn* knockdown[138]. This study was designed to reduce SMN in all myogenic precursors, since Myf5 is the earliest myogenic determination transcription factor expressed in the dermomyotome of the developing somite[139]. However, Myf5 is actually not expressed in all satellite cells. Lineage tracing studies have shown that 10% of $Pax7^+$ satellite cells never expressed Myf5, and that the $Pax7^+/Myf5^-$ cell population is actually more likely to repopulate the satellite cell niche, while the $Pax7^+/Myf5^+$ population is more likely to terminally differentiate[84]. This suggests that SMN knockdown driven by Myf5 would leave a small population of healthy satellite cells that are highly capable of proliferating and maintaining their stemness. Furthermore, in this study, SMN was only knocked down to ~30% of wild type levels, which was an approximate 3-fold increase relative to SMA mice. Therefore, it is possible that lower levels of SMN across all myogenic precursors would cause a skeletal muscle defect.

SMN threshold hypothesis

The aforementioned discrepancies highlight the fact that different cell types have differential tolerance for SMN deficiency. In fact, SMN expression substantially varies temporally, across tissues, and even within a specific cell population[110,140]. For example, in the severe "Taiwanese" SMA mouse model, which features ubiquitous SMN knockdown, SMN levels are initially highest in the brain and spinal cord at P2, but decrease significantly until P8, whereas SMN levels in the muscle and kidney are initially quite low and decrease even further over time[140]. The differential SMN threshold required for normal development and survival might underlie the selective susceptibility of motor neurons to SMN deficiency, and suggests that skeletal muscle may be relatively tolerant to the loss of SMN. Our data from Chapter 2 supports this hypothesis. When SMN was depleted completely in satellite cells of the *Pax7:SMN*-KO mouse model, we observed a severe muscle regeneration phenotype, leading to a complete absence of muscle fibers three weeks after cardiotoxin damage. However, when SMN was reduced to ~10% of controls, similar to levels observed in Type I SMA patients, muscle regeneration recovered substantially. We still observed significant satellite cell proliferation and muscle growth deficits, but the phenotype was far less severe than in the case of total SMN knockout. Therefore, while SMN deficiency impairs satellite cell-mediated muscle growth, muscle is more resistant than motor neurons to the loss of SMN.

Pro-myogenic effects of HDAC inhibition for the treatment of SMA

Our screen identified a large number of compounds across multiple drug classes that increase satellite cell proliferation, and our bioinformatics analysis demonstrated that these compounds collapse onto a subset of discrete pathways known to modulate satellite cell activity. These signaling pathways include FGF, p38-MAPK, and JAK/STAT[132,134,135,141,142]. In addition, a large number of hits were HDAC inhibitors, suggesting that this pathway may also be important for satellite cell

proliferation. Myogenesis is indeed regulated at multiple stages by various epigenetic mechanisms, including histone modifications and DNA methylation[137]. Similar to other stem cells, quiescent satellite cells are primed for lineage progression, with chromatin maintained in a transcriptionally permissive state[143,144]. For example, several myogenic determination genes, including MyoD and Myf5, contain activation histone marks at their transcription start sites, although they remain transcriptionally silent[145]. In proliferating myoblasts, however, myogenic differentiation genes contain histones with HDAC-catalyzed repressive marks, thus preventing terminal myogenic differentiation. For example, class I HDACs associate with MyoD and class II HDACs associate with MEF2 to inhibit myoblast differentiation[143,146]. Clearly, HDACS play an important and complex role in regulating myogenesis, but exactly how HDAC inhibition stimulates proliferation of activated satellite cells remains to be determined.

In addition, further studies are needed to understand if pracinostat directly targeted satellite cells to enhance muscle growth *in vivo*, or if the effects were mediated through a different mechanism, such as SMN upregulation in motor neurons. Multiple HDAC inhibitors have been shown to increase *SMN2* promoter activity and upregulate SMN expression, and we observed a slight increase in SMN protein in SMA muscle treated with pracinostat[126]. Given our findings that even small increases in SMN can dramatically improve muscle regeneration after damage, it is possible that this marginal SMN increase improved satellite cell function, in addition to promoting motor neuron survival. Regardless, we believe that HDAC inhibition is capable of directly stimulating satellite cell-autonomous proliferation independent of SMN, because multiple HDAC inhibitors had pro-proliferative effects on purified wild type satellite cells.

An alternative possibility is that HDAC inhibition mediates its benefit by blocking the expression of pro-atrophy genes. Previous studies have shown that in response to denervation, the upregulation of HDAC4 results in downstream activation of myogenin and muscle-specific

atrogenes[147]. In SMA mice, myogenin upregulation directly activates atrogene expression, and treatment with an HDAC inhibitor blocks atrogene promoter activity in myoblasts[104]. Therefore, in addition to SMN upregulation, HDAC inhibition may suppress myogenin-mediated atrogene induction in muscle, thus protecting against atrophy. If pracinostat had the same effect in our mouse models, this pathway could have contributed to the muscle growth we observed.

HDAC inhibitors have actually failed in clinical trials of SMA, presumably because they did not sufficiently rescue SMN levels[148,149]. However, with the recent FDA approval of nusinersen and AVXS-101, it would be interesting to determine if HDAC inhibition or other satellite cell-targeting mechanisms could complement SMN elevation to enhance muscle growth.

Therapeutic implications of satellite cell defects in SMA

Altogether, there are several interesting therapeutic implications of our work when placed in the context of the SMA literature. First, our results highlight the importance of systemic SMN restoration, and raise the concern that nusinersen, which is intrathecally administered, may not sufficiently protect against muscle-intrinsic growth deficits. Fortunately, two orally-bioavailable, SMN2 splice modifiers that are in clinical development show great promise for increasing SMN systemically[62].

Second, since satellite cells are major culprits responsible for muscle hypotrophy, merely elevating SMN levels in muscle that has already been formed, as in the case of all patients with milder forms of SMA, may not enhance muscle growth. Satellite cells become mostly quiescent after postnatal development, and it is unlikely that SMN elevation would drive these cells out of quiescence in the absence of external activating signals, such as those that occur after muscle damage. Interestingly, many studies have identified a critical early neonatal window within which SMN restoration is most beneficial. For example, in severe SMNΔ7 mice, SMN restoration at P4 increased median survival to

139 days, whereas SMN restoration at P10 resulted in no survival benefit[74]. This critical window has been attributed to the extent of damage/lack of maturation at the neuromuscular junction[75]. However, this period is clearly defined by robust postnatal skeletal muscle growth as well. Therefore, early correction of myogenic defects before satellite cells become quiescent may also contribute to the critical window of SMN restoration.

Third, in SMA patients living with chronic denervation for long periods, as is the case with any currently living SMA Types II-IV patients, it is possible that the satellite cell pool may be significantly reduced or have lost myogenic potential. This is the phenotype we observed in end-stage SMA mice, which contained reduced numbers of $Pax7^+$ satellite cells and a near complete absence of actively proliferating satellite cells. Additional studies are needed to determine if these satellite cells are capable of re-activating, or if they are instead senescent, terminally and irreversibly differentiated, or dying. Fortunately, we did observe substantial numbers of $Pax7^+$ cells remaining in human SMA patient muscle biopsies, but the myogenic potential of these cells remains to be determined. Since SMA pathologies present with a range of clinical severities, it is likely that satellite cell health may differ between older versus younger patients and severe versus intermediate/mild patients. Regardless, there are a number of muscle-targeted therapies that do not rely on satellite cell activation, instead directly bulking up muscle fibers via myostatin-inhibition or increasing muscle contractility. Such therapeutic agents hold promise for increasing muscle strength for a wide range of SMA patients.

Lastly, our findings suggest that it would be beneficial to devise a therapeutic strategy that increases the number of functional satellite cells in SMA muscle. Since satellite cell transplant therapy is neither existent nor feasible for a disease with such widespread muscle atrophy, our small molecule-based, satellite cell-targeted approach may prove beneficial. Indeed, we identified many compounds capable of proliferating satellite cells in a cell-autonomous and SMN-independent manner. However, such a therapy would need to be combined with SMN-elevating therapy, which is clearly important

for preventing motor neuron death. Furthermore, since SMN deficiency not only reduces satellite cell proliferation, but also impairs myoblast fusion into multinucleated myotubes, it would be important to both boost satellite cell proliferation and ensure that the satellite cells retain full myogenic function.

Feasibility of small molecule-based, satellite cell-targeted therapy

Stem cell-based regenerative medicine approaches are usually discussed in the context of cell transplant therapies[150,151]. In the skeletal muscle field, many cell-based therapies have been explored to combat muscle injury and disease, including the development of engraftable cells of both myogenic and non-myogenic origins. However, cell-based approaches are still hindered by many technical limitations, and none of these methods have been FDA-approved[152].

Therefore, the alternative approach of using systemically delivered therapeutic agents to modulate satellite cells and myoblasts *in situ* holds great promise. In the skeletal muscle field, growth factors have been administered to improve muscle repair after damage. For example, prolonged release of biomaterial-encased hepatocyte growth factor (HGF), which activates quiescent satellite cells and promotes their proliferation, improved muscle remodeling in a volumetric muscle loss injury model[153]. Insulin-like growth factor-1 (IGF-1) acting locally within skeletal muscle has been shown to stimulate satellite cell proliferation and muscle hypertrophy, and in SMNΔ7 mice, its overexpression increased muscle mass and improved survival[154,155]. Aside from growth factors, several satellite cell-targeted small molecules have proven efficacious at repairing muscle damage. For example, intramuscular injection of JAK-STAT inhibitors, which stimulate satellite cell proliferation *in vitro*, enhanced muscle repair and force generation after injury[132]. In our lab, we demonstrated that the RET-inhibitor CEP701 increased satellite cell proliferation and increased muscle size after damage (Buchanan and Price et al., manuscript in preparation).

Outside of the skeletal muscle field, other stem cell-targeted therapeutics are under investigation. For example, multiple small molecules have been identified that target oligodendrocyte progenitor cells (OPCs) to improve remyelination in multiple sclerosis (MS) models[156,157]. In addition, small molecules have been identified that stimulate the expansion of cochlear supporting cells, which differentiate into functional hair cells of the inner ear[158]. One such molecule is now in a Phase II clinical trial for the treatment of sensorineural hearing loss[159]. Altogether, the results of our study and others in the literature paint an optimistic picture for the use of satellite cell-targeted therapeutic agents for the treatment of muscle disorders.

Remaining hurdles for satellite cell-targeted therapy

Developing a satellite cell-targeted therapeutic paradigm will require additional knowledge about skeletal muscle pathologies in SMA. Specifically, we need to understand if satellite cells in SMA ever exist in an activated state due to chronic denervation or other pathological processes (i.e., if skeletal muscle in SMA behaves as if it is damaged). Our compound screen was performed on satellite cells that were freshly removed from the niche and were thus in an activated state. It is highly possible that these compounds may not have a pro-proliferative effect on quiescent satellite cells, as different pathways are responsible for maintaining quiescence versus supporting proliferation. In fact, our *in vivo* pracinostat results suggest that this may be a concern. In neonatal SMNΔ7 mice, which have actively proliferating satellite cells, pracinostat treatment increased muscle size. However, in the adult SMA model, pracinostat only improved denervated but not innervated skeletal muscle. We have not yet assessed the status of satellite cells in the adult model, but our results suggest that satellite cells may remain quiescent in fully innervated muscles. If satellite cells are not activated in SMA patients, we may need to develop therapeutic methods to drive satellite cells out of quiescence.

Developing a satellite-cell targeted approach will also require overcoming several technical hurdles. For example, many of the compounds identified in our screen are cancer drugs with cytotoxic effects in non-satellite cell types. Unsurprisingly, many of these promiscuous compounds were toxic in rapidly developing neonates when administered *in vivo*, since these compounds have broad effects across many tissues. Therefore, we are not necessarily proposing that any one of these specific molecules be advanced clinically. Instead, future studies should elucidate the mechanisms by which these compounds induce satellite cell proliferation, followed by the development of more targeted therapeutics acting on these pathways.

Consideration should also be given to how satellite cell-targeted therapies would be administered. Since satellite cells do not need to be continuously activated to enhance muscle growth, chronic treatment may not be necessary. Instead, cyclic treatment could potentially be administered as needed to increase myonuclear accretion. However, given that SMN deficiency causes premature terminal differentiation, there is a concern that artificially enhancing satellite cell proliferation could exhaust the stem cell pool. In future studies, it will be important to test the effects of satellite cell-targeted compounds *in vivo* over long-term treatment regimens.

Broader applications for satellite cell-targeted therapies

Aside from SMA, satellite cell-targeted therapy may be beneficial for other diseases that cause muscle weakness. Defective satellite cell function has been identified in many other muscle disorders. For example, in a severely symptomatic mouse model of X-linked myotubular myopathy, a severe congenital myopathy resulting from myotubularin deficiency, satellite cells were shown to be defective in proliferation and function during regeneration, correlating with disease progression[160]. In the limb-girdle muscular dystrophies (LGMDs), decreased satellite cell numbers have been observed in patients and myoblast proliferation deficits occur *in vitro*[161,162]. Interestingly, pharmacological HDAC inhibition

in the α-sarcoglycan-deficient LGMD mouse model restored myofiber size[163]. These and other disorders could benefit from therapies that protect against loss of muscle function by boosting the regenerative capacity of satellite cells.

In addition, many studies have shown that satellite cell dysfunction reduces the regenerative capacity of muscle during aging, potentially contributing to sarcopenia. This is likely due to disruption of pathways regulating satellite cell maintenance and myogenesis, such as JAK-STAT and p38-MAPK signaling[164]. Systemically administered, satellite cell-targeted therapies could potentially ameliorate age-related changes in skeletal muscle throughout the body. In fact, one study identified elevated JAK-STAT signaling in aged satellite cells and proved that *in vivo* treatment with a JAK-inhibitor enhanced muscle regeneration and force production after injury[132].

In addition to muscle disorders and sarcopenia due to aging, satellite cell-targeted therapy could be explored for neuromuscular conditions or to improve muscle regeneration after damage. In future studies, it would be interesting to replicate our screen and bioinformatics analysis using satellite cells derived from mouse models of aging and other muscle disorders.

CHAPTER 6

MATERIALS AND METHODS

Animal care

The following mouse strains were obtained from The Jackson Laboratory: B6.129-Smn1tm1Jme/J (JAX #6146), B6.Cg-Pax7tm1(cre/ERT2)Gaka/J (JAX #17763), B6;129S6-Gt(ROSA)26Sortm9 (CAG-tdTomato)Hze/J(#7905)andFVB.CgGrm7Tg(SMN2)89AhmbSmn1tm1Msd Tg(SMN2* delta7)4299Ahmb/J (JAX #5025). All mice were housed under standard conditions and allowed free access to food and water ad libitum. All animal care protocols and procedures were reviewed and approved by the IACUC of Harvard University or the University of Southern California and were performed in accordance with institutional and federal guidelines.

DNA extraction and PCR

For mouse genotyping, DNA was extracted using the salting out method. Briefly, tails were incubated in lysis buffer (10 mM Tris-HCl, 200 mM NaCl, 20 mM EDTA, 0.5% SDS pH 8.0) containing 1 mg/ml Proteinase K. 5M NaCl was used to salt out the cellular proteins and DNA was precipitated from the clarified lysate with ethanol. Pellets were resuspended in nuclease-free water. To extract DNA from cells, pellets were lysed according to the manufacturer's instructions using the DirectPCR Cell Lysis Reagent (Viagen Biotech) containing 1 mg/ml Proteinase K. PCR was performed using KOD Hot Start Master Mix (VWR) and the primers listed in Table 1.

Protein extraction and western blotting

Cells and tissue were lysed in RIPA buffer with 2% SDS and phosphatase and protease inhibitors (Life Technologies). Protein concentration was determined from clarified lysates using the Pierce BCA Protein Assay Kit (ThermoFisher Scientific). Protein lysates were diluted in RIPA and Laemmli running buffer to normalize concentrations (8-20ug), run on SDS-glycine gels, then transferred to PVDF membranes. Membranes were blocked with 5% milk in TBS-T and incubated overnight with

primary anti-SMN (BD Biosciences) and anti-beta tubulin (Abcam) antibodies. Membranes were washed 3 times with TBS-T then incubated in secondary antibodies conjugated to horse radish peroxidase. Chemiluminescence signal was produced using the SuperSignal West Dura Extended Duration Substrate (ThermoFisher Scientific) and detected on film. Image analysis was performed on Image J.

Table 6.1. Primers for PCR analyses.

Gene	Primer Type	Sequence 5'-->3'	Expected bands
mSmn1	Common forward	CTC CGG GAT ATT GGG ATT G	Mutant = 500 bp Wild type = 800 bp
	Mutant reverse	GGT AAC GCC AGG GTT TTC C	
	Wild type reverse	TTT CTT CTG GCT GTG CCT TT	
hSMN2	Common forward	CTG ACC TAC CAG GGA TGA GG	Mutant = 300 bp Wild type = 400 bp
	Mutant reverse	GGT CTG TTC TAC AGC CAC AGC	
	Wild type reverse	CCC AGG TGG TTT ATA GAC TCA GA	
hSMNΔ7	Transgene	TCC ATT TCC TTC TGG ACC AC	Transgene = 270 bp Internal positive control = 200 bp
	Transgene	ACC CAT TCC ACT TCC TTT TT	
	Internal positive control forward	CAA ATG TTG CTT GTC TGG TG	
	Internal positive control reverse	GTC AGT CGA GTG CAC AGT TT	
$CreER^{T2}$	Common forward	GCT GCT GTT GAT TAC CTG GC	Mutant = 235 bp Wild type = 400 bp
	Mutant reverse	CAA AAG ACG GCA ATA TGG TG	
	WT reverse	CTG CAC TGA GAC AGG ACC G	
tdTomato	Mutant forward	CCA GGG ATT TCA GTC GAT GT	Mutant = 200 bp Wild type = 300 bp
	Mutant reverse	AAT CTG ACG CAG GCA GTT CT	
	Wild type forward	CGT GAT CTG CAA CTC CAG TC	
	Wild type reverse	GGA GCG GGA GAA ATG GAT ATG	
Smn-F7	Ex7sou1	AGA AGG AAA GTG CTC ACA TAC AAA TT	Mutant = 635 bp Wild type = 435 bp
	GS8	TGT CTA TAA TCC TCA TGC TAT GGA G	
Smn-F7Δ7	GS8	TGT CTA TAA TCC TCA TGC TAT GGA G	Smn-F7Δ7 = 450 bp
	PHR5	TTC TCT TGA TTC CCA CTT TGT GGT TC	

Neonatal motor behavior tests

Neonatal behavioral tests were conducted to assess motor strength as described previously[128]. The righting latency assay measures the amount of time it takes for mice to right themselves onto four hind limbs when they are laid down on their right or left sides (maximum 30 seconds). The time upright assay measures how long the mice can stand upright on four hind limbs (maximum 60 seconds). For the tube hanging assay, mice were placed with their hind limbs draped over the edge of a 50ml conical tube with bedding at the bottom. The tube time measures how long the mice can hang onto the tube before falling. The tube score rates the positioning of the hind limbs and tail during the assay on a scale of 0-4, according to a previously published standardized rating system[128]. Stronger mice will splay their hind limbs while gripping the tube, while weaker mice will curl their feet inward and fall quickly. A total of three trials were performed for all assays and the average values were compared between conditions.

Immunofluorescence and image analysis

Cells and fresh tissue cryosections were fixed in 4% paraformaldehyde (PFA) for 5 minutes, washed thoroughly, and blocked in either 2% BSA/5% goat serum/0.2% triton/PBS (cells and muscle) or 10% donkey serum/0.3% triton/PBS (spinal cords) for one hour. Mouse tissue was additionally blocked using the Mouse on Mouse Blocking Reagent (Vector Laboratories) to reduce the non-specific background signal. Cells and tissues were incubated overnight using the following primary antibodies: anti-MyoD (5.8A clone, Santa Cruz Biotechnology), anti-MYH1E supernatant (MF20, DSHB), anti-Myogenin (F5D, DSHB), anti-Pax7 (DSHB), anti-laminin (Sigma or Novus for 647-conjugate), anti-ChAT (Millipore), and anti-RFP (VWR). After thorough washing, cells and tissue were incubated for one hour in isotype-matched secondary antibodies using the fluorophores Alexa 488, 546, or 647 (Life Technologies). Hoechst (Life technologies) was used to label nuclei. Images of cultured cells were

acquired with a high content Operetta imager (PerkinElmer) and analyzed with Columbus software (PerkinElmer), using manually designed scripts to automatically detect number of nuclei and cells positive for each fluorescence channel. Tissue sections were imaged on a Nikon Eclipse Ti fluorescence microscope and analyzed with NIS Elements software.

Muscle histology

To assess satellite cell and muscle fiber morphology, hind limb tibialis anterior and semispinalis muscles were dissected and immediately flash frozen in OCT using supercooled isopentane. In some cases when tdTomato expression needed to be preserved, dissected muscles were post-fixed for 1 hour in 0.5% paraformaldehyde (PFA), washed extensively in PBS, incubated in 30% sucrose overnight, then embedded in OCT. 10-12μm muscle cross sections were obtained and processed for immunofluorescence, hematoxylin and eosin (H&E) staining, or Masson's trichrome staining. H&E and Masson's staining was performed at the Harvard Stem Cell and Regenerative Biology Histology Core Facility. Adult mice (~3-12 months) were used for all *Pax7:SMN*-KO and *Pax7:SMN*-KD experiments.

Muscle regeneration assay

Muscle injury was performed in isoflurane-anesthetized mice as described previously[84]. Briefly, 50μl injections of a 10μM solution of *Naja pallida* cardiotoxin (CTX, Sigma-Aldrich) was injected into the tibialis anterior muscle in combination with mechanical damage by multiple intramuscular needle entries. Mice were monitored daily for 4 days to ensure recovery. TA muscles were dissected and processed as described above. The cross-sectional area of ~200 individual myofibers from damaged and contralateral undamaged TAs was measured using NIS Elements software. To account for muscle size differences between biological replicates (due to gender or age differences), individual values for

each damaged fiber were normalized to the mean undamaged myofiber area for the same mouse and then averaged.

In situ muscle force measurements

An Aurora Scientific 1300-A Whole Mouse Test System was used to gather force production data. Mice were placed ventrally on a heated stage while the animal was anesthetized with 2% isoflurane. The leg of interest was immobilized both at the knee joint and foot to ensure the leg remained in the same position throughout the testing procedure. An incision to expose the sciatic nerve was conducted as described previously, and the distal TA tendon was dissected and affixed to the motor lever[165]. We conducted both direct stimulation of the TA muscle with monopolar electrodes as well as indirect stimulation with a stimulatory cuff on the sciatic nerve and obtained highly similar results in both cases. Calibrated Dynamic Muscle Control and Analysis Software (Aurora Scientific) and a 701C Stimulator (Aurora Scientific) were used to acquire muscle force measurements. The optimal voltage was found by using course voltage adjustments and the InstantStim feature to determine what voltage yielded the most powerful twitches. Optimal force–length measurements were obtained by making micro adjustments on the length out feature of the machine. This stretching of the TA muscle allowed for optimal alignment of actin filaments in the muscle to obtain the Optimal Length (Lo). On the live data monitor, the force measurements were displayed in real time in response to the muscle stimulation. Once the Lo and optimal voltage were set, we ran a "Twitch" protocol, which administers a single electrical impulse equivalent to a single action potential to elicit a short, low force contraction. The pulse width in our protocol was 0.2ms and a 20-second rest period was allowed between each electrical pulse. The force elicited from the muscle was typically within the 100-150mN range. Once the setup was prepared, Ringer's solution was applied to the muscle and the exposed sciatic nerve. A tetanic stimulation frequency sequence from 50Hz, 100Hz, 150Hz to 200 Hz intervals was performed

to determine the maximum tetanic force produced by the muscle. A rest period of 2 minutes was given between each tetanic stimulation. Once the sequence was finished, a caliper tool was used to calculate the Lo measuring from the patellar tendon to the TA distal tendon and the body weight was recorded. To account for size variability between sample mice, the maximum muscle force produced by damaged TA muscles was normalized to the force produced by the undamaged, contralateral TA from the same mouse. Specific force measurements were calculated as per Gordon Lynch's SOP protocol.

Single muscle fiber isolation

Single muscle fibers were isolated from the extensor digitorum longus (EDL) hind limb muscle according to published protocols[166]. Briefly, the EDL was dissected and incubated in collagenase for 1 hour, followed by gentle trituration to release single fibers from the tendon. Muscle fibers were fixed in 4% PFA and stained with Hoechst to label nuclei. All myonuclei incorporated within single myofibers were quantified at 20X magnification. Only myofibers that were fully intact with angulated as opposed to fragmented ends were analyzed, and at least 10 myofibers were quantified per biological replicate.

Satellite cell isolation and primary myoblast line derivation

Mouse satellite cells were isolated from hind limb muscle as described previously[132]. Briefly, hind limb muscles were dissected and mechanically minced, then incubated and triturated in 0.4%collagenase/1% dispase (Roche) to allow enzymatic dissociation of fibers. Several rounds of filtration and wash steps were performed to clear large cellular debris. To isolate satellite cells, muscle lysates were prepared for fluorescence activated cell sorting (FACS) based on the cell surface marker profile CD45-CD11b-Ter119-CD31-Sca1-CXCR4+alpha7integrin+, similar to what has been described previously[167-169].

FACS was conducted on a BD FACSAria instrument at the Joslin Flow Cytometry Core facility. Cells were collected into FACS buffer (10% FBS/1mM EDTA in PBS) then spun and resuspended prior to seeding.

Myoblast derivation and proliferation/differentiation assays

To derive primary myoblast lines, FACS-purified satellite cells were expanded *in vitro* for several passages on collagen-coated plates in myoblast growth medium containing Hams F10 (Life Technologies or Westnet), 20% heat-inactivated fetal bovine serum (Life Technologies), 1X penicillin/streptomycin (Life Technologies), and 10ng/mL basic fibroblast growth factor (bFGF, Life Technologies). For the proliferation assay, *Pax7:SMN*-KD and *Pax7:SMN*-KO myoblasts were treated with 1μm 4-hydroxytamoxifen for 48 hours then maintained for an additional 3 days to ensure SMN depletion. Cells were trypsinized and seeded on collagen-coated 96-well plates at 2000 cells/well in myoblast growth medium and fixed at multiple time points. For the differentiation assay, 4-OHT-treated myoblasts were seeded at 20,000 cells/well and serum-stared in DMEM medium containing 10% heat-inactivated horse serum and 1X penicillin/streptomycin for 5 days.

EdU assays

For *in vitro* labeling, cells were incubated in 1μM EdU/DMSO 24 hours prior to fixing. For *in vivo* studies, mice were subcutaneously injected with 100μg EdU dissolved in 0.9% saline 6 hours prior to sacrifice. EdU detection was performed according to the manufacturer's instructions using the Click-iT Plus EdU Imaging kit (Invitrogen).

Satellite cell small molecule screen

Satellite cells were isolated from hind limb skeletal muscle of Tg:Pax7nGFP mice and FACS-purified based on GFP expression. Cells were plated at 150 cells/well on collagen-coated 96-well plates in StemSpan SFEM II medium (STEMCELL Technologies) supplemented with .05ng/ml bFGF. Cell were treated with LINCS1-4 compound libraries at 3 concentrations (0.1,0.3, and 1μM) in biological triplicate. The day cells were plated was considered Day 0. Compounds were added on Day 1 using an automated liquid dispensing robot (Matrix Hydra DT, Thermo Fisher). Cells were incubated without media change until Day 4 at which point they were fixed (EL406, Biotek instruments) and images were acquired with a high content Operetta imager (PerkinElmer) and analyzed with Columbus software (PerkinElmer). Quantification of cells was conducted using manually designed scripts to automatically detect number of $Hoechst^{+}$ nuclei and cells. For dose response assays, satellite cells were prepared by the same method and treated with hit compounds at 8 concentrations between 0.05-5μM. All compounds were resuspended in dimethylsulfoxide (DMSO, Sigma Aldrich). 0.1% DMSO was used as a negative control and 600nM Jak3 inhibitor VI was used as a positive control on all plates. Hoechst (Life technologies) was used to label nuclei. Relative fold change was normalized to the average of DMSO replicates per plate and subsequently averaged across biological replicate plates (n=3).

Drug clustering and metadrug analysis

The 'protein_chemical.links.detailed' file (version 5.0) was downloaded from the STITCH website (http://stitch.embl.de/cgi/download.pl). Protein-drug interactions for 54 drug hits uncovered by the satellite cell screen presented in Chapter 4 were extracted from the database and protein interactions with combined score < 500 were removed. A (54 × 54) matrix C was constructed such that $(C)_{i,j} = 0.01 +$ (# shared protein interactions between drugs i and $j)/\frac{1}{2}(N_i+N_j)$, where N_i is

the total number of interactions for drug i. Drugs were then clustered by the R 'hclust' function with default parameters using $1/C$ as a distance matrix. To compute metadrug scores, we first constructed a (gene × drug) matrix M of combined interaction scores from the STITCH database. M was then decomposed by non-negative matrix factorization into rank r matrices A_r and B_r such that $M \approx A_r B_r$ for $r = 2, \ldots, 15$. For each rank approximation r and gene g, a raw score $W_{r,g}$ was computed via

$$W_{r,g} = \sum_{j=1}^{N} (A_r)_{g,j},$$

and subsequently normalized to $Z_{r,g} = \left(W_{r,g} - \overline{W_r}\right)/\sigma_r$, where $\overline{W_r}$ and σ_r represent the mean and standard deviation of W-scores across all genes for rank r. The final per-gene metadrug score S_g is the mean of Z-scores across the rank approximations used:

$$S_g = \frac{1}{15} \sum_{i=2}^{15} Z_{i,g}$$

Genes not expressed in satellite cells (defined as below the 5th percentile of expression; data unpublished) were excluded from further analysis. NMF approximation was performed using the 'nmf' function from the R package NMF with default parameters.

3' DGE RNA sequencing

Pax7:*SMN*-KD control and mutant myoblast lines were cultured (2 biological replicates per condition with 3-4 individual growth replicates each) and treated for 48 hours with 1μm 4-OHT or an ethanol vehicle. After 3 days, RNA was extracted using a Total RNA Purification Plus kit (Norgen) and quantified using a Nanodrop (Thermo Fisher Scientific). 50ng of total RNA in 10μl of water was mixed with 10μl of 1X TCL lysis buffer with 1% (v/v) ß-mercaptoethanol (Qiagen). Each sample was

added to triplicate wells in 384 well plates and stored at -80°C. Prior to library construction, the plate was thawed, vortexed briefly, and centrifuged for 1 minute at 1000 rpm. 28μl of SPRI beads (Beckman Coulter Genomics) were added directly to the sample, mixed and incubated for 5 minutes. The plate was transferred to a magnetic rack to aggregate the beads and incubated for 5 minutes prior to removing the liquid. The beads were washed with 80% ethanol twice and allowed to dry for 1 minute. 20μl nuclease free water was added per well, the plate was removed from the magnetic rack and the beads were thoroughly resuspended. Following a 5 minute incubation, the plate was returned to the magnetic rack and incubated for an additional 5 minutes before transferring the supernatant to a fresh PCR plate. 5μl of the supernatant was transferred to a separate plate containing RT master mix and 3' and 5' adapters for reverse transcription and template switching, and incubated for 90 minutes at 42°C[170]. The cDNA was pooled and purified with a QIAquick PCR purification kit according to the manufacturer's directions with a final elution in 24μl of nuclease free water. This was followed by an exonuclease I treatment for 30 minutes at 37°C that was stopped with a 20 minute incubation at 80°C. The cDNA was then amplified using the Advantage 2 PCR Enzyme System (Takara) for 5 cycles and purified using AMPure XP magnetic beads (Beckman Coulter Genomics). Library preparation was completed with 55ng input using a Nextera DNA kit (Illumina) following the manufacturer's instructions, amplified 5 cycles, and purified with AMPure XP magnetic beads (Beckman Coulter Genomics). A Pippin PREP purification of the sample from 300-800bp was performed, then quantified by qPCR and sequenced on a single Illumina NextSeq run with 75bp paired end reads at the Harvard University Bauer Core Facility.

Table 6.2. RNA IDs for samples used in RNA sequencing analysis

RNA ID	Sample name	Treatment	Growth replicate number
R1001	*Pax7:SMN*-KD Control	Vehicle	1
R1023	*Pax7:SMN*-KD Control	Vehicle	2
R1047	*Pax7:SMN*-KD Control	Vehicle	3
R1066	*Pax7:SMN*-KD Control	Vehicle	4
R1002	*Pax7:SMN*-KD Control	4-OHT	1
R1011	*Pax7:SMN*-KD Control	4-OHT	2
R1028	*Pax7:SMN*-KD Control	4-OHT	3
R1040	*Pax7:SMN*-KD Control	4-OHT	4
R1003	*Pax7:SMN*-KD Mutant	Vehicle	1
R1024	*Pax7:SMN*-KD Mutant	Vehicle	2
R1029	*Pax7:SMN*-KD Mutant	Vehicle	3
R1067	*Pax7:SMN*-KD Mutant	Vehicle	4
R1004	*Pax7:SMN*-KD Mutant	4-OHT	1
R1012	*Pax7:SMN*-KD Mutant	4-OHT	2
R1043	*Pax7:SMN*-KD Mutant	4-OHT	3
R1065	*Pax7:SMN*-KD Mutant	4-OHT	4
R1007	*Pax7:SMN*-KD Control #2	Vehicle	1
R1046	*Pax7:SMN*-KD Control #2	Vehicle	2
R1064	*Pax7:SMN*-KD Control #2	Vehicle	3
R1008	*Pax7:SMN*-KD Control #2	4-OHT	1
R1044	*Pax7:SMN*-KD Control #2	4-OHT	2
R1045	*Pax7:SMN*-KD Control #2	4-OHT	3
R1009	*Pax7:SMN*-KD Mutant #2	Vehicle	1
R1041	*Pax7:SMN*-KD Mutant #2	Vehicle	2
R1042	*Pax7:SMN*-KD Mutant #2	Vehicle	3
R1010	*Pax7:SMN*-KD Mutant #2	4-OHT	1
R1014	*Pax7:SMN*-KD Mutant #2	4-OHT	2
R1063	*Pax7:SMN*-KD Mutant #2	4-OHT	3

Differential expression analysis

Reads were demultiplexed using a custom script and aligned to mm10 via bwa aln -l 24. Gene expression levels were determined by counting unique UMIs among reads with unambiguous gene mappings. Read counts were summed across technical replicates for each RNA library to produce a 28-column expression matrix. Sample R1011 was removed from further analysis due to having an unusually high RNA concentration prior to sequencing and very poor expression correlation with the remaining 27 samples. The expression matrix was further filtered by removing: (1) ribosomal genes (gene symbols beginning with MRPS, RPS, MRPL or RPL); (2) genes with fewer than 200 total reads across the 27 samples; and (3) genes with 0 reads in 8 or more samples. DESeq2 was run to determine

differentially expressed genes between samples R1002, R1028 and R1040 (wild type) and samples R1004, R1012, R1043 and R1065 (SMA). DESeq2 was run with $\alpha = 0.2$ and samples not in the wild type or SMA groups were included in DESeq2's model to help determine basal expression levels.

KEGG and GO analyses

First, expression values from DESeq2 were normalized using the rlog transform. The GAGE package was then used to determine KEGG pathways with significant perturbations. GAGE was run in both same.dir=FALSE and same.dir=TRUE modes to determine KEGG pathways with mixed expression changes and same-direction expression changes, respectively. GO analysis was also performed using GAGE, but only same-direction expression changes were considered. KEGG pathways and GO terms were taken from the gageData package (keg.sets.mm and go.sets.mm, respectively).

SMA patient tissue analysis

Frozen human muscle derived from patients with spinal muscular atrophy and age matched controls were obtained from Dr. Charlotte J. Sumner (Johns Hopkins University). Tissues were collected during standard autopsies or spinal fusion surgeries performed at JHMI or other institutions. Specimens were de-identified at the time of collection (IRB number: NA_00035399).

iPSC culture:

The following iPSC/ESC lines were obtained from the Harvard Stem Cell iPS Core: WA01, Hues66, E3-SipsA, and BJSipsD. The following SMA patient iPSC lines were obtained from the Rubin lab: SMA-15A, SMA-2-18C, and SMA-38D. iPSC/ESCs were maintained in supplemented StemFlex medium (ThermoFisher Scientific) on Matrigel-coated (BD Biosciences) plates. Cells were passaged at approximately 70% confluence using Gentle Cell Dissociation Reagent or Accutase (STEMCELL

Technologies). When dissociated to single cells, ROCK-inhibitor (EMD Millipore) was added to the culture for 24 hours.

Skeletal muscle directed differentiation

iPSC/ESCs were differentiated into skeletal muscle cells according to the manufacturer's protocol for the Skeletal Muscle Differentiation Kit (Genea Biocells). This proprietary kit contains three separate medium components: Skeletal Muscle Induction Medium (SKM01), Myoblast Cell Culture Medium (SKM02) and Myotube Fusion Medium (SKM03). Accutase-dissociated iPSC/ESCs were seeded at 4,500 cells/cm^2 on collagen I-coated plates with ROCK inhibitor for 24 hours then maintained in SKM01 for 7-10 days or until very confluent. To facilitate the transition from satellite-like cells to myoblasts, cultures were then dissociated with 0.25% Trypsin-EDTA (Life Technologies) and seeded at 10,000 cells/cm^2 on collagen I-coated plates in SKM02. Myoblasts were maintained for 5-7 days or until very confluent, then switched to SKM03 to facilitate myotube fusion for 2-4 days.

siRNA Transfections

iPSCs were transfected with 30 pmol of a pooled, SMN-specific siRNA (Santa Cruz Biotechnology) or a scrambled sequence control (Control siRNA-A; Santa Cruz Biotechnology) diluted in Opti-MEM and Lipofectamine RNAiMAX (ThermoFisher Scientific). Transfection mixtures were added directly to the cell culture medium for 24 hours. Transfections were performed in iPSCs 4 days and 2 days prior to initiating skeletal muscle differentiations, and again 2 days prior to switching between each SKM medium stage (total of 5 transfections). Western blots to confirm SMN knockdown were performed 48 hours after each transfection at the time of switching between differentiation stages.

REFERENCES

1 Werdnig, G. Zwei frühinfantile hereditäre Fälle von progressiver Muskelatrophie unter dem Bilde der Dystrophie, aber anf neurotischer Grundlage. *Archiv für Psychiatrie und Nervenkrankheiten* **22**, 437-480 (1891).

2 Hoffmann, J. Ueber chronische spinale Muskelatrophie im Kindesalter, auf familiärer Basis. *Deutsch. Z. Nervenheilk* **3**, 427-470 (1893).

3 Bowerman, M. *et al.* Therapeutic strategies for spinal muscular atrophy: SMN and beyond. *Dis Model Mech* **10**, 943-954, doi:10.1242/dmm.030148 (2017).

4 Verhaart, I. E. C. *et al.* Prevalence, incidence and carrier frequency of 5q-linked spinal muscular atrophy - a literature review. *Orphanet J Rare Dis* **12**, 124, doi:10.1186/s13023-017-0671-8 (2017).

5 Farrar, M. A. & Kiernan, M. C. The Genetics of Spinal Muscular Atrophy: Progress and Challenges. *Neurotherapeutics* **12**, 290-302, doi:10.1007/s13311-014-0314-x (2015).

6 Lefebvre, S. *et al.* Identification and characterization of a spinal muscular atrophy-determining gene. *Cell* **80**, 155-165, doi:10.1016/0092-8674(95)90460-3 (1995).

7 Burghes, A. H. When is a deletion not a deletion? When it is converted. *American Journal of Human Genetics* **61**, 9-15 (1997).

8 Burghes, A. H. & Beattie, C. E. Spinal muscular atrophy: why do low levels of survival motor neuron protein make motor neurons sick? *Nat Rev Neurosci* **10**, 597-609, doi:10.1038/nrn2670 (2009).

9 Liu, Q. & Dreyfuss, G. A novel nuclear structure containing the survival of motor neurons protein. *EMBO J* **15**, 3555-3565 (1996).

10 Chari, A. *et al.* An assembly chaperone collaborates with the SMN complex to generate spliceosomal SnRNPs. *Cell* **135**, 497-509, doi:10.1016/j.cell.2008.09.020 (2008).

11 Zhang, H. L. *et al.* Active transport of the survival motor neuron protein and the role of exon-7 in cytoplasmic localization. *J Neurosci* **23**, 6627-6637 (2003).

12 Winkler, C. *et al.* Reduced U snRNP assembly causes motor axon degeneration in an animal model for spinal muscular atrophy. *Genes Dev* **19**, 2320-2330, doi:10.1101/gad.342005 (2005).

13 Gabanella, F. *et al.* Ribonucleoprotein assembly defects correlate with spinal muscular atrophy severity and preferentially affect a subset of spliceosomal snRNPs. *PLoS One* **2**, e921, doi:10.1371/journal.pone.0000921 (2007).

14 Zhang, Z. *et al.* SMN deficiency causes tissue-specific perturbations in the repertoire of snRNAs and widespread defects in splicing. *Cell* **133**, 585-600, doi:10.1016/j.cell.2008.03.031 (2008).

15 Doktor, T. K. *et al.* RNA-sequencing of a mouse-model of spinal muscular atrophy reveals tissue-wide changes in splicing of U12-dependent introns. *Nucleic Acids Res* **45**, 395-416, doi:10.1093/nar/gkw731 (2017).

16 Custer, S. K. *et al.* Altered mRNA Splicing in SMN-Depleted Motor Neuron-Like Cells. *PLoS One* **11**, e0163954, doi:10.1371/journal.pone.0163954 (2016).

17 Zhang, H. *et al.* Multiprotein complexes of the survival of motor neuron protein SMN with Gemins traffic to neuronal processes and growth cones of motor neurons. *J Neurosci* **26**, 8622-8632, doi:10.1523/JNEUROSCI.3967-05.2006 (2006).

18 Custer, S. K., Todd, A. G., Singh, N. N. & Androphy, E. J. Dilysine motifs in exon 2b of SMN protein mediate binding to the COPI vesicle protein alpha-COP and neurite outgrowth in a cell culture model of spinal muscular atrophy. *Hum Mol Genet* **22**, 4043-4052, doi:10.1093/hmg/ddt254 (2013).

19 Ting, C. H. *et al.* The spinal muscular atrophy disease protein SMN is linked to the Golgi network. *PLoS One* **7**, e51826, doi:10.1371/journal.pone.0051826 (2012).

20 McWhorter, M. L., Monani, U. R., Burghes, A. H. & Beattie, C. E. Knockdown of the survival motor neuron (Smn) protein in zebrafish causes defects in motor axon outgrowth and pathfinding. *J Cell Biol* **162**, 919-931, doi:10.1083/jcb.200303168 (2003).

21 Jablonka, S., Beck, M., Lechner, B. D., Mayer, C. & Sendtner, M. Defective Ca2+ channel clustering in axon terminals disturbs excitability in motoneurons in spinal muscular atrophy. *J Cell Biol* **179**, 139-149, doi:10.1083/jcb.200703187 (2007).

22 Rossoll, W. *et al.* Smn, the spinal muscular atrophy-determining gene product, modulates axon growth and localization of beta-actin mRNA in growth cones of motoneurons. *J Cell Biol* **163**, 801-812, doi:10.1083/jcb.200304128 (2003).

23 Rochette, C. F., Gilbert, N. & Simard, L. R. SMN gene duplication and the emergence of the SMN2 gene occurred in distinct hominids: SMN2 is unique to Homo sapiens. *Hum Genet* **108**, 255-266, doi:10.1007/s004390100473 (2001).

24 Monani, U. R. Spinal muscular atrophy: a deficiency in a ubiquitous protein; a motor neuron-specific disease. *Neuron* **48**, 885-896, doi:10.1016/j.neuron.2005.12.001 (2005).

25 Miguel-Aliaga, I. *et al.* The Caenorhabditis elegans orthologue of the human gene responsible for spinal muscular atrophy is a maternal product critical for germline maturation and embryonic viability. *Hum Mol Genet* **8**, 2133-2143, doi:10.1093/hmg/8.12.2133 (1999).

26 Imlach, W. L. *et al.* SMN is required for sensory-motor circuit function in Drosophila. *Cell* **151**, 427-439, doi:10.1016/j.cell.2012.09.011 (2012).

27 Chang, H. C. *et al.* Modeling spinal muscular atrophy in Drosophila. *PLoS One* **3**, e3209, doi:10.1371/journal.pone.0003209 (2008).

28 Rajendra, T. K. *et al.* A Drosophila melanogaster model of spinal muscular atrophy reveals a function for SMN in striated muscle. *J Cell Biol* **176**, 831-841, doi:10.1083/jcb.200610053 (2007).

29 Schrank, B. *et al.* Inactivation of the survival motor neuron gene, a candidate gene for human spinal muscular atrophy, leads to massive cell death in early mouse embryos. *Proc Natl Acad Sci U S A* **94**, 9920-9925, doi:10.1073/pnas.94.18.9920 (1997).

30 Monani, U. R. *et al.* The human centromeric survival motor neuron gene (SMN2) rescues embryonic lethality in Smn(-/-) mice and results in a mouse with spinal muscular atrophy. *Hum Mol Genet* **9**, 333-339, doi:10.1093/hmg/9.3.333 (2000).

31 Le, T. T. *et al.* SMNDelta7, the major product of the centromeric survival motor neuron (SMN2) gene, extends survival in mice with spinal muscular atrophy and associates with full-length SMN. *Hum Mol Genet* **14**, 845-857, doi:10.1093/hmg/ddi078 (2005).

32 Ling, K. K., Lin, M. Y., Zingg, B., Feng, Z. & Ko, C. P. Synaptic defects in the spinal and neuromuscular circuitry in a mouse model of spinal muscular atrophy. *PLoS One* **5**, e15457, doi:10.1371/journal.pone.0015457 (2010).

33 Kong, L. *et al.* Impaired synaptic vesicle release and immaturity of neuromuscular junctions in spinal muscular atrophy mice. *J Neurosci* **29**, 842-851, doi:10.1523/JNEUROSCI.4434-08.2009 (2009).

34 Kariya, S. *et al.* Reduced SMN protein impairs maturation of the neuromuscular junctions in mouse models of spinal muscular atrophy. *Hum Mol Genet* **17**, 2552-2569, doi:10.1093/hmg/ddn156 (2008).

35 Park, G. H., Maeno-Hikichi, Y., Awano, T., Landmesser, L. T. & Monani, U. R. Reduced survival of motor neuron (SMN) protein in motor neuronal progenitors functions cell autonomously to cause spinal muscular atrophy in model mice expressing the human centromeric (SMN2) gene. *J Neurosci* **30**, 12005-12019, doi:10.1523/JNEUROSCI.2208-10.2010 (2010).

36 Hua, Y. *et al.* Peripheral SMN restoration is essential for long-term rescue of a severe spinal muscular atrophy mouse model. *Nature* **478**, 123-126, doi:10.1038/nature10485 (2011).

37 Hua, Y. *et al.* Motor neuron cell-nonautonomous rescue of spinal muscular atrophy phenotypes in mild and severe transgenic mouse models. *Genes Dev* **29**, 288-297, doi:10.1101/gad.256644.114 (2015).

38 Shababi, M. *et al.* Cardiac defects contribute to the pathology of spinal muscular atrophy models. *Hum Mol Genet* **19**, 4059-4071, doi:10.1093/hmg/ddq329 (2010).

39 Shanmugarajan, S. *et al.* Bone loss in survival motor neuron (Smn(-/-) SMN2) genetic mouse model of spinal muscular atrophy. *J Pathol* **219**, 52-60, doi:10.1002/path.2566 (2009).

40 Poruk, K. E. *et al.* Observational study of caloric and nutrient intake, bone density, and body composition in infants and children with spinal muscular atrophy type I. *Neuromuscul Disord* **22**, 966-973, doi:10.1016/j.nmd.2012.04.008 (2012).

41 Sintusek, P. *et al.* Histopathological Defects in Intestine in Severe Spinal Muscular Atrophy Mice Are Improved by Systemic Antisense Oligonucleotide Treatment. *PLoS One* **11**, e0155032, doi:10.1371/journal.pone.0155032 (2016).

42 Araujo, A., Araujo, M. & Swoboda, K. J. Vascular perfusion abnormalities in infants with spinal muscular atrophy. *J Pediatr* **155**, 292-294, doi:10.1016/j.jpeds.2009.01.071 (2009).

43 Bowerman, M. *et al.* Defects in pancreatic development and glucose metabolism in SMN-depleted mice independent of canonical spinal muscular atrophy neuromuscular pathology. *Hum Mol Genet* **23**, 3432-3444, doi:10.1093/hmg/ddu052 (2014).

44 Somers, E., Stencel, Z., Wishart, T. M., Gillingwater, T. H. & Parson, S. H. Density, calibre and ramification of muscle capillaries are altered in a mouse model of severe spinal muscular atrophy. *Neuromuscul Disord* **22**, 435-442, doi:10.1016/j.nmd.2011.10.021 (2012).

45 Rudnik-Schoneborn, S. *et al.* Digital necroses and vascular thrombosis in severe spinal muscular atrophy. *Muscle Nerve* **42**, 144-147, doi:10.1002/mus.21654 (2010).

46 Lipnick, S. L. *et al.* Systemic nature of spinal muscular atrophy revealed by studying insurance claims. *PLoS One* **14**, e0213680, doi:10.1371/journal.pone.0213680 (2019).

47 Kablar, B. & Rudnicki, M. A. Development in the absence of skeletal muscle results in the sequential ablation of motor neurons from the spinal cord to the brain. *Dev Biol* **208**, 93-109, doi:10.1006/dbio.1998.9184 (1999).

48 Grieshammer, U., Lewandoski, M., Prevette, D., Oppenheim, R. W. & Martin, G. R. Muscle-specific cell ablation conditional upon Cre-mediated DNA recombination in transgenic mice leads to massive spinal and cranial motoneuron loss. *Dev Biol* **197**, 234-247, doi:10.1006/dbio.1997.8859 (1998).

49 Giudice, J. & Taylor, J. M. Muscle as a paracrine and endocrine organ. *Curr Opin Pharmacol* **34**, 49-55, doi:10.1016/j.coph.2017.05.005 (2017).

50 Yin, H., Price, F. & Rudnicki, M. A. Satellite cells and the muscle stem cell niche. *Physiol Rev* **93**, 23-67, doi:10.1152/physrev.00043.2011 (2013).

51 Li, L., Xiong, W. C. & Mei, L. Neuromuscular Junction Formation, Aging, and Disorders. *Annu Rev Physiol* **80**, 159-188, doi:10.1146/annurev-physiol-022516-034255 (2018).

52 Relaix, F. & Zammit, P. S. Satellite cells are essential for skeletal muscle regeneration: the cell on the edge returns centre stage. *Development* **139**, 2845-2856, doi:10.1242/dev.069088 (2012).

53 Ripolone, M. *et al.* Impaired Muscle Mitochondrial Biogenesis and Myogenesis in Spinal Muscular Atrophy. *JAMA Neurol* **72**, 666-675, doi:10.1001/jamaneurol.2015.0178 (2015).

54 Lee, Y. I., Mikesh, M., Smith, I., Rimer, M. & Thompson, W. Muscles in a mouse model of spinal muscular atrophy show profound defects in neuromuscular development even in the absence of failure in neuromuscular transmission or loss of motor neurons. *Dev Biol* **356**, 432-444, doi:10.1016/j.ydbio.2011.05.667 (2011).

55 Ling, K. K., Gibbs, R. M., Feng, Z. & Ko, C. P. Severe neuromuscular denervation of clinically relevant muscles in a mouse model of spinal muscular atrophy. *Hum Mol Genet* **21**, 185-195, doi:10.1093/hmg/ddr453 (2012).

56 Murray, L. M. *et al.* Selective vulnerability of motor neurons and dissociation of pre- and post-synaptic pathology at the neuromuscular junction in mouse models of spinal muscular atrophy. *Hum Mol Genet* **17**, 949-962, doi:10.1093/hmg/ddm367 (2008).

57 Bricceno, K. V. *et al.* Survival motor neuron protein deficiency impairs myotube formation by altering myogenic gene expression and focal adhesion dynamics. *Hum Mol Genet* **23**, 4745-4757, doi:10.1093/hmg/ddu189 (2014).

58 Shafey, D., Cote, P. D. & Kothary, R. Hypomorphic Smn knockdown C2C12 myoblasts reveal intrinsic defects in myoblast fusion and myotube morphology. *Exp Cell Res* **311**, 49-61, doi:10.1016/j.yexcr.2005.08.019 (2005).

59 Cifuentes-Diaz, C. *et al.* Deletion of murine SMN exon 7 directed to skeletal muscle leads to severe muscular dystrophy. *J Cell Biol* **152**, 1107-1114, doi:10.1083/jcb.152.5.1107 (2001).

60 Nicole, S. *et al.* Intact satellite cells lead to remarkable protection against Smn gene defect in differentiated skeletal muscle. *J Cell Biol* **161**, 571-582, doi:10.1083/jcb.200210117 (2003).

61 Martinez, T. L. *et al.* Survival motor neuron protein in motor neurons determines synaptic integrity in spinal muscular atrophy. *J Neurosci* **32**, 8703-8715, doi:10.1523/JNEUROSCI.0204-12.2012 (2012).

62 Howell, K., Gibbs, R. M. & Rubin, L. L. Spinal Muscular Atrophy: Huge Steps. *Cerebrum* (2019).

63 Hua, Y., Vickers, T. A., Okunola, H. L., Bennett, C. F. & Krainer, A. R. Antisense masking of an hnRNP A1/A2 intronic splicing silencer corrects SMN2 splicing in transgenic mice. *Am J Hum Genet* **82**, 834-848, doi:10.1016/j.ajhg.2008.01.014 (2008).

64 Finkel, R. S. *et al.* Nusinersen versus Sham Control in Infantile-Onset Spinal Muscular Atrophy. *N Engl J Med* **377**, 1723-1732, doi:10.1056/NEJMoa1702752 (2017).

65 Mercuri, E. *et al.* Nusinersen versus Sham Control in Later-Onset Spinal Muscular Atrophy. *N Engl J Med* **378**, 625-635, doi:10.1056/NEJMoa1710504 (2018).

66 Ramos, D. M. *et al.* Age-dependent SMN expression in disease-relevant tissue and implications for SMA treatment. *J Clin Invest* **129**, 4817-4831, doi:10.1172/JCI124120 (2019).

67 Dominguez, E. *et al.* Intravenous scAAV9 delivery of a codon-optimized SMN1 sequence rescues SMA mice. *Hum Mol Genet* **20**, 681-693, doi:10.1093/hmg/ddq514 (2011).

68 Foust, K. D. *et al.* Rescue of the spinal muscular atrophy phenotype in a mouse model by early postnatal delivery of SMN. *Nat Biotechnol* **28**, 271-274, doi:10.1038/nbt.1610 (2010).

69 Mendell, J. R. *et al.* Single-Dose Gene-Replacement Therapy for Spinal Muscular Atrophy. *N Engl J Med* **377**, 1713-1722, doi:10.1056/NEJMoa1706198 (2017).

70 Naryshkin, N. A. *et al.* Motor neuron disease. SMN2 splicing modifiers improve motor function and longevity in mice with spinal muscular atrophy. *Science* **345**, 688-693, doi:10.1126/science.1250127 (2014).

71 Palacino, J. *et al.* SMN2 splice modulators enhance U1-pre-mRNA association and rescue SMA mice. *Nat Chem Biol* **11**, 511-517, doi:10.1038/nchembio.1837 (2015).

72 Sumner, C. J. & Crawford, T. O. Two breakthrough gene-targeted treatments for spinal muscular atrophy: challenges remain. *J Clin Invest* **128**, 3219-3227, doi:10.1172/JCI121658 (2018).

73 Swoboda, K. J. *et al.* Natural history of denervation in SMA: relation to age, SMN2 copy number, and function. *Ann Neurol* **57**, 704-712, doi:10.1002/ana.20473 (2005).

74 Lutz, C. M. *et al.* Postsymptomatic restoration of SMN rescues the disease phenotype in a mouse model of severe spinal muscular atrophy. *J Clin Invest* **121**, 3029-3041, doi:10.1172/JCI57291 (2011).

75 Kariya, S. *et al.* Requirement of enhanced Survival Motoneuron protein imposed during neuromuscular junction maturation. *J Clin Invest* **124**, 785-800, doi:10.1172/JCI72017 (2014).

76 Hwu, W. Outcomes after 1-year in presymptomatic infants with genetically diagnosed spinal muscular atrophy (SMA) treated with nusinersen: interim results from the NURTURE study. *Neuromuscul Disord* **27**, S212 (2017).

77 McPherron, A. C., Lawler, A. M. & Lee, S. J. Regulation of skeletal muscle mass in mice by a new TGF-beta superfamily member. *Nature* **387**, 83-90, doi:10.1038/387083a0 (1997).

78 Pirruccello-Straub, M. *et al.* Blocking extracellular activation of myostatin as a strategy for treating muscle wasting. *Sci Rep* **8**, 2292, doi:10.1038/s41598-018-20524-9 (2018).

79 Long, K. K. *et al.* Specific inhibition of myostatin activation is beneficial in mouse models of SMA therapy. *Hum Mol Genet* **28**, 1076-1089, doi:10.1093/hmg/ddy382 (2019).

80 Cytokinetics, I. (2018).

81 Mauro, A. Satellite cell of the skeletal muscle fiber. *Journal of Biophysical and Biochemical Cytology* **9**, 493-495 (1961).

82 Pourquie, O. Vertebrate somitogenesis: a novel paradigm for animal segmentation? *Int J Dev Biol* **47**, 597-603 (2003).

83 Moss, F. P. & Leblond, C. P. Satellite cells as the source of nuclei in muscles of growing rats. *Anat Rec* **170**, 421-435, doi:10.1002/ar.1091700405 (1971).

84 Kuang, S., Kuroda, K., Le Grand, F. & Rudnicki, M. A. Asymmetric self-renewal and commitment of satellite stem cells in muscle. *Cell* **129**, 999-1010, doi:10.1016/j.cell.2007.03.044 (2007).

85 Schultz, E. Satellite cell proliferative compartments in growing skeletal muscles. *Dev Biol* **175**, 84-94, doi:10.1006/dbio.1996.0097 (1996).

86 White, R. B., Bierinx, A. S., Gnocchi, V. F. & Zammit, P. S. Dynamics of muscle fibre growth during postnatal mouse development. *BMC Dev Biol* **10**, 21, doi:10.1186/1471-213X-10-21 (2010).

87 Delhaas, T., Van der Meer, S. F., Schaart, G., Degens, H. & Drost, M. R. Steep increase in myonuclear domain size during infancy. *Anat Rec (Hoboken)* **296**, 192-197, doi:10.1002/ar.22631 (2013).

88 Lepper, C., Partridge, T. A. & Fan, C. M. An absolute requirement for Pax7-positive satellite cells in acute injury-induced skeletal muscle regeneration. *Development* **138**, 3639-3646, doi:10.1242/dev.067595 (2011).

89 Gavrilina, T. O. *et al.* Neuronal SMN expression corrects spinal muscular atrophy in severe SMA mice while muscle-specific SMN expression has no phenotypic effect. *Hum Mol Genet* **17**, 1063-1075, doi:10.1093/hmg/ddm379 (2008).

90 Hayhurst, M., Wagner, A. K., Cerletti, M., Wagers, A. J. & Rubin, L. L. A cell-autonomous defect in skeletal muscle satellite cells expressing low levels of survival of motor neuron protein. *Dev Biol* **368**, 323-334, doi:10.1016/j.ydbio.2012.05.037 (2012).

91 Li, D. K. *et al.* A cell system for phenotypic screening of modifiers of SMN2 gene expression and function. *PLoS One* **8**, e71965, doi:10.1371/journal.pone.0071965 (2013).

92 Wishart, T. M. *et al.* SMN deficiency disrupts brain development in a mouse model of severe spinal muscular atrophy. *Hum Mol Genet* **19**, 4216-4228, doi:10.1093/hmg/ddq340 (2010).

93 Iascone, D. M., Henderson, C. E. & Lee, J. C. Spinal muscular atrophy: from tissue specificity to therapeutic strategies. *F1000Prime Rep* **7**, 04, doi:10.12703/P7-04 (2015).

94 Murphy, M. M., Lawson, J. A., Mathew, S. J., Hutcheson, D. A. & Kardon, G. Satellite cells, connective tissue fibroblasts and their interactions are crucial for muscle regeneration. *Development* **138**, 3625-3637, doi:10.1242/dev.064162 (2011).

95 Liu, W. *et al.* Loss of adult skeletal muscle stem cells drives age-related neuromuscular junction degeneration. *Elife* **6**, doi:10.7554/eLife.26464 (2017).

96 Sampath, S. C. *et al.* Induction of muscle stem cell quiescence by the secreted niche factor Oncostatin M. *Nat Commun* **9**, 1531, doi:10.1038/s41467-018-03876-8 (2018).

97 Frugier, T. *et al.* Nuclear targeting defect of SMN lacking the C-terminus in a mouse model of spinal muscular atrophy. *Hum Mol Genet* **9**, 849-858, doi:10.1093/hmg/9.5.849 (2000).

98 Madisen, L. *et al.* A robust and high-throughput Cre reporting and characterization system for the whole mouse brain. *Nat Neurosci* **13**, 133-140, doi:10.1038/nn.2467 (2010).

99 McGovern, V. L. *et al.* SMN expression is required in motor neurons to rescue electrophysiological deficits in the SMNDelta7 mouse model of SMA. *Hum Mol Genet* **24**, 5524-5541, doi:10.1093/hmg/ddv283 (2015).

100 Pawlikowski, B., Pulliam, C., Betta, N. D., Kardon, G. & Olwin, B. B. Pervasive satellite cell contribution to uninjured adult muscle fibers. *Skelet Muscle* **5**, 42, doi:10.1186/s13395-015-0067-1 (2015).

101 Hardy, D. *et al.* Comparative Study of Injury Models for Studying Muscle Regeneration in Mice. *PLoS One* **11**, e0147198, doi:10.1371/journal.pone.0147198 (2016).

102 Roman, W. & Gomes, E. R. Nuclear positioning in skeletal muscle. *Semin Cell Dev Biol* **82**, 51-56, doi:10.1016/j.semcdb.2017.11.005 (2018).

103 Supek, F., Bosnjak, M., Skunca, N. & Smuc, T. REVIGO summarizes and visualizes long lists of gene ontology terms. *PLoS One* **6**, e21800, doi:10.1371/journal.pone.0021800 (2011).

104 Bricceno, K. V. *et al.* Histone deacetylase inhibition suppresses myogenin-dependent atrogene activation in spinal muscular atrophy mice. *Hum Mol Genet* **21**, 4448-4459, doi:10.1093/hmg/dds286 (2012).

105 Cifuentes-Diaz, C. *et al.* Neurofilament accumulation at the motor endplate and lack of axonal sprouting in a spinal muscular atrophy mouse model. *Hum Mol Genet* **11**, 1439-1447, doi:10.1093/hmg/11.12.1439 (2002).

106 Liu, W., Wei-LaPierre, L., Klose, A., Dirksen, R. T. & Chakkalakal, J. V. Inducible depletion of adult skeletal muscle stem cells impairs the regeneration of neuromuscular junctions. *Elife* **4**, doi:10.7554/eLife.09221 (2015).

107 Carlson, B. M. The Biology of Long-Term Denervated Skeletal Muscle. *Eur J Transl Myol* **24**, 3293, doi:10.4081/ejtm.2014.3293 (2014).

108 Rodrigues Ade, C. & Schmalbruch, H. Satellite cells and myonuclei in long-term denervated rat muscles. *Anat Rec* **243**, 430-437, doi:10.1002/ar.1092430405 (1995).

109 Ng, S. Y. *et al.* Genome-wide RNA-Seq of Human Motor Neurons Implicates Selective ER Stress Activation in Spinal Muscular Atrophy. *Cell Stem Cell* **17**, 569-584, doi:10.1016/j.stem.2015.08.003 (2015).

110 Rodriguez-Muela, N. *et al.* Single-Cell Analysis of SMN Reveals Its Broader Role in Neuromuscular Disease. *Cell Rep* **18**, 1484-1498, doi:10.1016/j.celrep.2017.01.035 (2017).

111 Yang, Y. M. *et al.* A small molecule screen in stem-cell-derived motor neurons identifies a kinase inhibitor as a candidate therapeutic for ALS. *Cell Stem Cell* **12**, 713-726, doi:10.1016/j.stem.2013.04.003 (2013).

112 van der Wal, E. *et al.* Large-Scale Expansion of Human iPSC-Derived Skeletal Muscle Cells for Disease Modeling and Cell-Based Therapeutic Strategies. *Stem Cell Reports* **10**, 1975-1990, doi:10.1016/j.stemcr.2018.04.002 (2018).

113 Darabi, R. *et al.* Human ES- and iPS-derived myogenic progenitors restore DYSTROPHIN and improve contractility upon transplantation in dystrophic mice. *Cell Stem Cell* **10**, 610-619, doi:10.1016/j.stem.2012.02.015 (2012).

114 Tanaka, A. *et al.* Efficient and reproducible myogenic differentiation from human iPS cells: prospects for modeling Miyoshi Myopathy in vitro. *PLoS One* **8**, e61540, doi:10.1371/journal.pone.0061540 (2013).

115 Chal, J. *et al.* Differentiation of pluripotent stem cells to muscle fiber to model Duchenne muscular dystrophy. *Nat Biotechnol* **33**, 962-969, doi:10.1038/nbt.3297 (2015).

116 Caron, L. *et al.* A Human Pluripotent Stem Cell Model of Facioscapulohumeral Muscular Dystrophy-Affected Skeletal Muscles. *Stem Cells Transl Med* **5**, 1145-1161, doi:10.5966/sctm.2015-0224 (2016).

117 Quadrato, G., Brown, J. & Arlotta, P. The promises and challenges of human brain organoids as models of neuropsychiatric disease. *Nat Med* **22**, 1220-1228, doi:10.1038/nm.4214 (2016).

118 Wurster, C. D. & Ludolph, A. C. Nusinersen for spinal muscular atrophy. *Ther Adv Neurol Disord* **11**, 1756285618754459, doi:10.1177/1756285618754459 (2018).

119 Lee, S. J. *et al.* Role of satellite cells versus myofibers in muscle hypertrophy induced by inhibition of the myostatin/activin signaling pathway. *Proc Natl Acad Sci U S A* **109**, E2353-2360, doi:10.1073/pnas.1206410109 (2012).

120 Collins, C. A. *et al.* Stem cell function, self-renewal, and behavioral heterogeneity of cells from the adult muscle satellite cell niche. *Cell* **122**, 289-301, doi:10.1016/j.cell.2005.05.010 (2005).

121 Oh, J., Lee, Y. D. & Wagers, A. J. Stem cell aging: mechanisms, regulators and therapeutic opportunities. *Nat Med* **20**, 870-880, doi:10.1038/nm.3651 (2014).

122 Gussoni, E., Blau, H. M. & Kunkel, L. M. The fate of individual myoblasts after transplantation into muscles of DMD patients. *Nat Med* **3**, 970-977, doi:10.1038/nm0997-970 (1997).

123 Skuk, D. & Tremblay, J. P. Clarifying misconceptions about myoblast transplantation in myology. *Mol Ther* **22**, 897-898, doi:10.1038/mt.2014.57 (2014).

124 Sambasivan, R. *et al.* Distinct regulatory cascades govern extraocular and pharyngeal arch muscle progenitor cell fates. *Dev Cell* **16**, 810-821, doi:10.1016/j.devcel.2009.05.008 (2009).

125 Makhortova, N. R. *et al.* A screen for regulators of survival of motor neuron protein levels. *Nat Chem Biol* **7**, 544-552, doi:10.1038/nchembio.595 (2011).

126 Mohseni, J., Zabidi-Hussin, Z. A. & Sasongko, T. H. Histone deacetylase inhibitors as potential treatment for spinal muscular atrophy. *Genet Mol Biol* **36**, 299-307, doi:10.1590/S1415-47572013000300001 (2013).

127 Novotny-Diermayr, V. *et al.* SB939, a novel potent and orally active histone deacetylase inhibitor with high tumor exposure and efficacy in mouse models of colorectal cancer. *Mol Cancer Ther* **9**, 642-652, doi:10.1158/1535-7163.MCT-09-0689 (2010).

128 El-Khodor, B. F. *et al.* Identification of a battery of tests for drug candidate evaluation in the SMNDelta7 neonate model of spinal muscular atrophy. *Exp Neurol* **212**, 29-43, doi:10.1016/j.expneurol.2008.02.025 (2008).

129 Feng, Z. *et al.* Pharmacologically induced mouse model of adult spinal muscular atrophy to evaluate effectiveness of therapeutics after disease onset. *Hum Mol Genet* **25**, 964-975, doi:10.1093/hmg/ddv629 (2016).

130 Kuhn, M., von Mering, C., Campillos, M., Jensen, L. J. & Bork, P. STITCH: interaction networks of chemicals and proteins. *Nucleic Acids Res* **36**, D684-688, doi:10.1093/nar/gkm795 (2008).

131 Jones, N. C. *et al.* The p38alpha/beta MAPK functions as a molecular switch to activate the quiescent satellite cell. *J Cell Biol* **169**, 105-116, doi:10.1083/jcb.200408066 (2005).

132 Price, F. D. *et al.* Inhibition of JAK-STAT signaling stimulates adult satellite cell function. *Nat Med* **20**, 1174-1181, doi:10.1038/nm.3655 (2014).

133 Moyle, L. A. *et al.* Ret function in muscle stem cells points to tyrosine kinase inhibitor therapy for facioscapulohumeral muscular dystrophy. *Elife* **5**, doi:10.7554/eLife.11405 (2016).

134 Tierney, M. T. *et al.* STAT3 signaling controls satellite cell expansion and skeletal muscle repair. *Nat Med* **20**, 1182-1186, doi:10.1038/nm.3656 (2014).

135 Cosgrove, B. D. *et al.* Rejuvenation of the muscle stem cell population restores strength to injured aged muscles. *Nat Med* **20**, 255-264, doi:10.1038/nm.3464 (2014).

136 Yablonka-Reuveni, Z., Danoviz, M. E., Phelps, M. & Stuelsatz, P. Myogenic-specific ablation of Fgfr1 impairs FGF2-mediated proliferation of satellite cells at the myofiber niche but does not abolish the capacity for muscle regeneration. *Front Aging Neurosci* **7**, 85, doi:10.3389/fnagi.2015.00085 (2015).

137 Segales, J., Perdiguero, E. & Munoz-Canoves, P. Regulation of Muscle Stem Cell Functions: A Focus on the p38 MAPK Signaling Pathway. *Front Cell Dev Biol* **4**, 91, doi:10.3389/fcell.2016.00091 (2016).

138 Iyer, C. C. *et al.* Low levels of Survival Motor Neuron protein are sufficient for normal muscle function in the SMNDelta7 mouse model of SMA. *Hum Mol Genet* **24**, 6160-6173, doi:10.1093/hmg/ddv332 (2015).

139 Chal, J. & Pourquie, O. Making muscle: skeletal myogenesis in vivo and in vitro. *Development* **144**, 2104-2122, doi:10.1242/dev.151035 (2017).

140 Groen, E. J. N. *et al.* Temporal and tissue-specific variability of SMN protein levels in mouse models of spinal muscular atrophy. *Hum Mol Genet* **27**, 2851-2862, doi:10.1093/hmg/ddy195 (2018).

141 Chakkalakal, J. V., Jones, K. M., Basson, M. A. & Brack, A. S. The aged niche disrupts muscle stem cell quiescence. *Nature* **490**, 355-360, doi:10.1038/nature11438 (2012).

142 Bernet, J. D. *et al.* p38 MAPK signaling underlies a cell-autonomous loss of stem cell self-renewal in skeletal muscle of aged mice. *Nat Med* **20**, 265-271, doi:10.1038/nm.3465 (2014).

143 Puri, D., Gala, H., Mishra, R. & Dhawan, J. High-wire act: the poised genome and cellular memory. *FEBS J* **282**, 1675-1691, doi:10.1111/febs.13165 (2015).

144 Rumman, M., Dhawan, J. & Kassem, M. Concise Review: Quiescence in Adult Stem Cells: Biological Significance and Relevance to Tissue Regeneration. *Stem Cells* **33**, 2903-2912, doi:10.1002/stem.2056 (2015).

145 Liu, L. *et al.* Chromatin modifications as determinants of muscle stem cell quiescence and chronological aging. *Cell Rep* **4**, 189-204, doi:10.1016/j.celrep.2013.05.043 (2013).

146 Lu, J., McKinsey, T. A., Zhang, C. L. & Olson, E. N. Regulation of skeletal myogenesis by association of the MEF2 transcription factor with class II histone deacetylases. *Mol Cell* **6**, 233-244, doi:10.1016/s1097-2765(00)00025-3 (2000).

147 Moresi, V. *et al.* Myogenin and class II HDACs control neurogenic muscle atrophy by inducing E3 ubiquitin ligases. *Cell* **143**, 35-45, doi:10.1016/j.cell.2010.09.004 (2010).

148 Swoboda, K. J. *et al.* SMA CARNI-VAL trial part I: double-blind, randomized, placebo-controlled trial of L-carnitine and valproic acid in spinal muscular atrophy. *PLoS One* **5**, e12140, doi:10.1371/journal.pone.0012140 (2010).

149 Kissel, J. T. *et al.* SMA CARNIVAL TRIAL PART II: a prospective, single-armed trial of L-carnitine and valproic acid in ambulatory children with spinal muscular atrophy. *PLoS One* **6**, e21296, doi:10.1371/journal.pone.0021296 (2011).

150 Brody, H. Regenerative medicine. *Nature* **540**, S49, doi:10.1038/540S49a (2016).

151 Tabar, V. & Studer, L. Pluripotent stem cells in regenerative medicine: challenges and recent progress. *Nat Rev Genet* **15**, 82-92, doi:10.1038/nrg3563 (2014).

152 Qazi, T. H. *et al.* Cell therapy to improve regeneration of skeletal muscle injuries. *J Cachexia Sarcopenia Muscle* **10**, 501-516, doi:10.1002/jcsm.12416 (2019).

153 Grasman, J. M., Do, D. M., Page, R. L. & Pins, G. D. Rapid release of growth factors regenerates force output in volumetric muscle loss injuries. *Biomaterials* **72**, 49-60, doi:10.1016/j.biomaterials.2015.08.047 (2015).

154 Bosch-Marce, M. *et al.* Increased IGF-1 in muscle modulates the phenotype of severe SMA mice. *Hum Mol Genet* **20**, 1844-1853, doi:10.1093/hmg/ddr067 (2011).

155 Musaro, A. *et al.* Localized Igf-1 transgene expression sustains hypertrophy and regeneration in senescent skeletal muscle. *Nat Genet* **27**, 195-200, doi:10.1038/84839 (2001).

156 Deshmukh, V. A. *et al.* A regenerative approach to the treatment of multiple sclerosis. *Nature* **502**, 327-332, doi:10.1038/nature12647 (2013).

157 Neumann, B. *et al.* Metformin Restores CNS Remyelination Capacity by Rejuvenating Aged Stem Cells. *Cell Stem Cell* **25**, 473-485 e478, doi:10.1016/j.stem.2019.08.015 (2019).

158 McLean, W. J. *et al.* Clonal Expansion of Lgr5-Positive Cells from Mammalian Cochlea and High-Purity Generation of Sensory Hair Cells. *Cell Rep* **18**, 1917-1929, doi:10.1016/j.celrep.2017.01.066 (2017).

159 *FX-322 in Adults With Stable Sensorineural Hearing Loss*, <https://clinicaltrials.gov/ct2/show/NCT04120116?term=fx-322&rank=2> (2019).

160 Lawlor, M. W. *et al.* Myotubularin-deficient myoblasts display increased apoptosis, delayed proliferation, and poor cell engraftment. *Am J Pathol* **181**, 961-968, doi:10.1016/j.ajpath.2012.05.016 (2012).

161 Higuchi, I. *et al.* Statistically significant differences in the number of CD24 positive muscle fibers and satellite cells between sarcoglycanopathy and age-matched Becker muscular dystrophy patients. *Intern Med* **38**, 412-415, doi:10.2169/internalmedicine.38.412 (1999).

162 Miyagoe-Suzuki, Y. *et al.* Reduced proliferative activity of primary POMGnT1-null myoblasts in vitro. *Mech Dev* **126**, 107-116, doi:10.1016/j.mod.2008.12.001 (2009).

163 Minetti, G. C. *et al.* Functional and morphological recovery of dystrophic muscles in mice treated with deacetylase inhibitors. *Nat Med* **12**, 1147-1150, doi:10.1038/nm1479 (2006).

164 Hwang, A. B. & Brack, A. S. Muscle Stem Cells and Aging. *Curr Top Dev Biol* **126**, 299-322, doi:10.1016/bs.ctdb.2017.08.008 (2018).

165 Quarta, M. *et al.* Bioengineered constructs combined with exercise enhance stem cell-mediated treatment of volumetric muscle loss. *Nat Commun* **8**, 15613, doi:10.1038/ncomms15613 (2017).

166 Pasut, A., Jones, A. E. & Rudnicki, M. A. Isolation and culture of individual myofibers and their satellite cells from adult skeletal muscle. *J Vis Exp*, e50074, doi:10.3791/50074 (2013).

167 Cerletti, M. *et al.* Highly efficient, functional engraftment of skeletal muscle stem cells in dystrophic muscles. *Cell* **134**, 37-47, doi:10.1016/j.cell.2008.05.049 (2008).

168 Maesner, C. C., Almada, A. E. & Wagers, A. J. Established cell surface markers efficiently isolate highly overlapping populations of skeletal muscle satellite cells by fluorescence-activated cell sorting. *Skelet Muscle* **6**, 35, doi:10.1186/s13395-016-0106-6 (2016).

169 Sherwood, R. I. *et al.* Isolation of adult mouse myogenic progenitors: functional heterogeneity of cells within and engrafting skeletal muscle. *Cell* **119**, 543-554, doi:10.1016/j.cell.2004.10.021 (2004).

170 Soumillon, M., Cacchiarelli, D., Semrau, S., can Oudenaarden, A. & Mikkelsen, T. S. Characterization of directed differentiation by high-throughput single-cell RNA-Seq. *bioRxiv* (2014).

APPENDIX A

SUPPLEMENTARY FIGURES

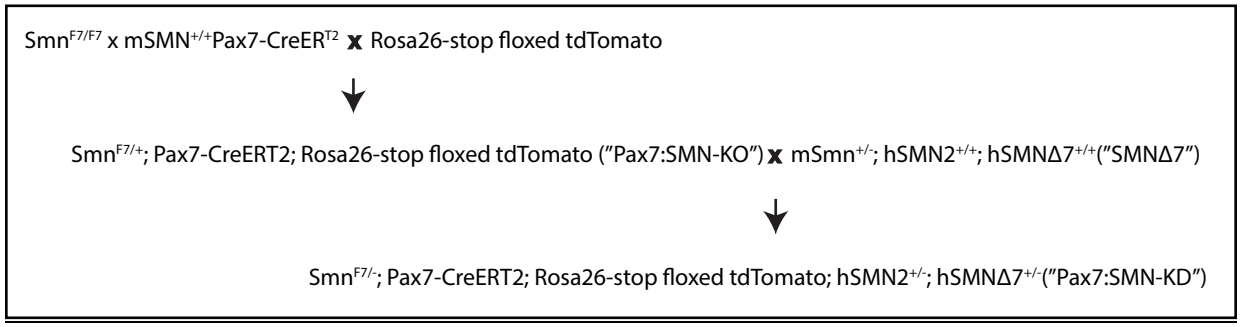

Supplementary Figure 2.1. Breeding schematic showing generation of *Pax7:SMN*-KO and *Pax7:SMN*-KD mice. To generate *Pax7:SMN*-KO mice, SMN$^{F7/F7}$ mice were bred to Pax7-CreER^{T2} and Rosa-tdTomato mice. Triple homozygous offspring were bred to SMNΔ7 to generate the *Pax7:SMN*-KD model.

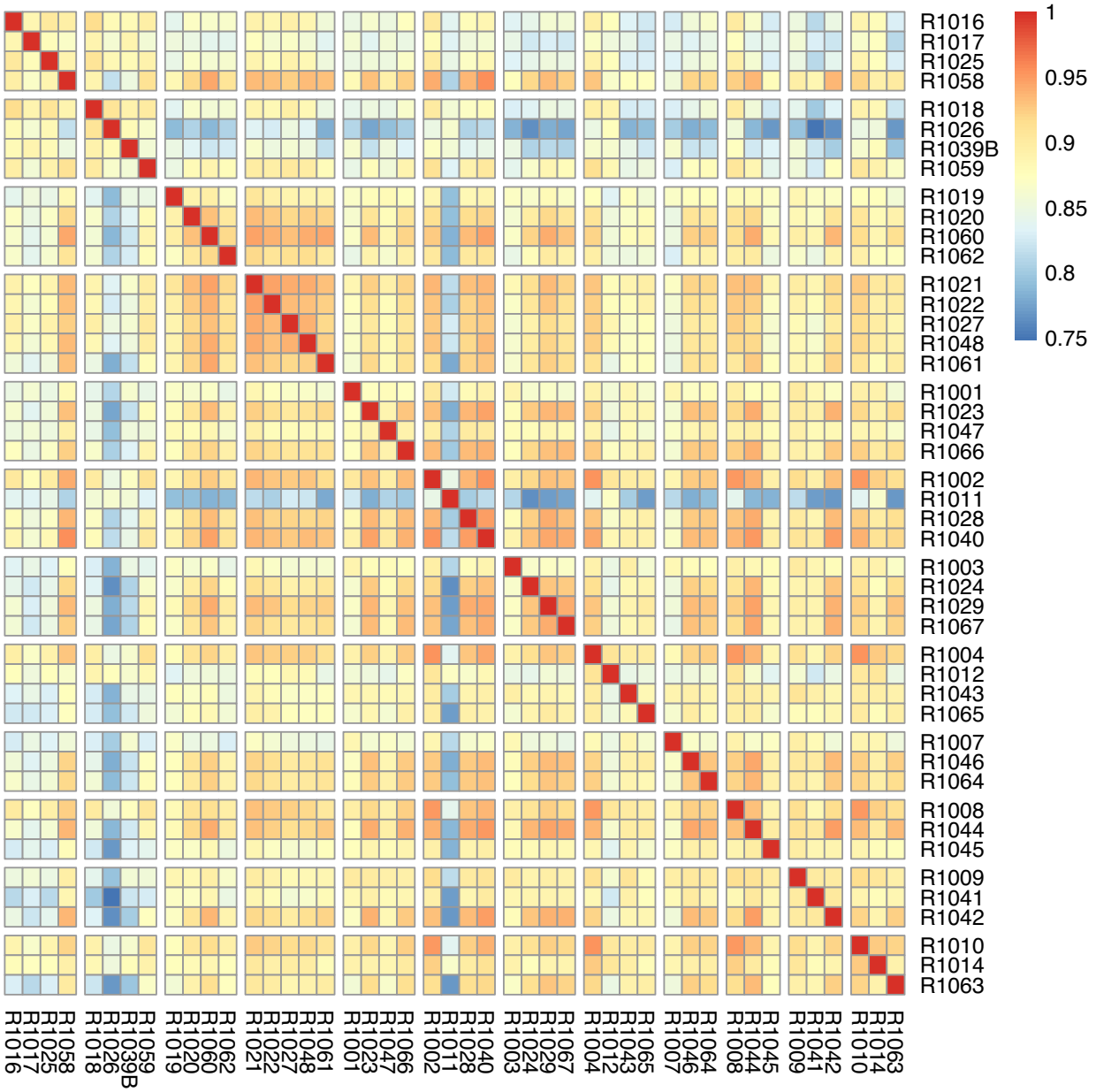

Supplementary Figure 2.2. Sample correlation for RNA sequencing read counts. Myoblast RNA-sequencing expression counts were first filtered to remove genes with fewer than 50 unique UMIs across all samples. Pearson correlation coefficients were then computed on log10 transformed UMI counts. Samples are grouped by cell type and treatment. Sample R1011 was excluded from the analysis due to low correlation with all other samples.

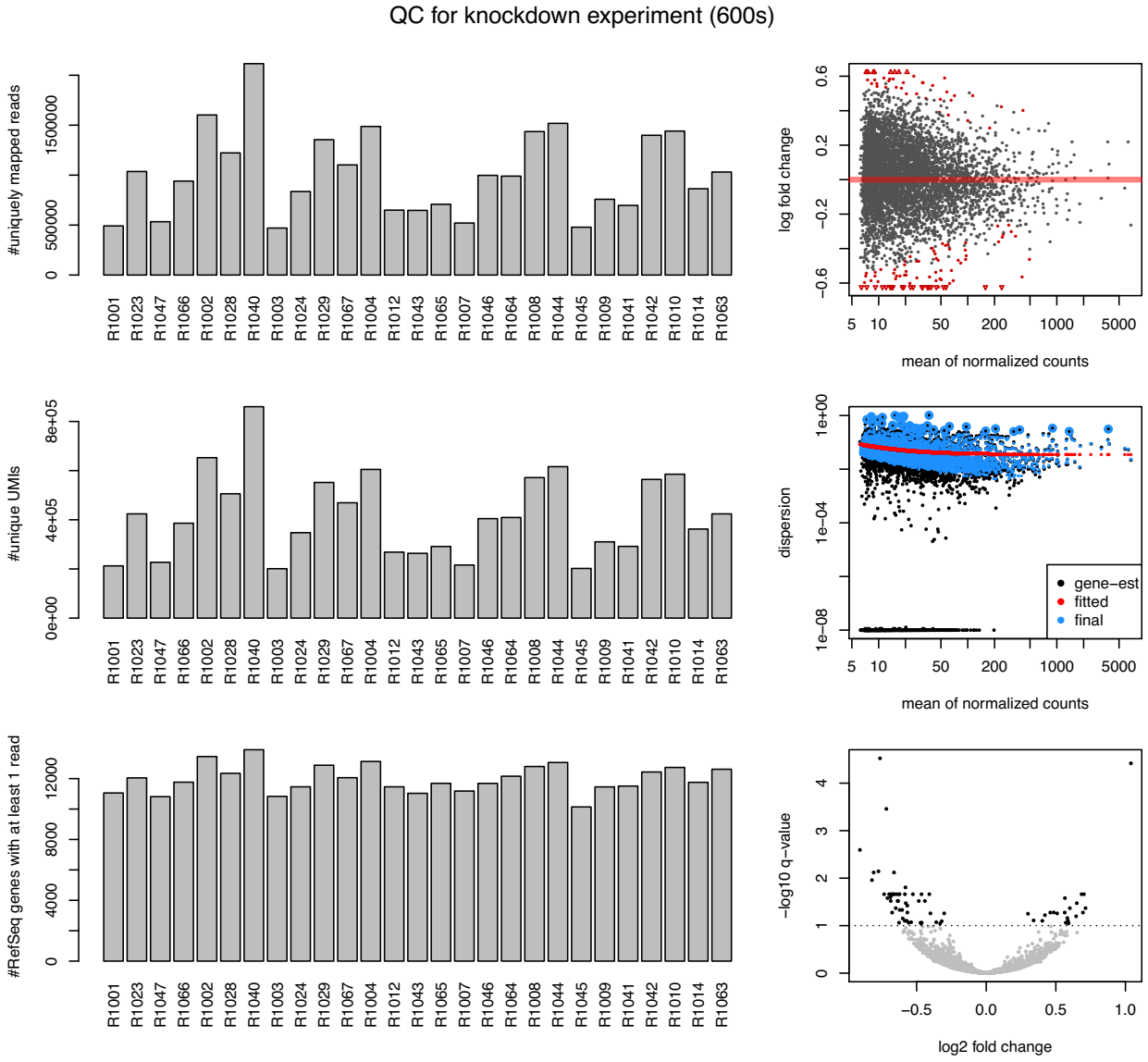

Supplemental Figure 2.3. Quality assessment of RNA sequencing analysis for *Pax7:SMN*-KD myoblasts. A) Total number of reads that uniquely mapped to mm10 RefSeq genes. B) Total number of unique UMIs mapped to mm9 RefSeq genes. C) Number of genes detected per library. D) MA plot: each dot represents one gene. X-axis: Mean normalized read count per gene; Y-axis: log2fold change of SMA versus WT. Red points indicate significant differential expression. E) DESeq2 dispersion model: X-axis: Mean normalized count per gene; Y-axis: Variance of read count over all samples. F) Volcano plot showing log2fold change of SMA versus WT against -log10 q-values. Horizontal line denotes a false discovery rate (FDR) cutoff of 0.1. Black points are called as differentially expressed genes.

Supplementary Table 2.1. Differentially expressed genes in *Pax7:SMN*-KD control versus mutant myoblasts

Gene	log2 Fold Change	q value	Gene	log2 Fold Change	q value	Gene	log2 Fold Change	q value
Hist1h1c	1.039	0	Spc24	-0.688	0.025	Sptbn1	0.509	0.055
Hmgb2	-0.718	0	Clspn	-0.709	0.026	Cd81	0.3	0.056
Hmgn2	-0.763	0	Snrpa1	0.565	0.026	Atp6v1g1	0.422	0.06
Prim1	-0.908	0.003	Dhfr	-0.637	0.03	Hsd11b1	0.646	0.064
Lig1	-0.774	0.007	Kif23	-0.633	0.03	Map2k1	0.583	0.069
Hist1h1b	-0.809	0.008	Kpna2	-0.485	0.03	Hmmr	-0.6	0.071
Lrrc17	-0.662	0.008	Mest	-0.686	0.03	Gabarap	0.34	0.078
Cdca3	-0.821	0.011	Srsf7	-0.441	0.03	2810417H13Rik	-0.585	0.079
Pcna	-0.58	0.016	2700094K13Rik	-0.578	0.034	Cd59a	0.587	0.079
Amotl2	0.685	0.022	Hist1h2bc	0.651	0.034	Ctsd	0.403	0.079
Atf5	0.701	0.022	Nasp	-0.567	0.038	Fen1	-0.572	0.079
Birc5	-0.686	0.022	Gna13	0.713	0.043	Erh	-0.32	0.08
Ccnb1	-0.623	0.022	Kif22	-0.65	0.043	Hnrnpf	-0.359	0.085
Cdca8	-0.628	0.022	Pold4	0.601	0.043	Prdx4	-0.54	0.085
Cdk1	-0.666	0.022	Asf1b	-0.622	0.047	2810025M15Rik	-0.472	0.087
Ddx39	-0.527	0.022	Top2a	-0.604	0.047	Cenpa	-0.558	0.087
Dnmt1	-0.673	0.022	Dhrs3	0.695	0.053	Fn1	0.59	0.087
Fam64a	-0.734	0.022	H2afz	-0.566	0.053	Lsm5	-0.464	0.087
Grcc10	-0.409	0.022	Mdm2	0.564	0.053	Ptpra	0.571	0.087
Hmgb1	-0.465	0.022	Rad51ap1	-0.676	0.053	Rnf219	-0.626	0.087
Mad2l1	-0.698	0.022	Sqstm1	0.46	0.053	Hdac1	-0.468	0.09
Prc1	-0.584	0.022	Timp2	0.485	0.053	Hspd1	-0.332	0.09
Stmn1	-0.648	0.022	H3f3b	-0.302	0.055	Pmaip1	0.59	0.09
Uhrf1	-0.666	0.022	Smc1a	-0.401	0.055			

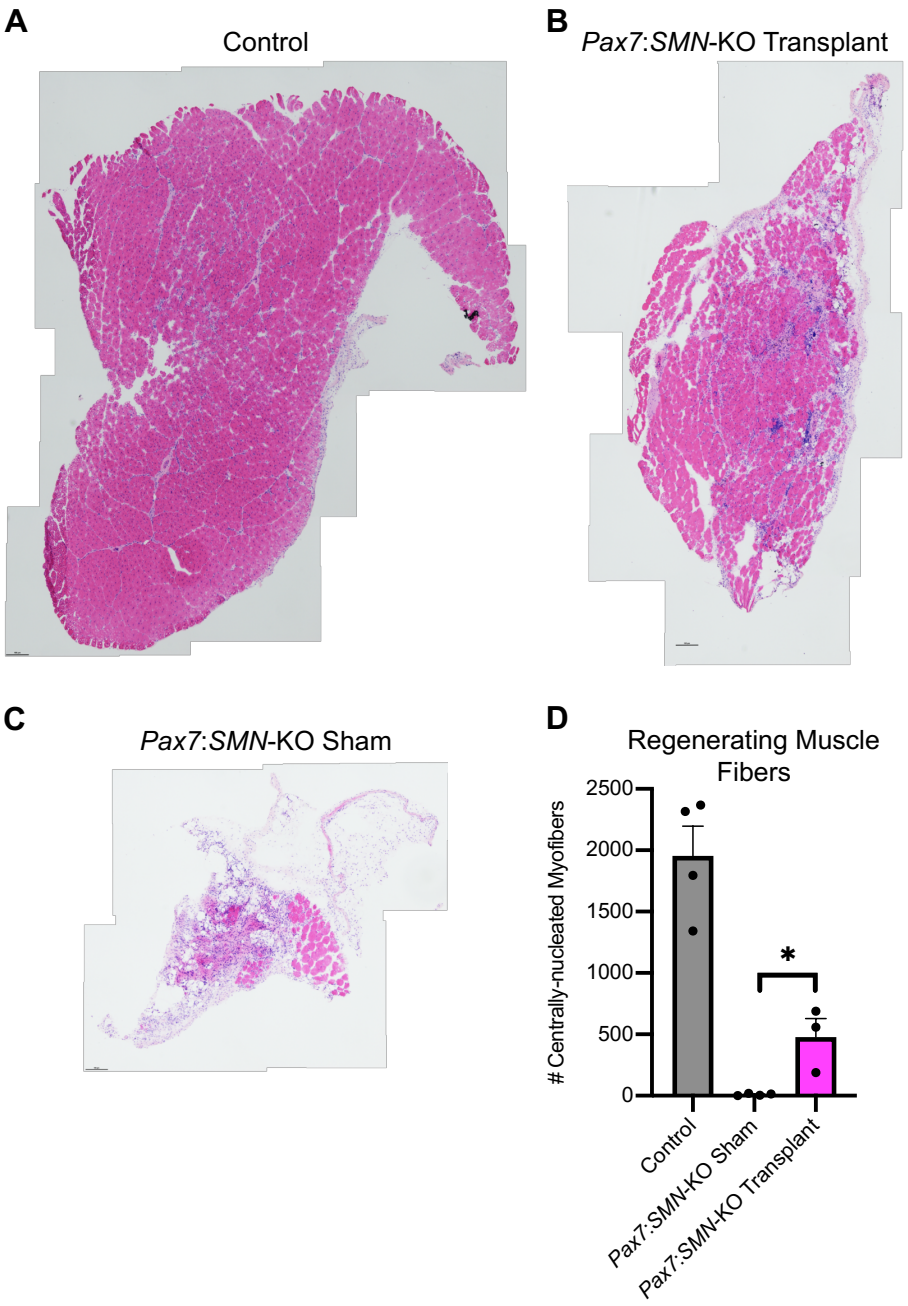

Supplementary Figure 4.1. Satellite cell transplant in *Pax7:SMN*-KO mice after muscle damage rescues regeneration. Wild type satellite cells FACS-purified from Tg:Pax7-nGFP mice were injected into TA muscles of tamoxifen-treated *Pax7:SMN*-KO control and mutant mice 24 hours post-cardiotoxin damage (10,000 cells transplanted per muscle). Regeneration was assessed after 3 weeks by quantifying the number of centrally-nucleated myofibers per muscle section. A-C) H&E images of Cre-only control, *Pax7:SMN*-KO transplant, and *Pax7:SMN*-KO sham TA muscles. D) Quantification showing rescue of regenerating fibers after transplant. N=3-4 per group, p=0.0136, unpaired t test. Data presented as mean ± SEM.

Supplementary Table 4.1. Full list of hit compounds from wild type satellite cell screen.

Compound	Annotation	Fold Change Relative to Vehicle	Max Fold Change Concentration (uM)	Standard Deviation	Significance
VX-702	p38 MAPK inhibitor	6.390	5	2.051	*
Doramapimod	p38 MAPK inhibitor (MK14)	5.499	5	1.126	***
NG25	Tgf-b activated kinase (Tak1) inhibitor	5.147	0.8	1.325	*
Ralimetinib	p38 MAPK inhibitor	4.635	3	1.913	*
Bosutinib	Bcr-Abl inhibitor	4.580	3	2.157	*
PH-797804	p38 MAPK inhibitor	4.554	5	0.740	***
SB 239063	p38 MAPK inhibitor	4.414	5	0.957	***
SB202190	p38 MAPK inhibitor	4.303	3	1.138	*
URMC-099	MLK and DLK inhibitor	3.697	0.8	1.405	*
BI-D1870	RSK inhibitor	3.641	3	1.009	**
SB 203580	p38 MAPK inhibitor (MK14)	3.505	5	0.317	***
Losmapimod	p38 MAPK inhibitor	3.080	5	0.630	**
XMD8-92	BMK1/ERK5 inhibitor	2.670	3	0.160	***
Vorinostat	HDAC1 - linked to cell differentiation	2.636	0.4	0.316	***
XMD8-85	BMK1/ERK5 and BRD4 inhibitor	2.584	3	0.303	***
XMD11-50	LRRK2 inhibitor	2.556	0.8	0.491	***
I-BET GSK525762A	BET bromodomain inhibitor	2.456	0.4	0.117	***
Pracinostat	HDAC inhibitor	2.445	0.2	0.596	***
I-BET151 GSK1210151A	BET bromodomain inhibitor	2.416	0.8	0.114	***
VX-745	p38α inhibitor	2.325	5	0.211	***
Rocilinostat ACY-1215	HDAC6 inhibitor	2.300	3	0.188	***
Entinostat MS-27-275	HDAC1 and HDAC3 inhibitor	2.106	0.4	0.716	***
(+)-JQ1 (S)-JQ1	BET bromodomain inhibitor	2.025	0.1	0.362	***
HG-6-64-01	B-Raf inhibitor	2.007	0.05	0.045	***
AZ-628	pan-Raf inhibitor	1.956	3	0.224	**
PFI-1	BET bromodomain inhibitor	1.922	0.8	0.248	***
Mocetinostat MGCD0103	HDAC inhibitor	1.922	0.2	0.422	**
Nilotinib	Bcr-Abl inhibitor (abl1)	1.908	5	0.304	***
GDC-0879	B-Raf inhibitor	1.774	3	0.210	***
Sorafenib	Multikinase inhibitor (Raf-1, B-Raf, VEGFR-2)	1.770	1	0.450	**
Neratinib	HER2 and EGFR inhibitor	1.769	0.8	0.135	***

Table 4.1 (continued)

Compound	Annotation	Fold Change Relative to Vehicle	Max Fold Change Concentration (uM)	Standard Deviation	Significance
Belinostat PXD101	HDAC inhibitor	1.768	0.2	0.375	**
Sunitinib	RTK inhibitor (Flk-1, PDGFRβ)	1.588	0.8	0.292	**
Y-27632	ROCK inhibitor	1.577	0.1	1.212	
SB590885 GSK2118436	B-Raf inhibitor	1.528	0.8	0.263	*
NVP-BHG712 KIN001-265	EphB4 (also activity against VEGFR, c-Raf)	1.450	1	0.218	
pseudoXL765	PIK3C inhibitor	1.374	0.8	0.202	**
Y39983	ROCK inhibitor	1.256	0.8	0.105	*
KIN001-055HY-11067	JAK3, MKNK1 inhibitor	1.123	1	0.141	
MK2206	Akt inhibitor	1.023	0.1	0.077	

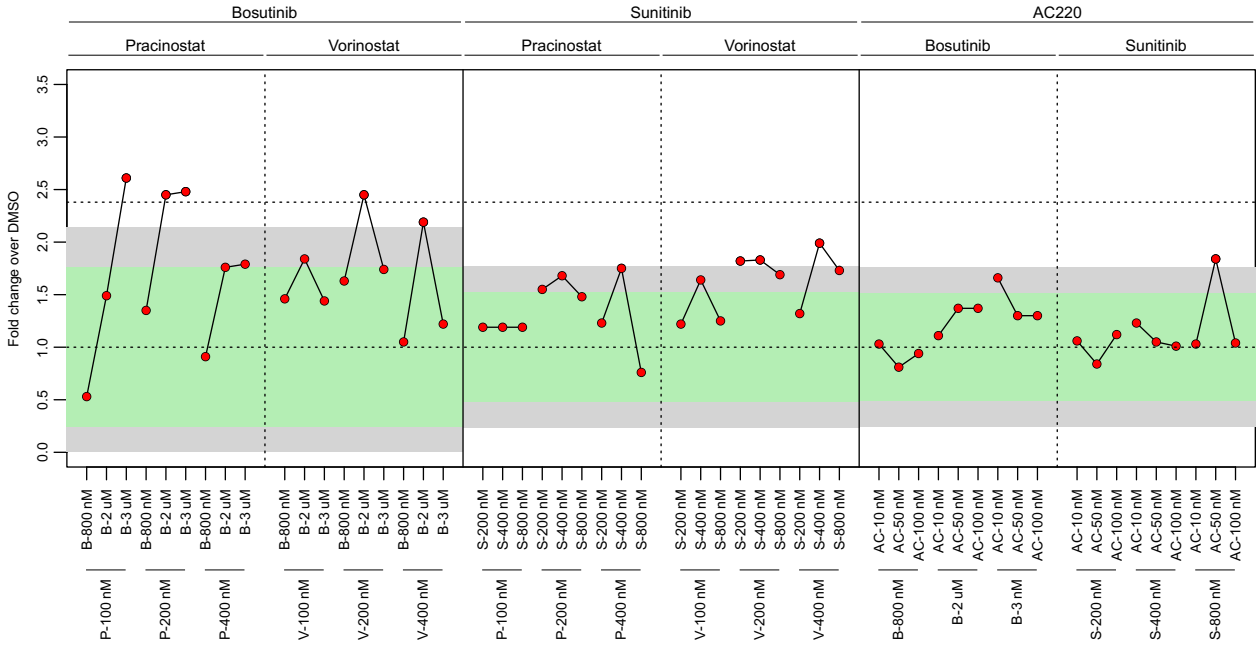

Supplementary Figure 4.2. Compound synergy assay in wild type satellite cells. Plot showing the effect of 3 doses each of various combinations of compounds on stimulating wild type satellite cell proliferation. The Y-axis represents fold change in satellite cell number relative to DMSO control. The rectangles show 2X (green) and 3X (grey) the DMSO standard deviation per plate.

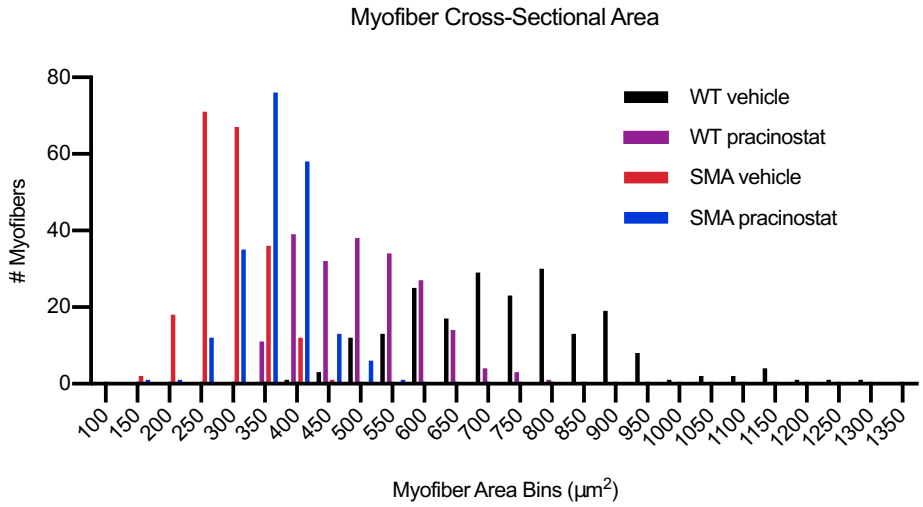

Supplementary Figure 4.3. Pracinostat increases muscle fiber size relative to wild type controls in severe SMA mice *in vivo*. Histogram showing distribution of TA individual myofiber cross-sectional area in SMNΔ7 mutant and wild type mice treated with pracinostat or DMSO.

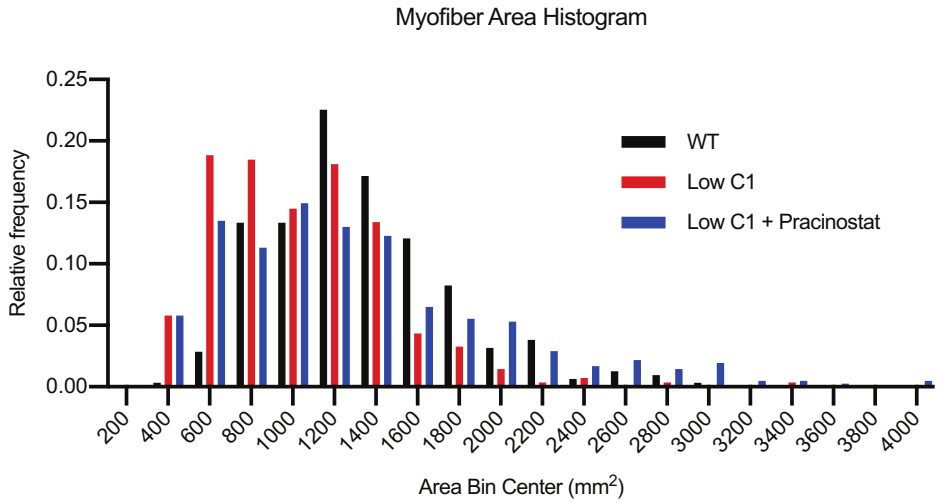

Supplementary Figure 4.4. Pracinostat ameliorates muscle atrophy relative to wild type controls in intermediate pharmacological SMA mice *in vivo*. Histogram showing distribution of semispinalis individual myofiber cross-sectional area in pharmacological SMA mice treated with a low dose of C1 alone or with C1 + pracinostat.

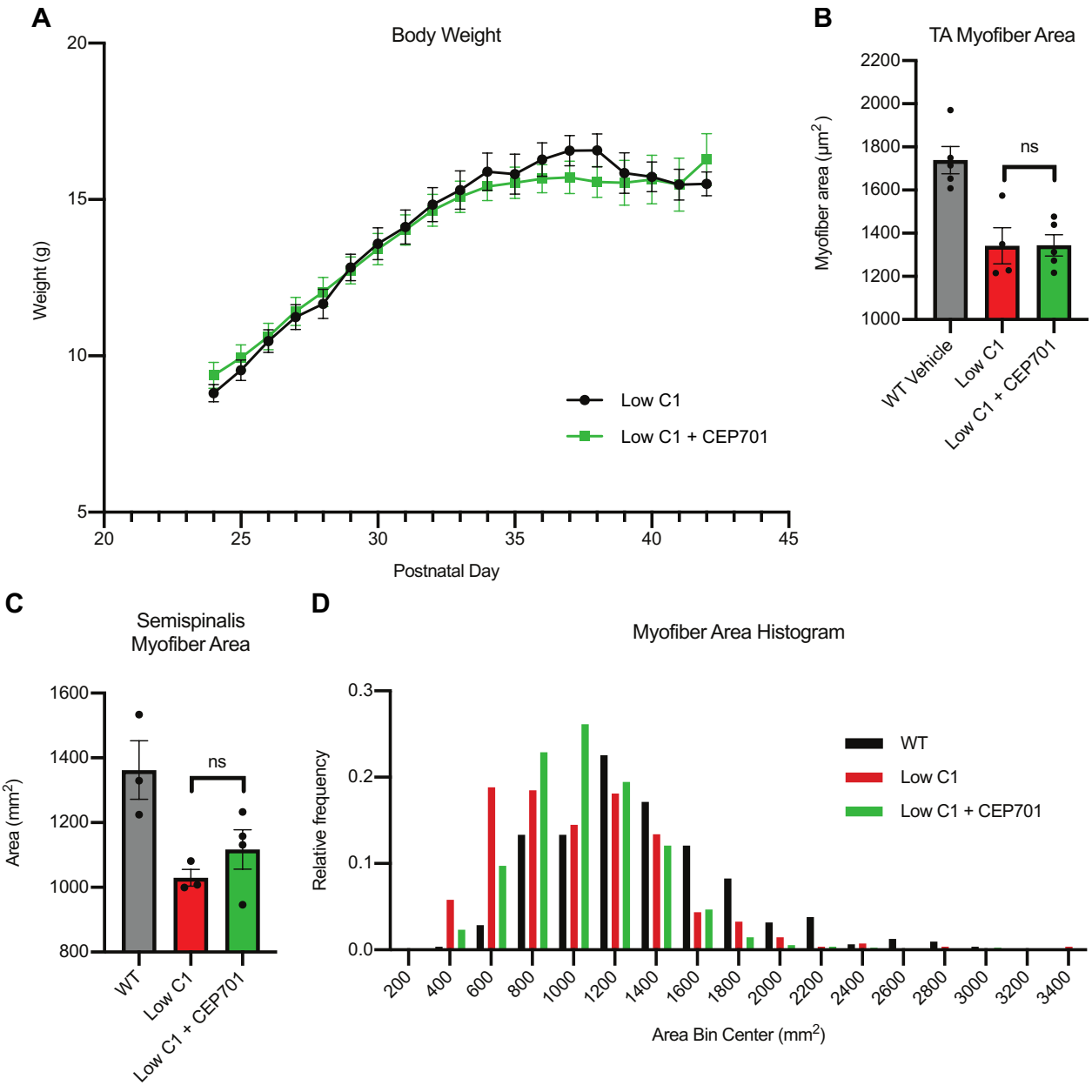

Supplementary Figure 4.5. CEP701 does not ameliorate muscle atrophy in intermediate pharmacological SMA mice *in vivo*. A) Daily body weight of SMNΔ7 mutant mice treated with a low dose of C1 only or a low dose of C1 and CEP701. B) Hind limb TA individual myofiber area at P42. N=4-5 per group, p=>0.05, unpaired t test. C) Semispinalis individual myofiber area at P42. N=3-4 per group, p=>0.05, unpaired t test. D) Histogram showing distribution of semispinalis individual myofiber cross-sectional area.

APPENDIX B

PUBLISHED REVIEW ARTICLE

Toward Precision Medicine for Neurological and Neuropsychiatric Disorders

Cell Stem Cell, 23(1):21-24

Rebecca M. Gibbs[1,2], Scott Lipnick[1,2,3], Joel W. Bateman[1,4], Lloyd Chen[1,4], Henry C. Cousins[1,4], Elizabeth G. Hubbard[1,4], Geraldine Jowett[1,2,4], Darren S. LaPointe[1,4], Maxine J. McGredy[1,4], Michelle N. Odonkor[1,4], Giuliana Repetti[1,2,4], Elizabeth Thomas[1,4], and Lee L. Rubin[1,2]

[1]Department of Stem Cell and Regenerative Biology, Harvard University, Cambridge, MA 02138, USA

[2]Harvard Stem Cell Institute, Harvard University, Cambridge, MA 02138, USA

[3]Department of Biomedical Informatics, Harvard Medical School, Boston, MA 02115, USA

[4]These authors contributed equally

Contribution:

Manuscript written by Rebecca Gibbs and edited by Dr. Lee Rubin. Concepts and research for this Forum were conceived as part of an undergraduate course at Harvard College (SCRB 195) taught by Dr. Lee Rubin (Professor) and Rebecca Gibbs (Teaching Fellow).

Cell Stem Cell
Forum

Toward Precision Medicine for Neurological and Neuropsychiatric Disorders

Rebecca M. Gibbs,[1,2] Scott Lipnick,[1,2,3] Joel W. Bateman,[1,4] Lloyd Chen,[1,4] Henry C. Cousins,[1,4] Elizabeth G. Hubbard,[1,4] Geraldine Jowett,[1,2,4] Darren S. LaPointe,[1,4] Maxine J. McGredy,[1,4] Michelle N. Odonkor,[1,4] Giuliana Repetti,[1,2,4] Elizabeth Thomas,[1,4] and Lee L. Rubin[1,2,*]
[1]Department of Stem Cell and Regenerative Biology, Harvard University, Cambridge, MA 02138, USA
[2]Harvard Stem Cell Institute, Harvard University, Cambridge, MA 02138, USA
[3]Department of Biomedical Informatics, Harvard Medical School, Boston, MA 02115, USA
[4]These authors contributed equally
*Correspondence: lee_rubin@harvard.edu
https://doi.org/10.1016/j.stem.2018.05.019

The genetic complexity, clinical variability, and inaccessibility of affected tissue in neurodegenerative and neuropsychiatric disorders have largely prevented the development of effective disease-modifying therapeutics. A precision medicine approach that integrates genomics, deep clinical phenotyping, and patient stem cell models may facilitate identification of underlying biological drivers and targeted drug development.

Neurological disorders are a leading cause of disability and fatality worldwide, accounting for 17% of global deaths and 10% of disability-adjusted life-years (GBD 2015 Neurological Disorders Collaborator Group, 2017). The prevalence of these conditions has increased substantially over the past three decades and will continue to grow due to population expansion and increasing life expectancy, leading to a staggering health and economic burden. Despite massive research efforts, effective preventative and disease-modifying treatments remain elusive. A pervasive challenge hindering drug development is the traditional classification of central nervous system (CNS) diseases as single disorders defined by end-stage clinical symptoms and pathologies, instead of a disease continuum comprising a range of genetic and pathological subclasses. We believe that CNS therapeutics development will benefit from a precision medicine approach, which will require integrated methodologies that combine genomics, electronic medical records (EMRs), and patient-derived stem cell models. The confluence of these modern tools could enable identification of more homogeneous patient populations early in disease progression and development of more precise, subtype-matched therapeutics that target shared pathological mechanisms.

Lessons from Precision Medicine in Oncology

The field of oncology has paved the way for more precise clinical subtyping and targeted drug treatment, but this has not always been the case. Traditional chemotherapy and radiation treatments broadly inhibit proliferation, thus causing high toxicity by failing to distinguish between cancer cells and rapidly dividing healthy cells. Two decades ago, oncologists recognized that cancers with similar pathological phenotypes or those arising in individual organs were actually distinct tumor subtypes that could be targeted with more precise and selective treatments. The most notable early success was the development of the BCR-ABL inhibitor Gleevec for the treatment of chronic myeloid leukemia, which substantially improved survival rates (Shin et al., 2017). It is now almost universally accepted that targeting specific molecular pathways driving tumor growth is superior to traditional, less specific treatments like chemotherapy. Clinical trials such as NCI-MATCH (ClinicalTrials.gov number NCT02465060) have begun accounting for interpatient and intratumor heterogeneity by selecting targeted treatments based on tumor mutation profiles.

Similar to cancer, CNS disorders result from a complex interplay between genetics and environment, and likely represent a broad categorization of many different molecular pathologies leading to uniform clinical presentations (Figure 1). However, the precision medicine approach that has been successful in oncology may be far more challenging to achieve for the treatment of CNS disorders. First, neural tissue cannot be biopsied to identify particular molecular pathways at play. Second, CNS disorders present with highly variable phenotypes, penetrance, and age of onset. Although clinical diagnostics and imaging methods are helpful, these approaches do not provide sufficient granularity to distinguish each CNS disease subtype on a molecular level. Third, the genetic mutations underlying cancer are largely somatic and can often be identified by comparison to adjacent unaffected tissue. In CNS disorders, inherited genomic variation is a critical factor and thus requires population comparison for detection. Although neural diseases sometimes arise from highly penetrant mutations, genome-wide association studies have indicated that they more commonly result from the integrated effects of hundreds of common genetic variants with small effect sizes converging on common phenotypic endpoints, such as neural dysfunction and neuroinflammation followed by neuronal death. However, genomics studies have not yet predicted which variants act together to produce different disease types. Overall, although genetics sets a foundation for disease risk, the biological pathways driving key pathogenic processes remain largely unknown, making it difficult to identify discrete drug targets that modify disease progression.

Developing Targeted Therapeutics for Stratified Patient Populations

Drugs developed for CNS disorders typically target common phenotypes or symptoms (i.e., the final convergence point in Figure 1). For example, antibodies

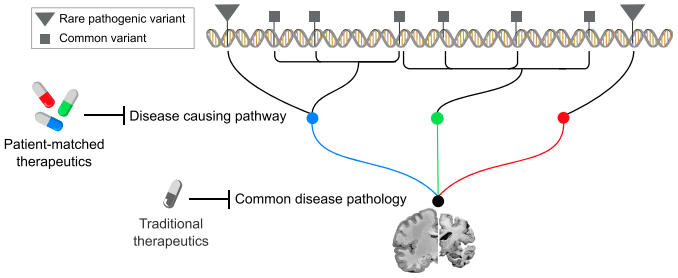

Figure 1. Common Clinical Phenotypes in Neurodegenerative and Neuropsychiatric Disorders Result from Complex Genetic Variation Converging on Multiple Pathogenic Pathways

Identification of intermediate convergence points may lead to novel disease-modifying therapeutics that target specific biological disease drivers.

against amyloid-β peptide have been extensively explored as a therapy for Alzheimer's disease (AD) due to the pathological accumulation of amyloid-β plaques in all AD patients. Analogous to chemotherapy for cancer, broad therapeutics may prove helpful. However, similar to cancer, neural disorders are driven by multiple molecular pathways and may therefore require targeted therapeutics. Thus, it may be preferable to employ a precision medicine approach by developing drugs that target narrow groups of patients with similar underlying genetic variation (i.e., disease-contributing variants in Figure 1). For example, although hundreds of mutations in the *CFTR* gene have been shown to cause cystic fibrosis, the drug Kalydeco (Vertex Pharmaceuticals) was initially FDA approved specifically for patients with the G551D mutation, which causes faulty ion channel gating (Quon and Rowe, 2016). Kalydeco's indication has since been expanded to include patients with additional *CFTR* gating mutations. Given the polygenicity of CNS disorders, this approach may only be feasible if the shared functional consequences of multiple gene products can be identified, and if there is a large enough population to justify the hefty drug development costs. In spite of Kalydeco's expansion to additional patients, the treatment costs more than $300,000 per year due to the very small number of treatable patients. To avoid the prohibitively high costs of developing therapeutics for ultra-rare patient populations, it would be ideal to develop therapies that perturb shared mechanistic pathways and that are reasonably effective across an economically practical patient base (i.e., therapies that target the intermediate convergence points in Figure 1).

Implementing Precision Medicine for CNS Diseases

If we acknowledge that CNS disorders need to be more precisely defined for the purposes of identifying targeted therapeutics, how do we begin to subtype these complex diseases? An important first step in implementing precision medicine for neurodegenerative and neuropsychiatric disorders will be improving methodologies to parse out the intermediate pathways leading to neuronal dysfunction in different forms of CNS disorders. Genome sequencing has proven useful in unraveling the genetic architecture of CNS diseases, but understanding how multitudes of risk variants translate to neural pathologies requires more than genomic data alone. We believe that an integrated approach combining patients' genomic data, EMRs, and molecular phenotyping of patient stem cell-derived models will help to identify therapeutically valid pathogenic mechanisms shared by defined patient populations (Figure 2). EMRs provide large amounts of clinical information about neural diseases, including pathologies in peripheral tissues, the temporal relationship between pathologies, and other factors that modulate CNS dysfunction. Furthermore, capturing patients' genomes in induced pluripotent stem cells (iPSCs) provides a valuable system to functionalize genetic contributions to cellular behavior and extend the power of genetic and EMR data.

Genomics for Patient Stratification

Genetic data have played an important role in understanding neural disease transmission and etiology. Familial studies of most CNS disorders have shown a high degree of heritability and have occasionally identified highly penetrant, causal variants and risk genes. Clinical trials have evolved from enrolling broad and heterogeneous patient populations to a more modern paradigm of treating small, genetically homogeneous populations in early disease stages, using disease variants as inclusion criteria. These early precision medicine attempts have been most noteworthy in AD. For example, following several clinical failures in genetically heterogeneous cohorts of patients with mild to moderate AD, anti-amyloid-β monoclonal antibody therapy is now being tested in individuals with known AD-causing mutations prior to cognitive symptom onset, with the hope that prevention trials in genetically similar patients are more likely to result in positive outcomes (the DIAN trial; ClinicalTrials.gov number NCT01760005). However, despite attempts to stratify patients into more homogeneous cohorts and implement early treatment, the DIAN trial is still testing a therapy that targets a very broad clinical phenotype, analogous to chemotherapy in cancer. Additional tools other than genotyping highly penetrant variants will be needed to develop more precisely tailored therapeutics.

Integrating Genomics and Clinical Data from EMRs

What other tools can enable us to functionalize genomics data? One interesting approach is to combine clinical data derived from EMRs with the vast amounts of genetic data now available. Well curated EMRs contain a wealth of clinical information about large populations, including patient symptoms, drug history, and results of diagnostic tests. EMRs are maintained longitudinally over many years, allowing researchers to track clinical phenotypes even prior to disease onset and to assess disease progression. Large-scale, unbiased EMR exploration can provide insight into important phenotypic differences related to a disease of

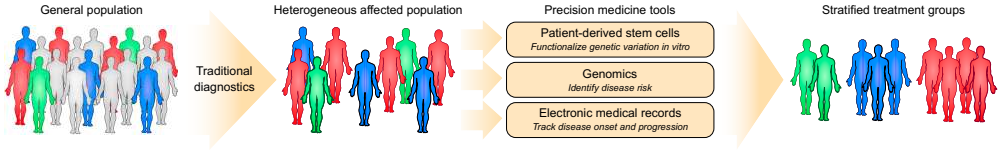

Figure 2. Genomics, EMRs, and Patient-Derived Stem Cells Collapse Patient Genotype and Clinical Phenotype Data into Tractable Computational and Biological Models
While traditional diagnostic methods can identify heterogeneous patient populations affected by a neurological disease, the integration of precision medicine tools could facilitate development of more precise therapeutics targeting stratified patient populations with shared pathogenic mechanisms.

interest, as well as unexpected peripheral characteristics that could reveal information about disease subtypes.

Cross-referencing EMR data with genetic data could provide insight into the relationship between susceptibility loci, clinical symptoms, and drug responsiveness, potentially facilitating both the identification of novel therapeutic candidates targeting impaired neural pathways and improved clinical trial design. For example, a recent study coupled high-throughput exome sequencing of more than 50,000 patients with longitudinal EMRs spanning a median of 14 years (Dewey et al., 2016). By linking sequence data with EMR-derived phenotype data, the researchers discovered novel associations between many genetic variants and a wide range of clinical phenotypes, including 58 variants associated with total cholesterol. The study also used predicted loss-of-function variants as an equivalency model for drug target antagonism and identified associations between lipid levels and variants in genes encoding lipid-lowering drug targets, providing a proof of concept that large-scale sequencing and EMR-based studies can provide insight into therapeutically valid pathways. Taking a similar approach using neurological phenotypes could illuminate how genetic variation relates to neurological symptoms and facilitate the discovery of pathways leading to neuronal decline.

Aside from complementing genomics data, EMRs could also directly predict neuronal disease onset and progression, thus providing an opportunity for early intervention. Recent studies have developed predictive models based on EMR data to identify prodromal diagnoses in neurodegenerative diseases. For example, bladder dysfunction is strongly associated with a future diagnosis of Multiple System Atrophy (MSA), and constipation is moderately associated with a future diagnosis of Parkinson's disease (PD) (LaHue et al., 2016). However, neither symptom predicts disease with any certainty. Therefore, the goal of EMR analyses will be to provide a more comprehensive set of clinical symptoms in patients with specific forms of diseases. Since we are unable to directly monitor neural deterioration in a patient's brain, at least until more sophisticated imaging methods are developed, understanding how clinically observable prodromal pathologies relate to genetic risk may facilitate the discovery of early disease-driving mechanisms.

Using Stem Cells in Precision Medicine

Although sequence data and EMRs provide important genetic and phenotypic information for applying precision medicine to neurology, it will also be critical to incorporate a tractable experimental system that faithfully recapitulates human biology. One of the key limitations in drug development for neurological disorders is the inaccessibility of neural tissue and the lack of adequate preclinical models with high predictive power. Although multiple upstream pathways lead to common downstream neuronal phenotypes, a method to study and therapeutically target these pathways is necessary. Advances in human induced pluripotent stem cell (iPSC) technology within the last decade may finally overcome these limitations. iPSCs reprogrammed from patient somatic cells collapse the complex genetic backgrounds of individual patients into observable phenotypes, hopefully offering more predictive models for studying disease mechanisms and for drug discovery and preclinical validation.

The field of cardiology has already begun using stem cell models to explore a precision medicine paradigm. For example, iPSCs derived from a congenital long QT syndrome patient with a known potassium channel mutation demonstrated prolonged action potential duration and arrhythmogenicity *in vitro*, reminiscent of clinical symptoms (Itzhaki et al., 2011). These *in vitro* phenotypes were rescued with several novel compounds, suggesting that iPSC models can be used to identify drugs tailored to patients with specific forms of a disease. Transcriptome profiling of iPSC-derived cardiomyocytes has also been used to predict individual patient susceptibility to drug cardiotoxicity, validating iPSCs as a model for safety pharmacology and highlighting the possibility of using stem cells to risk-stratify patients (Matsa et al., 2016). However, predicting drug response based on compounds with known mechanisms of action is only the first step. Next it will be important to discover novel compounds for defined disease subclasses and validate these compounds clinically. Although cardiac iPSC modeling has not yet led to improved therapeutics, such studies have demonstrated the future potential of guiding therapy using stem cells.

Outside of cardiology, there have been many attempts to model neurodegenerative and neuropsychiatric diseases using patient iPSCs (Falk et al., 2016). iPSCs can be differentiated into most major neuronal classes, allowing the study of a broad range of neurological afflictions. Furthermore, 3D culture methods allow the formation of iPSC-derived cerebral organoids, which provide regional specification of diverse brain structures and functional neural circuits for studying complex neural physiology (Quadrato and Arlotta, 2017). In addition, improved

gene editing technologies now allow researchers to engineer stem cell lines with specific neural disease-associated mutations. For example, our lab recently performed CRISPR-Cas9-mediated knockout of *PARKIN*, *DJ-1*, and *ATP13A2* in control iPSC-derived midbrain dopaminergic neurons to model PD. PD is a typical neurodegenerative disease associated with multiple disease-causing genes, risk genes, and suspected environmental factors that superimpose to produce specific forms of the disease. Using whole-genome transcriptomics and quantitative proteomics, we detected dysregulation of pathways predicted to be disrupted in PD and discovered novel PD-associated pathologies. This approach allowed us to understand phenotypes related to specific genetic forms of PD and to ask which forms of the disease are most similar to one another. This could be useful for identifying therapeutics that correct discrete phenotypes associated with genetics and environment acting together.

Since CNS disorders often result from integrated effects of many common variants, it is important to look beyond iPSC models of rare, high-penetrance mutations. To understand the role of common variation, it may be necessary to identify disease-associated cellular phenotypes in large numbers of lines derived from idiopathic patient cohorts. Because these phenotypes often cannot be predicted, it will be important to use techniques capable of simultaneously evaluating many different cellular features, such as single-cell RNA-sequencing or high-content, image-based morphological profiling. However, because of the substantial genetic heterogeneity and line-to-line variability of iPSC systems, experiments to detect differences caused by the small effects of common variants must be carefully designed and well-powered (Hoffman et al., 2018). Any informative cellular and molecular phenotypes could be cross-referenced with genetic and EMR data to identify critical disease pathways and to cluster patients into defined treatment cohorts.

The Evolution of Precision Medicine

While precision medicine offers an attractive approach to tackle neurodegenerative and neuropsychiatric diseases, many challenges remain in its implementation. The simple precision medicine strategy that is revamping the field of oncology cannot sufficiently address the complexities of neural disorders. Instead, precision medicine will need to evolve to a more sophisticated form that integrates genomics data, clinical phenotype data, and human biology to subclassify CNS disorders more precisely and identify druggable targets matched to more homogeneous patient populations. Fortunately, we have an emerging toolbox that may enable researchers to make precision medicine in neurology a reality.

ACKNOWLEDGMENTS

Concepts and research for part of this Forum were conceived as part of an undergraduate course at Harvard College (SCRB 195).

WEB RESOURCES

ClinicalTrials.gov, https://clinicaltrials.gov/ct2/show/NCT01760005
ClinicalTrials.gov, https://clinicaltrials.gov/ct2/show/NCT02465060

REFERENCES

Dewey, F.E., Murray, M.F., Overton, J.D., Habegger, L., Leader, J.B., Fetterolf, S.N., O'Dushlaine, C., Van Hout, C.V., Staples, J., Gonzaga-Jauregui, C., et al. (2016). Distribution and clinical impact of functional variants in 50,726 whole-exome sequences from the DiscovEHR study. Science *354*, aaf6814.

Falk, A., Heine, V.M., Harwood, A.J., Sullivan, P.F., Peitz, M., Brüstle, O., Shen, S., Sun, Y.M., Glover, J.C., Posthuma, D., and Djurovic, S. (2016). Modeling psychiatric disorders: from genomic findings to cellular phenotypes. Mol. Psychiatry *21*, 1167–1179.

GBD 2015 Neurological Disorders Collaborator Group (2017). Global, regional, and national burden of neurological disorders during 1990-2015: a systematic analysis for the Global Burden of Disease Study 2015. Lancet Neurol. *16*, 877–897.

Hoffman, G.E., Schrode, N., Flaherty, E., and Brennand, K.J. (2018). New considerations for hiPSC-based models of neuropsychiatric disorders. Mol. Psychiatry. https://doi.org/10.1038/s41380-018-0029-1.

Itzhaki, I., Maizels, L., Huber, I., Zwi-Dantsis, L., Caspi, O., Winterstern, A., Feldman, O., Gepstein, A., Arbel, G., Hammerman, H., et al. (2011). Modelling the long QT syndrome with induced pluripotent stem cells. Nature *471*, 225–229.

LaHue, S., Albers, K., Goldman, S., Leimpeter, A., Van Den Eeden, S., and Tanner, C. (2016). Prodromal Diagnoses in the Electronic Medical Record (EMR) Differ in Parkinson's Disease (PD), Dementia with Lewy Bodies (DLB), Multiple System Atrophy (MSA), and Progressive Supranuclear Palsy (PSP). Neurology *86*, P3.347.

Matsa, E., Burridge, P.W., Yu, K.H., Ahrens, J.H., Termglinchan, V., Wu, H., Liu, C., Shukla, P., Sayed, N., Churko, J.M., et al. (2016). Transcriptome Profiling of Patient-Specific Human iPSC-Cardiomyocytes Predicts Individual Drug Safety and Efficacy Responses In Vitro. Cell Stem Cell *19*, 311–325.

Quadrato, G., and Arlotta, P. (2017). Present and future of modeling human brain development in 3D organoids. Curr. Opin. Cell Biol. *49*, 47–52.

Quon, B.S., and Rowe, S.M. (2016). New and emerging targeted therapies for cystic fibrosis. BMJ *352*, i859.

Shin, S.H., Bode, A.M., and Dong, Z. (2017). Precision medicine: the foundation of future cancer therapeutics. npj Precision Oncology *1*, 12.

APPENDIX C

CO-AUTHORED PUBLICATION

Blocking p62-dependent SMN degradation ameliorates spinal muscular atrophy disease phenotypes

The Journal of Clinical Investigation, 128(7):3008-3023

Natalia Rodriguez-Muela,[1,2] Andrey Parkhitko,[3] Tobias Grass,[1,2] **Rebecca M. Gibbs**,[1,2] Erika M. Norabuena,[1,2] Norbert Perrimon,[3,4] Rajat Singh,[5] and Lee L. Rubin[1,2]

[1]Department of Stem Cell and Regenerative Biology, Harvard University, Cambridge, Massachusetts, USA.

[2]Harvard Stem Cell Institute, Cambridge, Massachusetts, USA.

[3]Department of Genetics, Harvard Medical School, Boston, Massachusetts, USA.

[4]Howard Hughes Medical Institute, Boston, Massachusetts, USA.

[5]Department of Medicine, Albert Einstein College of Medicine, Bronx, New York, USA.

Contribution:

Performed *in vivo* analysis of myofiber size and neuromuscular junction innervation in SMA mice carrying a heterozygous autophagy receptor p62 knockout allele. We found that p62 depletion increased skeletal muscle size and improved neuromuscular junction innervation in SMA mice.

Blocking p62-dependent SMN degradation ameliorates spinal muscular atrophy disease phenotypes

Natalia Rodriguez-Muela,[1,2] Andrey Parkhitko,[3] Tobias Grass,[1,2] Rebecca M. Gibbs,[1,2] Erika M. Norabuena,[1,2] Norbert Perrimon,[3,4] Rajat Singh,[5] and Lee L. Rubin[1,2]

[1]Department of Stem Cell and Regenerative Biology, Harvard University, Cambridge, Massachusetts, USA. [2]Harvard Stem Cell Institute, Cambridge, Massachusetts, USA. [3]Department of Genetics, Harvard Medical School, Boston, Massachusetts, USA. [4]Howard Hughes Medical Institute, Boston, Massachusetts, USA. [5]Department of Medicine, Albert Einstein College of Medicine, Bronx, New York, USA.

Spinal muscular atrophy (SMA), a degenerative motor neuron (MN) disease, caused by loss of functional survival of motor neuron (SMN) protein due to *SMN1* gene mutations, is a leading cause of infant mortality. Increasing SMN levels ameliorates the disease phenotype and is unanimously accepted as a therapeutic approach for patients with SMA. The ubiquitin/proteasome system is known to regulate SMN protein levels; however, whether autophagy controls SMN levels remains poorly explored. Here, we show that SMN protein is degraded by autophagy. Pharmacological and genetic inhibition of autophagy increases SMN levels, while induction of autophagy decreases these levels. SMN degradation occurs via its interaction with the autophagy adapter p62 (also known as SQSTM1). We also show that SMA neurons display reduced autophagosome clearance, increased p62 and ubiquitinated proteins levels, and hyperactivated mTORC1 signaling. Importantly, reducing p62 levels markedly increases SMN and its binding partner gemin2, promotes MN survival, and extends lifespan in fly and mouse SMA models, revealing p62 as a potential new therapeutic target for the treatment of SMA.

Introduction

Spinal muscular atrophy (SMA) is an early-onset, autosomal recessive neuromuscular disease caused by low levels of survival motor neuron (SMN) protein (1). SMA is primarily characterized by the degeneration of motor neurons (MNs) of the spinal cord and skeletal muscle atrophy. However, recent studies have revealed a wide range o f pathologies in multiple peripheral tissues in humans and mice (2). Because of a gene duplication event, humans harbor 0–6 copies of *SMN2*, a paralog to *SMN1*. A single nucleotide difference between *SMN1* and *SMN2* leads to alternative splicing of *SMN2* (3, 4). While *SMN1* primarily produces a full-length SMN (SMN-FL) transcript, approximately 90% of the *SMN2* gene product lacks exon 7 (SMNΔ7), a highly unstable form of the protein (5, 6). *SMN2* is a major SMA disease modifier, with higher *SMN2* copy numbers correlating with delayed disease onset and better prognosis. SMN is ubiquitously expressed, localized in the cytoplasm and nuclear foci, termed gems, and plays an essential housekeeping role in the biogenesis of spliceosomal small nuclear ribonucleoprotein particles (snRNPs) (7) and axonal transport of mRNA (8). A large body of evidence suggests that increasing SMN levels repairs the disease phenotype. Although a number of compounds that increase SMN levels by stimulating its transcription or altering the *SMN2* splicing pattern have been identified (9–14), SMN is also regulated at the level of protein degradation. We and others have shown that SMN protein is degraded by the ubiquitin-proteasome system (UPS) (15–20). However, the role of macroautophagy (hereafter referred to as autophagy) in regulating SMN protein levels has not been investigated. Autophagy is a highly conserved intracellular degradative pathway that eliminates cell components to maintain cellular homeostasis (21). While the proteasome degrades short-lived proteins, autophagy turns over damaged, redundant, and aggregated proteins as well as cellular organelles in bulk but also in a selective manner through a number of proteins, called autophagy receptors, that specifically recognize certain cargo and deliver it to autophagosomes (APs) for degradation (22, 23). The role of autophagy in neurodegenerative disorders has been extensively studied (24–28). However, its contribution to the pathophysiology of SMA remains unknown.

Here, we demonstrate that SMN protein levels are regulated by autophagy. We show that lysosomal inhibition increases the levels of total SMN protein, ubiquitinated SMN, SMN-binding partner gemin2, and the number of nuclear gems as well as levels of partially functional SMNΔ7. We also show that SMN degradation is mediated by its ubiquitination and interaction with the autophagy receptor p62 (also known as SQSTM1). Our study unravels a highly activated mTOR pathway in SMA-affected cells that contributes to the deficient AP clearance and subsequent accumulation of ubiquitinated proteins and p62. Importantly, depletion of p62 levels markedly rescues MN death in vitro and extends the lifespan of SMA fly and mouse models. Taken together, our results point to new therapeutic possibilities for the treatment of SMA by dampening autophagy-dependent SMN degradation.

Results

Autophagy regulates SMN protein levels. Restoring SMN protein levels above a certain threshold is the most common approach to treating SMA. While SMN protein levels are controlled at tran-

Authorship note: AP and TG contributed equally to this work.
Conflict of interest: The authors have declared that no conflict of interest exists.
Submitted: May 18, 2017; **Accepted:** April 12, 2018.
Reference information: *J Clin Invest*. 2018;128(7):3008–3023.
https://doi.org/10.1172/JCI95231.

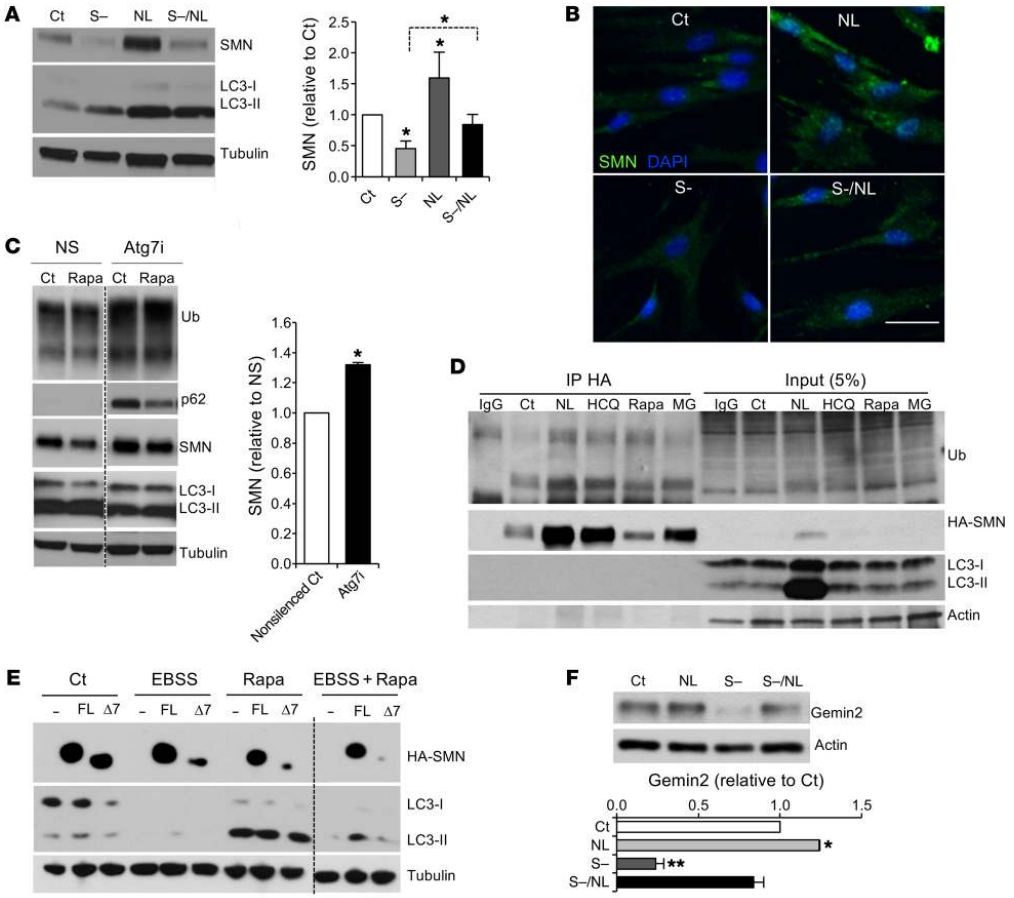

Figure 1. Autophagy regulates SMN protein levels. (**A**) Representative immunoblot and quantification of protein lysates from human control fibroblasts after treatment with lysosomal inhibitors (NL), serum starvation (S–), or a combination of both (S–/NL) for 24 hours (n = 5 independent experiments). (**B**) Representative image of immunostaining against SMN (green) on human control fibroblasts after the indicated treatments (nuclei are labeled with DAPI, blue). Scale bar: 50 μm. (**C**) Representative immunoblot and quantification of protein lysates from WT mouse ESC–derived MNs infected with lentivirus carrying shRNA against Atg7 (Atg7i) or empty control (NS) for 7 days and treated for the last 24 hours of the culture with rapamycin or control media (results are expressed relative to NS control cells; n = 3 independent experiments). (**D**) Representative IP from HEK293T lysates transfected with HA-SMN plasmid and treated with lysosomal inhibitors (NL and HCQ), rapamycin, or the proteasome inhibitor MG132 (MG) for 24 hours and immunoblotted against ubiquitin, HA, LC3, and actin. (**E**) Representative immunoblot from HEK293T lysates transfected with empty vector (–) or the HA-tagged versions of SMN-FL or SMNΔ7 (Δ7) and cultured in control or amino acid–free media (EBSS), rapamycin, or both for 24 hours. (**F**) Representative immunoblot and quantification from human control fibroblasts after a 24-hour treatment with serum-free media, NL, or both, showing the levels of the SMN-binding partner gemin2 (member of the SMN complex) (n = 3 independent experiments). *P < 0.05 and **P < 0.01, by 2-tailed t test. All results are shown as the mean ± SEM. Ct, control; Rapa, rapamycin; Ub, ubiquitin.

scriptional and posttranscriptional levels, in the past few years, therapeutic strategies have focused primarily on the transcriptional regulation of SMN. It is thought that SMN degradation occurs mainly via the UPS (15–20). However, since SMN is part of large multi-protein complexes including the SMN complex, formed by SMN and gemins (2–8) (key components of spliceosomes) (7), stress granules (29), and axonal granules involved in axonal transport (8), we wondered whether SMN degradation occurred in bulk as part of these large protein complexes via autophagy.

To determine whether autophagy regulates SMN degradation, we first exposed human fibroblasts to the best-known autophagy inducer, starvation, by depriving them of serum and blocked lysosomal degradation by exposing cells to the lysosomal inhibitors ammonium chloride and leupeptin (NL). We found that, not only did SMN levels decrease with serum starvation, but, importantly, SMN levels were elevated when autophagy activity was blocked (Figure 1, A and B), indicating that SMN is degraded via autophagy. We also sought to determine whether autophagy controls

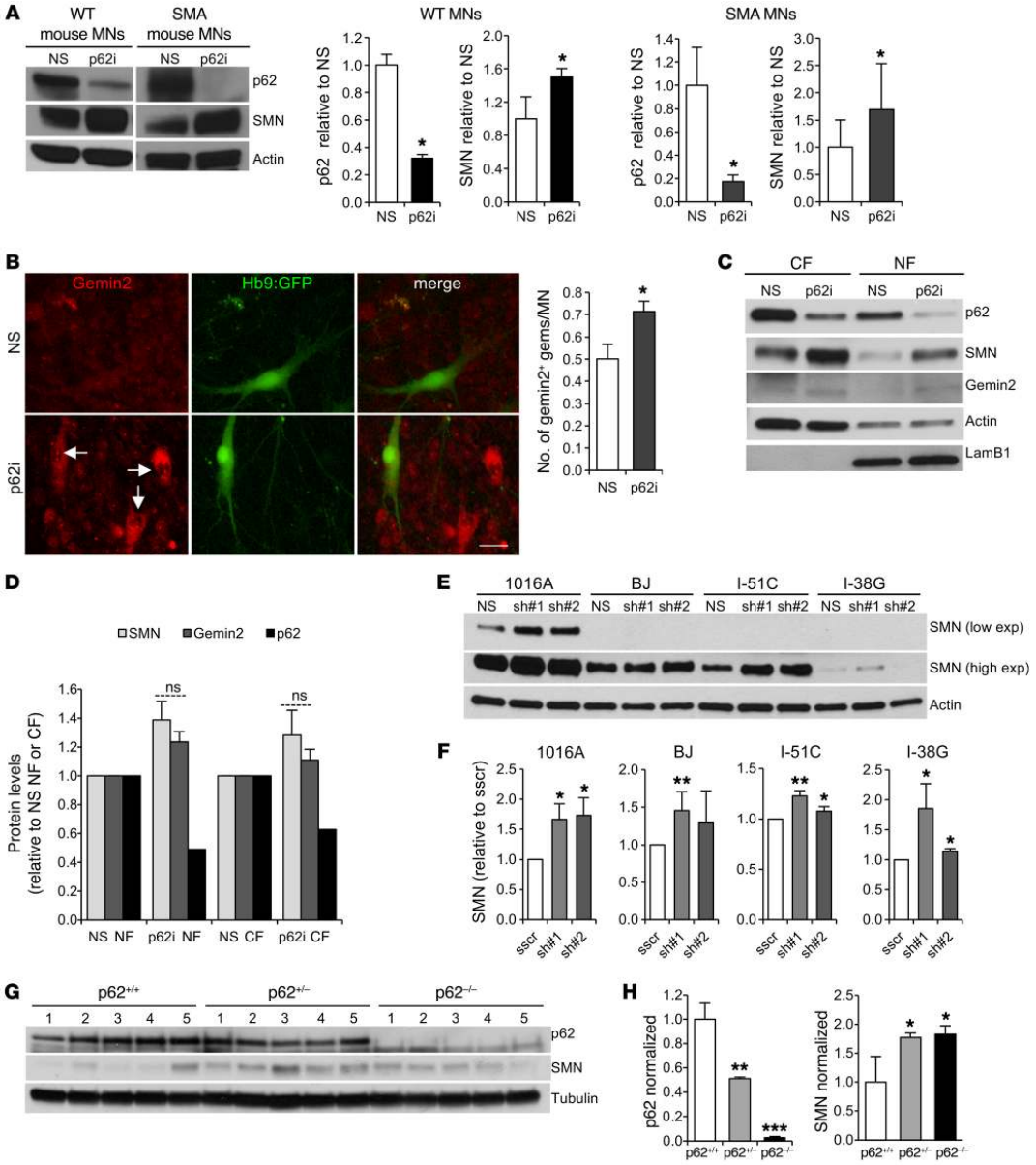

Figure 2. SMN degradation by autophagy is specifically mediated by p62. (**A**) Representative immunoblot of protein lysates from WT and SMA mouse ESC–derived MNs 7 days after infection with the nonsilencing control (NS) or shRNA against p62 (p62i). Graph shows quantification of p62 and SMN protein levels (results are expressed relative to the nonsilenced control cells; $n = 5$ independent experiments). (**B**) Immunostaining against gemin2 and quantification of the number of gemin2$^+$ nuclear gems in SMA mouse ESC–derived MNs. Scale bar: 25 μm (results are expressed relative to NS control cells ($n = 3$ independent experiments; 600 MNs per condition were counted). (**C** and **D**) Representative immunoblot and quantification of subcellular fractionation 3T3 protein lysates 6 days after infection with lentivirus carrying shRNA against p62 or NS control (ns, not significant). CF, cytoplasmic fraction; NF, nuclear fraction. (**E**) Representative immunoblot of human iPSC–derived MN lysates from healthy control cells (1016A and BJ) and SMA patients with different disease severities (type II, I-51C; type I, I-38G). MNs were infected with a lentivirus expressing NS shRNA control or p62 shRNA and lysed 7 days after infection. exp, expression. (**F**) Quantification of SMN and p62 protein levels. Results are expressed relative to scramble-silenced (sscr) cells ($n = 7$, 6, 4, and 3 independent experiments, from left to right). (**G** and **H**) Representative immunoblot and quantification of protein lysates obtained from p62$^{-/-}$, heterozygotic (p62$^{+/-}$), or WT (p62$^{+/-}$) adult mouse brains (results are expressed relative to p62$^{+/+}$ mice; $n = 5$ mice per group). $^*P < 0.05$, $^{**}P < 0.01$, and $^{***}P < 0.001$, by 2-tailed t test. All results are shown as the mean ± SEM.

SMN protein levels in MNs, the most severely affected cell type in the disease. Given that autophagy is not efficiently triggered by starvation in neurons (21), we used shRNA delivery to reduce the expression of *Atg7*, a crucial gene required for autophagosome formation, in mouse embryonic stem cell–derived (ESC-derived) MNs. As expected, we found that MNs with reduced *Atg7* showed increased levels of the autophagy substrate p62, accumulation of ubiquitinated proteins, as well as reduced levels of the AP marker LC3-II (Figure 1C). As anticipated, we also noted an increase in the levels of SMN when compared with levels in control cultures (Figure 1C), confirming that autophagy meditates SMN degradation. It is traditionally accepted that, upon ubiquitination, SMN degradation occurs solely via the UPS. Our results led us to explore whether ubiquitinated SMN is also degraded by autophagy. In fact, when HA-SMN-FL–expressing HEK293T cells were treated with modulators of autophagy (the inhibitors NL and weak base hydroxychloroquine [HCQ] and a well-known activator of autophagy, rapamycin) or the proteasome inhibitor MG132 and subjected to IP using an anti-HA antibody, we detected an accumulation of ubiquitinated SMN upon both proteasomal and lysosomal blockage (Figure 1D).

Given these findings, we next determined whether the truncated form of SMN protein, SMNΔ7, is also an autophagy substrate. Cells from patients with SMA express higher levels of SMNΔ7 than SMN-FL. Although SMNΔ7 is highly unstable, it retains some function, at least in the presence of SMN-FL (5, 6, 30). While it has been reported that SMNΔ7 is quickly degraded by the proteasome (16), its oligomerization with SMN-FL increases its stability (30). Because SMNΔ7 binds to SMN-FL, we postulated that SMNΔ7 might also be degraded by autophagy. To answer this question, we transfected HEK293T cells with HA-tagged forms of both proteins and induced autophagy by subjecting the cells to amino acid starvation (EBSS media), rapamycin, or both. Indeed, induction of autophagy led to decreased levels of SMN-FL and SMNΔ7, which were more pronounced upon combining both autophagy-inducing stimuli (Figure 1E), demonstrating that SMNΔ7 protein levels are also under autophagy control. Interestingly, the levels of gemin2, an SMN-binding protein and essential spliceosome component, were also decreased upon autophagy induction (with serum starvation), and increased upon lysosomal inhibition (NL) (Figure 1F). Taken together, these data demonstrate that autophagy degrades ubiquitinated SMN and other components of the SMN complex, such as gemin2, which in turn suggests that the pool of SMN degraded by autophagy is the one associated with SMN complexes.

SMN degradation by autophagy is mediated by p62. Autophagy is not only an in-bulk catabolic process, it also selectively targets specific substrates for degradation. Several autophagy cargo recognition proteins, or autophagy receptors, have been identified, including p62, NBR1, optineurin, NDP52, and NIX (22, 23). They share key domains that allow binding to autophagic cargo for their delivery for lysosomal degradation. Through their ubiquitin-binding domain (UBA motif), these receptors bind to polyubiquitinated cargo, and via their LC3-binding domain (LC3-interacting region [LIR] motif), they interact with LC3, which coats the inner membrane of autophagosomes (22, 31–33). These proteins are also autophagy substrates and, hence, serve as markers for autophagy flux.

To investigate whether autophagy receptors mediate SMN degradation, we focused first on the best-characterized autophagy receptor, p62. Depletion of p62 levels with shRNAs markedly increased SMN protein levels in WT mouse MNs (Figure 2A), without increasing *SMN* mRNA expression levels (Supplemental Figure 1A; supplemental material available online with this article; https://doi.org/10.1172/JCI95231DS1). These results led us to explore whether the same was true in SMA MNs. We obtained ESCs from a severe SMA mouse model, SMNΔ7, in which *Smn* has been deleted, and 2 copies of the human *SMN2* transgene and 2 copies of the human *SMN2* transgene lacking exon 7 have been inserted into the genome (*Smn*$^{-/-}$ *SMN2*$^{+/+}$ SMNΔ7$^{+/+}$ *Hb9::GFP*) (30). SMN protein levels in both ESCs and MNs derived from these mice were reduced by approximately 70% when compared with levels in WT controls (Supplemental Figure 1, B and C). Knockdown of p62 in SMNΔ7 MNs led to increases in SMN protein levels similar to those detected in WT MNs (Figure 2A).

We also studied the number of nuclear gems. Gems are multiprotein nuclear structures composed of SMN molecules, gemins2–7 and snRNPs involved in the transcription and processing of many types of nuclear RNAs (7). A reduction of their number per cell is an SMA hallmark. Interestingly, p62 downregulation led to an increase in the number of gemin2^{+} and SMN^{+} nuclear gems in SMA MNs and also in other neurons in the culture (non-MN population) (Figure 2B and Supplemental Figure 1D). This finding led us to explore whether the effect of p62 depletion on increases in SMN protein levels is more marked in the nucleus than in the cytoplasm. However, cellular fractionation assays of p62-knockdown NIH3T3 cells that also exhibited significantly higher SMN levels in total lysates when compared with the nonsilenced control (NS) (Supplemental Figure 1E) showed similar increases in SMN and gemin2 levels in both cellular fractions, which indicates that stabilization of these proteins occurs in both the nucleus and cytoplasm (Figure 2, C and D).

We extended these results by showing that p62 regulates SMN protein levels in human MNs. We derived MNs from induced pluripotent stem cells (iPSCs) from healthy control and SMA patients affected by different disease severities — a severe line (type II, I-51C) and a very severe line (type I, I-38G) — that we have previously described (34, 35). These iPSCs and the derived MNs express amounts of SMN that reflect their disease severities (35). Similar to what we observed in mouse MNs, depletion of p62 levels in human MNs also led to an increase in SMN protein levels (Figure 2, E and F, and Supplemental Figure 1F). To verify the importance of p62 as a mediator of SMN degradation, we studied SMN protein levels in brains from adult p62-null (p62$^{-/-}$) mice. Confirming our results, brains from heterozygous and p62$^{-/-}$ mice showed markedly increased SMN protein levels when compared with levels in littermate controls (Figure 2, G and H). Together, these data indicate that p62 regulates SMN and gemin2 protein levels in all cell types studied, including human control and SMA iPSC–derived MNs, and in mice.

p62 interacts with SMN. Given our findings, we next explored how p62 functions as an autophagy receptor to target SMN for degradation. We performed co-IP analysis after transfecting HEK293T cells with HA-SMN and Myc-p62 or various combinations of plasmids used as negative controls (HA-GFP plus Myc-p62

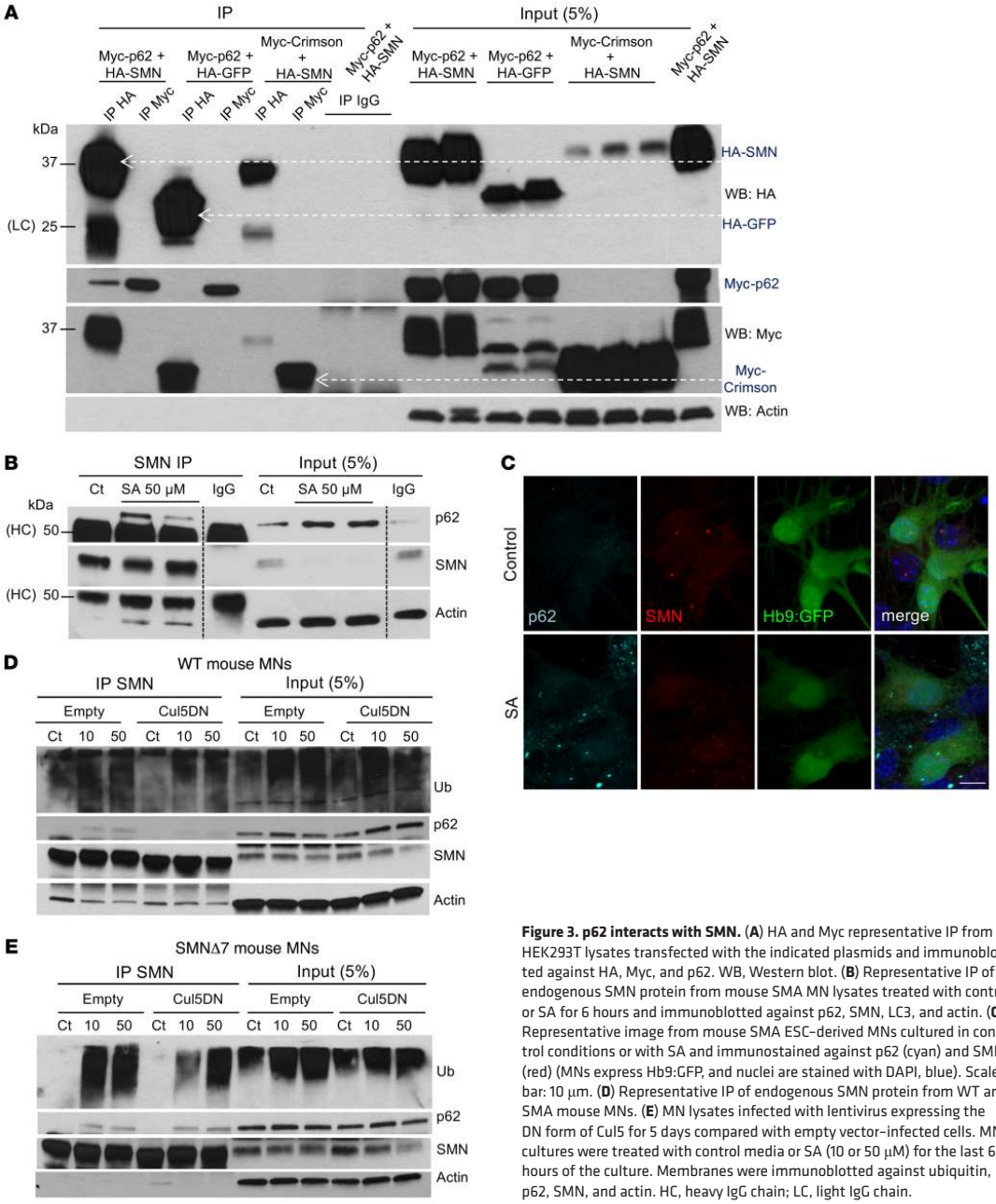

Figure 3. p62 interacts with SMN. (**A**) HA and Myc representative IP from HEK293T lysates transfected with the indicated plasmids and immunoblotted against HA, Myc, and p62. WB, Western blot. (**B**) Representative IP of endogenous SMN protein from mouse SMA MN lysates treated with control or SA for 6 hours and immunoblotted against p62, SMN, LC3, and actin. (**C**) Representative image from mouse SMA ESC–derived MNs cultured in control conditions or with SA and immunostained against p62 (cyan) and SMN (red) (MNs express Hb9:GFP, and nuclei are stained with DAPI, blue). Scale bar: 10 μm. (**D**) Representative IP of endogenous SMN protein from WT and SMA mouse MNs. (**E**) MN lysates infected with lentivirus expressing the DN form of Cul5 for 5 days compared with empty vector–infected cells. MN cultures were treated with control media or SA (10 or 50 μM) for the last 6 hours of the culture. Membranes were immunoblotted against ubiquitin, p62, SMN, and actin. HC, heavy IgG chain; LC, light IgG chain.

and HA-SMN plus Myc-E2-crimson, a far-red fluorescent protein). We found that, while Myc-p62 IP did not pull down HA-SMN, HA-SMN did coimmunoprecipitate with Myc-p62 (Figure 3A). Co-IPs of HA-GFP with Myc-p62 and of HA-SMN with Myc-E2-crimson were negative, as we expected (Figure 3A). These results indicate that SMN and p62 indeed interact with one another. To confirm these data, we performed IP of endogenous proteins in mouse MNs. Interestingly we did not detect interaction between SMN and p62 under basal conditions. However, binding of SMN to p62 was detected when we induced the incorporation of SMN into

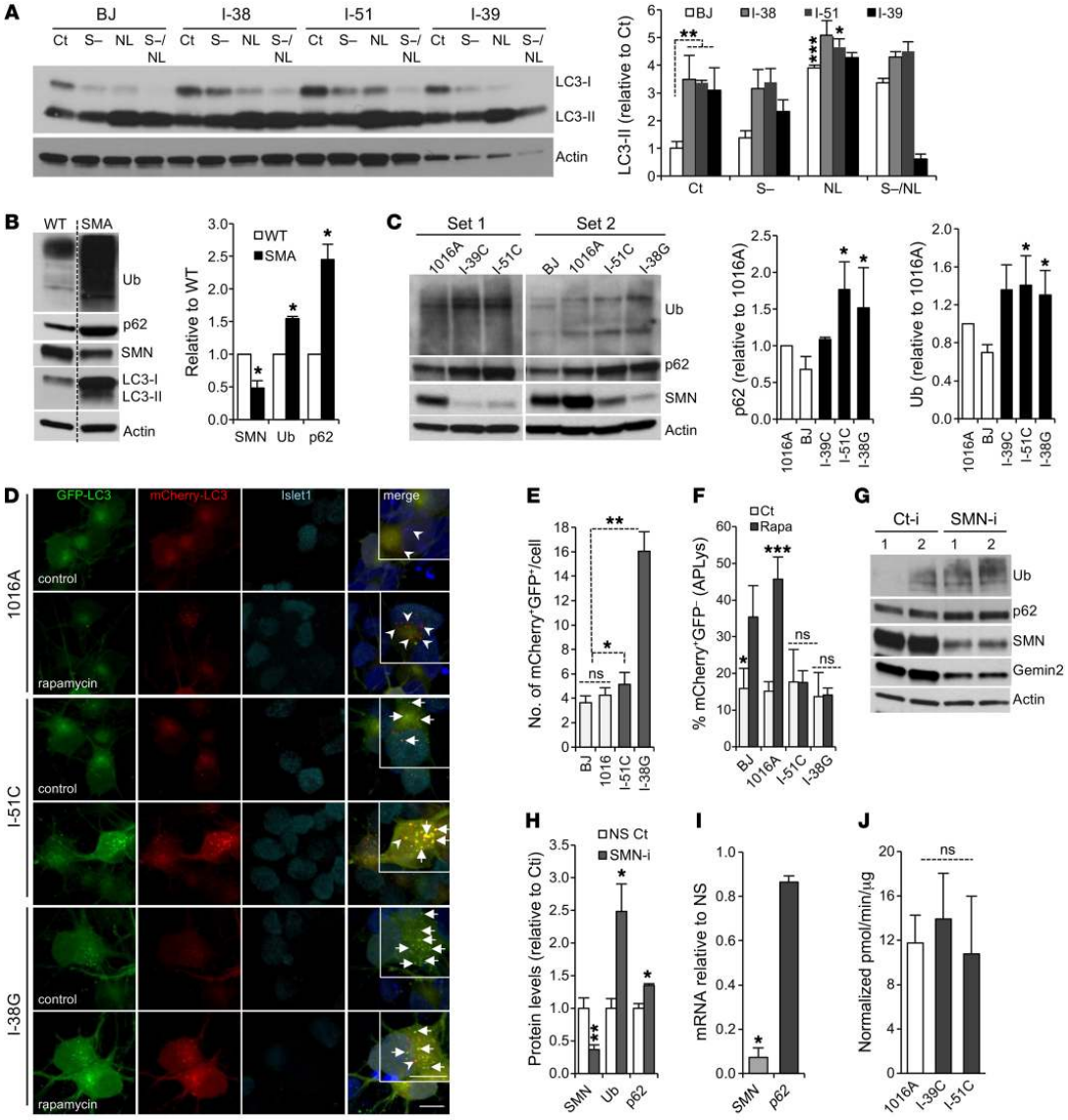

Figure 4. Autophagy activity is impaired upon SMN deficiency. (**A**) Representative immunoblot to determine autophagy flux from human control and SMA fibroblast protein lysates. Cells were treated in the presence or absence of serum (S–) for 24 hours, with or without lysosomal inhibitors (NL) for the last 4 hours of the culture. Graph shows the quantification of LC3-II levels. (**B**) Representative immunoblot of protein lysates from WT and SMA mouse ESC–derived MNs. Graph shows quantification (results are expressed relative to WT MNs; $n = 3$ independent experiments). (**C**) Representative immunoblot from human iPSC–derived MN lysates from control cells (1016A and BJ) and SMA patients with different disease severities (type III, I-39C; type II, I-51C; type I, I-38G). Graphs show quantifications (results are expressed relative to 1016A control MNs; $n = 5$ independent experiments). (**D**) Representative confocal images of human control and SMA iPSC–derived MNs infected with mCherry-GFP-LC3 lentivirus. MNs were fixed 8 days after infection. Magnifications are shown in the insets. Scale bars: 10 µm. (**E** and **F**) Graphs show the quantification of APs (yellow, marked by arrows) and the percentage of APLys (red, marked by arrowheads). $n = 146, 44, 114$, and 86 transduced MNs for BJ, 1016A I-51C, and I-38G cells, respectively. (**G**) Representative immunoblot of HEK293T cells transfected with SMN RNAi (SMN-i) or control RNAi (Ct-i) for 3 days (duplicates are shown). (**H**) Quantification of protein levels (results are expressed relative to NS control cells; $n = 3$ independent experiments). (**I**) qRT-PCR showing *p62* mRNA expression upon SMN RNAi–mediated knockdown in HEK293T cells. Gene expression is indicated as the fold change of $2^{-\Delta\Delta Ct}$ with respect to actin, normalized to RNAi control cells (results are expressed relative to NS control cells; $n = 2$ independent experiments). (**J**) Quantification of the chymotrypsin-like activity in control versus SMA human MNs. $^*P < 0.05$, $^{**}P < 0.01$, and $^{***}P < 0.001$, by 2-tailed t test. All results are shown as the mean ± SEM.

protein complexes. It has been reported that besides being distributed throughout the cytoplasm and localizing to the nucleus when assembled into gems, SMN can also cluster in cytoplasmic structures called stress granules (SGs) in response to oxidative stress (29). SGs are mainly composed of RNA-binding proteins such as Tia1, TIAR, FUS, and SMN, among others (29, 36), and mRNA, and their main function is to prevent the translation of mRNA during cellular stress (29). To test whether p62 interacts with SMN in SGs, we induced oxidative stress in HEK293T cells transfected with combinations of the constructs described above by exposing them to 10 and 50 μM sodium arsenite (NaAsO, referred to hereafter as SA) for 6 hours, a commonly used method to induce SG formation. We observed that HA-SMN strongly coimmunoprecipitated with Myc-p62 upon SG formation (Supplemental Figure 2A).

To explore the reproducibility of these findings with endogenous proteins, we subjected mouse SMA MNs to similar analyses. Importantly, upon treatment with SA, endogenous SMN coimmunoprecipitated with p62 (Figure 3B). Interestingly, in WT MNs, exposure to SA resulted in a lower ratio of immunoprecipitated SMN to SMN in total lysates when compared with controls (Supplemental Figure 2B). By contrast, in SMA MNs, this difference was not as pronounced, indicating that upon SA-induced SG formation, the pool of SMN present in SGs (and therefore not available in protein lysates because of their incorporation into large aggregates and not extracted by a mild lysis detergent) was possibly larger in WT cells than in SMA MNs. These results agree with those of previous studies reporting that SMN-deficient cells have impaired SG formation, which increases their susceptibility to death (37). Second, we noted that co-IP of SMN with p62 was more efficient in SMA MNs (Figure 3B) than in WT MNs (Supplemental Figure 2B) and that localization of p62 in aggregates upon SA treatment was more evident in SMA MNs (Figure 3C and Supplemental Figure 2C). Therefore, the incorporation of SMN in SGs, or SG formation itself, might be impaired in SMA cells; however, the interaction between SMN and p62 is enhanced in the diseased cells.

Recently published data from our laboratory suggest that SMN is ubiquitinated by Cullin5-E3 ubiquitin ligase (Cul5), targeting it for degradation, and that overexpression of a dominant-negative (DN) form of Cul5 stabilizes SMN (35). We postulated that ubiquitinated SMN could at least be a fraction of the SMN protein that is recognized by p62 and degraded via autophagy. To test this possibility, we infected mouse SMA and WT ESC–derived MNs with lentiviruses carrying Cul5DN or a control empty vector, and we exposed them to SA to induce the localization of SMN in stress granules. We performed SMN IP and, as expected, we observed that for both types of MNs, there was a reduction in the amount of pulled-down, ubiquitinated SMN after Cul5DN expression (Figure 3, D and E). As a result, in WT MNs, the interaction of SMN with p62 was reduced in Cul5DN-expressing MNs compared with that seen in the empty vector–treated MNs (Figure 3D). Interestingly, and in agreement with our previous results, the binding between SMN and p62 was still maintained after Cul5DN overexpression in SMA MNs. This again suggests that in the diseased cells, the fraction of p62 that binds to SMN, at least under SG-formation conditions, is larger, or p62-SMN interaction stronger, than in WT cells (Figure 3E). Taken together, these data suggest that p62 interacts readily with the pool of SMN that is assembled in protein complexes. Furthermore, these data indicate that preventing SMN ubiquitination reduces its ability to bind p62.

SMN deficiency leads to autophagy failure and accumulation of p62/ubiquitinated proteins. Autophagy dysfunction has been widely described in multiple neurodegenerative diseases; however, its participation in the pathophysiology of SMA remains largely unexplored. Thus, we decided to investigate autophagy function in SMA cells. First, fibroblasts from patients with different SMA severities (type I, I-38; type II, I-51; and type III, I-39) showed higher levels of LC3-I and LC3-II than did control fibroblasts (Figure 4A and Supplemental Figure 3A), suggesting that AP formation remains intact in SMA. To determine whether the increase in LC3-II represents an increase in AP formation and not a block in its fusion with lysosomes or its degradation, we studied autophagy flux by measuring LC3-II turnover in the presence and absence of lysosomal inhibitors. If autophagy flux occurs properly, the amount of LC3-II should be higher in the presence of lysosomal inhibitors (38). In SMA fibroblasts, we observed that the increase in LC3-II following lysosomal blockage under control and starvation conditions was reduced when compared with control fibroblasts (Figure 4A), indicating a defect in autophagy flux. This was accompanied by increased p62 protein levels in SMA fibroblasts — a hallmark of autophagy blockage (Supplemental Figure 3B). These data suggest that SMN deficiency impairs autophagy in human fibroblasts.

In order to validate these results, we explored whether a similar dysfunction in autophagy occurs in SMA MNs. Indeed, murine SMA MNs showed higher levels of p62 (while mRNA expression remained unchanged, Supplemental Figure 3C) and ubiquitinated proteins compared with WT MNs and higher levels of LC3-I and LC3-II (Figure 4B), which correlated with increased LC3 immunostaining in MNs in culture (Supplemental Figure 3D). We confirmed these results in human iPSC–derived MNs that showed higher levels of p62 and ubiquitinated proteins in SMA compared with healthy MNs (Figure 4C and Supplemental Figure 3E). To investigate how relevant these results from in vitro MNs are to the disease in vivo, we immunostained cervical spinal cord sections from SMNΔ7 mice and WT littermates for p62 and ubiquitin. In line with our in vitro results, we observed that Hb9:GFP$^+$ ventral MNs from P10 SMNΔ7 mice showed increased p62 and ubiquitin staining compared with that seen in WT MNs (Supplemental Figure 3F). These results demonstrate that autophagy is impaired in both mouse and human MNs.

Autophagy can be dysregulated at several steps, and in the context of neurodegenerative diseases, a growing number of studies have reported that alterations at each of these steps can lead to autophagy failure (39). Our results indicate that AP clearance is partially impaired in SMA cells. To further explore this possibility, we studied autophagy flux by using an mCherry-GFP-LC3 construct. This allowed us to distinguish APs (both green and red giving rise to yellow puncta) from autophagolysosomes (APLys, red) since fusion with acidic lysosomes leads to loss of GFP fluorescence at low pH and unmasking of the mCherry fluorescence (40). Consequently, we infected human iPSC–derived MNs with lentiviruses expressing this construct and analyzed the presence of APs (yellow) and APLys (red) by confocal microscopy. SMA MN cultures had an increased number of APs under basal conditions (Figure 4,

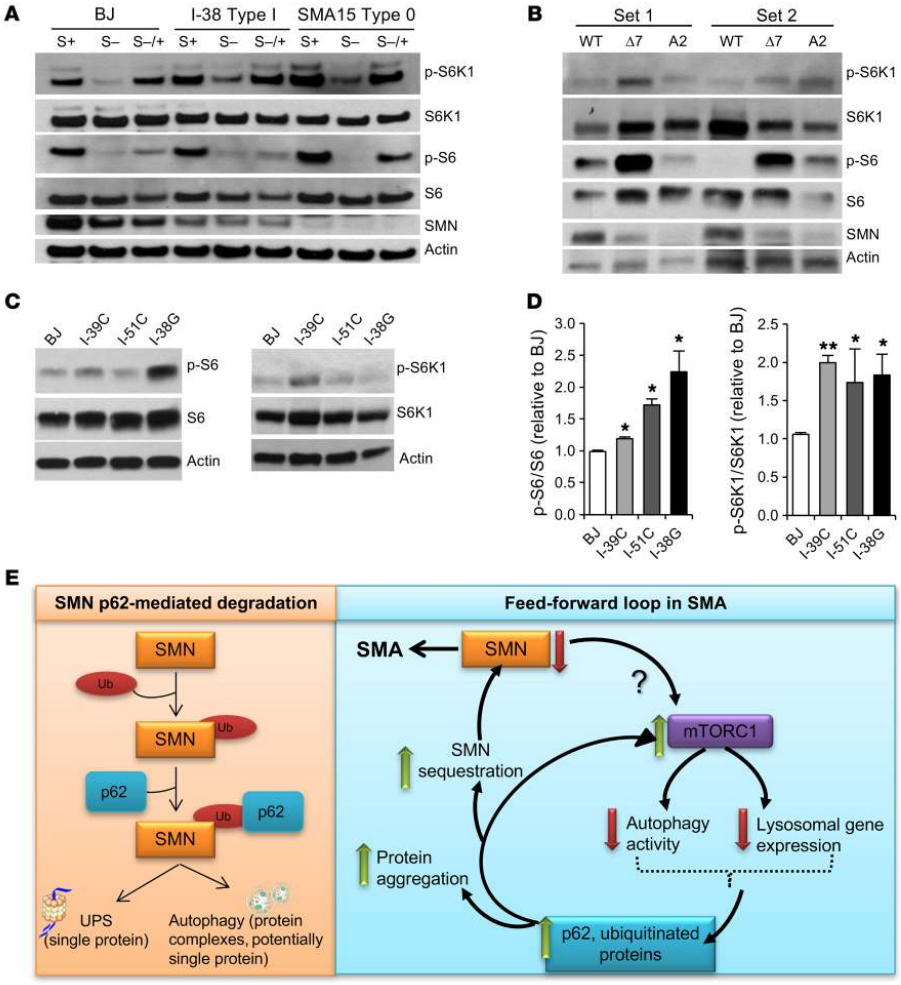

Figure 5. SMN deficiency results in mTOR activation, which could contribute to the autophagy impairment observed in SMA cells. (**A**) Representative immunoblot from human healthy control and SMA types I and 0 fibroblast lysates. Cells were cultured in the presence of 10% serum (S+), deprived of serum (S–) for 16 hours, or deprived of serum and then incubated for an additional 30 minutes with serum (S–/+). Phosphorylated and total levels of the mTOR targets S6K1 and S6 were measured. Quantifications are shown in Supplemental Figure 4A. (**B**) Representative immunoblot of mouse WT and SMA (SMNΔ7 and A2) MN lysates to measure mTOR pathway activity. Quantifications are shown on Supplemental Figure 4B. (**C**) Representative immunoblot from human healthy control and SMA MN lysates to measure mTOR pathway activity. (**D**) Quantifications of p-S6/S6 and p-S6K1/S6K1 ratios from human healthy control and SMA MN lysates. $*P < 0.05$ and $**P < 0.01$, by 2-tailed t test ($n = 6$ independent experiments). Data indicate the mean ± SEM, expressed relative to BJ healthy control MNs. (**E**) Scheme of the interplay between low SMN-p62-mTOR–defective autophagy.

D and E) and a reduced increase in the percentage of APLys upon autophagy induction with rapamycin when compared with WT MN cultures (Figure 4, D and F), suggesting that the formation of APs is not impaired in SMA MNs, but rather their clearance.

We next questioned whether the defect in autophagy activity detected in SMA cells was an indirect consequence of long-term SMN deficiency or whether, by contrast, acute reduction in SMN levels per se could lead to autophagy impairment. To answer this question, and since MNs have poor transfection efficiency, we used HEK293T cells to silence *SMN1* with siRNA and determined the levels of p62 and ubiquitination by Western blotting. We observed that both markers were increased after acute loss of SMN when compared with controls (Figure 4, G and H), while *p62* mRNA expression levels remained unchanged (Figure 4I), indicating that p62 accumulation was nontranscriptional and occurred in essence from reduced turnover. Finally, to rule out the possibility that UPS activity dysfunction was responsible for the accumulation of p62 and ubiquitin in SMA MNs, we quantified chymotrypsin-like activ-

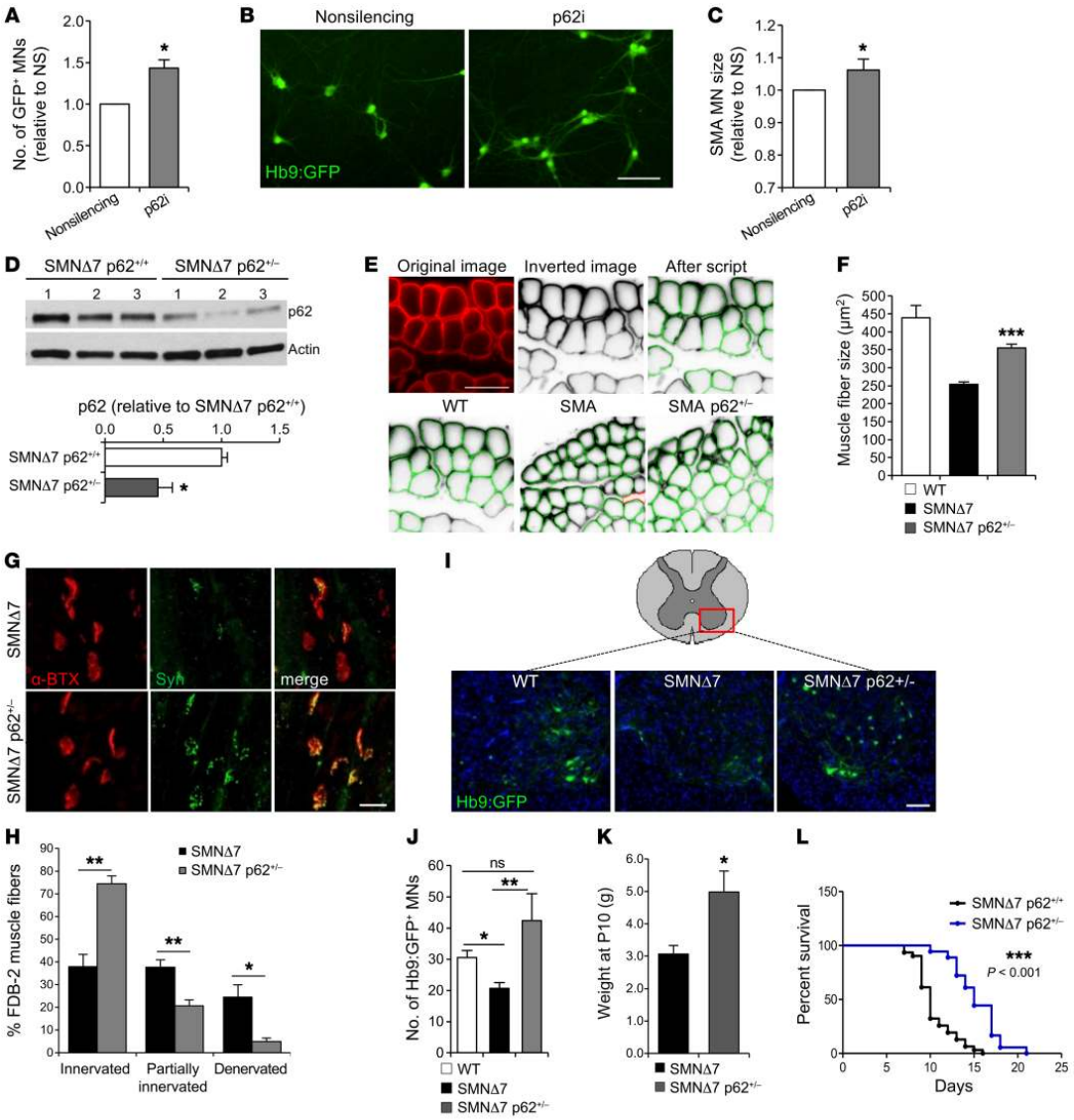

Figure 6. p62 knockdown promotes MN survival in vitro and ameliorates the disease phenotype of SMA models in vivo. (**A**) Quantification of Hb9:GFP+ SMA mouse ESC–derived MNs 9 days after infection with p62 shRNA lentivirus compared with the NS-infected cells (results are expressed relative to NS-treated MNs; $n = 6$ independent experiments) and (**B**) representative image. Scale bar: 50 μm. (**C**) Quantification of SMA MN soma size after p62 knockdown ($n = 4{,}100$ NS; $n = 5{,}500$ p62i MNs measured). (**D**) Representative immunoblot and quantification of spinal cord protein lysates of SMNΔ7 mice and SMNΔ7 hemizygotes for p62 ($n = 5$ SMNΔ7 $p62^{+/+}$ mice, $n = 3$ SMNΔ7 $p62^{+/-}$ mice). (**E**) Representative images of cryosectioned TA muscles. Top: Original image showing laminin immunostaining (red), signal inverted by Columbus script, and individual muscle fibers recognized by the script, highlighted in green. Bottom: TA sections from WT, SMNΔ7, and SMNΔ7 $p62^{+/-}$ P10 mice. Scale bar: 50 μm. (**F**) Quantification of TA fiber size ($n = 5$ WT mice, $n = 4$ SMNΔ7 mice, $n = 4$ SMNΔ7 $p62^{+/-}$ mice). (**G**) Immunofluorescence images of SMNΔ7 and SMNΔ7 $p62^{+/-}$ FDB-2 P10 muscles showing neuromuscular junctions immunostained for nerve terminals (anti-synaptophysin [Syn], green) and endplates (α-bungarotoxin [α-BTX], red). Scale bar: 20 μm. (**H**) Quantification of fully innervated, partially innervated, and fully denervated endplates ($n = 4$ SMNΔ7 mice, $n = 4$ SMNΔ7 $p62^{+/-}$ mice). (**I**) Representative images of cervical spinal cord cryosections from P10 WT, SMNΔ7, and SMNΔ7 $p62^{+/-}$ mice showing Hb9:GFP+ MNs (nuclei are stained with DAPI; central canals are outlined with dotted circles). Scale bar: 100 μm. (**J**) Average number of MNs per section ($n = 10$ WT mice, $n = 9$ SMNΔ7 mice, $n = 4$ SMNΔ7 $p62^{+/-}$ mice). (**K**) Weight measurements of P10 mice ($n = 12$ SMNΔ7 mice, $n = 8$ SMNΔ7 $p62^{+/-}$ mice). (**L**) Kaplan-Meier plot showing survival curves for SMNΔ7 $p62^{+/+}$ mice (black line) and SMNΔ7 $p62^{+/-}$ (blue line) mice. $n = 31$ SMNΔ7 $p62^{+/+}$ mice; $n = 18$ SMNΔ7 $p62^{+/-}$ mice. $^{*}P < 0.05$, $^{**}P < 0.01$, and $^{***}P < 0.001$, by 2-tailed t test (**A**, **C**, **D**, **F**, **H**, **J**, and **K**) and Mantel-Cox and Gehan-Breslow-Wilcoxon tests (**L**). All results are shown as the mean ± SEM.

ity in protein lysates from control and SMA iPSC–derived MNs and observed that at least this activity associated with the proteasome complex was not reduced in diseased cells (Figure 4J). Together, these data indicate that the lack of SMN leads to an impairment of autophagy function that in turn results in accumulation of p62/ubiquitinated proteins in MNs and non-MNs. However, autophagy activity is not completely blocked, and we postulated that it can still sequester p62-SMN protein complexes for degradation.

SMN deficiency leads to mTORC1 activation. We next sought to explore how deficiency in SMN protein levels led to the autophagy malfunction that eventually resulted in the build-up of protein aggregates or toxic species (24, 41–43). It has been reported that p62, besides serving as an autophagy cargo adaptor, also mediates mTOR activation by promoting its localization to the lysosomal membrane (44, 45). The protein kinase mTOR is the master regulator of cellular metabolism and growth and is part of 2 protein complexes, mTORC1 and mTORC2 (46). When active, mTORC1 suppresses autophagy at different levels (47–49). Given the accumulation of p62 that we and others have observed in SMA cells (50, 51) and the associated autophagy activity dysfunction, we sought to determine whether decreased SMN levels affect mTOR activity. To address this question, we compared healthy control human fibroblasts with fibroblasts from patients affected by the most severe forms of the disease, SMA type I and type 0, with the latter type carrying only 1 *SMN2* copy. We deprived the fibroblasts of serum overnight and then incubated them with full media for 30 minutes to measure mTOR activity. We observed that not only did the control-treated SMA fibroblasts show increased phosphorylated levels of the mTOR downstream targets S6K1 and S6 when compared with healthy fibroblasts (Figure 5A and Supplemental Figure 4A), but the decrease in their phosphorylation upon starvation was less pronounced than in control cells, suggesting a higher basal mTOR activity in the diseased fibroblasts. Next, we investigated whether mTOR activity was also enhanced in SMA mouse and human MNs of different severities and obtained similar results, i.e., higher levels of phosphorylated S6K1 (p-S6K1) and p-S6 compared with healthy controls (Figure 5B, Supplemental Figure 4B, and Figure 5, C and D, respectively). These data indicate that SMN deficiency results in mTOR pathway activation. It has been previously reported that p62 activates mTOR (44, 45). We postulate that these results, together with the elevated p62 levels observed in SMA-affected cells, suggest that the increase in mTORC1 activity in SMA leads to the accumulation of p62 protein, which in turn activates mTOR and results in a feed-forward cycle that results in further autophagy dysfunction and SMN sequestration (Figure 5E).

Reducing p62 levels promotes MN survival in vitro and increases the lifespan of fly and mouse SMA models. Our data show that a reduction of p62 protein levels leads to notable increases in SMN and other proteins of the SMN complex including gemin2. Consequently, we explored whether this stabilization of SMN and its binding partners is associated with cytoprotection of SMA cells. We have previously shown that higher SMN levels directly correlate with better survival of both WT and SMA MNs under any kind of stress (34, 35). Thus, we decided to investigate the effect on MN survival of a p62-mediated increase in SMN. We knocked down p62 by lentiviral infection in mouse SMA MNs and quantified the number of surviving Hb9:GFP$^+$ MNs 10 days later. p62 knockdown resulted in a 50% increase in MN survival compared with cultures infected with a scramble control virus (NS) (Figure 6, A and B). In addition, p62-knockdown SMA MNs had a larger soma size, an indication of better overall neuronal health (Figure 6C). We also explored whether reducing p62 levels in WT MNs could reduce the basal rates of death due to culture-intrinsic stress. Indeed, we observed that WT MNs also had better survival and a larger soma size when p62 was knocked down compared with the NS-treated MNs (Supplemental Figure 5, A–C).

These results prompted us to investigate whether reducing p62 levels caused an amelioration of the SMA disease phenotype in vivo. We first studied a fly model of SMA, in which the expression of an RNAi targeting Smn is activated only in adult flies using a ubiquitous tubulin-Gal4 driver, which is under the control of the temperature-sensitive GAL80 protein (Gal80ts). Larvae were raised at 18°C, when tubulin-Gal4 is inactive, to prevent SMN reduction from having developmental effects, and adult flies were then switched to 29.5°C to drive expression of the RNAi. We used the actin gene-switch–inducible (actin-GS–inducible) Gal4-UAS expression system (52, 53), in which UAS RNAi expression is driven by Gal4 when flies are fed mifepristone (RU486). As expected, RNAi against a control gene (Contr-i) did not affect lifespan (Supplemental Figure 6, A and B), and Smn RNAi (Smn-i) decreased *Smn* mRNA levels by 70% (Supplemental Figure 6A). We did not expect that Smn RNAi would produce a strong decrease in lifespan, given that its expression is only activated during adult life. Indeed, we observed a small, although significant, reduction of the mean lifespan when it was coexpressed with the control RNAi (Supplemental Figure 6, A and C). Next, we analyzed the effects of reducing p62 expression on SMN protein levels and found that it resulted in enhanced SMN protein expression (Supplemental Figure 6, D and E), without affecting *Smn* mRNA expression (Supplemental Figure 6F). In addition, we tested whether p62 downregulation affected the lifespan of *Smn*-deficient flies by coexpressing *Smn*-i with *p62*-i. Importantly, while reducing p62 levels alone did not affect lifespan (Supplemental Figure 6, G and H), the flies expressing *Smn*-i and *p62*-i showed a complete rescue of the *Smn* RNAi–induced shortened lifespan (Supplemental Figure 6, I and J). These results indicate that decreasing p62 levels increases SMN protein in vivo and rescues the shortened lifespan of SMN-deficient flies.

We next sought to explore whether these observations could be reproduced in the SMA SMNΔ7 mouse, which in our colony survived an average of 10 days. Given than p62-KO mice are fertile and relatively healthy until they reach a mature age, when they develop obesity and bone and metabolic problems (54), we aimed to measure the disease manifestations in p62-KO SMNΔ7 mice. However, breeding SMNΔ7 p62-KO mice resulted in embryonic lethality of SMNΔ7 pups (data not shown), presumably because p62 is a scaffold protein with multiple modules that interact with other key signaling proteins (55). Instead, we crossed SMNΔ7 mice with p62-KO mice in order to obtain SMNΔ7 p62 heterozygotic mice (*smn*$^{-/-}$ h*SMN2*$^{+/+}$ h*SMN*Δ7$^{+/+}$ Hb9:GFP$^+$ p62$^{+/-}$ or just SMNΔ7 p62$^{+/-}$ for simplicity). We confirmed that p62 protein levels in spinal cords from SMNΔ7 p62$^{+/-}$ mice were indeed reduced by half (Figure 6D) and then studied several aspects of the mouse SMA disease phenotype. We first used an unbiased, automated method to measure muscle fiber size of tibialis anterior (TA) muscle

cryosections at the disease end stage (P10). We found that SMNΔ7 p62$^{+/-}$ TA muscle fibers had a significant increase in size compared with TA muscle fibers from SMNΔ7 mice (homozygous for p62) (Figure 6, E and F). Next, we evaluated the innervation status of the flexor digitorum brevis 2 (FDB-2) appendicular muscle, which is reported to show strong denervation in SMNΔ7 mice (56). Fully innervated endplates were defined by the complete overlap of presynaptic nerve terminals and immunostained with synaptophysin, and postsynaptic motor endplate acetylcholine receptors were labeled with α-bungarotoxin. Partially denervated endplates were identified by the partial overlap of pre- and postsynaptic labeling, and fully denervated endplates were devoid of any presynaptic labeling (Supplemental Figure 5D). Quantification of the percentage of denervated endplates revealed a robust amelioration of this pathologic phenotype in SMNΔ7 p62 mice. While in P10 SMNΔ7 muscles, only 40% of the endplates were fully innervated (Figure 6, G and H), nearly 80% of the endplates in SMNΔ7 p62 muscles were fully innervated and only approximately 5% were denervated (Figure 6, G and H). Additionally, we analyzed the spinal MN loss characteristically seen in this SMA mouse model (30) and observed that, while SMNΔ7 mice at P10 displayed a 50% reduction in the number of MNs, SMNΔ7 p62$^{+/-}$ P10 mice had similar numbers of ventral MNs compared with WT mice (Figure 6, I and J). This notable improvement in muscle, MNs numbers, and muscle innervation correlated with a significant increase in the body weight of SMNΔ7 p62$^{+/-}$ mice compared with that of SMNΔ7 mice (Figure 6K). Importantly, the rescue of multiple SMA-associated phenotypes translated to a 50% increase in the mean lifespan (5 more days) (Figure 6L). These data validate our in vitro results and confirm that p62 plays an important role in SMA pathology. Additionally, this work shows that reducing p62 levels, which are aberrantly increased in the disease, could represent a new strategy for developing SMA therapeutics.

Discussion

In this study, we have identified the autophagy receptor p62 as a regulator of SMN protein levels and discovered a molecular mechanism that explains the autophagy dysfunction affecting SMA cells. Our data reveal that mTOR overactivation causes such a dysfunction in SMA MNs, resulting in the accumulation of ubiquitinated proteins and p62. We suggest that abnormally high p62 levels aggravate the autophagy impairment and constitute the basis for the buildup of toxic species that increase susceptibility to cell death.

SMA is an early-onset neuromuscular disease associated with loss-of-function mutations or complete loss of the *SMN1* gene, resulting in very low SMN protein levels. Therefore, it is commonly accepted that approaches aimed at increasing SMN levels will have therapeutic value in treating the disease. Several of these approaches have recently entered clinical trials after showing promising results in in vitro and in vivo models (57), with one, Spinraza (nusinersen), having been recently approved. However, most of these approaches focus on modifying the expression or splicing of the *SMN2* gene or on directly replacing the *SMN1* gene via viral delivery. SMN is also controlled at the posttranscriptional level, but to date the approaches targeting this aspect of SMN biology have not achieved therapeutic success. Therefore, one main focus of our work has been to identify new pathways that mediate SMN protein degradation, with a view toward stabilizing the protein and therefore increasing its levels. It is known that SMN forms part of protein complexes (gems, SGs, complexes along axons) whose disassembly and degradation mechanisms are unclear. Since the UPS, previously shown to regulate SMN levels, only targets single proteins, we focused on the other major cellular catabolic pathway, the autophagy-lysosomal system, which is in charge of degrading protein complexes, protein aggregates, and organelles. We postulated that autophagy could also regulate SMN protein levels by at least targeting the fraction that is localized to protein complexes. With this study, we found that, indeed, autophagy degrades SMN — not only SMN-FL, but also the most abundantly transcribed form of SMN in SMA patients, SMNΔ7, which is partially functional, and therefore blocking its degradation may be quite relevant for slowing disease progression. Our data also show that the autophagy receptor p62 is a mediator of selective SMN degradation. SMN and p62 interact, and this interaction is partially blocked when SMN ubiquitination is inhibited. We also demonstrate that reducing p62 levels leads to a significant enhancement not only of SMN, but also of some of its main binding partners, such as gemin2 and the number of SMN^{+}, gemin2^{+} nuclear gems. Importantly, such increases had functional consequences, since they improved the survival of SMA MNs in vitro, abolished the shortening effect on fly lifespan induced by Smn-i, and notably improved multiple aspects of the disease pathology of SMNΔ7 mice, including increasing their lifespan by 50%.

One recently published study also implicated autophagy in the control of SMN protein levels (51). This work, however, showed that inducing autophagy increases SMN levels, while at the same time, it claimed that SMA cells exhibit increased autophagy. Although, there are differences between our studies, both of them demonstrated the critical role of autophagy in SMA pathogenesis, and our study, using multiple cell types and models, further uncovers the mechanistic control of SMN degradation by selective autophagy via the molecular adaptor p62. Additional studies will be required to understand the discrepancies between our findings and the previously published results.

For many years, autophagy was considered a bulk degradation process induced by nutrient deprivation and lacking specificity. However, almost 20 years ago, selective autophagy was reported in yeast (58), and since then, multiple studies have confirmed that autophagy is a more selective process than originally thought (59). Indeed, p62 and other proteins with similar amino acid domains, such as NBR1, optineurin, NDP52, and others, have been shown to function as autophagy cargo recognition proteins (31, 32). A hallmark of most neurodegenerative diseases is the accumulation of misfolded and aggregation-prone proteins and damaged organelles (39, 60). Numerous studies have reported the importance of autophagy receptors in delivering protein aggregates and organelles to APs for degradation (22). To date, the presence of these toxic species in SMA had not been reported. However, recent studies have identified intracellular trafficking problems that affect mitochondria (61), the endosomal-lysosomal system (62, 63), and axonal transport, growth, or morphology (26, 64–66). An impairment of the last steps of the autophagic process could well be another consequence of SMN deficiency, but such an autophagy dysfunction could also be the source of those cellular defects,

similar to what has been reported for other neurological disorders. These studies, together with the data presented in this work, suggest that SMA shares more neurodegenerative disease hallmarks than previously recognized.

Since autophagy, through p62, plays a role in mediating SMN degradation, and since most neurodegenerative disorders involve defects in autophagy activity, we investigated whether this pathway was functioning properly in SMA. Indeed, we observed that all SMA cells analyzed — human fibroblasts as well as mouse and human iPSC–derived MNs — had higher amounts of LC3-I and LC3-II, which correlates with increased number of APs and impaired AP turnover (Figure 4). We observed that this defect was accompanied by increased levels of p62 and ubiquitinated proteins and that an acute decrease in SMN protein levels produced the same results. Our findings agree with those of recent studies that reported autophagy alterations upon SMN downregulation in cell lines (50, 67, 68) and answer the previously unresolved question of why autophagy is dysfunctional in SMA and explain the nature of the interplay between SMN and autophagy activity. We postulate that, as a consequence of SMN deficiency–induced autophagy impairment, ubiquitinated proteins and p62 accumulate. This is likely to increase the appearance of misfolded and aggregated proteins, leading to additional problems in cellular trafficking and AP clearance. This hypothesis is in line with a previous study from Komatsu and colleagues demonstrating that p62 plays an important role in inclusion body formation when autophagy is deficient (69). Another possible consequence of enhanced p62 protein levels is overactivation of mTORC1, which would in turn further interfere with autophagy activity (70, 71). There is also some disagreement as to the role that mTOR plays in SMA. On the one hand, several studies in SMA mice suggest that mTOR is downregulated and that increasing its activity can promote MN survival and enhance lifespan (72–74). On the other hand, another study showed that SMA type III muscle shows overexpression of mTOR (75). It is therefore possible that the activity of mTOR in SMA differs between different tissues or even cell populations. The increased mTOR activity that we detected in SMA cells could be a cellular response to limit further accumulation of APs and aggregation-prone material, but at the same time, it could be blocking autophagy reactivation via its inhibitory effect on TFEB, the master transcriptional regulator of lysosomal and autophagy genes (76, 77). Further studies are needed to understand whether the observed alterations of autophagy/lysosomal function and the mTORC1 signaling pathway in SMA MNs are direct, and maybe independent, consequences of SMN loss of function, or the indirect result of accumulative events triggered by the deficiency of the protein.

In summary, in this study, we have identified a pathway that controls SMN levels in cells including MNs, a finding that may uncover new avenues for identifying potential targets for therapeutic intervention. Furthermore, we have revealed an autophagy dysfunction in SMA MNs that is possibly caused by mTOR overactivation, resulting in the accumulation of ubiquitinated proteins and p62. p62 is a key protein that links autophagy, mTORC1, ubiquitination, and, now, SMN protein levels. We postulate that abnormally high p62 levels may aggravate autophagy impairment and constitute the basis for the buildup of toxic species that enhance susceptibility to cell death. Understanding the molecular mechanisms that control this loop, as well as whether compromised autophagy contributes to SMA progression, will be essential for the future development of therapeutics that act on this pathway to prevent neuronal degeneration.

Methods

Mouse colonies. FVB mice were obtained from Charles River Laboratories. The original breeding pair of heterozygous SMNΔ7 mice (*Smn*$^{+/-}$ h*SMN2*$^{+/+}$ h*SMNΔ7*$^{+/+}$) on a FVB background and the *Hb9:GFP* mice on a C57Bl/6 background were provided by The Jackson Laboratory and backcrossed with mice on a FVB background for more than 10 generations. *p62 SQSTM1*$^{-/-}$ mice on a C57Bl/6 background were provided by Toru Yanagawa (University of Tsukuba, Tsukuba, Japan) and backcrossed with mice a FVB background for more than 7 generations.

Spinal MN and muscle histology. The spinal cord and TA muscles were dissected from WT, SMNΔ7, and SMNΔ7 p62$^{+/-}$ mice euthanized at P10 and were fixed in 4% paraformaldehyde in PBS overnight. The spinal cords were processed as previously described (35), and images were captured with an LSM 700 Inverted Confocal Microscope (Leica). For evaluation of the innervation state of the FDB-2 muscle, hind paws were fixed in 4% paraformaldehyde in PBS overnight and then rinsed in PBS. The FDB-2 muscles were dissected, permeabilized in 0.5% Triton X-100, and blocked in 5% normal goat serum (NGS) under constant shaking for 1 hour, and then incubated with anti-synaptophysin antibody for 24 hours at 4°C. Samples were subsequently washed with several changes of PBS with shaking for 6 hours, incubated with secondary antibody overnight at 4°C, and then washed with PBS with shaking for 6 hours. Finally, samples were incubated with α-bungarotoxin for 1 hour at room temperature to label acetylcholine receptors (AChRs), washed again for 1 hour, and mounted and imaged as described above.

Mouse MN differentiation. Mouse WT SMN$^{+/+}$ SMN2$^{+/+}$ Hb9:GFP and SMA SMN$^{-/-}$ SMN2$^{+/+}$ Hb9:GFP, and SMN$^{-/-}$ SMN2$^{+/+}$ SMNΔ7 Hb9:GFP ES cells were maintained and differentiated as described previously (35). Briefly, ESCs were differentiated into MNs using an embryoid body method with treatments of retinoic acid (Sigma-Aldrich) and a hedgehog agonist (Curis, Inc.). After 7 days, MNs were dissociated and plated onto poly-ornithine coated plates (PerkinElmer).

Human MN differentiation. The iPSCs were grown on Matrigel-coated dishes (BD Biosciences), cultured with mTeSR (STEMCELL Technologies), and split using Gentle Cell Dissociation Reagent (STEMCELL Technologies) until the initiation of the MN differentiation protocol, when they were dissociated with Accutase (STEMCELL Technologies) and cultured in mTeSR as embryoid bodies in ultra-low attachment dishes (Corning). LDN (1 μM, Stemgent) and SB 431542 (10 μM, Stemgent) were added 1 day later (day 1) to induce neural differentiation and media gradually changed to knockout serum replacement and DMEM media (Life Technologies, Thermo Fisher Scientific). Retinoic acid (1 μM , Sigma-Aldrich) and BDNF (10 ng/ml) were added 2 days later (day 3), and 1 μM smoothened agonist 1.3 (EMD Millipore) was added 5 days later (day 8). DAPT (2.5 μM, R&D Systems) was added on day 10 along with, 2 μM cytosine arabinoside (Ara-c, Sigma-Aldrich) to eliminate progenitors and dividing cells. From day 5 to day 10, media were gradually changed to DMEM/F12 supplemented with 2% B27 and 1% N2 (Life Technologies, Thermo Fisher Scientific).

After 14 days of differentiation, the cultures were dissociated with papain/DNase solution (Worthington) and plated in 50 μg/ml poly-lysin (EMD Millipore), 10 μg/ml laminin (Life Technologies, Thermo Fisher Scientific) and 10 μg/ml fibronectin-coated (Corning) plates (Greiner). The medium used was Neurobasal containing 2% B27 and 1% N2, supplemented with Glutamax (Life Technologies, Thermo Fisher Scientific), NEAA (EMD Millipore), 20% glucose, 0.2 μM ascorbic acid (Sigma-Aldrich), and 20 ng/ml of BDNF, GDNF, and CNTF (R&D Systems).

Immunocytochemistry and image analysis. Cells were fixed in 4% paraformaldehyde (PFA) at room temperature for 20 minutes. Following standard protocols, cells were immunostained with primary antibodies followed by fluorescently labeled secondary antibodies (Life Technologies, Thermo Fisher Scientific) as previously described (35). For quantification of mCherry-LC3$^+$ APLys and mCherry-GFP-LC3$^+$ APs, human iPSC–derived MNs were cultured in 12-mm glass coverslips and images captured using a ×63 objective on an LSM 700 Inverted Confocal Microscope (Leica). Quantification was performed on images of 40 to 100 lentivirus-transduced neurons per line and per treatment, with maximum projection of all *Z*-stack sections using ImageJ software (NIH). Three independent experiments were performed. TA muscle fiber size was measured in images taken from random visual fields using a ×20 objective on a Nikon Eclipse Ti microscope. Subsequent image quantification was automatically performed using the PerkinElmer Columbus Image Data Storage and Analysis System. The muscle fibers (2,000–3,000 per mouse) were measured. Innervation of FDB-2 muscles was quantified in images taken with a ×20 objective on a LSM 700 inverted confocal microscope. The innervation status of postsynaptic endplates was determined according to the extent to which the endplate overlaid with presynaptic components. Fully innervated endplates were defined by the complete overlap of presynaptic (i.e., synaptophysin) and postsynaptic (α-bungarotoxin) labeling. Partially denervated endplates were those with only part of the endplate being covered by presynaptic labeling. Fully denervated endplates were devoid of any presynaptic labeling. Endplates (300–700 per mouse) were analyzed from randomly selected visual fields. The quantification was performed by an investigator blinded to the muscle genotypes.

Chemicals, antibodies, and plasmids. For mammalian cell experiments, the following antibodies were used: rat HA and mouse β-actin (Cell Signaling Technology, 3700S); rabbit β-tubulin (Abcam, ab6046); rabbit islet 1 (Abcam, ab109517); SQSTM1/p62 (Abcam, ab56416); rabbit gemin2 (Abcam, ab150383); rabbit lamin B1 (Abcam, ab16048); mouse SMN (BD Biosciences, 610647); rabbit ubiquitin (Santa Cruz Biotechnology, SC-9133); mouse c-Myc (Novus Biologicals, NB600-302); rabbit LC3 (2775); rabbit p-P70S6K1 (Thr389, Cell Signaling Technology, 9234S); rabbit P70S6K1 (Cell Signaling Technology, 2708S); rabbit p-S6 (Ser235/236, Cell Signaling Technology, 2211s); rabbit S6 (Cell Signaling Technology, 2217S); synaptophysin (Synaptic Systems, 101002); and laminin (Sigma-Aldrich, L9393). For NMJ analysis, Alexa Fluor 555–conjugated α-bungarotoxin (Life Technologies, Thermo Fisher Scientific, B35451) was used. For fly experiments, SMN (gift of Spyros Artavanis-Tsakonas, Harvard Medical School, Boston, Massachusetts, USA, and Gregory Matera, University of North Carolina, Chapel Hill, North Carolina, USA) and tubulin (Sigma-Aldrich, T5168) antibodies were used. cDNAs encoding human HA-tagged SMN-FL protein or a truncated SMN protein carrying a deletion of exon 7 (Δ7) were subcloned into the pEF-DEST51 vector using the Gateway cloning system (Life Technologies, Thermo Fisher Scientific). Myc-p62 plasmid was provided by María T. Diaz-Meco (Sanford Burnham Prebys Medical Discovery Institute, La Jolla, California, USA), and HA-GFP and Myc-E2-crimson plasmids were purchased from Addgene (plasmid numbers 22612 and 38770, respectively).

Transfection and lentiviral transduction. For overexpression of SMN-FL and SMN-Δ7 proteins, HEK293T cells were transfected with Lipofectamine 2000 (Life Technologies, Thermo Fisher Scientific) with the HA-tagged forms of the proteins following the manufacturer's instructions. A pool of RNAi (20 nM) against p62 (SQSTM1) or SMN (Santa Cruz Biotechnology, sc-29679 and sc-36510, respectively) or control RNAi (QIAGEN, 1027280) was transfected into HEK293T cells and mouse MNs (Santa Cruz Biotechnology, sc-29828) using Lipofectamine RNAiMAX Transfection Reagent (Life Technologies, Thermo Fisher Scientific) following the manufacturers' instructions. Cells were exposed to the silencing mix for 6 hours, following which silencing medium was replaced with fresh complete media. Lentiviral shRNA plasmids targeting Atg7 and a nonsilencing control, as well as mCherry-GFP-LC3 constructs were provided by Ana M. Cuervo (Albert Einstein College of Medicine, New York, New York, USA) and previously published (40, 78). Plasmids encoding the DN form of human Cul5 in PHAGE vector and empty PHAGE vector were purchased from Addgene (plasmid numbers 41916 and 44012, respectively) and used for lentiviral production. Vectors encoding short hairpins against mouse (TRCN0000238133 and TRCN0000098615) and human (TRCN0000430110 and TRCN0000007234) p62 (SQSTM1) were purchased from Sigma-Aldrich. Lentiviral stocks were prepared by Lipofectamine transfection of these vectors and the packaging vectors pMDLg/pRRE, pRSV-Rev, and pMD2.VSVG into HEK293T cells. Supernatants were collected over a 72-hour period, titered, and used for infection. The efficiency of infection at 72 hours, determined by the percentage of GFP$^+$ cells or the percentage of cells surviving 1 μM puromycin treatment, depending on the vector, exceeded 90% for all constructs.

Cell culture treatments. For serum or amino acid removal, cells were washed with PBS followed by culture in DMEM or EBSS for 24 hours, respectively. The lysosomal inhibitors leupeptin (Fisher BioReagents, Thermo Fisher Scientific), ammonium chloride (Sigma-Aldrich) and HCQ (Sigma-Aldrich) were used at 100 μM, 20 mM, and 10 μM, respectively, for 4 to 6 hours. Rapamycin (R&D Systems) was used at 200 nM and MG132 (Sigma-Aldrich) at 100 nM. For SG formation induction, cells were exposed to 10 or 50 μM sodium arsenate for 6 hours. Details on IP, cellular fractionation, and immunoblot analysis are provided in the Supplemental Experimental Procedures.

Chymotrypsin-like activity measurement. Human iPSC–derived MNs were washed in PBS, homogenized with 0.5% NP-40, and centrifuged for 15 minutes at 4°C at 16,200 *g*. Supernatant were collected and the assay performed using the Proteasome Activity Assay Kit (Abcam, ab107921) according to the manufacturer's instructions.

Reverse transcription PCR. Total RNA was extracted with the TRIzol Reagent (Life Technologies, Thermo Fisher Scientific), followed by DNase digestion using RQ1 RNase-Free DNase (Promega). Total RNA was reverse transcribed with the iScript cDNA Synthesis Kit (Bio-Rad). Quantitative reverse transcription PCR (qRT-PCR) was performed with iQ SYBR Green Supermix (Bio-Rad) and a CFX96 Real-Time PCR Detection System (Bio-Rad). Relative quantitations

of mRNA levels were determined using the comparative Ct method. For mammalian cell experiments, 18s and actin were used as housekeeping genes, and for fly experiments, RpL32 and α-tubulin 84B were used as a normalization reference. The following mouse primers were used: *SMN*, forward, 5′-AAGGCACAGCCAGAAGAAAA-3′, *SMN*, reverse, 5′-TCACAGGTCGGGGAAAGTAG-3′; *p62*, forward, 5′-GCTGCCCTAACCCACATCT-3′, *p62*, reverse, 5′-CGCCTTCATCCGAGAAAC-3′; and *IL6*, forward, 5′-AGTTGCCTTCTTGGGACTGA-3′, *IL6*, reverse, 5′-TCCACGATTTCCCAGAGAAC-3′. The following human primers were used: *SMN*, forward, 5′-AACATCAAGCCCAAATCTGC-3′, *SMN*, reverse, 5′-TGGTCCAGAAGGAAATGGAG-3′; and *p62*, forward, 5′-AGAACGTTGGGGAGAGTGTG-3′, *p62*, reverse, 5′-GCGATCTTCCTCATCTGCTC-3′. The following primers were used for fly: *Smn*, forward, 5′-AGCGGAAAGAAAAAGACACC-3′, *Smn*, reverse, 5′-TCGAAAAGATGTGATGTGATGA-3′; *ref(2)P(p62)*, forward, 5′-AATCGAGCTGTATCTTTTCCAGG-3′, *ref(2)P(p62)*, reverse, 5′-AACGTGCATATTGCTCTCGCA-3′.

Fly lifespan analysis. For survival analysis, flies were collected within 24 hours from eclosion, sorted by sex under light CO_2 anesthesia, and reared at standard density (20–25 flies per vial) on cornmeal, soy flour, and yeast fly food at 25°C and 60% humidity and a 12-hour light/12-hour dark cycle. Flies were transferred to fresh vials every 2 days and dead flies counted. RU486 (Mifepristone) dissolved in ethanol was administered in the media at a final concentration of 150 μg/ml. The efficiency of Smn and p62 RNAi lines was tested using the ubiquitous actin5c-Gal4 driver. As a control, we used RNAi against the white gene, responsible for the eye color that we and others have showed does not affect lifespan when it is mutated or suppressed with RNAi (79). The following RNAi lines were used: control RNAi (HMS00017), Smn-i (JF02057), p62-551i (HMS00551), and p62-938i (HMS00938).

Statistics. Statistical significance was determined using a 2-tailed Student's *t* test for groups of 2 and by ANOVA for groups of 3 or more. A CI of 95% was used for all comparisons. The statistical significance for the Kaplan-Meier analysis was determined by Mantel-Cox and Wilcoxon tests. A *P* value of less than 0.05 was considered statistically significant.

Study approval. All animal studies were reviewed and approved by the IACUC of Harvard University and performed in accordance with institutional and federal guidelines. The Pediatric Neuromuscular Clinical Research Network recruited SMA patients and collected the fibroblasts later obtained by the Rubin laboratory for the derivation of iPS cell lines. Tissue collections for all human subjects who donated tissue used in this research were conducted with consent under protocols that were approved by the Columbia University IRB. Subsequent use of the SMA patients' samples in the Rubin laboratory at Harvard University was reviewed by the Harvard University Committee on the Use of Human Subjects (CUHS). The generation of iPSC lines by the Harvard iPSC Core was conducted in a fee-for-service capacity. The information regarding both the SMA iPSC lines and the healthy control cell lines BJ and 1016A has been previously published (35).

See complete unedited blots in the supplemental material.

Author contributions

NRM and AP conceived the study. NRM, AP, and TG designed the study methodology. NRM and AP performed formal analysis. NRM, AP, RMG, and TG conducted the studies. EMN provided research assistance. NRM, AP, NP, and LLR provided resources. NRM wrote the original draft of the manuscript. NRM, AP, TG, NP, RS, and LLR reviewed and edited the manuscript. NRM and LLR were responsible for funding acquisition.

Acknowledgments

We thank the Pediatric Neuromuscular Clinical Research Network for recruiting SMA patients and the Harvard Stem Cell Institute iPSC Core Facility for generating the iPSCs from SMA patients' fibroblasts. We thank Catherine McGillivary and Diane Faria (Department of Stem Cell and Regenerative Biology, Histology Core, Harvard University, Cambridge, Massachusetts, USA) for histology assistance. We thank Patricia Boya (Department of Cellular and Molecular Biology, Centro de Investigaciones Biológicas, CSIC) for critically reviewing this manuscript. We are grateful to Lance S. Davidow for image analysis support and J. LaLonde(Department of Stem Cell and Regenerative Biology, Harvard University, and Harvard Stem Cell Institute, Cambridge, Massachusetts, USA) for editorial assistance. This work was supported by the Muscular Dystrophy Association (MDA376743, to NRM); the SMA Foundation (to LLR); the National Institute of Neurological Disorders and Stroke (NINDS) (P01NS066888, to LLR); and the National Institute of General Medical Sciences (R01-AG043517, to RS and R01-GM084947, to NP). AP is supported by a LAM Foundation Fellowship Award (LAM00105E01-15).

Address correspondence to: Natalia Rodriguez-Muela or Lee L. Rubin, 7 Divinity Avenue, Sherman Fairchild G53 (N. Rodriguez-Muela), Sherman Fairchild G60 (L.L. Rubin), Cambridge, Massachusetts 02138, USA. Phone: 617.384.8105; Email: natalia_rodriguezmuela@harvard.edu (N. Rodriguez-Muela); lee_rubin@harvard.edu (L.L. Rubin).

1. Lefebvre S, et al. Identification and characterization of a spinal muscular atrophy-determining gene. *Cell*. 1995;80(1):155–165.
2. Iascone DM, Henderson CE, Lee JC. Spinal muscular atrophy: from tissue specificity to therapeutic strategies. *F1000Prime Rep*. 2015;7:04.
3. Lorson CL, Hahnen E, Androphy EJ, Wirth B. A single nucleotide in the SMN gene regulates splicing and is responsible for spinal muscular atrophy. *Proc Natl Acad Sci U S A*. 1999;96(11):6307–6311.
4. Monani UR, et al. A single nucleotide difference that alters splicing patterns distinguishes the SMA gene SMN1 from the copy gene SMN2. *Hum Mol Genet*. 1999;8(7):1177–1183.
5. Lorson CL, et al. SMN oligomerization defect correlates with spinal muscular atrophy severity. *Nat Genet*. 1998;19(1):63–66.
6. Cho S, Dreyfuss G. A degron created by SMN2 exon 7 skipping is a principal contributor to spinal muscular atrophy severity. *Genes Dev*. 2010;24(5):438–442.
7. Gubitz AK, Feng W, Dreyfuss G. The SMN complex. *Exp Cell Res*. 2004;296(1):51–56.
8. Fallini C, et al. Dynamics of survival of motor neuron (SMN) protein interaction with the mRNA-binding protein IMP1 facilitates its trafficking into motor neuron axons. *Dev Neurobiol*. 2014;74(3):319–332.
9. Lim SR, Hertel KJ. Modulation of survival motor neuron pre-mRNA splicing by inhibition of alternative 3′ splice site pairing. *J Biol Chem*. 2001;276(48):45476–45483.
10. Hua Y, Vickers TA, Okunola HL, Bennett CF, Krainer AR. Antisense masking of an hnRNP A1/A2 intronic splicing silencer corrects SMN2 splicing in transgenic mice. *Am J Hum Genet*. 2008;82(4):834–848.
11. Williams JH, Schray RC, Patterson CA, Ayitey SO,

Tallent MK, Lutz GJ. Oligonucleotide-mediated survival of motor neuron protein expression in CNS improves phenotype in a mouse model of spinal muscular atrophy. *J Neurosci*. 2009;29(24):7633–7638.
12. Osman EY, et al. Morpholino antisense oligonucleotides targeting intronic repressor Element1 improve phenotype in SMA mouse models. *Hum Mol Genet*. 2014;23(18):4832–4845.
13. Dickson A, Osman E, Lorson CL. A negatively acting bifunctional RNA increases survival motor neuron both in vitro and in vivo. *Hum Gene Ther*. 2008;19(11):1307–1315.
14. Naryshkin NA, et al. Motor neuron disease. SMN2 splicing modifiers improve motor function and longevity in mice with spinal muscular atrophy. *Science*. 2014;345(6197):688–693.
15. Kwon DY, Motley WW, Fischbeck KH, Burnett BG. Increasing expression and decreasing degradation of SMN ameliorate the spinal muscular atrophy phenotype in mice. *Hum Mol Genet*. 2011;20(18):3667–3677.
16. Burnett BG, Muñoz E, Tandon A, Kwon DY, Sumner CJ, Fischbeck KH. Regulation of SMN protein stability. *Mol Cell Biol*. 2009;29(5):1107–1115.
17. Makhortova NR, et al. A screen for regulators of survival of motor neuron protein levels. *Nat Chem Biol*. 2011;7(8):544–552.
18. Kwon DY, et al. The E3 ubiquitin ligase mind bomb 1 ubiquitinates and promotes the degradation of survival of motor neuron protein. *Mol Biol Cell*. 2013;24(12):1863–1871.
19. Han KJ, et al. Ubiquitin-specific protease 9x deubiquitinates and stabilizes the spinal muscular atrophy protein-survival motor neuron. *J Biol Chem*. 2012;287(52):43741–43752.
20. Xu C, Kim NG, Gumbiner BM. Regulation of protein stability by GSK3 mediated phosphorylation. *Cell Cycle*. 2009;8(24):4032–4039.
21. Mizushima N, Komatsu M. Autophagy: renovation of cells and tissues. *Cell*. 2011;147(4):728–741.
22. Xu Z, Yang L, Xu S, Zhang Z, Cao Y. The receptor proteins: pivotal roles in selective autophagy. *Acta Biochim Biophys Sin (Shanghai)*. 2015;47(8):571–580.
23. Zaffagnini G, Martens S. Mechanisms of selective autophagy. *J Mol Biol*. 2016;428(9 Pt A):1714–1724.
24. Hara T, et al. Suppression of basal autophagy in neural cells causes neurodegenerative disease in mice. *Nature*. 2006;441(7095):885–889.
25. Pickford F, et al. The autophagy-related protein beclin 1 shows reduced expression in early Alzheimer disease and regulates amyloid beta accumulation in mice. *J Clin Invest*. 2008;118(6):2190–2199.
26. Komatsu M, et al. Essential role for autophagy protein Atg7 in the maintenance of axonal homeostasis and the prevention of axonal degeneration. *Proc Natl Acad Sci U S A*. 2007;104(36):14489–14494.
27. Fimia GM, et al. Ambra1 regulates autophagy and development of the nervous system. *Nature*. 2007;447(7148):1121–1125.
28. Liang CC, Wang C, Peng X, Gan B, Guan JL. Neural-specific deletion of FIP200 leads to cerebellar degeneration caused by increased neuronal death and axon degeneration. *J Biol Chem*. 2010;285(5):3499–3509.
29. Protter DS, Parker R. Principles and properties of stress granules. *Trends Cell Biol*. 2016;26(9):668–679.
30. Le TT, et al. SMNDelta7, the major product of the centromeric survival motor neuron (SMN2) gene, extends survival in mice with spinal muscular atrophy and associates with full-length SMN. *Hum Mol Genet*. 2005;14(6):845–857.
31. Kirkin V, McEwan DG, Novak I, Dikic I. A role for ubiquitin in selective autophagy. *Mol Cell*. 2009;34(3):259–269.
32. Slobodkin MR, Elazar Z. The Atg8 family: multifunctional ubiquitin-like key regulators of autophagy. *Essays Biochem*. 2013;55:51–64.
33. Pankiv S, et al. p62/SQSTM1 binds directly to Atg8/LC3 to facilitate degradation of ubiquitinated protein aggregates by autophagy. *J Biol Chem*. 2007;282(33):24131–24145.
34. Ng SY, et al. Genome-wide RNA-Seq of human motor neurons implicates selective ER stress activation in spinal muscular atrophy. *Cell Stem Cell*. 2015;17(5):569–584.
35. Rodriguez-Muela N, et al. Single-cell analysis of SMN reveals its broader role in neuromuscular disease. *Cell Rep*. 2017;18(6):1484–1498.
36. Hua Y, Zhou J. Survival motor neuron protein facilitates assembly of stress granules. *FEBS Lett*. 2004;572(1-3):69–74.
37. Zou T, Yang X, Pan D, Huang J, Sahin M, Zhou J. SMN deficiency reduces cellular ability to form stress granules, sensitizing cells to stress. *Cell Mol Neurobiol*. 2011;31(4):541–550.
38. Klionsky DJ, et al. Guidelines for the use and interpretation of assays for monitoring autophagy (3rd edition). *Autophagy*. 2016;12(1):1–222.
39. Frake RA, Ricketts T, Menzies FM, Rubinsztein DC. Autophagy and neurodegeneration. *J Clin Invest*. 2015;125(1):65–74.
40. Kimura S, Noda T, Yoshimori T. Dissection of the autophagosome maturation process by a novel reporter protein, tandem fluorescent-tagged LC3. *Autophagy*. 2007;3(5):452–460.
41. Komatsu M, et al. Loss of autophagy in the central nervous system causes neurodegeneration in mice. *Nature*. 2006;441(7095):880–884.
42. Boya P, et al. Inhibition of macroautophagy triggers apoptosis. *Mol Cell Biol*. 2005;25(3):1025–1040.
43. Korolchuk VI, Mansilla A, Menzies FM, Rubinsztein DC. Autophagy inhibition compromises degradation of ubiquitin-proteasome pathway substrates. *Mol Cell*. 2009;33(4):517–527.
44. Duran A, et al. p62 is a key regulator of nutrient sensing in the mTORC1 pathway. *Mol Cell*. 2011;44(1):134–146.
45. Dibble CC, Manning BD. Signal integration by mTORC1 coordinates nutrient input with biosynthetic output. *Nat Cell Biol*. 2013;15(6):555–564.
46. Saxton RA, Sabatini DM. mTOR signaling in growth, metabolism, and disease. *Cell*. 2017;169(2):361–371.
47. Ganley IG, Lam du H, Wang J, Ding X, Chen S, Jiang X. ULK1.ATG13.FIP200 complex mediates mTOR signaling and is essential for autophagy. *J Biol Chem*. 2009;284(18):12297–12305.
48. Jung CH, et al. ULK-Atg13-FIP200 complexes mediate mTOR signaling to the autophagy machinery. *Mol Biol Cell*. 2009;20(7):1992–2003.
49. Kim J, Kundu M, Viollet B, Guan KL. AMPK and mTOR regulate autophagy through direct phosphorylation of Ulk1. *Nat Cell Biol*. 2011;13(2):132–141.
50. Custer SK, Androphy EJ. Autophagy dysregulation in cell culture and animals models of spinal muscular atrophy. *Mol Cell Neurosci*. 2014;61:133–140.
51. Periyakaruppiah A, de la Fuente S, Arumugam S, Bahí N, Garcera A, Soler RM. Autophagy modulators regulate survival motor neuron protein stability in motoneurons. *Exp Neurol*. 2016;283(Pt A):287–297.
52. Osterwalder T, Yoon KS, White BH, Keshishian H. A conditional tissue-specific transgene expression system using inducible GAL4. *Proc Natl Acad Sci U S A*. 2001;98(22):12596–12601.
53. Roman G, Endo K, Zong L, Davis RL. P[Switch], a system for spatial and temporal control of gene expression in Drosophila melanogaster. *Proc Natl Acad Sci U S A*. 2001;98(22):12602–12607.
54. Rodriguez A, et al. Mature-onset obesity and insulin resistance in mice deficient in the signaling adapter p62. *Cell Metab*. 2006;3(3):211–222.
55. Katsuragi Y, Ichimura Y, Komatsu M. p62/SQSTM1 functions as a signaling hub and an autophagy adaptor. *FEBS J*. 2015;282(24):4672–4678.
56. Ling KK, Gibbs RM, Feng Z, Ko CP. Severe neuromuscular denervation of clinically relevant muscles in a mouse model of spinal muscular atrophy. *Hum Mol Genet*. 2012;21(1):185–195.
57. Faravelli I, Nizzardo M, Comi GP, Corti S. Spinal muscular atrophy--recent therapeutic advances for an old challenge. *Nat Rev Neurol*. 2015;11(6):351–359.
58. Hutchins MU, Veenhuis M, Klionsky DJ. Peroxisome degradation in Saccharomyces cerevisiae is dependent on machinery of macroautophagy and the Cvt pathway. *J Cell Sci*. 1999;112(Pt 22):4079–4087.
59. Ichimura Y, Kominami E, Tanaka K, Komatsu M. Selective turnover of p62/A170/SQSTM1 by autophagy. *Autophagy*. 2008;4(8):1063–1066.
60. Wong E, Cuervo AM. Autophagy gone awry in neurodegenerative diseases. *Nat Neurosci*. 2010;13(7):805–811.
61. Miller N, Shi H, Zelikovich AS, Ma YC. Motor neuron mitochondrial dysfunction in spinal muscular atrophy. *Hum Mol Genet*. 2016;25(16):3395–3406.
62. Dimitriadi M, et al. Decreased function of survival motor neuron protein impairs endocytic pathways. *Proc Natl Acad Sci U S A*. 2016;113(30):E4377–E4386.
63. Hosseinibarkooie S, et al. The power of human protective modifiers: PLS3 and CORO1C unravel impaired endocytosis in spinal muscular atrophy and rescue SMA phenotype. *Am J Hum Genet*. 2016;99(3):647–665.
64. Wang QJ, et al. Induction of autophagy in axonal dystrophy and degeneration. *J Neurosci*. 2006;26(31):8057–8068.
65. Friedman LG, et al. Disrupted autophagy leads to dopaminergic axon and dendrite degeneration and promotes presynaptic accumulation of α-synuclein and LRRK2 in the brain. *J Neurosci*. 2012;32(22):7585–7593.
66. Rodríguez-Muela N, Germain F, Mariño G, Fitze PS, Boya P. Autophagy promotes survival of retinal ganglion cells after optic nerve axotomy in mice. *Cell Death Differ*. 2012;19(1):162–169.
67. Garcera A, Bahi N, Periyakaruppiah A, Arumugam S, Soler RM. Survival motor neuron protein reduc-

tion deregulates autophagy in spinal cord motoneurons in vitro. *Cell Death Dis*. 2013;4:e686.
68. Piras A, et al. Inhibition of autophagy delays motoneuron degeneration and extends lifespan in a mouse model of spinal muscular atrophy. *Cell Death Dis*. 2017;8(12):3223.
69. Komatsu M, et al. Homeostatic levels of p62 control cytoplasmic inclusion body formation in autophagy-deficient mice. *Cell*. 2007;131(6):1149–1163.
70. Hara K, et al. Raptor, a binding partner of target of rapamycin (TOR), mediates TOR action. *Cell*. 2002;110(2):177–189.
71. Linares JF, Duran A, Yajima T, Pasparakis M, Moscat J, Diaz-Meco MT. K63 polyubiquitination and activation of mTOR by the p62-TRAF6 complex in nutrient-activated cells. *Mol Cell*. 2013;51(3):283–296.
72. Ning K, et al. PTEN depletion rescues axonal growth defect and improves survival in SMN-deficient motor neurons. *Hum Mol Genet*. 2010;19(16):3159–3168.
73. Tseng YT, Chen CS, Jong YJ, Chang FR, Lo YC. Loganin possesses neuroprotective properties, restores SMN protein and activates protein synthesis positive regulator Akt/mTOR in experimental models of spinal muscular atrophy. *Pharmacol Res*. 2016;111:58–75.
74. Kye MJ, et al. SMN regulates axonal local translation via miR-183/mTOR pathway. *Hum Mol Genet*. 2014;23(23):6318–6331.
75. Millino C, et al. Different atrophy-hypertrophy transcription pathways in muscles affected by severe and mild spinal muscular atrophy. *BMC Med*. 2009;7:14.
76. Sardiello M, et al. A gene network regulating lysosomal biogenesis and function. *Science*. 2009;325(5939):473–477.
77. Settembre C, et al. A lysosome-to-nucleus signalling mechanism senses and regulates the lysosome via mTOR and TFEB. *EMBO J*. 2012;31(5):1095–1108.
78. Rodríguez-Muela N, et al. Balance between autophagic pathways preserves retinal homeostasis. *Aging Cell*. 2013;12(3):478–488.
79. Parkhitko AA, Binari R, Zhang N, Asara JM, Demontis F, Perrimon N. Tissue-specific down-regulation of S-adenosyl-homocysteine via suppression of dAhcyL1/dAhcyL2 extends health span and life span in Drosophila. *Genes Dev*. 2016;30(12):1409–1422.